Development of a new pharmacokinetic model using in silico studies, drug delivery systems and analytical methods

Abigail Filipe Ferreira

Tese de Doutoramento apresentada à

Faculdade de Ciências da Universidade do Porto

Bioquímica

2021

Development of a new pharmacokinetic model using in silico studies, drug delivery systems and analytical methods

Abigail Filipe Ferreira

Programa Doutoral em Química Sustentável

2021

Orientador

Rui Alexandre Santos Lapa, Professor Associado, Faculdade de Farmácia da Universidade do Porto

Coorientador

Nuno Filipe de Sousa Vale, Professor Auxiliar Convidado, Faculdade de Medicina da Universidade do Porto

U.PORTO
FACULDADE DE CIÊNCIAS
UNIVERSIDADE DO PORTO

Todas as correções determinadas pelo
júri, e só essas, foram efetuadas.

Pelos orientadores,

Porto, 09 / 12 / 2021

AGRADECIMENTOS (ACKNOWLEDGEMENTS)

A realização deste projeto de doutoramento só foi possível graças às instituições envolvidas e à orientação do Professor Doutor Rui Lapa e do Professor Doutor Nuno Vale. Este trabalho não seria igualmente possível sem o apoio e a colaboração de todos os que contribuíram para os estudos concretizados e incluídos nesta tese.

Às universidades responsáveis pelo Programa Doutoral em Química Sustentável (Universidade do Porto, Universidade de Aveiro e Universidade Nova de Lisboa) agradeço o apoio institucional e formativo. À Fundação para a Ciência e a Tecnologia (FCT) agradeço o financiamento da bolsa de doutoramento PD/BD/135120/2017.

Ao Professor Doutor Rui Lapa muito agradeço a confiança que depositou em mim e a oportunidade de realizar este projeto.

Ao Professor Doutor Nuno Vale não me chegam as palavras para agradecer todas as oportunidades que me proporcionou, a motivação e otimismo que sempre me transmitiu, o esforço que dedicou para o sucesso deste projeto, e por não me deixar desistir nas fases mais difíceis deste trajeto.

Ao Professor Doutor Jorge Gonçalves, agradeço a oportunidade de desenvolver parte do trabalho no Laboratório de Farmacologia do Departamento de Ciências do Medicamento da Faculdade de Farmácia da Universidade do Porto.

Pela oportunidade de fazer um estágio no Serviço de Química Clínica do Centro Hospitalar Universitário do Porto e de recolher os dados que permitiram a realização dos trabalhos da segunda parte desta tese, muito agradeço ao Professor Doutor José Carlos Oliveira. À Doutora Helena Martins tenho que agradecer o tempo que dedicou, a disponibilidade que sempre me mostrou e todos os ensinamentos que me transmitiu. A realização deste estágio foi uma experiência muito enriquecedora para mim.

Pelo infindável companheirismo, paciência, ajuda e compreensão das colegas de laboratório que partilharam a maior jornada deste percurso comigo, muito agradeço à Diana Duarte, Sara Silva e Ana Salomé Correia. Derramámos sangue, suor e lágrimas, partilhámos e ultrapassámos muita coisa, e não tenho dúvidas que superaremos esta etapa com sucesso e mais fortes que nunca! Após as adversidades, permanecerão as boas memórias. Muito obrigada a vocês!

Um especial agradecimento também à Bárbara Costa, Cristiana Correia, Joana Santos, Maria João Gouveia e Sara Moreira, colegas e coautoras de alguns dos trabalhos desenvolvidos.

Obrigada à Filipa Amaro, ao Dany Silva e às assistentes técnicas Maria do Céu Pereira e Mónica Caldas pelas boas recordações que guardarei da minha passagem pela FFUP.

Quero também deixar um cumprimento a todos os meus colegas da edição 2017/2018 do PDQS. Obrigada pela boa atmosfera que se formou durante a parte curricular do PDQS, que me ajudou a superá-la, pelos bons momentos passados e amizades criadas. Uma palavra especial à Karen: FORÇA!

Aos meus amigos que continuaram a apoiar-me e a aturar as minhas frustrações e desabafos, muito obrigada! Valérie, Rita Neves, Margarida, Mariana Santos, Fernando, … vocês são uma inspiração.

À minha família, um enorme OBRIGADA! Obrigada pela vossa motivação, pela vossa força, pela vossa paciência e compreensão, pelo esclarecimento das minhas dúvidas existenciais de inglês (Vanessa e Tina) e obrigada Paulo Jorge por me ajudares a começar a escrever esta tese. De soldado maçarico a 2º Cabo (e todos os postos que ainda alcançarás), para mim serás sempre o Topo Gigio que virou indígena XD. A todos vocês, o meu maior obrigada.

E aos meus pais. Porque a vocês devo TUDO. Esta tese é para vocês.

RESUMO

A farmacocinética (*pharmacokinetics*, PK) é uma área da farmacologia presente e de vital importância para a investigação e desenvolvimento de novos fármacos, monitorização pós-comercialização e contínuas otimizações em contexto clínico. O seu objetivo fundamental é melhorar os desfechos clínicos dos pacientes, aumentando a eficácia dos agentes terapêuticos e reduzindo os efeitos adversos que podem causar, contribuindo também para a medicina de precisão.

Neste projeto de doutoramento, a farmacocinética foi a base dos trabalhos desenvolvidos, que abordaram dois problemas de saúde para os quais são urgentemente necessárias alternativas terapêuticas: o cancro e infeções bacterianas graves. Estas temáticas foram abordadas na Parte I e Parte II desta tese, respetivamente.

A primeira parte desta tese foi dedicada à avaliação de novas estratégias para melhorar a terapia oncológica. O cancro é uma das principais causas de morte a nível mundial e as opções terapêuticas atualmente disponíveis apresentam ainda inúmeras limitações no que diz respeito à sua eficácia e aos efeitos secundários adversos que provocam.

Neste projeto foram exploradas e estudadas alternativas para aumentar a eficácia do agente quimioterapêutico gemcitabina (Gem). Estas incluíram (a) o estudo da farmacocinética da Gem e de conjugados Gem-CPP (péptidos penetradores celulares, CPP), (b) a determinação da permeabilidade de conjugados Gem-CPP6, (c) a proposta de uma nova via de administração para a Gem (oral) e (d) a combinação de Gem e 5-FU (outro agente usado em quimioterapia) com fármacos reaproveitados (itraconazole, tacrina ou verapamil).

Estes estudos confirmaram a utilidade dos CPP como veículos de entrega de fármacos, demonstrada pela permeabilidade e bioatividade dos conjugados Gem-CPP aqui avaliados. A via de administração oral para a gemcitabina foi avaliada como farmacocineticamente viável. Foi também identificada como promissora a combinação de gemcitabina e de 5-FU com itraconazole, pela sua melhorada bioatividade e previsto perfil farmacocinético e desempenho *in vivo* favorável.

Na segunda parte deste trabalho foi abordado o tratamento de infeções graves. Considerando que muitos antibióticos apresentam uma estreita janela terapêutica e atuam de forma muito variável entre diferentes indivíduos, o que pode facilmente conduzir a tratamentos não eficazes ou a efeitos tóxicos devidos a sobredosagem, é essencial otimizar o uso destes fármacos.

Foram analisados dados clínicos e demográficos de pacientes em internamento hospitalar devido a infeções graves e a receber terapia antibiótica com amicacina, gentamicina, tobramicina ou vancomicina. O perfil farmacocinético destes antibióticos foi analisado, avaliando diferentes regimes terapêuticos e a influencia de parâmetros individuais dos pacientes, como o sexo, a idade, o peso e a função renal.

Nestes estudos, foi destacada a importância de monitorizar estes pacientes e realçado o impacto da função renal nos níveis plasmáticos de vancomicina.

Foi ainda realizado um estudo complementar, analisando diferentes equações utilizadas para prever a clearance da creatinina a partir dos níveis séricos e de características dos pacientes.

Palavras-chave: farmacocinética, antibióticos, amicacina, gentamicina, tobramicina, vancomicina, cancro, gemcitabina, péptidos penetradores celulares, ferramentas *in silico*, modelação e simulação PBPK, GastroPlus™.

ABSTRACT

Pharmacokinetics (PK) is a branch of pharmacology present and of vital importance for the research and development (R&D) of new drugs, post-market monitoring, and continued optimizations in clinical contexts. Its fundamental purpose is to improve patients' clinical outcomes, enhancing the efficacy of therapeutic agents and reducing possible adverse side effects, also contributing towards precision medicine.

In this PhD project, PK was the core of the developed studies, that focused on two concerning health problems for which therapeutic alternatives are urgently needed: cancer and serious bacterial infections. These were addressed in Part I and Part II of this thesis, respectively.

The first part of this thesis was dedicated to the evaluation of new strategies to improve cancer therapy. Cancer is one of the leading causes of death worldwide, with currently available therapeutic options still presenting many shortcomings, regarding their efficacy and severe side effects.

Here, alternatives to enhance the bioactivity and efficacy of a drug used in chemotherapy, gemcitabine (Gem), were explored and evaluated. These included (a) the study of the PK properties of Gem and Gem-CPP (Cell-Penetrating Peptides) conjugates, (b) the experimental determination of the permeability of Gem-CPP6 conjugates, (c) proposing a new administration route for Gem (oral), and (d) the combination of Gem and 5-FU (also a chemotherapeutic agent) with repurposed drugs itraconazole, tacrine or verapamil.

These studies have confirmed the value of CPPs as drug delivery vehicles, demonstrated by the enhanced permeability and bioactivity of the Gem-CPP conjugates assessed here. The oral route of administration for gemcitabine was evaluated as pharmacokinetically viable. The combination of Gem and 5-FU with itraconazole was also identified as promising, considering its improved *in vitro* activity, and predicted favorable PK profile and *in vivo* performance.

In the second part of this thesis, the treatment of serious infections was studied. Considering many antibiotics present a narrow therapeutic window and perform significantly differently amongst different individuals, easily leading to not effective treatments or toxic effects caused by overdosing, it is essential to optimize the use of these drugs.

Clinical and demographic data from inpatients receiving antibiotic therapy with amikacin, gentamicin, tobramycin, or vancomycin for the treatment of severe infections was analyzed. The PK profile of these antibiotics was assessed, and different dosing regimens, as well as the impact of individual parameters as sex, age, body weight, and renal function, were evaluated.

These studies highlighted the importance of therapeutic drug monitoring (TDM) for patients treated with these antibiotics and emphasized the impact of renal function on vancomycin plasma concentrations.

An additional study was performed, where different equations used to predict creatinine clearance from serum creatinine concentration and considering patients' sex, age, and body composition were evaluated.

Keywords: pharmacokinetics, antibiotics, amikacin, gentamicin, tobramycin, vancomycin, cancer, gemcitabine, cell-penetrating peptides, *in silico* tools, PBPK modeling and simulation, GastroPlus™.

CONTENTS

AGRADECIMENTOS (ACKNOWLEDGEMENTS) ..... **v**

RESUMO ..... **vii**

ABSTRACT ..... **ix**

CONTENTS ..... **xi**

LIST OF FIGURES ..... **xiii**

ABBREVIATIONS ..... **xv**

INTRODUCTION **3**

PHARMACOKINETICS (PK) 3

RESEARCH AND DEVELOPMENT (R&D) OF NEW DRUGS 5

Early drug discovery 6

Preclinical studies 6

Clinical development and trials 6

Regulatory review and approval 7

Post-market surveillance 7

PK MODELING AND SIMULATION AND PREDICTION OF ADME 8

Noncompartmental PK analysis (NCA) 9

Compartmental models 9

Physiologically based pharmacokinetic models 9

Population PK 10

THERAPEUTIC DRUG MONITORING (TDM) 14

Target concentration intervention (TCI) 15

Model-informed precision dosing (MIPD) 16

CANCER 18

Prodrug conjugates with Cell-Penetrating Peptides (CPPs) 20

Gemcitabine 21

INFECTIONS AND ANTIBIOTIC THERAPY 23

Antibiotics and the need for TDM and dosage adjustment 24

PART I 27

CHAPTER 1

Combination of Gemcitabine with Cell-Penetrating Peptides: A Pharmacokinetic Approach Using *In Silico* Tools 29

CHAPTER 2

Permeability evaluation of gemcitabine-CPP6 conjugates in Caco-2 cells 43

CHAPTER 3

Permeability of Gemcitabine and PBPK Modeling to Assess Oral Administration 53

CHAPTER 4

New *in vitro-in silico* approach for the prediction of *in vivo* performance of drug combinations 65

PART II 91

CHAPTER 5

In silico pharmacokinetic study of vancomycin using PBPK modeling and therapeutic drug monitoring 93

CHAPTER 6

PBPK modeling and simulation of antibiotics amikacin, gentamicin, tobramycin, and vancomycin used in hospital practice 109

CHAPTER 7

A retrospective study comparing creatinine clearance estimation using different equations on a population-based cohort 139

FINAL REMARKS AND FUTURE PERSPECTIVES 155

SUPPORTING INFORMATION 157

- Amino Acids in the Development of Prodrugs 159
- Development of potent CPP6–gemcitabine conjugates against human prostate cancer cell line (PC-3) 221

REFERENCES 229

LIST OF FIGURES

Figure 1: An overview and summarized description of ADME. Reproduced from [4]. 3

Figure 2: Diversity of applications of PK. 5

Figure 3: Outline and summary of the stages of new drugs R&D. Reproduced from [10]. 5

Figure 4: "Summary of the PBPK literature analyzed. The number of articles per year that contain one or more PBPK models of pharmaceutical agents in humans is shown in (A). The distribution of the PBPK model applications in the original data papers is shown in (B).". Reproduced from [33]. 11

Figure 5: Simulations Plus, Inc. and GastroPlus™ logos. 12

Figure 6: GastroPlus™ Advanced Compartmental Absorption and Transit Model (ACAT). Reproduced from [44]. 13

Figure 7: “Schematic graphical representation of the interpretation of a TDM result for imatinib, measured at 845 µg/L in a 35 years, 90 kg male patient 9 hours after the last intake of his 400 mg q.d. dosing regimen. **(A)** Population percentiles showing the expected range of concentrations in the general population. **(B)** *A priori* percentiles showing concentrations expected in patients having similar individual characteristics (covariates). **(C)** *A posteriori* percentiles deduced by Bayesian inference from the *a priori* expectation and from the patient's observation (represented as the red dot, with whiskers depicting the associated intra-individual error). **(D)** *A posteriori* percentiles predicted after adjustment of the dosage to 600 mg q.d., able to drive the patient's trough concentration close to the target and the associated prediction range into the acceptance interval (represented as the blue horizontal line and band, respectively).” Reproduced from [49]. 16

Figure 8: CPPs as delivery vectors – intracellular delivery of CPP-cargo complexes. Reproduced from [98]. 20

Figure 9: Mechanism of intracellular activation and deactivation of gemcitabine. Adapted from [114]. 22

Figure 10: The core elements for antibiotic stewardship programs. Reproduced from [120]. 24

Figure 11: Model-Informed Precision Dosing workflow. Reproduced from [140]. 156

ABBREVIATIONS

5-FU: fluorouracil

ACAT: advanced compartmental and transit model

ADME: absorption, distribution, metabolism, and elimination

ADMET or ADME-Tox: absorption, distribution, metabolism, elimination, and toxicity

AMP: antimicrobial peptide

AUC: area under the curve

CPP: cell-penetrating peptide

DMPK: drug metabolism and pharmacokinetics

FDA: U.S. Food and Drug Administration

Gem: gemcitabine

IVIVE: in vitro-to-in vivo extrapolations

LADME: liberation, absorption, distribution, metabolism, and elimination

MAP: membrane active peptide

MIPD: model-informed precision dosing

MVA: multivariate analysis

NCA: noncompartmental analysis

PBBM: physiologically based biopharmaceutics modeling

PBPK: physiologically based pharmacokinetics

PCA: principal component analysis

PD: pharmacodynamics

PK: pharmacokinetics

q.d.: “*quaque die*" (in Latin, once a day).

QSAR: quantitative structure–activity relationships

R&D: research and development

TDM: therapeutic drug monitoring

INTRODUCTION

INTRODUCTION

INTRODUCTION

PHARMACOKINETICS (PK)

Pharmacokinetics is the branch of **pharmacology** that studies the route and fate of substances administered to a living organism until their elimination (*how the organism affects the drug*), while **pharmacodynamics** studies the biochemical and physiologic effects of drugs (*how a drug affects an organism*) [1,2]. The International Union of Pure and Applied Chemistry (IUPAC) defines PK as the "*Process of the uptake of drugs by the body, the biotransformation they undergo, the distribution of the drugs and their metabolites in the tissues, and the elimination of the drugs and their metabolites from the body over a period of time*." [3]. The acronym **ADME** encompasses the PK stages: **A**bsorption, **D**istribution, **M**etabolism, and **E**xcretion (Figure 1). The acronym LADME introduces considerations regarding **L**iberation of the active substance from the delivery system; ADME-Tox or ADMET add the **T**oxicological aspect.

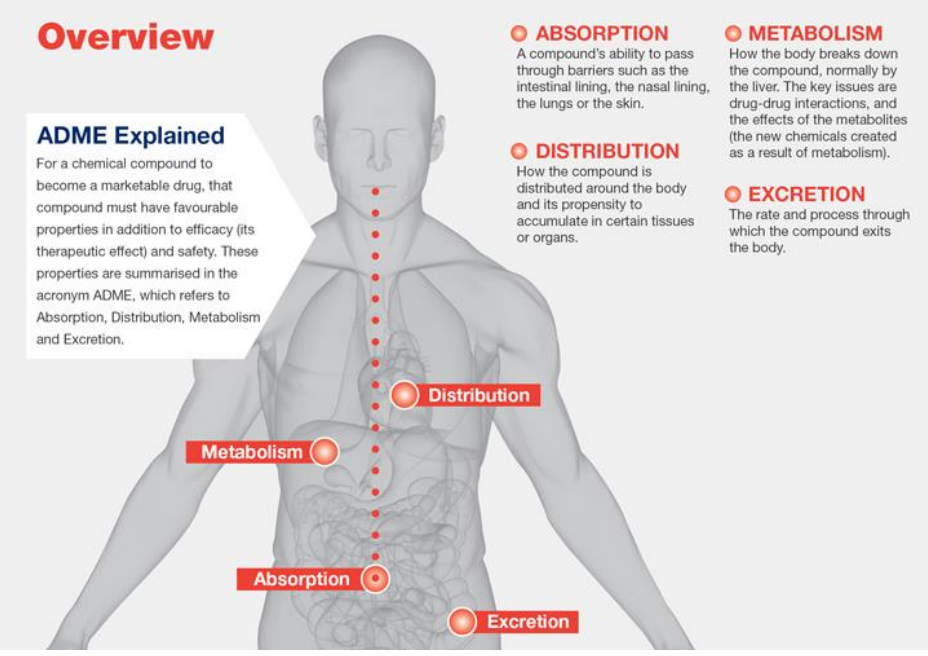

Figure 1: An overview and summarized description of ADME. Reproduced from [4].

The first stage, **Absorption**, begins with the drug's administration and analyzes the processes until the active substance reaches the bloodstream. Bioavailability, the fraction of the active form of a drug that enters the bloodstream, is predominantly dependent on the route of administration (e.g., drugs given intravenously are instantly delivered to the bloodstream and thus bioavailability is 100%). Other elements influencing absorption and bioavailability are medicine's formulation, substances' chemical properties, administered dose, and possible interactions with blood components, food and/or other drugs.

The **Distribution** phase entails the movement of the drug from the absorption site to different tissues around the body, and is influenced by many factors, including blood flow, drug's lipophilicity, molecular size, and interaction with blood components, such as plasma proteins.

As for **Metabolism**, the chemical alterations most drugs go through are mainly catalyzed by enzymes of the superfamily Cytochrome P450 (CYPs), leading to the formation of metabolites, that can be inactive and even toxic, or the actual active form of the drug (a type of prodrug) [4,5]. Metabolism is ruled by genetic factors (enzyme polymorphisms) and is also dependent on age, overall liver function (the main organ where metabolism takes place), and drug-drug interactions (enzyme inhibition or induction).

Finally, a drug and its metabolites need to be **Excreted** from the body, or their accumulation can adversely affect normal body functions and metabolism. The main route of excretion is through the kidneys, resulting in elimination in the urine. This process involves mechanisms of active secretion of free or protein-bound drug by transporters and glomerular filtration of unbound drug. Drugs can also be eliminated via biliary or fecal excretion, and through the lungs in the expired air (in the case of volatile compounds, like anesthetic gases and alcohol). To a lesser extent, drugs can be excreted in sweat, saliva, milk (via lactation), or other body fluids. Renal function, age and pathologies affecting renal blood flow (e.g., congestive heart failure and kidney disease) influence the rate and efficiency of drug elimination.

PK is a comprehensive science, an integral part of many fields, with countless applications and inestimable value. It has an important role throughout the process of research and development (R&D) of new drugs, extended to its vital significance in clinical settings and in improving patients' care and outcome (Figure 2).

During R&D of new therapeutic agents, some of the most important factors to consider and evaluate are related to LADME properties, and include solubility, lipophilicity, permeability, modification or degradation due to chemical stability and metabolism, transport, specificity, and targeting. Then, bioactivity and toxicology are crucial PD aspects to assess.

Figure 2: Diversity of applications of PK.

RESEARCH AND DEVELOPMENT (R&D) OF NEW DRUGS

The R&D for new therapeutic agents is long, complex, difficult and expensive, and a multitude of procedures are required until a new drug can be approved and commercialized. Only about 12 percent of drugs entering clinical trials are ultimately approved for introduction by the FDA and recent studies estimate the development and approval of new drugs takes on average seven to nine years and the cost of introducing a new drug can range from $1 billion to more than $2 billion USD [6-8]. This process can be divided into 5 stages, depicted in Figure 3 and described below [9].

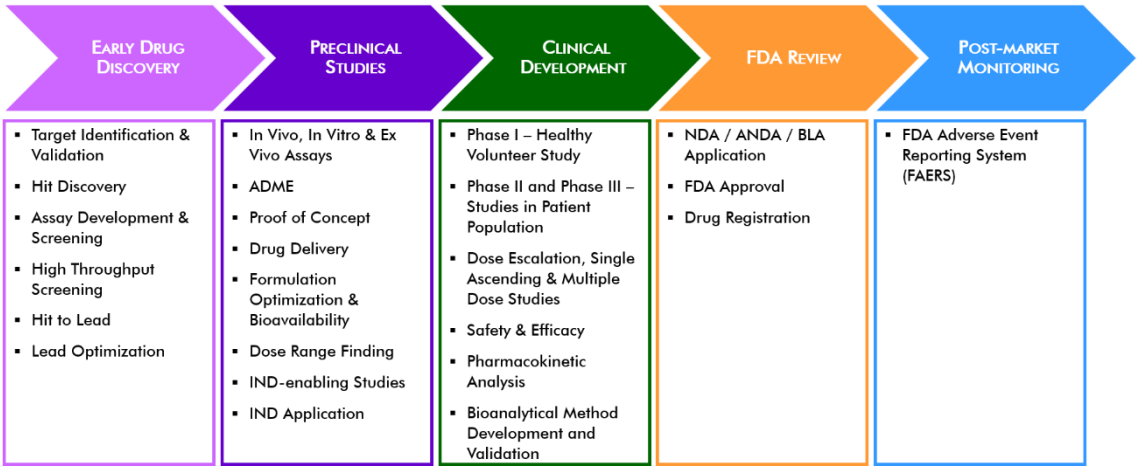

Figure 3: Outline and summary of the stages of new drugs R&D. Reproduced from [10].

Early drug discovery

The development of new drugs can be driven by (1) unfavorable results of previously existing treatments (inefficiency, or unanticipated and possibly toxic effects), (2) new insights and knowledge about biological and pathophysiological processes or disease mechanisms, that may include new targets or biomarkers identification to allow compounds to be designed to prevent, stop or reverse particular effects, (3) high throughput screening of an enormous selection of compounds to find possible candidates for a variety of conditions, or (4) technological advances that provide new possibilities and benefits.

During this early stage, there can be thousands of compounds being evaluated and these studies can last 3 to 5 years. It usually begins with targets identification and validation, and using High Throughput Screening (HTS) and *in silico* tools to identify hit compounds. Compounds are evaluated regarding their physicochemical properties and PK aspects related to ADME profile, mainly based on previous knowledge, extrapolations and using *in silico* tools. These include molecular weight (MW), lipophilicity (partition and distribution coefficients, logP and logD), solubility, permeability, acid dissociation constant (pKa), polar surface area (PSA), interaction and affinity to known transporters and other biomarkers of interest, and also with enzymes that can affect their metabolism [11]. After the initial evaluations, only a small number of candidates will be considered promising enough to move to the next stage.

Preclinical studies

After the Hit to Lead (H2L) process and lead generation and optimization, these drug candidates are evaluated to determine their efficacy and safety in *in vitro*, *in vivo* and *ex vivo* assays. During this stage (around 1-2 years), researchers evaluate ADME properties and PK/PD profile, assess drug delivery and optimize formulation to reach maximum bioavailability, and determine a suitable dose range to study in the following clinical stage. A proof-of-concept can be established investigating mechanisms of drug action/effects (target engagement/PD) and pathways that contribute to the particular condition or disease.

Clinical development and trials

With the results from the preclinical phase, one or more final drug candidates are evaluated on human participants. Prior to the beginning of any clinical trial, an Investigational New Drug (IND) Application must be filed to the regulatory entity, presenting the results from the preclinical studies and requesting authorization for clinical investigations. There are 3 main phases of clinical trials [12].

During phase I, drugs are administered to and tested in a typically small group of healthy volunteers (20-80) concerning their safety. Different administration routes may be assessed, and the appropriate and safe dosage ranges must be verified. PD effects, such as side effects, must be recorded and reported.

When these aspects are refined, phase II is initiated in patients suffering from the studied health condition, to confirm if the drug will demonstrate the desirable effects in human patients. Typically, a larger group is enrolled in this phase to explore drug activity, measuring efficacy while also investigating observed short-term adverse reactions.

Finally, the phase III of clinical trials will enroll an even larger group of patients to further confirm efficacy and monitor side effects, thus validating drug response signature.

Throughout all stages of clinical trials, patients undergo pharmacokinetic evaluation that includes blood sample collection in established time-points, to measure drug and possible metabolites' concentration. This requires a previous validation of the necessary protocols and analytical methods, including High-Performance Liquid Chromatography (HPLC) and Mass Spectrometry (MS). Dose escalation, single ascending and multiple dose studies can be carried out in all stages of clinical trials. Ideally, during the course of and by the end of a clinical trial, if a heterogenous enough population is studied, researchers will have gained insights into how the drug candidate may differently affect people of different groups (such as by gender, race, or ethnicity) and interact with other drugs patients may be receiving for the treatment of other comorbidities. If previous treatments for the studied condition were previously available, comparisons in effectiveness and overall benefits will be analyzed.

Regulatory review and approval

After the conclusion of a clinical trial, the results will be reviewed by a regulatory entity (such as the FDA, EMA, or China Food and Drug Administration (CFDA)) in a New Drug Application (NDA) formal request. The reviewing process can take 1-2 years and if the drug is approved, it will be registered, and manufacturing and commercialization will be initiated [13].

Post-market surveillance

Nevertheless, monitoring of drugs never ceases. Post-market monitoring and surveillance will always have mechanisms in place, including the FDA Adverse Event Reporting System (FAERS) [14], to monitor the efficacy, safety, risk, and benefits of long-term use by the general population. This system may also lead to label expansion, when a drug seems to have positive impacts for additional types of patients/diseases beyond the original use for which the drug was approved for marketing.

In summary, PK is present and a key element throughout the entire process of research, development, clinical and post clinical evaluation of drugs. In fact, poor PK properties, such as low bioavailability, were responsible for the failure of about 40% of lead compounds 30 years ago and still remain one of the main motives preventing progression of new drug candidates to further stages [15]. Since then, with the acknowledgement of ADME properties as major impactors on clinical outcome, technological innovations, and the development of ***in silico* tools** and software packages, dramatic changes and reductions have been seen on the time, human resources, and financial investment necessary to achieve new advancements, both in the R&D process and in clinical applications.

Predicting many of the relevant physicochemical, pharmacological, and pharmacokinetic properties and the disposition attributes of drugs using *in silico* methods can rapidly identify PK liabilities, such as poor bioavailability, high metabolism and clearance, potential for drug-food and drug-drug interactions (DDI), the need for dose adjustments, and particular alterations in special populations. This has become essential from the early stages of R&D of new drugs, to the clinical setting and in ensuring the best outcome and minimal side effects for patients.

As such, there has been an increased interest and investment in drug metabolism and pharmacokinetics (DMPK) and PK/PD relationship studies, including in the development of improved software packages. Most modern tools to model and simulate PK profiles can accelerate drug discovery, but also help design clinical trials, analyze clinical data in all stages of clinical evaluation, regulatory approval, and post market monitoring and surveillance and quickly identify adequate therapeutic solutions [16-20].

PK MODELING AND SIMULATION AND PREDICTION OF ADME

Numerous methods have been explored to predict and study human pharmacokinetics. These include interspecies allometric scaling [21], *in vitro*-to-*in vivo* extrapolations (IVIVE) [22], quantitative statistical methods such as Quantitative Structure–Activity Relationships (QSAR) or Quantitative Structure–Property Relationships (QSPR) [23,24], Principal Component Analysis (PCA), Multivariate Analysis (MVA) [25], and other *in silico* methods [26]. These quantitative and mechanistic

approaches define processes in complex systems of mathematical equations. Earlier, preclinical and clinical PK studies were merely descriptive. Currently, many commercial platforms and software packages are available and are more user-friendly, making PK modeling and simulation more accessible, without requiring extensive mathematical, modeling and/or programming experience.

PK models are often used to describe the plasma or relevant tissue drug concentration throughout time and are built using compartments as “building blocks” with increasing complexity, from non-compartmental models, models with 1, 2, or 3 compartments, to more intricate models, such as whole-body or physiologically based pharmacokinetic (PBPK) models and population PK models [27,28].

Noncompartmental PK analysis (NCA)

The most elementary PK information can be provided by **NCA**. This relies on simple algebraic equations to analyze peak concentration and elimination half-life and estimate PK parameters. NCA is a much faster and cost-efficient method, convenient for the characterization of new drug products, helping the guidance of development at various stages [29].

Compartmental models

Different organs and tissues of the body can be defined by **compartmental models**, kinetically interconnected [30]. Typically, a central compartment representing plasma is linked to one or two peripheral compartments via rate constants. Although more complex than NCA, there is potential for more variability since certain assumptions are made to build and parameterize the PK model. Though these models generally do not hold any physiological meaning, they can provide important PK descriptors, as clearance and volume of distribution, and thus, effective drug half-life or “residence” time.

Physiologically based pharmacokinetic models

Using similar mathematical frameworks and a series of differential equations, **PBPK** models have a larger number of compartments, parameterized with physiological knowledge of specific organs or tissues and flow rates connecting the system. These dynamic models can predict most PK attributes and the concentration-time profile after drug administration. PBPK models can be used for a wide variety of purposes and applications (described below) and present numerous advantages compared to other methods, since PBPK models account for sequential metabolism and permeability limited processes [31-35].

Population PK

While individual PK studies are the best approach when rapid processing of PK parameters is needed, or when complete individual PK profiles are to be defined, **population PK (popPK)** analysis and modeling approaches are of value to study variability in drug concentrations within a population of patients receiving clinically relevant doses of a drug of interest. This method requires concentration-time data from multiple individuals and can incorporate covariate information as age, sex, weight, race, renal/hepatic function, and even data about concomitant medications that can lead to DDIs. This is a more technically convoluted analysis and tends to use complex mathematical and compartmental methods to reach conclusions. User-friendly popPK software has been developed to support all stages of drug development and surveillance, as assessing the sources of PK variability can be essential for drug safety and efficacy, and appropriate dosages can be selected for a given population or subgroup with information granted by popPK models [36,37].

As aforementioned, there has been an increasing interest and investment in pharmacokinetic studies, including the development of tools and software for prediction of PK attributes, modeling and simulation of profiles. Some of the available software that can be used for PK studies are GastroPlus™ and Monolix® by Simulations Plus, Inc. (Lancaster, California, USA), Simcyp®, NONMEM (ICON plc), Phoenix® WinNonlin® and Phoenix® NLME™ by Certara (UK Limited, Sheffield, UK), and PK-Sim® (OSP, Open Systems Pharmacology).

Sager et al. conducted a systematic review on publications between 2008 and May 2014 related to PBPK models [33]. Searching the PubMed database for papers that included the terms “PBPK” and “physiologically based pharmacokinetic model”, a total of 366 articles were analyzed regarding the models’ development and applications. The number of these publications has been steadily increasing, from 9 papers in 2008, to 94 in 2014 (Figure 4A). The most common applications were the study of drug-drug interactions (DDI) (28%), prediction of interindividual variability and general clinical pharmacokinetics (23%), absorption kinetics (12%), and age-related changes in pharmacokinetics (10%) (Figure 4B). For FDA regulatory filings, models were primarily used for DDI predictions (60%), followed by pediatrics (21%) and absorption (6%) predictions.

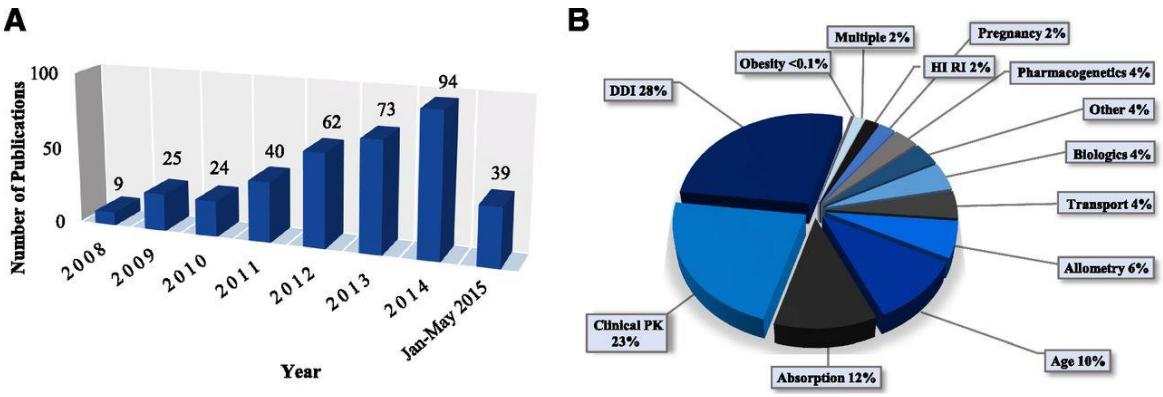

Figure 4: "Summary of the PBPK literature analyzed. The number of articles per year that contain one or more PBPK models of pharmaceutical agents in humans is shown in (A). The distribution of the PBPK model applications in the original data papers is shown in (B).". Reproduced from [33].

In this PhD project, GastroPlus™ software package, including ADMET Predictor™, developed by Simulations Plus, Inc., was explored to predict PK attributes, concentration-time profiles, and evaluate different dosing regimens, the impact of patients' individual characteristics, namely age, biological sex, weight, and renal function, and of choosing different administration routes.

Simulations Plus, Inc. is celebrating 25 years of extensive knowledge in pharmacology, and provides consulting solutions, tools, and user-friendly software packages for model-based drug development, to make better data-driven decisions, accelerate and reduce the costs of R&D. This company and its product are well established and acclaimed.

> *"We are a leading provider of modeling and simulation software and consulting services supporting drug discovery, development research, and regulatory submissions. With our subsidiaries, Cognigen, DILIsym Services, and Lixoft, we offer solutions that bridge machine learning, physiologically based pharmacokinetics* [pharmacometrics and ADMET property prediction]*, quantitative systems pharmacology/toxicology, and population PK/PD modeling approaches. Our technology is licensed and applied by major pharmaceutical, biotechnology, chemical, consumer goods companies, and regulatory agencies worldwide."* [38].

Some of the pharmaceutical companies and regulatory entities that use and acknowledge their products include Orion, Novartis, Sanofi, Pfizer, Merck, AstraZeneca, Janssen, the U.S. Food and Drug Administration (FDA), European Medicines Agency (EMA), the China Food and Drug Administration (CFDA), the Centers for Disease Control and Prevention (CDC), the National Institutes of Health (NIH), and the National Cancer Institute (NCI) [39].

> *"**GastroPlus** is a mechanistically based simulation software package that simulates intravenous, oral, oral cavity, ocular, inhalation, dermal, subcutaneous, and intramuscular absorption, biopharmaceutics, pharmacokinetics, and pharmacodynamics in humans and animals. This smoothly integrated platform combines a user-friendly interface with powerful science to help you make faster and more informed project decisions!" [40].*

Figure 5: Simulations Plus, Inc. and GastroPlus™ logos.

This software package was specifically designed for PK studies, particularly physiologically based pharmacokinetics (PBPK) and physiologically based biopharmaceutics modeling (PBBM). Its features and capabilities allow the prediction of drug absorption and disposition, and simulation of absorption, pharmacokinetics, and pharmacodynamics in humans and many preclinical species, thanks to preinstalled physiological parameters and an integrated advanced compartmental and transit (ACAT) model (Figure 6). Thus, it supports model-based drug development and PK assessments in all phases of drug discovery, translational research, and clinical development. This not only improves decision making throughout clinical drug development, but also enables the design and optimization of dosing regimens and formulations, increasing the chances of the drug to reach its target with the desired concentration and drug plasma concentration to be maintained within the therapeutic window [11,31,33,41-43].

GastroPlus™ can incorporate 10 additional modules (individually licensed to meet each user's needs): ADMET Predictor™ module (for the prediction of physicochemical and PK parameters of compounds), PKPlus™ and PBPKPlus™ modules for an even deeper insight into the PK of drugs, and IVIVCPlus™, Additional Dosage Routes, Metabolism & Transporter, Drug-Drug Interaction (DDI), PDPlus™, Biologics, and Optimization modules.

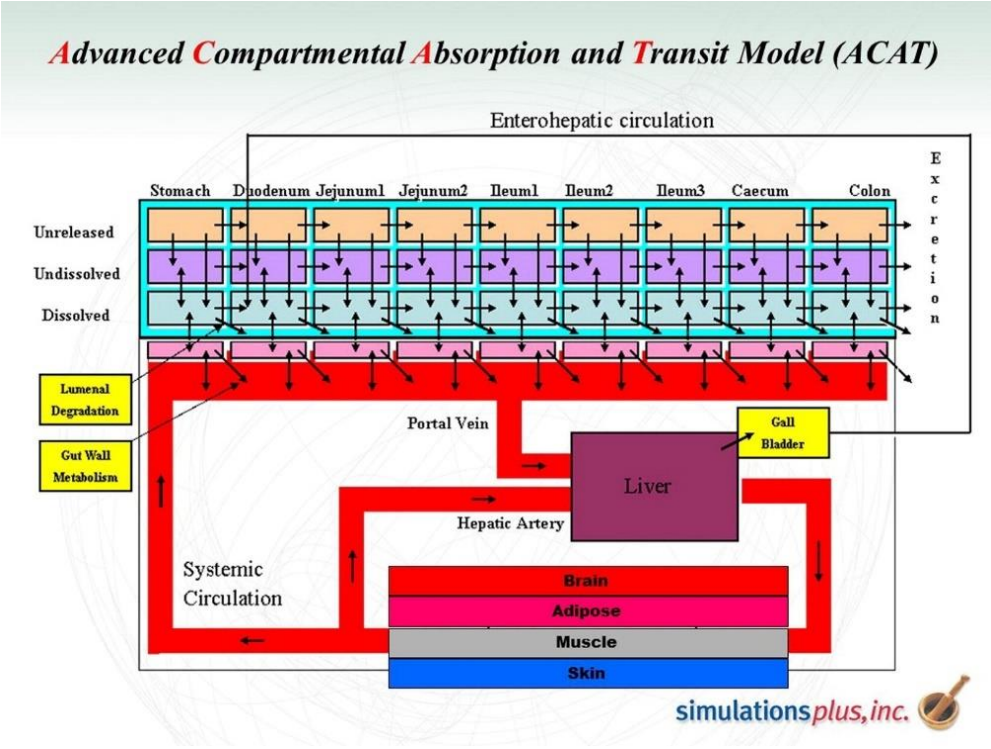

Figure 6: GastroPlus™ Advanced Compartmental Absorption and Transit Model (ACAT). Reproduced from [44].

Calculations and simulations rely on the numerical integration of differential equations that coordinate a set of well-characterized physical events that occur and are interconnected as a result of diverse physicochemical and biologic phenomena. Despite its sophistication, GastroPlus™ is relatively easy for someone with a background in ADME to learn and use, and quality and highly customizable PBPK models can be easily developed due to its intuitive and modern graphical user interface, that enables a rapid and smooth transition from setting up inputs to evaluating results. Simulation studies can be initiated based on a drug's structure and a small set of collected data to predict the most important parameters in pharmacokinetics (PK), such as the maximum concentration reached in plasma and liver, time necessary to reach such concentrations, fraction absorbed and bioavailability, and area under the curve (AUC).

Additionally, GastroPlus™ not only calculates PK attributes but draws a graphical representation of concentration over time profiles, for quicker interpretation of simulation results. Furthermore, parameter sensitivity analysis (PSA) and population PK analyses (including Population Estimates for Age-Related Physiology, PEAR) can also be performed in GastroPlus™.

Thus far in this thesis, the prominence of PK has been addressed, from its central role in the R&D process to its clinical relevance. In fact, applied pharmacokinetics is valuable in countless pharmacological evaluations, whether for academic purposes, drug development and clinical research, and in clinical medicine, for therapeutic drug monitoring and individualized dosing, towards precision medicine.

THERAPEUTIC DRUG MONITORING (TDM)

Even after the myriad of studies and optimizations that were required to approve a drug with a determined therapeutic application and recommended dosing regimens (label and guidelines), not all drugs will perform as a “one-size-fits-all”. Due to certain pharmacological characteristics of some drugs and drug classes, their dosing regimens will need to be adjusted and customized for each patient [45,46]. This can be accomplished through **therapeutic drug monitoring (TDM)**.

This branch of clinical chemistry and clinical pharmacology specializes in the measurement of circulating drug concentrations to adjust dosing regimens, so as to reach a defined target exposure associated with optimal efficacy and minimal toxicity [47,48]. TDM can be traced back to the late 1960s and the efforts of clinicians to improve patient care and clinical outcome [48]. The cases that required such dosage individualization have been extensively reviewed and TDM is now indicated and recommended for critically ill patients undergoing sufficiently long treatment to justify dosage adjustment efforts and for drugs that have the following pharmacological properties [49]:

1. Poorly predictable PK and significant interpatient variability, resulting in a wide range of concentration levels between patients after standard dosage administration;
2. Narrow therapeutic window, that combined with interpatient variability, poses a high risk of misdoing. Standard dosage could be subtherapeutic for some patients, but the use of very high standard doses in all patients to ensure overall efficacy is forbidden due to the risk of toxicity [50];
3. Consistent concentration exposure and response and/or toxicity (PD) relationships. Also, effects following changes in drug exposure should be reversible, enabling the definition of a range of concentrations associated with optimal efficacy and minimal toxicity;

4. Lack of readily assessable PD markers and quick response to dosage changes;
5. Acceptable PK stability, considering within-patient PK variability over time (inter-occasion variability) and assay and/or model-related errors [51].

TDM has been proven favorable and recommended for hundreds of therapeutic agents, including anticancer drugs [52], anti-infectives [53], antiretrovirals [54], biologic therapeutic agents [55], psychotropic agents [56], etc. Traditionally, clinicians would analyze the results from the TDM and empirically modify a patient's dosage to approximate circulating concentrations to the identified target therapeutic window. Advantages of this approach include its quite simple interpretation of the TDM data and undemanding implementation, as the adjustment can generally be done based on a mathematical "rule of three", changing either dose or dosing interval (Dettli rules [57]). Some conventional therapeutic ranges have been extended to nomograms that can assist in the adjustment decision.

Notwithstanding its simplicity and usefulness, traditional TDM holds some limitations. The blood samples to determine drug concentration need to be collected only after steady-state is reached, typically meaning dosage will only be adjusted 3-4 days after beginning of treatment. While this is a suitable timespan for many drugs, in the case of infections and antibiotic treatment, the PK/PD target should be promptly achieved. Moreover, some antibiotics exhibit nonlinear PK and are concentration and/or time dependent. In such cases, dosage adjustment cannot be based on the "rule of three". Another weakness of this approach is likewise related to sampling, as a single sample determination (as C_{peak} or C_{trough}) is frequently an insufficient indicator of drug exposure. Also, timing of both dose administration and sample collection is a critical factor to ensure accurate interpretation of results and appropriate adjustments [49].

Consequently, dosage adjustments based on traditional TDM are considered a passive procedure, as therapeutic ranges are often wide and due to the interpatient variability and other factors described above, PK/PD targets and successful clinical outcome may not by achieved. Improvements to this practice are thus needed.

Target concentration intervention (TCI)

Taking advantage of the increasing computational power and advances in computer sciences, TCI has been introduced as a more adequate approach. Computer-assisted solutions for the interpretation of TDM results in a clinical setting have arisen and mathematical models have been developed to further inform clinicians decisions [58].

Model-informed precision dosing (MIPD)

MIPD has emerged as an integrative approach to precision medicine, considered the next milestone of medical progress after evidence based medicine [59]. These mathematical models are built with the input from observational population PK studies to interpret the measured drug concentration and predict personalized dosing beyond a specific approach or technique. When in significant number, these studies assemble data on drugs' average PK parameters, and identify the most impacting covariates or individual factors contributing to inter and intraindividual variability. The latter can be accounted for using both parametric and nonparametric approaches [60,61]. The main difference is that in nonparametric approaches, support points are estimated from the clinical data, while parametric approaches use a defined distribution of PK parameters.

The most recurrently recognized covariates include age, body weight, biological sex, and serum creatinine (important to evaluate renal function). Genetic aspects, comorbidities, clinical status of the patient (disease status, renal/hepatic function, biological markers, treatment tolerance, etc.), as well as comedications also influence PK attributes [62].

Bayesian inference is also of undeniable value for TDM and MIPD (Figure 7). The main components of the Bayesian approach are prior distribution, likelihood principle, posterior probabilities, decision rules, and predictive probability [63-65].

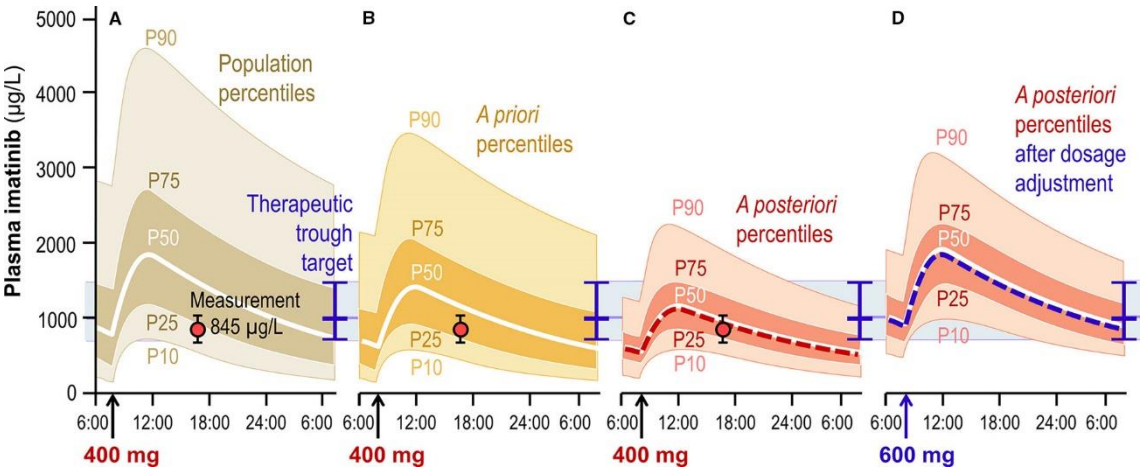

Figure 7: "Schematic graphical representation of the interpretation of a TDM result for imatinib, measured at 845 µg/L in a 35 years, 90 kg male patient 9 hours after the last intake of his 400 mg q.d. dosing regimen. **(A)** Population percentiles showing the expected range of concentrations in the general population. **(B)** *A priori* percentiles showing concentrations expected in patients having similar individual characteristics (covariates). **(C)** *A posteriori* percentiles deduced by Bayesian inference from the *a priori* expectation and from the patient's observation (represented as the red dot, with whiskers depicting the associated intra-individual error). **(D)** *A posteriori* percentiles predicted after adjustment of the dosage to 600 mg q.d., able to drive the patient's trough concentration close to the target and the associated prediction range into the acceptance interval (represented as the blue horizontal line and band, respectively)." Reproduced from [49].

Medicine has witnessed admirable advances, and countless therapeutic agents are currently available for the treatment of most diseases and maladies. Nevertheless, new drugs are unceasingly being investigated and developed for the treatment of diseases for which there is still no existing therapeutic options, for new conditions that emerge occasionally (e.g., due to the Zika virus and, more recently, SARS-CoV-2), for diseases with increasing incidence, and when currently available therapeutic options are insufficient and alternatives are needed. This is the case for **cancer** and **severe infections**, a leading cause of death worldwide, and a growing concern due to the high risk of misdoing and rising antibiotic resistance, respectively.

In summary, in this PhD project, PK properties were evaluated and PBPK models were developed and explored to assess delivery, permeability and efficacy of a chemotherapeutic agent conjugated with CPPs (gemcitabine-CPP prodrugs) and combinations of anticancer agents with repurposed drugs, and to further analyze impacting variability factors on antibiotic disposition.

These studies add insights that can contribute to new further refined MIPD.

CANCER

Worldwide, cancer is one of the most concerning, severe and fatal diseases, being among the leading causes of death. An estimated 9.6 million deaths, or one in six deaths, in 2018, were due to cancer. The prevalence of this condition has been growing at an alarming rate, and 18 million new cases were reported in 2018. There are disparities in the incidence of cancers between sexes, age and ethnic groups, and in different regions of the globe. Globally, prostate, lung, and colorectal cancers are the most prevalent in men (about 43%), while breast, lung, and colorectal cancers affect women the most (around 50%) [66,67].

The management and treatment of cancer is extremely difficult, mainly due to the complexity of this multifactorial condition. In fact, a team of multidisciplinary professionals is usually involved throughout the progression of a patient's journey. Cancer treatment options include surgery, chemotherapy and radiotherapy, and a combination of these is often recommended and employed. The management of this condition depends on numerous factors, including the stage and progression of the disease, the general health status of the patient, and the available treatment options for each specific diagnosis [68].

Despite the remarkable advancements in the development of new therapeutic options and overall treatment improvement, that has resulted in the amelioration of patients' clinical outcomes, currently available cancer treatments still present several shortcomings.

The complexity in recognizing the cancer altered cells and distinguishing them from normal healthy cells, the intratumoral and intertumoral heterogeneity and interindividual variability, the difficulty in reaching metastases, and the development of drug resistance represent the main difficulties in cancer therapy and are responsible for low treatment efficacy [69]. Additionally, adverse side effects are frequent, and can include fatigue, nausea, vomiting, appetite and weight changes, hair loss, hematologic alterations including anemia, among others [69,70].

Thus, new alternatives are incessantly being researched, aiming at increasing the overall treatment efficacy and reducing the associated side effects. These include the development of new therapeutic agents and prodrugs, drug repurposing and drug combinations, immunotherapy and gene therapy [71,72].

The **combination** of two or more antineoplastic agents (or polychemotherapy) has been approved by the FDA and is standard treatment for several cancers [73]. For breast cancer, antimetabolites (methotrexate and 5-fluorouracil) are traditionally combined with alkylating agents (such as cyclophosphamide) [74]; in the case of lung cancer, in

particular metastatic small-cell lung cancer, a combination chemotherapy, generally including platinum-based agents plus etoposide or irinotecan, is the core first-line treatment [75]. This approach is widely accepted, as it results in higher response rates than single-agent chemotherapy.

Repurposed drugs (drugs that have been approved for other applications but have shown potential por cancer treatment) as single-therapy or in combination with traditional chemotherapeutic agents, have been extensively studied [76-78]. Some of these combinations have reached clinical trials, but none has been approved so far. A proof-of-concept clinical trial is evaluating the combination of 9 repurposed drugs with metronomic temozolomide for recurrent glioblastoma (NCT02770378). In this project, this strategy was explored, and the combination of gemcitabine or 5-FU with itraconazole, tacrine or verapamil was evaluated regarding bioactivity and PK features.

Regarding **prodrugs** for the treatment of cancer, designing for selective activation in target tissues is undoubtedly the most efficient and attractive approach [79-81]. Other strategies involve the improvement of physicochemical properties, as solubility and lipophilicity, enhancement of permeability and transport and of pharmacokinetic properties [78,82-84].

In this context, **prodrugs using amino acid or peptide moieties** have demonstrated very promising results, with improvements in several physicochemical and pharmacokinetic properties, namely enhanced solubility, lipophilicity, permeability, bioavailability, specificity with accurate delivery to target tissues or organs, prevention of fast metabolism, and decreased toxicity [85,86].

Although **amino acids** are basic constituents of a cell structure, they require specialized transport systems to cross the plasma membrane. Amino acid transporters are ubiquitous and have overlapping substrate specificity. They can transport not only amino acids but also amino acid related compounds, acting as delivery vehicles, and can be used for targeting drug delivery, for example to the corneal epithelium, taking advantage of endogenous nutrient transporters that are over-expressed in certain tissues and organs [87]. The importance of these transporters in PK has been recognized through several studies that report an improved bioavailability of amino acid linked compounds [88-90]. Moreover, amino acids are the building blocks for proteins and are thus generally regarded as safe [86]. Amino acid prodrugs have been developed for cancer treatment, including amino acid esters of gemcitabine [91] and an amino acid ester prodrug of brivanib, in phase III clinical trials for the treatment of hepatocellular

carcinoma and colon-rectal cancer [92]. A review on “Amino Acids in the Development of Prodrugs” was prepared and is presented in the Supporting Information of this thesis.

The same rationale has been applied for the development of **peptide prodrugs**. Adding peptide moieties to existing drugs has also resulted in improved physicochemical, pharmacological and pharmacokinetic properties [93-97].

Prodrug conjugates with Cell-Penetrating Peptides (CPPs)

A particularly interesting class of peptides are Membrane Active Peptides (MAPs). Two classes of MAPs are Cell-Penetrating Peptides (CPPs) and Anti-Microbial Peptides (AMPs). CPPs are small sequences of amino acids (typically less than 40 residues) that have proven efficacy in transposing cell membranes via transporter and receptor-independent mechanisms, mainly endocytosis. Importantly, CPPs can also intrinsically carry and deliver a wide variety of cargos inside cells in a non-cytotoxic manner (and maintaining the integrity of the cell in opposition to AMP), with no restriction with respect to the size or type of cargo, from small therapeutic molecules with low molecular weight, such as some drugs and nucleic acids, imaging agents useful to diagnostics, to large plasmid DNA, antibodies, or even entire proteins. These can be covalently or noncovalently bound to the CPP. Moreover, these peptides and CPP-cargo conjugates are versatile, and usually easy to synthesize, functionalize, and characterize. Using this transport system, bioactive cargos can be delivered directly inside cells, and obtain high levels of protein activation/inactivation, gene expression or silencing, or tumor targeting, for example. As such, CPP-drug conjugates can become excellent prodrugs (Figure 8).

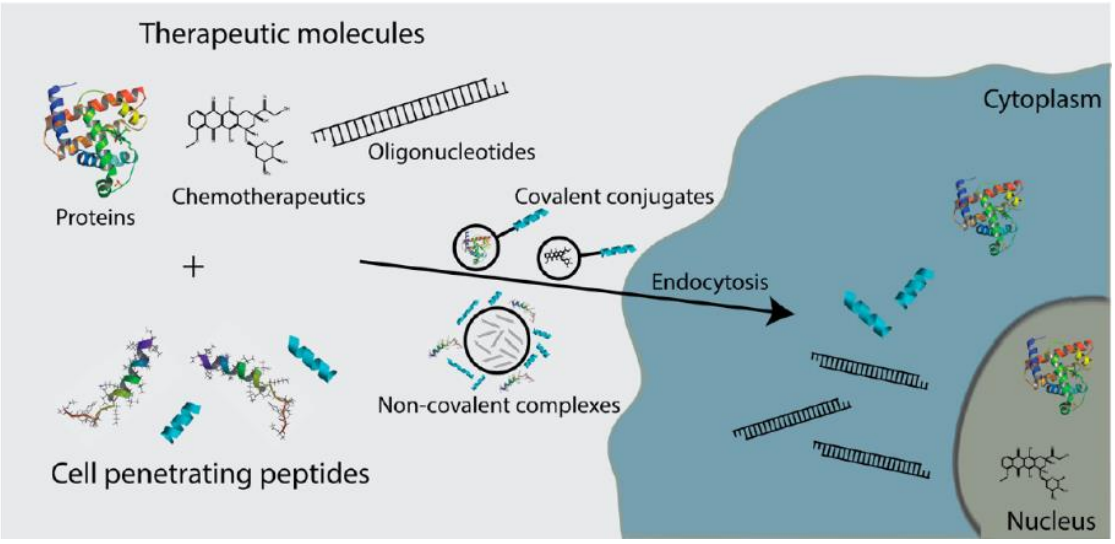

Figure 8: CPPs as delivery vectors – intracellular delivery of CPP-cargo complexes. Reproduced from [98].

CPP-drug conjugates have been developed for the treatment of cancers [99,100], involving doxorubicin [101,102], methotrexate [103], paclitaxel [104], and gemcitabine [105].

During this PhD project, various Gem-CPP conjugates were developed and studied in Part I. An original research paper where gemcitabine was conjugated with cell-penetrating hexapeptides (yielding CPP6-gemcitabine conjugates) and identified as promising for the treatment of prostate cancer after evaluation in different cell lines is presented in the Supporting Information of this thesis. Moreover, a review on "Cell-penetrating peptides in oncologic pharmacotherapy" was prepared [106].

Gemcitabine

Many chemotherapy drugs are based on the use of nucleoside analogues. One of such analogues is 2′,2′-difluorodeoxycytidine, or Gemcitabine (Gem). Gemcitabine has many distinctive properties from other nucleoside analogues, including its broad spectrum of activity [107]. This drug is particularly effective against pancreatic cancer, and the use of its hydrochloride salt was approved by the FDA in 1996 as first-line treatment for patients with locally advanced (non-resectable Stage II or Stage III) or metastatic (Stage IV) pancreatic adenocarcinoma previously treated with fluorouracil (5-FU) [108].

Currently, it is known that Gem is efficient against a wide range of solid tumors, and is approved and indicated by the FDA for the treatment of advanced ovarian cancer (that has relapsed at least 6 months after completion of platinum-based therapy) in combination with carboplatin; as first-line treatment of metastatic breast cancer (after failure of prior anthracycline-containing adjuvant chemotherapy, unless anthracyclines were clinically contraindicated) in combination with paclitaxel; and for the treatment of non-small cell lung cancer in combination with cisplatin. For the treatment of pancreatic cancer, gemcitabine is used as a single agent [109]. It is also being investigated in other cancer and tumor types, such as advanced biliary tract carcinomas [110], bladder cancer [111], and sarcomas [112].

This metabolic inhibitor is a polar drug with low membrane permeability and oral bioavailability, and is primarily administered by intravenous infusions. However, the efficacy of gemcitabine is hindered by a number of factors. Gemcitabine is rapidly metabolized and enzymatically converted in the blood stream, liver, kidney, and even various tumor tissues to an inactive form, mainly by cytidine deaminase (CDA). Thus, it has a short plasma circulation time and elimination half-life, that is dependent on the

infusion time, age and gender of patients, and ranges from 42 to 94 min for short infusions [109]. Nucleoside transporters are required to transpose the membrane and enter cells and multiple kinases are needed to active gemcitabine to gemcitabine triphosphate (dFdCTP), the active form of this drug (Figure 9). Poor efficacy or even resistance to gemcitabine are common, due to under-expression or depletion of transporters or activating kinases [107,113].

Furthermore, similarly to other chemotherapeutic agents, treatment with gemcitabine also causes side effects. The most common (≥ 20%) adverse reactions reported for gemcitabine as a single agent are nausea/vomiting, anemia, increased alanine aminotransferase (ALT), increased aspartate aminotransferase (AST), neutropenia, increased alkaline phosphatase, proteinuria, fever, hematuria, rash, thrombocytopenia, dyspnea, and edema [109].

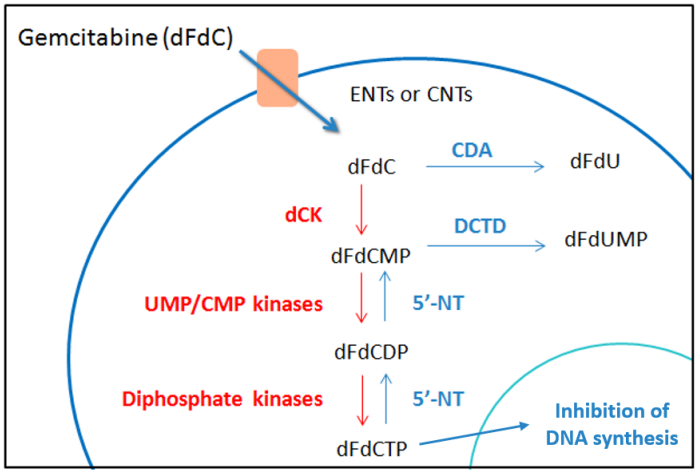

Figure 9: Mechanism of intracellular activation and deactivation of gemcitabine. Adapted from [114].

As such, in this project, prodrugs of Gem consisting of conjugates with CPPs (providing protection from metabolic deactivation, and transport and delivery) were evaluated concerning their permeability and PK properties and profile. Also, the PK of the combination of Gem or a similar antineoplastic agent, 5-FU, with repurposed drugs itraconazole, verapamil or tacrine was analyzed *in silico* to predict *in vivo* performance.

The work developed in the first part of this project has also provided the experience in the development of PBPK models, helpful for the studies carried out in the second part, regarding the application of these models to assess the optimization of antibiotic use and dosage personalization.

INFECTIONS AND ANTIBIOTIC THERAPY

Infections are a serious health threat. They are caused by infectious agents (also called pathogens) such as virus, microorganisms like bacteria, fungi, parasites, and even arthropods. The immune system is able to fight many infections, but specific medication is often needed, especially since some of these agents are becoming more and more aggressive. Additionally, severe consequences can arise from the infectious agents reaching the bloodstream and spreading to other locations, and also from sepsis, a life-threatening condition where tissues and organs are gravely affected by the own body's response to infection. This project focused on the anti-infective class of antibiotics.

The first antibiotic ever discovered was penicillin, by Alexander Fleming in 1928. Since then, and more predominantly after the 1940s, antibiotics have revolutionized the treatment of patients with severe bacterial infections, significantly reducing morbidity and mortality. However, these drugs have been overused and are currently one of the most widely, and often injudiciously, prescribed and used therapeutic drugs worldwide. This has led to a bacterial selection of resistant strains.

Nowadays, antibiotic resistance is one of the biggest public health concerns, being a major problem both in hospital environments and in outpatient situations. A report by the World Health Organization (WHO) revealed antibiotic resistance is a "*serious threat (that) is no longer a prediction for the future, it is happening right now in every region of the world and has the potential to affect anyone, of any age, in any country. Antibiotic resistance – when bacteria change so antibiotics no longer work in people who need them to treat infections – is now a major threat to public health*." [115,116].

This is a major reason supporting the importance of monitoring and optimizing antibiotics use, and also the implementation of Antibiotic Stewardship Programs (ASP). The Centers for Disease Control and Prevention (CDC) identified 7 core elements of antibiotic stewardship in 2014 and recommend that all hospitals have an ASP (Figure 10) [117]. Tracking (monitoring process measures), reporting information on antibiotic use and resistance, and education of clinicians and health care providers are 3 of these core elements. Optimizing the use of antibiotics leads to the maximization of therapeutic success and will extend the clinical lifespan of currently available antimicrobial agents, by limiting the emergence of resistance [118,119].

Figure 10: The core elements for antibiotic stewardship programs. Reproduced from [120].

Antibiotics and the need for TDM and dosage adjustment

As discussed earlier, monitoring patients and adjusting their dosing regimens can be vital to ensure their successful clinical outcome, with minimized side effects. It has been extensively demonstrated that this is crucial in the case of antibiotics, with confirmed beneficial results [121-126].

This project focused on aminoglycosides amikacin, gentamicin and tobramycin, and glycopeptide vancomycin. These antibiotics are widely used to treat severe infections, caused by Gram-negative (aminoglycosides) and Gram-positive (vancomycin) bacteria. They are also the most frequently monitored in inpatients, which can be explained by their narrow therapeutic indexes and potential to cause adverse effects, namely nephrotoxicity, particularly in prolonged treatments [127-129]. Though historically, TDM was implemented mostly to prevent toxic adverse effects, mainly for glycopeptides and aminoglycosides, the assessment of trough and peak concentrations is considered diagnostically and therapeutically important, and strongly recommended for patients using the aforementioned antibiotics. The value of TDM of these antibiotics has been demonstrated [125,126,130-138]. Although TDM has been recommended for these antibiotics, it is still not a routine clinical practice, for reasons still not systematically reviewed. Not only does this process entails costs, it is also a massive challenge particularly for intensive care units, since these patients often present altered PK and significant inter- and intra-individual pharmacokinetic (PK) variability [139].

The Clinical Chemistry Service of the Department of Pathology in *Centro Hospitalar Universitário do Porto* (CHUP) monitors inpatients receiving antibiotic therapy that includes aminoglycosides amikacin, gentamicin, and tobramycin, and glycopeptide vancomycin. The health condition and welfare of patients is supervised by a team of medical professionals, and biological samples, mainly blood, are collected and biochemically analyzed regularly. Therapeutic drug monitoring (TDM) evaluates drug concentrations and other biochemical markers (among which, in the case of these antibiotics, creatinine is of key importance to assess renal function) to ensure the appropriate dose is being administered to the patients, continuously recommending dosing adjustments to optimize clinical outcome without developing severe side effects.

Thanks to a collaboration with this service, demographic and clinical information from a pool of inpatients with serious infections receiving therapy with these antibiotics was accessed and analyzed. This data was used to study the drug disposition and PK profile of these four antibiotics (amikacin, gentamicin, tobramycin, and vancomycin) using PKPB modeling and population simulations, and to evaluate the influence of patients' biological sex, age, weight, and renal function. These PBPK models not only confirmed the impact of renal function, but also alerted to the fleetness of increasing levels of vancomycin in plasma, that can quickly reach toxic levels and cause severe adverse effects.

PART I

PART I

CHAPTER 1

Combination of Gemcitabine with Cell-Penetrating Peptides: A Pharmacokinetic Approach Using *In Silico* Tools

Abigail Ferreira, Rui Lapa, Nuno Vale

Biomolecules, **2019**, 9(11), pp. 693. DOI: 10.3390/biom9110693.

This initial work aimed at the preliminary assessment of the PK attributes of gemcitabine and derived prodrug conjugates with Cell-Penetrating Peptides (CPPs). These conjugates had been previously synthesized and evaluated for their stability, gemcitabine release and bioactivity in three cancer cell lines within the research group.

In the first approach to PBPK modeling and simulations using software package GastroPlus™, the main PK properties of these drugs were predicted and the disposition profile evaluated.

Moreover, to provide further insight on the relationship between amino acid sequences and CPPs' penetration ability, the physicochemical properties of the 20 natural amino acids were calculated to build a z-scale. Then, this z-scale was applied to a database of peptides (CPPs and non-CPPs), and quantitative structure-activity relationships (QSAR), principal component analysis (PCA), and multivariate analysis (MVA) were used to correlate peptide properties with cellular penetration power.

biomolecules

MDPI

Article

Combination of Gemcitabine with Cell-Penetrating Peptides: A Pharmacokinetic Approach Using in Silico Tools

Abigail Ferreira [1,2,*], Rui Lapa [2] and Nuno Vale [1,3,4,5]

1 Laboratory of Pharmacology, Department of Drug Sciences, Faculty of Pharmacy, University of Porto, Rua de Jorge Viterbo Ferreira, 228, 4050-313 Porto, Portugal; nuno.vale@ff.up.pt
2 LAQV/REQUIMTE, Laboratory of Applied Chemistry, Department of Chemical Sciences, Faculty of Pharmacy, University of Porto, Rua de Jorge Viterbo Ferreira, 228, 4050-313 Porto, Portugal; ruilapa@ff.up.pt
3 Institute of Molecular Pathology and Immunology of the University of Porto (IPATIMUP), Rua Júlio Amaral de Carvalho, 45, 4200-135 Porto, Portugal
4 Instituto de Investigação e Inovação em Saúde (i3S), University of Porto, Rua Alfredo Allen, 208, 4200-135 Porto, Portugal
5 Department of Molecular Pathology and Immunology, Abel Salazar Biomedical Sciences Institute (ICBAS), University of Porto, Rua de Jorge Viterbo Ferreira, 228, 4050-313 Porto, Portugal
* Correspondence: abigail.ferreira@fc.up.pt; Tel.: +351-22-042-8500

Received: 23 September 2019; Accepted: 1 November 2019; Published: 4 November 2019

Abstract: Gemcitabine is an anticancer drug used to treat a wide range of solid tumors and is a first line treatment for pancreatic cancer. Our group has previously developed novel conjugates of gemcitabine with cell-penetrating peptides (CPP), and here we report some preliminary data regarding the pharmacokinetics of gemcitabine, two gemcitabine-CPP conjugates and respective CPP gathered from GastroPlus™, and analyze these results considering our previous evaluation of gemcitabine release and conjugates' bioactivity. Additionally, seeking to shed some light on the relation between the penetration ability of CPP and their physicochemical properties, chemical descriptors for the 20 natural amino acids were calculated, a new principal property scale (z-scale) was created and CPP prediction models were developed, establishing quantitative structure-activity relationships (QSAR). The z-scores of the peptides conjugated with gemcitabine are presented and analyzed with the aforementioned data.

Keywords: gemcitabine; cell-penetrating peptides (CPP); in silico; pharmacokinetics; GastroPlus™; z-scale

1. Introduction

Gemcitabine (2′,2′-difluoro-2′-deoxycytidine, dFdC, Gem, Figure 1) is a drug considered as 'first-line treatment' for various types of solid tumors and is clinically used in the treatment of various cancers including pancreatic cancer, non-small cell lung cancer (NSCLC), bladder, ovarian, and breast cancer, as well as some blood cancers, such as non-Hodgkin's lymphoma [1–3]. Like most anticancer drugs, gemcitabine is administered intravenously. Its cellular uptake is primarily facilitated and governed by the human equilibrative nucleoside transporter 1 (hENT1) and human concentrative nucleoside transporter 3 (hCNT3) [4,5]. Inside cells, gemcitabine acts as an antimetabolite, but first needs to be activated by phosphorylation to its triphosphate form (dFdCTP) by deoxycytidine kinase (dCK) and other intracellular kinases. dFdCTP is incorporated into DNA, leading to DNA strand termination after the incorporation of one more nucleotide, and also competes with deoxycytidine triphosphate (dCTP) as an inhibitor of DNA polymerase. The incorporation of this extra nucleotide into DNA appears

to be resistant to the normal mechanisms of DNA. Moreover, gemcitabine diphosphate (dFdCdP) is a potent inhibitor of ribonucleotide reductase (RNR), resulting in depletion of deoxyribonucleotides necessary for DNA synthesis, further potentiating the effects of dFdCTP in causing cell death by apoptosis [6,7].

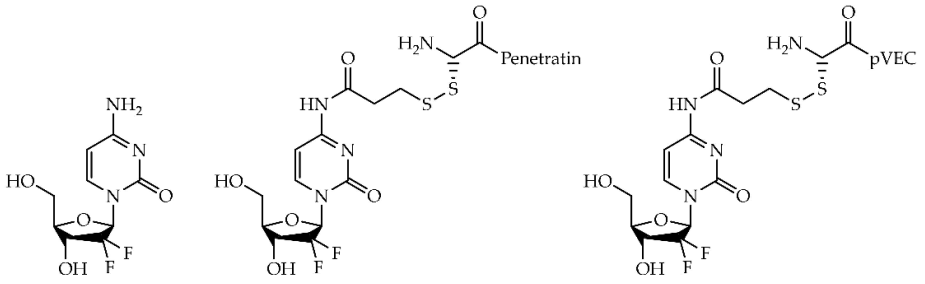

Figure 1. Chemical structures of gemcitabine and gemcitabine-CPP conjugates Gem-Cys-Pen and Gem-Cys-pVEC.

However, there are some factors hindering the full potential of gemcitabine: (a) gemcitabine may rapidly undergo deamination to its inactive uridine metabolite (2′,2′-difluorodeoxyuridine, dFdU), by cytidine deaminase (CDA), which is present at high levels in both human plasma and liver; (b) gemcitabine monophosphate (dFdCMP) is deaminated into dFdUMP by deoxycytidylate deaminase (DCTD); (c) the phosphorylated metabolites of gemcitabine are inactivated via reduction by cellular 5′-nucleotidase (5′-NT). Enzymatic conversion of gemcitabine rapidly clears it from the body [7,8]. Additionally, some tumor cells can develop resistance to gemcitabine related to nucleoside transporter deficiency [5]. As the adverse effects associated with chemotherapeutic agents remain severe, many efforts have been made to maximize therapeutic efficacy and attenuate the nocuous side manifestations. Numerous gemcitabine prodrugs have been developed to alter some of the unfavorable physicochemical properties of the drug and ideally improve its oral bioavailability.

Recently, our group has synthesized two gemcitabine-CPP conjugates (Figure 1), in an effort to both retard or prevent deamination of gemcitabine (masking its aniline moiety) and facilitate its delivery into cancer cells [9], taking advantage of the fact that all CPP are able to efficiently pass through cell membranes while being non-cytotoxic and carrying a wide variety of cargos inside cells [9,10]. CPP Penetratin (Pen, RQIKIWFQNRRMKWKK-NH_2) and pVEC (LLIILRRRIRKQAHAHSK-NH_2) were selected for conjugation with gemcitabine [9]. These are two well-known CPP and have both been reported in numerous cancer studies over the last two decades [11,12]. An additional cysteine residue (Cys) was coupled to the N-terminus of both CPP, producing Cys-Pen and Cys-pVEC, to allow the subsequent binding to parent drug. The time-dependent kinetics of gemcitabine release from hydrolysis of these new conjugates was studied in phosphate-buffered saline (PBS) at pH 7.4, 37 °C, and their biological activity was evaluated against three human tumoral cell lines: MKN-28 (human gastric cancer), Caco-2 (heterogeneous human epithelial colorectal adenocarcinoma) and HT-29 (human colon adenocarcinoma). The results were promising, revealing an increase in the anti-proliferative activity of gemcitabine in vitro upon conjugation with the CPP [9].

In this work, we used computational tools to study the pharmacokinetics (PK) of drug gemcitabine, gemcitabine-CPP conjugates and respective CPP, and to establish a possible relation between penetration potency of CPP and their physicochemical properties. The PK data was acquired using GastroPlus™; amino acid properties were calculated in Schrödinger's Maestro software; principal component analysis (PCA), multivariate analysis (MVA) and partial least square discriminant analysis (PLS-DA) were used to build CPP prediction models in SIMCA by Umetrics. GastroPlus™ is a powerful

mechanistically based simulation and modeling software for pharmaceutical research. With Advanced Compartmental Absorption and Transit (ACAT™) and Physiologically Based Pharmacokinetic (PBPK) models, it has features and capabilities to support model-based drug development in all phases of drug discovery, translational research, and clinical development. This software has been used in numerous academic studies and by pharmaceutical companies of excellence, along with the U.S. Food and Drug Administration (FDA), the Centers for Disease Control and Prevention (CDC), the National Institutes of Health (NIH), the National Cancer Institute (NCI) and the China Food and Drug Administration (CFDA).

Peptides and proteins have been the subject of considerable interest in medicine, research, and drug development due to some of their specific properties and a wide variety of applications [13,14]. In particular, CPP have the intrinsic property to efficiently deliver covalently or noncovalently bound therapeutic molecules (nucleic acids, proteins, drugs, imaging agents, etc.) into a variety of cell types and tissues in a nontoxic manner, via receptor-independent mechanisms (primarily endocytosis) [10,15,16]. Besides their ability to be uptaken by cells and act as an excellent therapeutic delivery vehicle, it has been established that CPP are generally relatively short peptides (less than 40 amino acids), have low cytotoxicity, dose-dependent efficiency, and no restriction with respect to the size or type of cargo. Additionally, CPP can enhance the water solubility of drugs [17].

The rational design and prediction of new CPP requires an understanding of the defining properties and similarities of these peptides. For example, almost every CPP sequence involves positively charged amino acids and it has also been shown that secondary structure, specifically helicity, is a key factor governing the interactions of a given CPP with cell membranes, and peptides with an α-helical region can enter cells more efficiently [18].

Theoretical and computational methods are powerful and very often useful tools to predict new CPP sequences, based on previously available experimental data and calculations of several amino acid and peptide properties. Initially, principal components analysis (PCA) and binary classification were explored for pattern recognition models [19,20]. With the determination of physicochemical properties of amino acids and peptides, quantitative structure activity relationship studies (QSAR), partial least squares (PLS) regression and multivariate analysis (MVA) can also be used as tools [21–24]. Hellberg et al. developed a tridimensional scale (z1–z3) for the 20 natural amino acids to perform quantitative structure-activity relationship (QSAR) of peptides, using 29 physicochemical properties [23]. This method and these scales have since been extended to include more amino acids and descriptive properties in the search for new CPP sequences.

In this project, we followed the same methodology and selected 12 physicochemical properties of the 20 natural amino acids to extract 3 z-scores. This tridimensional z-scale was used to build several CPP prediction models and to discuss the properties of amino acids and peptides that seem to play an important role in the penetration ability of these peptide sequences. Although it is possible to create models that allow for amino acid position-based optimization, the models created here were to predict a binary classification: CPP or non-CPP, using various calculated global peptide descriptors. This has been applied in multiple previous studies regarding peptide modeling with varying successful results [21,25].

2. Methods

2.1. Amino Acids–Structure, Physicochemical Properties and Creation of a Z-Scale

The structures of the 20 natural amino acids were drawn in Maestro (version 10.4, Schrödinger, LLC, New York, NY, USA). All amino acids were capped using C-terminal amidation and *N*-terminal acetylation to better simulate an amino acid as part of a peptide chain, linked through amide bonds. Maestro's LigPrep tool was used to simultaneously minimize the structures and generate possible charge states at pH 7.0 (histidine was only included in its charged, deprotonated state).

Physicochemical properties of the amino acids were calculated by Maestro's QikProp tool. This data was imported into SIMCA (version 13.0 ed, Umetrics AB, Umeå, Sweden) where it was scaled and centered. After principal component analysis (PCA) of the data, 3 principal components were extracted. These scores (designated z1, z2 and z3) constitute a z-scale used to quantitatively describe each amino acid and the peptide sequences. The 12 selected properties for PCA were: number of rotatable bonds (#rotor), molecular weight (mol MW), volume, solvent accessible surface area (SASA), number of hydrogen bond donors (donorHB), number of hydrogen bond acceptors (accptHB), globularity (glob), octanol/water partition coefficient (QPlogPo/w), polar surface area (PSA), net charge (Tot Q), and ratios FISA/SASA (FISA is the hydrophilic component of SASA) and FOSA/SASA (FOSA is the hydrophobic component of SASA).

In general, the relation of the PCs with the physicochemical properties suggests the first PC (z1) is mainly related to properties describing size and shape properties, such as volume, SASA, globularity and molecular weight; the second PC (z2) seems to be more related to the polarity of the amino acids and the descriptors QPlogPo/w, accptHB, donorHB, FISA/SASA and PSA; finally, z3 seems to be predominantly influenced by electronic properties (in this case described by charge).

2.2. *Peptides*

2.2.1. Datasets

Peptide sequences were extracted from the different CellPPD (Designing of Cell Penetrating Peptides) databases, available from http://crdd.osdd.net/raghava/cellppd/dataset.php. This provided a main dataset of experimentally validated cell-penetrating (900 CPP) and both validated and randomly generated non-active peptides (1148 non-CPP) after removal of duplicates.

The lack of experimentally validated non-CPP is a known problem [26,27] and creating balanced datasets, which has been demonstrated to be very crucial in modeling [26,28,29], is therefore a major problem. To try to overcome this issue, the main dataset was reduced to contain only 900 non-CPP, the same number of CPP present. The deleted 248 peptides were selected randomly.

To study the influence of terminal chains, all peptides were truncated to originate 6 other datasets. First, the peptides were divided in half, generating an N-terminal and a C-terminal dataset. In the cases of peptides with an odd number of amino acids, the N-terminal was the longer chain. Then, five residues were taken from each terminal, originating the "first 5AA" and "last 5AA" datasets. Finally, the same process was used, but to create "first 10AA" and "last 10AA" datasets.

2.2.2. Peptide Descriptors

Every peptide is described as a sequence of the z-scores of their amino acids. The mean of the z-scores across the entire sequence was calculated (mean z1, mean z2 and mean z3). The absolute difference between terminals was calculated (|Nt − Ct|), as well as the absolute difference between the first and last 5 or 10 amino acids. Using an extension of the Eisenberg's equation where the hydrophilicity descriptor of the original equation was replaced with the generated z-scale values (Equation (1)), as established by Maccari et al. [30], the z-scale moment was calculated for each dataset.

Equation (1): Original Eisenberg's equation; N: number of amino acids in the peptide sequence; n: order number of the specific amino acid examined; H: experimental hydrophilicity of a specific amino acid; δ: angle between two adjacent amino acids, which in the case of an alpha helical structure is defined as 100°.

$$\mu = \sqrt{\left(\sum_{n=1}^{N} H_n \cdot \sin(\delta n)\right)^2 + \left(\sum_{n=1}^{N} H_n \cdot \cos(\delta n)\right)^2} \quad (1)$$

Some properties of the peptides were calculated and applied as descriptors to the models. These properties included the peptides' steric bulk (calculated as the mean number of non-hydrogen atoms in the amino acid side chains), the mean net donating hydrogen bonds (calculated as the accepted

hydrogen bonds subtracted from the donated hydrogen bonds), the total charge of the peptide sequences as well as the mean net charge, which takes into consideration the total number of amino acids in each sequence. Additionally, the total number of Arg, His, Lys, Asp and Glu residues, and the total number and ratio of positively and negatively charged amino acids were also considered when building the prediction models.

2.3. Prediction Model Generation and Optimization

Using SIMCA and Partial Least Square Discriminant Analysis (PLS-DA), numerous prediction models were generated by varying the included properties and descriptors.

To be able to perform external validation of the built models, a test set composed of peptides not included in the generation of the models is needed. So, 50% of the main dataset peptides were randomly extracted and selected as the test set.

Internal classification predictive value, Q^2, and fit measurements were calculated and analyzed in the optimization process. Four performance measurements to access the predictability of the different models were calculated based on the number of true positives (TP), true negatives (TN), false positives (FP) and false negatives (FN). These measurements were sensitivity, specificity, accuracy and Matthew's correlation coefficient (MCC), a quality measurement for binary classifications (Equations (2) to (5)).

Equations (2) to (5): Sensitivity, representing the percentage of correctly predicted positive sequences; specificity, representing the percentage of correctly predicted negative sequences; accuracy, representing the percentage of correctly predicted sequences overall; and Matthew's correlation coefficient (MCC), a quality measurement for binary classifications.

$$(\text{Sensitivity}) : \frac{TP}{TP + FN} \times 100 \quad (2)$$

$$(\text{Specificity}) : \frac{TN}{TN + FP} \times 100 \quad (3)$$

$$(\text{Accuracy}) : \frac{TP + TN}{TP + FN + TN + FP} \times 100 \quad (4)$$

$$(\text{MCC}) : \frac{(TP \times TN) - (FP \times FN)}{\sqrt{(TP + FP) \times (TP + FN) \times (TN + FP) \times (TN + FN)}} \times 100 \quad (5)$$

2.4. Pharmacokinetic Assessment of Gemcitabine, Cpp and Gemcitabine-Cpp Conjugates

The pharmacokinetic study of gemcitabine, CPP and conjugates was performed in GastroPlus™ (version 9.5, Simulations Plus, Inc., Lancaster, California, USA), a mechanistically based simulation and modeling software for pharmaceutical research. GastroPlus™ builds physiologically based pharmacokinetic (PBPK) models and can run simulations based on a drug's structure and collected data to predict the most important parameters in pharmacokinetics (PK), such as the maximum concentration reached in plasma and liver, time necessary to reach such concentrations, binding to plasma proteins, fraction absorbed and bioavailability. It also draws a graphical representation of plasmatic concentration over time and calculates the area under the curve (AUC). GastroPlus™ not only simulates human PK, but can also be used to study mice, rats, monkeys, beagles, cats, rabbits and minipigs, based on preinstalled human and animal physiological parameters. This software has been used to successfully and accurately predict PK profiles, an important tool in early on drug discovery [31].

All the simulations in the scope of this project were performed to predict the PK for 24 h after intravenous administration of 1250 mg (1 h perfusion), using the Compartmental model of GastroPlus™. The software did not provide an estimated clearance for any of the molecules studied here, thus, gemcitabine's clearance value of 168 L/h was input into the software, according to this drug's FDA label and information deposited on DrugBank [32–34].

The general workflow of PBPK modeling has been described in publications and tutorials [35–37]. The preliminary model in this case was based on the physicochemical data from ADMET Predictor™ module of GastroPlus™, using a standard compartmental PBPK model.

3. Results and Discussion

The choice of amino acids and their combination in a peptide sequence when designing new CPP are fundamental. Properties such as size, polarity and charge vary greatly within the 20 natural amino acids, and to better understand how these properties correlate with CPP penetration ability, 12 physicochemical properties were selected and PCA was performed to extract 3 principal components (PCs), forming a tridimensional z-scale, presented in Table 1. The relation of the PCs with the physicochemical properties can be seen in Figure 2.

Table 1. Extracted z-scores for the 20 natural amino acids and their physicochemical properties.

Amino Acid	z1	z2	z3	Amino Acid Properties
Ala (A)	−3.4535	−0.8314	0.8710	Non-polar, aliphatic
Arg (R)	5.9227	−0.7707	1.9428	Positively charged
Asn (N)	0.4104	−4.0436	−0.5900	Polar
Asp (D)	0.1502	−2.2592	−1.7815	Negatively charged
Cys (C)	−1.8132	0.7809	−0.0062	Polar
Gln (Q)	2.5410	−2.5906	0.0520	Polar
Glu (E)	1.4594	−1.6961	−1.7366	Negatively charged
Gly (G)	−3.2706	−1.7938	0.5308	Non-polar, aliphatic
His (H)	1.4195	0.2462	0.6037	Positively charged
Ile (I)	−1.3560	1.8903	0.6660	Non-polar, aliphatic
Leu (L)	−1.5348	1.8836	0.7144	Non-polar, aliphatic
Lys (K)	2.7685	0.6670	2.5607	Positively charged
Met (M)	−0.0676	2.3168	0.4266	Non-polar, aliphatic
Phe (F)	−0.0247	2.9087	−1.2433	Aromatic
Pro (P)	−3.3838	−0.4244	−0.0096	Polar
Ser (S)	−1.6519	−1.4774	0.3484	Polar
Thr (T)	−1.3364	−0.5600	0.3103	Polar
Trp (W)	1.7531	3.3182	−1.7406	Aromatic
Tyr (Y)	2.0819	1.7453	−1.1132	Aromatic
Val (V)	−2.9262	0.7588	0.6271	Non-polar, aliphatic

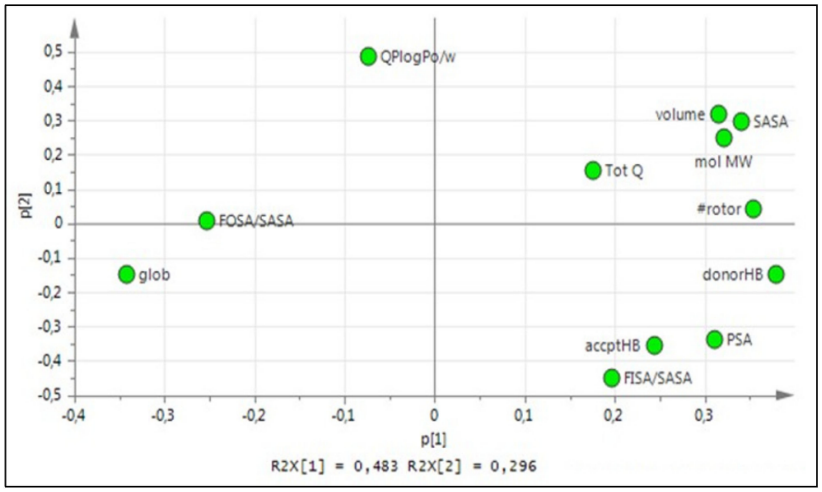

Figure 2. Loading plot explaining PC1 vs. PC2 for the 20 natural amino acids z-scale PCA.

Every peptide was described as a sequence of the z-scores of their amino acids and peptide descriptors were calculated for every peptide in the main dataset. PCA was performed to extract 3 PCs for each peptide. Several prediction models were generated by varying the included properties and descriptors, and Pen, Cys-Pen, pVEC and Cys-pVEC were predicted as CPP; their z-scores are presented in Table 2. All the models created in this project showed a decent ability to predict CPP, with an average of 79% sensitivity, 80% specificity, 81% accuracy, 61% MCC and 0.406 Q^2.

These results show Pen and Cys-Pen have z1 scores 2-fold higher than the z1 scores calculated for pVEC and Cys-pVEC. The same difference was observed for the z2 scores. However, regarding the third PC, pVEC and Cys-pVEC z3 scores are higher than the ones calculated for Pen and Cys-Pen. Adding a Cys residue to the original CPP sequences seems to have had a bigger impact on the PC related to size and shape, z1, where it was possible to differentiate the original CPP from the modified Cys-CPP, whereas z2 and z3 scores are very similar for the CPP and Cys-CPP.

As previously mentioned, charged has long been appointed as one of the most important features/characteristics of CPP. In Table 3, the number of charged amino acids and ratio of hydrophilic residues to total number of residues are presented. The difference in the content of positively charged amino acids in Pen and pVEC can explain the higher z3 scores calculated for pVEC (and Cys-pVEC).

With respect to the in vitro results previously observed by our group, there was a significant improvement in the biological activity of gemcitabine upon conjugation of the drug with either CPP, with Gem-Cys-pVEC conjugate showing the best results in MKN-28 and HT-29 cells (Table 4).

In Table 5 are the input data used in GastroPlus™ to simulate plasma concentration. Concentration curves were then compared to that of parental drug (GEMZAR®, gemcitabine for injection) and the approximation between values has been achieved.

Despite the promising in vitro bioactivity, favorable pharmacokinetic properties are required for the success of therapies in vivo. According to the simulations carried out in GastroPlus™, conjugates' bioavailability is ensured and plasma concentration should reach therapeutic levels (Table 6).

Table 2. Extracted z-scores for the studied peptides.

Peptide	z1 (Size and Shape)	z2 (Polarity)	z3 (Charge)
Pen	2.3233	0.4802	0.6731
Cys-Pen	2.0865	0.5016	0.6364
pVEC	1.0880	0.2586	1.0435
Cys-pVEC	0.9411	0.2895	0.9911

Table 3. Electronic and hydrophilic properties of the studied CPP.

	Sequence	#AA[1]	#Arg[1]	#Lys[1]	#His[1]	HR[2] (%)	Pred.[3]	Exp.[4]	Ref.
Pen	RQIKIWFQNRRMKWKK	16	3	4	0	63	+	+	[38]
Cys-Pen	CRQIKIWFQNRRMKWKK	17	3	4	0	59	+	N.D.	
pVEC	LLIILRRRIRKQAHAHSK	18	4	2	2	44	+	+	[39]
Cys-pVEC	CLLIILRRRIRKQAHAHSK	19	4	2	2	42	+	N.D.	

[1] # indicates number of total or indicated amino acid residues; [2] hydrophilic ratio (calculated at www.bachem.com/service-support/peptide-calculator); [3] predicted penetration ability; [4] experimentally verified penetration ability. N.D.: not determined.

Table 4. Biological activity and half-life of the studied molecules.

Compound	Caco-2 IC50/μM [9]	MKN-28 IC50/μM [9]	HT-29 IC50/μM [9]	$t_{1/2}$ (PBS, 37 °C)/h
Gem	>100	>100	>100	>2 [40]
Cys-Pen	>100	>100	>100	N.D.
Cys-pVEC	>100	>100	>100	N.D.
Gem-Cys-Pen	67.13 ± 2.92	46.99 ± 5.91	47.26 ± 11.3	230 [9]
Gem-Cys-pVEC	>100	20.68 ± 6.81	45.20 ± 1.04	42 [9]

N.D.: not determined.

Table 5. Input data used in GastroPlus™ to simulate plasma concentration of GEMZAR®.

Parameter	Value	Reference/Data Source
Solubility	5.01 mg/mL at pH 7.92	ADMET Predictor™
pKa	3.54 (DrugBank[a]: 3.6)	ADMET Predictor™
LogP	−1.32 (DrugBank[a]: 1.4)	ADMET Predictor™
Dose	1250 mg	FDA (Ref. ID: 3503046)[b]
Effective permeability, P_{eff}	0.59 cm/s × 10^{-4}	Caco-2 (Nuno Vale Lab)
Blood/plasma ratio	1.12	ADMET Predictor™
Clearance	168 L/h	[41]
Physiology	Human, fasting conditions	FDA (Ref. ID: 3503046)[b]
Body weight (Kg)	70	FDA (Ref. ID: 3503046)[b]

[a] From Reference 33; [b] From highlights of prescribing information [42].

Table 6. Predicted pharmacokinetic properties of studied molecules determined with GastroPlus™.

Compound	F_{up} [1] (%)	B/P ratio[2]	V_c [3]	F (%) [4]	Fa (%) [5]	AUC 0-inf [6]	AUC 0-t [7]	C_{max} [8]	$C_{max\ liver}$ [9]	Sol. [10]
Gem	84.61	1.12	1.45	99.949	99.949	7.4368	7.4367	5.9505	5.8709	5.01
Pen	22.50	0.93	0.14	99.999	99.999	7.4404	7.4404	7.4403	7.4398	1.83
Cys-Pen	26.72	0.92	0.11	99.999	99.999	7.4404	7.4404	7.4401	7.4394	4.66
Gem-Cys-Pen	12.91	0.98	0.17	100.000	100.000	7.4405	7.4404	7.4404	7.4403	1.26
pVEC	13.35	1.13	0.16	100.000	100.000	7.4405	7.4405	7.4404	7.4403	28.94
Cys-pVEC	15.53	1.12	0.11	100.000	100.000	7.4405	7.4404	7.4404	7.4403	17.34
Gem-Cys-pVEC	42.89	1.20	0.18	99.998	99.999	7.4404	7.4403	7.4400	7.4393	5.39

[1] percentage of drug that is not bound to plasma proteins (100 = fully unbound); [2] blood/plasma concentration ratio (ratio of concentrations of the drug in whole blood and plasma); [3] distribution volume, in L/kg; [4] bioavailability; [5] fraction absorbed as a percent of the dose (crossing the lumen and entering enterocytes); [6] area under the plasma concentration–time curve, in µg-h/mL, extrapolated to infinity; [7] area under the plasma concentration–time curve, in µg-h/mL, for the time of the simulation; [8] maximum plasma concentration reached in the central compartment, in µg/mL; [9] maximum concentration reached in the liver, in µg/mL; [10] solubility in mg/mL.

The calculated AUC for the conjugates was comparable to the AUC calculated for gemcitabine, yet, estimated C_{max} was higher for all peptides and conjugates analyzed compared to gemcitabine alone (Figure 3). Gem- Cys-pVEC conjugate binds less extensively to plasma proteins (>F_{up}, 42.89%). Considering this conjugate showed the best bioactivity in MKN-28 and HT-29 cells, and released gemcitabine in PBS faster than Gem-Cys-Pen conjugate (50% over 42 h, versus 9.6 days for Gem-Cys-Pen [8]), we believe Gem-Cys-pVEC conjugate has the best suitable profile for drug delivery. Binding to plasma proteins acts as a protection from quick biotransformation and degradation due to the action of plasma circulating enzymes [40] (such as proteases and CDA). This increases circulation time and can also be advantageous to biodistribution. However, it is important that there is a significant percentage/amount of the drug/compound free in circulation so that it can reach its target and exert its pharmacologic action. Differences in V_c of gemcitabine and the conjugates can be explained by their different affinity to bind to plasma proteins.

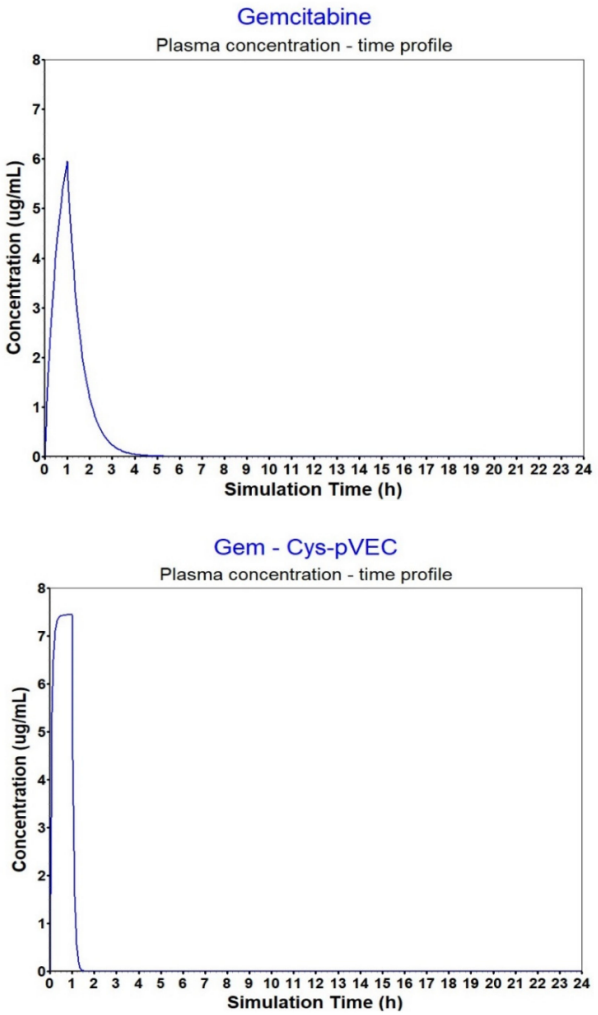

Figure 3. Plasma concentration–time profiles for gemcitabine and the Gem-Cys-pVEC conjugate after IV infusion (1 h).

4. Conclusions

The main goal of this study was to combine the in vitro and in silico approaches to highlight the potential clinical applications of CPP in drug delivery. The development of an amino acid z-scale and the calculation of peptide descriptors was important to understand some factors impacting penetration ability. We believe this method is of great value for pharmaceutical design using CPP for drug delivery. Given the results of this work, we intend to continue studying this approach and these conjugates, and to carry out in vivo experiments, considering Gem-Cys-pVEC our therapeutic lead as it showed the most promising results regarding in silico calculated properties, pharmacokinetic potential and in vitro bioactivity.

Author Contributions: Conceptualization, A.F. and N.V.; methodology, A.F. and N.V.; software, A.F., R.L. and N.V.; validation, R.L. and N.V.; formal analysis, A.F., R.L. and N.V.; investigation, A.F. and N.V.; resources, R.L. and N.V.; writing—original draft preparation, A.F.; writing—review and editing, A.F., R.L and N.V.; supervision, R.L. and N.V.; project administration, N.V.

Funding: This work has been financed by Fundo Europeu de Desenvolvimento Regional (FEDER) funds through the COMPETE 2020—Operational Programme for Competitiveness and Internationalisation (POCI) and Portugal 2020, and Portuguese funds through Fundação para a Ciência e a Tecnologia (FCT, Portugal), in the framework of the project "Institute for Research and Innovation in Health Sciences" (POCI-01-0145-FEDER-007274), and through grant UID/QUI/50006/2019 (LAQV-REQUIMTE). NV also acknowledges support from FCT and FEDER (European Union), award number IF/00092/2014/CP1255/CT0004. AF thanks FCT for a doctoral fellowship (PD/BD/135120/2017).

Acknowledgments: NV thanks FCT for the IF position and the Fundação Manuel António da Mota (FMAM, Porto, Portugal) and Pfizer (Portugal) for supporting the Nuno Vale research group. The contents of this article are solely the responsibility of the authors and do not necessarily represent the official views of FCT, FMAM or Pfizer. The authors thank Professor Christian Sköld (BMC, Uppsala University) for providing access to his Lab and assisting in the development of the CPP prediction models, as well as Professor Anja Sandström (BMC, Uppsala University) and Doctor Rebecca Fransson (AstraZeneca) for scientific support and collaboration.

Conflicts of Interest: The authors declare no conflict of interest.

References

1. Rybka, J.; Jurczak, W.; Giza, A.; Paszkiewicz-Kozik, E.; Kumiega, B.; Drozd-Sokolowska, J.; Butrym, A.; Kuliczkowski, K.; Wrobel, T. Gemcitabine-Based Treatment in Poor-Prognosis Patients with Relapsed and Refractory Hodgkin Lymphoma and Non-Hodgkin Lymphoma–a Multicenter Polish Experience. *Adv. Clin. Exp. Med.* **2015**, *24*, 783–789. [CrossRef] [PubMed]
2. Wong, A.; Soo, R.A.; Yong, W.P.; Innocenti, F. Clinical pharmacology and pharmacogenetics of gemcitabine. *Drug Metab. Rev.* **2009**, *41*, 77–88. [CrossRef] [PubMed]
3. Mini, E.; Nobili, S.; Caciagli, B.; Landini, I.; Mazzei, T. Cellular pharmacology of gemcitabine. *Ann. Oncol.* **2006**, *17*, 7–12. [CrossRef] [PubMed]
4. Ciccolini, J.; Mercier, C.; Dahan, L.; Andre, N. Integrating pharmacogenetics into gemcitabine dosing–time for a change? *Nat. Rev. Clin. Oncol.* **2011**, *8*, 439–444. [CrossRef] [PubMed]
5. Marechal, R.; Mackey, J.R.; Lai, R.; Demetter, P.; Peeters, M.; Polus, M.; Cass, C.E.; Young, J.; Salmon, I.; Deviere, J.; et al. Human equilibrative nucleoside transporter 1 and human concentrative nucleoside transporter 3 predict survival after adjuvant gemcitabine therapy in resected pancreatic adenocarcinoma. *Clin. Cancer. Res.* **2009**, *15*, 2913–2919. [CrossRef] [PubMed]
6. Huang, P.; Chubb, S.; Hertel, L.W.; Grindey, G.B.; Plunkett, W. Action of 2′,2′-difluorodeoxycytidine on DNA synthesis. *Cancer Res.* **1991**, *51*, 6110–6117. [PubMed]
7. Alvarellos, M.L.; Lamba, J.; Sangkuhl, K.; Thorn, C.F.; Wang, L.; Klein, D.J.; Altman, R.B.; Klein, T.E. PharmGKB summary: Gemcitabine pathway. *Pharm. Genom.* **2014**, *24*, 564. [CrossRef] [PubMed]
8. Kroep, J.; Van Moorsel, C.; Veerman, G.; Voorn, D.; Schultz, R.; Worzalla, J.; Tanzer, L.; Merriman, R.; Pinedo, H.; Peters, G. *Role of Deoxycytidine Kinase (dCK), Thymidine Kinase 2 (TK2), and Deoxycytidine Deaminase (dCDA) in the Antitumor Activity of Gemcitabine (dFdC). Purine and Pyrimidine Metabolism in Man Ix*; Springer: Boston, MA, USA, 1998; pp. 657–660. [CrossRef]

9. Vale, N.; Ferreira, A.; Fernandes, I.; Alves, C.; Araujo, M.J.; Mateus, N.; Gomes, P. Gemcitabine anti-proliferative activity significantly enhanced upon conjugation with cell-penetrating peptides. *Bioorg. Med. Chem. Lett.* **2017**, *27*, 2898–2901. [CrossRef]
10. Copolovici, D.M.; Langel, K.; Eriste, E.; Langel, U. Cell-penetrating peptides: Design, synthesis, and applications. *ACS Nano* **2014**, *8*, 1972–1994. [CrossRef]
11. Nan, Y.H.; Park, I.S.; Hahm, K.S.; Shin, S.Y. Antimicrobial activity, bactericidal mechanism and LPS-neutralizing activity of the cell-penetrating peptide pVEC and its analogs. *J. Pept. Sci.* **2011**, *17*, 812–817. [CrossRef]
12. Liu, C.; Tai, L.; Zhang, W.; Wei, G.; Pan, W.; Lu, W. Penetratin, a potentially powerful absorption enhancer for noninvasive intraocular drug delivery. *Mol Pharm* **2014**, *11*, 1218–1227. [CrossRef] [PubMed]
13. Reissmann, S. Cell penetration: Scope and limitations by the application of cell-penetrating peptides. *J. Pept. Sci.* **2014**, *20*, 760–784. [CrossRef] [PubMed]
14. Silva, S.; Almeida, A.J.; Vale, N. Combination of Cell-Penetrating Peptides with Nanoparticles for Therapeutic Application: A Review. *Biomolecules* **2019**, *9*, 22. [CrossRef] [PubMed]
15. Wang, F.; Wang, Y.; Zhang, X.; Zhang, W.; Guo, S.; Jin, F. Recent progress of cell-penetrating peptides as new carriers for intracellular cargo delivery. *J. Control. Release* **2014**, *174*, 126–136. [CrossRef]
16. Regberg, J.; Srimanee, A.; Langel, U. Applications of cell-penetrating peptides for tumor targeting and future cancer therapies. *Pharmaceuticals (Basel)* **2012**, *5*, 991–1007. [CrossRef]
17. Stewart, K.M.; Horton, K.L.; Kelley, S.O. Cell-penetrating peptides as delivery vehicles for biology and medicine. *Org. Biomol. Chem.* **2008**, *6*, 2242–2255. [CrossRef]
18. Tang, H.; Yin, L.; Kim, K.H.; Cheng, J. Helical Poly(arginine) Mimics with Superior Cell-Penetrating and Molecular Transporting Properties. *Chem. Sci.* **2013**, *4*, 3839–3844. [CrossRef]
19. Wold, S. Pattern recognition by means of disjoint principal components models. *Pattern Recognit* **1976**, *8*, 127–139. [CrossRef]
20. Kirschner, G.L.; Kowalski, B.R. The application of pattern recognition to drug design. *Drug Design* **1978**, *8*, 73–131.
21. Hällbrink, M.; Kilk, K.; Elmquist, A.; Lundberg, P.; Lindgren, M.; Jiang, Y.; Pooga, M.; Soomets, U.; Langel, Ü. Prediction of cell-penetrating peptides. *Int. J. Pept. Res. Ther.* **2005**, *11*, 249–259. [CrossRef]
22. Sandberg, M.; Eriksson, L.; Jonsson, J.; Sjostrom, M.; Wold, S. New chemical descriptors relevant for the design of biologically active peptides. A multivariate characterization of 87 amino acids. *J. Med. Chem.* **1998**, *41*, 2481–2491. [CrossRef] [PubMed]
23. Hellberg, S.; Sjostrom, M.; Skagerberg, B.; Wold, S. Peptide quantitative structure-activity relationships, a multivariate approach. *J. Med. Chem.* **1987**, *30*, 1126–1135. [CrossRef] [PubMed]
24. Jonsson, J.; Norberg, T.; Carlsson, L.; Gustafsson, C.; Wold, S. Quantitative sequence-activity models (QSAM)—tools for sequence design. *Nucleic Acids Res.* **1993**, *21*, 733–739. [CrossRef] [PubMed]
25. Hansen, M.; Kilk, K.; Langel, U. Predicting cell-penetrating peptides. *Adv Drug Deliv Rev* **2008**, *60*, 572–579. [CrossRef] [PubMed]
26. Gautam, A.; Chaudhary, K.; Kumar, R.; Sharma, A.; Kapoor, P.; Tyagi, A.; Open Source Drug Discovery Consortium; Raghava, G.P. In silico approaches for designing highly effective cell penetrating peptides. *J. Transl. Med.* **2013**, *11*, 74. [CrossRef]
27. Lata, S.; Sharma, B.K.; Raghava, G.P. Analysis and prediction of antibacterial peptides. *BMC Bioinformatics* **2007**, *8*, 263. [CrossRef]
28. Sanders, W.S.; Johnston, C.I.; Bridges, S.M.; Burgess, S.C.; Willeford, K.O. Prediction of cell penetrating peptides by support vector machines. *PLoS Comput. Biol.* **2011**, *7*, e1002101. [CrossRef]
29. Camacho, F.L.; Torres, R.; PolláN, R.R. *Classification of Antimicrobial Peptides with Imbalanced Datasets. Proceedings of 11th International Symposium on Medical Information Processing and Analysis, Cuenca, Ecuador, 17–19 November 2015*; Eduardo, R., Natasha, L., Juan, D.G.-A., Jorge, B., Eds.; SPIE—International Society For Optics and Photonics: Bellingham, Washington, DC, USA, 2015; p. 96810T.
30. Maccari, G.; Di Luca, M.; Nifosi, R.; Cardarelli, F.; Signore, G.; Boccardi, C.; Bifone, A. Antimicrobial peptides design by evolutionary multiobjective optimization. *PLoS Comput. Biol.* **2013**, *9*, e1003212. [CrossRef]
31. Hosea, N.A.; Jones, H.M. Predicting pharmacokinetic profiles using in silico derived parameters. *Mol Pharm* **2013**, *10*, 1207–1215. [CrossRef]

32. GEMZAR®. (Gemcitabine HCl) for injection; FDA label. Available online: https://www.accessdata.fda.gov/drugsatfda_docs/label/2011/020509s069lbl.pdf (accessed on 15 March 2019).
33. Gemcitabine on DrugBank Database. Available online: https://www.drugbank.ca/drugs/DB00441 (accessed on 15 March 2019).
34. Wishart, D.S.; Feunang, Y.D.; Guo, A.C.; Lo, E.J.; Marcu, A.; Grant, J.R.; Sajed, T.; Johnson, D.; Li, C.; Sayeeda, Z.; et al. DrugBank 5.0: A major update to the DrugBank database for 2018. *Nucleic Acids Res.* **2018**, *46*, D1074–D1082. [CrossRef]
35. Thelen, K.; Coboeken, K.; Willmann, S.; Burghaus, R.; Dressman, J.B.; Lippert, J. Evolution of a detailed physiological model to simulate the gastrointestinal transit and absorption process in humans, part 1: Oral solutions. *J. Pharm. Sci.* **2011**, *100*, 5324–5345. [CrossRef] [PubMed]
36. Thelen, K.; Coboeken, K.; Willmann, S.; Dressman, J.B.; Lippert, J. Evolution of a detailed physiological model to simulate the gastrointestinal transit and absorption process in humans, part II: Extension to describe performance of solid dosage forms. *J. Pharm. Sci.* **2012**, *101*, 1267–1280. [CrossRef] [PubMed]
37. Parrott, N.J.; Yu, L.J.; Takano, R.; Nakamura, M.; Morcos, P.N. Physiologically Based Absorption Modeling to Explore the Impact of Food and Gastric pH Changes on the Pharmacokinetics of Alectinib. *AAPS J.* **2016**, *18*, 1464–1474. [CrossRef] [PubMed]
38. Derossi, D.; Calvet, S.; Trembleau, A.; Brunissen, A.; Chassaing, G.; Prochiantz, A. Cell internalization of the third helix of the Antennapedia homeodomain is receptor-independent. *J. Biol. Chem.* **1996**, *271*, 18188–18193. [CrossRef]
39. Elmquist, A.; Lindgren, M.; Bartfai, T.; Langel, U. VE-cadherin-derived cell-penetrating peptide, pVEC, with carrier functions. *Exp. Cell Res.* **2001**, *269*, 237–244. [CrossRef]
40. Tsume, Y.; Drelich, A.J.; Smith, D.E.; Amidon, G.L. Potential Development of Tumor-Targeted Oral Anti-Cancer Prodrugs: Amino Acid and Dipeptide Monoester Prodrugs of Gemcitabine. *Molecules* **2017**, *22*, 1322. [CrossRef]
41. Peters, G.J.; Clavel, M.; Noordhuis, P.; Geyssen, G.J.; Laan, A.C.; Guastalla, J.; Edzes, H.T.; Vermorken, J.B. Clinical phase I and pharmacology study of gemcitabine (2′, 2′-difluorodeoxycytidine) administered in a two-weekly schedule. *J. Chemother.* **2007**, *19*, 212–221. [CrossRef]
42. Available online: https://www.accessdata.fda.gov/drugsatfda_docs/label/2014/020509s077lbl.pdf (accessed on 15 March 2019).

CHAPTER 2

Permeability evaluation of gemcitabine-CPP6 conjugates in Caco-2 cells

Abigail Ferreira, Sara Moreira, Rui Lapa, Nuno Vale

ADMET and DMPK, **2021**, 9(1), pp. 41-48. DOI: 10.5599/admet.882

As part of the efforts to study and further understand some of the mechanisms underlying the improved activity of conjugates of CPPs with conventional anticancer drugs, the absorption and permeability of three of these conjugates was evaluated using the *in vitro* standard model, a monolayer of human colon carcinoma cells, Caco-2. These three cell-penetrating hexapeptides (CPP6) conjugates with Gem were previously developed by this research group, and their bioactivity assessed in different cell lines.

In this work, the transport of Gem-CCP6 conjugates across a monolayer of Caco-2 cells was analyzed and compared to that of isolated gemcitabine and the respective CPP6. The Gem-CPP6-2 conjugate and respective CPP6-2 (KLPVMW) revealed the highest permeability, crossing the monolayer of Caco-2 cells to a greater extent.

ADMET & DMPK 9(1) (2021) 41-48; doi: https://dx.doi.org/10.5599/admet.882

ADMET

Open Access : ISSN : 1848-7718

http://www.pub.iapchem.org/ojs/index.php/admet/index

Original scientific paper

Permeability evaluation of gemcitabine-CPP6 conjugates in Caco-2 cells

Abigail Ferreira[1,2], Sara Moreira[1,3], Rui Lapa[2] and Nuno Vale[1,4*]

[1] *OncoPharma Research Group, Center for Health Technology and Services Research (CINTESIS), Rua Dr. Plácido da Costa, 4200-450 Porto, Portugal*
[2] *LAQV/REQUIMTE, Laboratory of Applied Chemistry, Department of Chemical Sciences, Faculty of Pharmacy, University of Porto, Rua de Jorge Viterbo Ferreira, 228, 4050-313 Porto, Portugal*
[3] *Faculty of Sciences, University of Porto, Rua do Campo Alegre, 687, 4169-007 Porto, Portugal*
[4] *Faculty of Medicine, University of Porto, Al. Prof. Hernâni Monteiro, 4200-319 Porto, Portugal*

*Corresponding Author: E-mail: nunovale@med.up.pt; Tel.: +351-225513600; Fax: +351-225513601

Received: July 04, 2020; Revised: October 13, 2020; Published: October 26, 2020

Abstract

Cancer is one of the most alarming diseases due to its high mortality and still increasing incidence rate. Currently available treatments for this condition present several shortcomings and new options are continuously being developed and evaluated, aiming at increasing the overall treatment efficiency and reducing associated adverse side effects. Gemcitabine has proven activity and is used in chemotherapy. However, its therapeutic efficiency is limited by its low bioavailability as a result of rapid enzymatic inactivation. Additionally, tumor cells often develop drug resistance after initial tumor regression related to transporter deficiency. We have previously developed three gemcitabine conjugates with cell-penetrating hexapeptides (CPP6) to facilitate intracellular delivery of this drug while also preventing enzymatic deamination. The bioactivity of these new prodrugs was evaluated in different cell lines and showed promising results. Here, we assessed the absorption and permeability across Caco-2 monolayers of these conjugates in comparison with gemcitabine and the respective isolated cell-penetrating peptides (CPPs). CPP6-2 (KLPVMW) and respective Gem-CPP6-2 conjugate showed the highest permeability in Caco-2 cells.

Keywords

Cell-Penetrating Peptides; Permeability; Solubility; Caco-2; DMPK.

Introduction

Cancer is the second leading cause of death worldwide. There were 18 million new cases and 9.6 million cancer related deaths in 2018. Globally, about one in six deaths is due to cancer. Lung and prostate cancers are the most prevalent in men, while breast and colorectum cancers affect women the most [1]. Drug resistance and overall treatment inefficacy are responsible for the high mortality of this multifactorial disease. Difficulty in recognizing altered cells and distinguishing them from normal cells as well as reaching metastases are the main hurdles of cancer therapy. Research in this field strives to maximize efficacy while reducing adverse side effects.

Gemcitabine (Gem, dFdC or 2′,2′-difluoro-2′-deoxycytidine, Scheme 1) is a cytotoxic nucleoside analogue used as a chemotherapeutic drug. It is effective against an extensive range of solid tumors, such as pancreatic, non-small cell lung, breast and ovarian cancers, and is often a first-line treatment in clinical settings [2]. Despite being administered intravenously, treatment with gemcitabine has limited efficacy largely due to its short half-life (8-17 min), since gemcitabine is rapidly inactivated metabolically in the serum through deamination of its 4-N amine by cytidine deaminase (CDA), present in high levels in both human plasma and liver. As such, much higher doses are required to reach an effective plasma concentration, increasing toxicity and the risk of adverse side effects. Another major obstacle is the drug resistance related to nucleoside transporter deficiency, which is developed by some tumor cells after initial tumor regression. As a hydrophilic drug, gemcitabine cellular uptake is primarily facilitated by the human equilibrative nucleoside transporter 1 (hENT1). Thus, the expression of this transporter plays a key role in gemcitabine intracellular uptake [3]. There have been many efforts to improve gemcitabine clinical efficacy and numerous derivatives and prodrugs have been designed to alter some of the unfavorable physicochemical properties of gemcitabine and ideally improve its oral bioavailability [4]. Our research group has previously developed gemcitabine conjugates with cell-penetrating peptides (CPPs) to facilitate intracellular delivery of this drug [5-6]. In three of these new prodrugs, a cell-penetrating hexapeptide (CPP6) was covalently conjugated to the aniline moiety of gemcitabine through suitable bio-/chemo-reversible bonds. Two CPP5 (KLPVM and VPMLK) with reported high percentage of cell-penetration were selected. One tryptophan (Trp) residue was added to the terminal of these CPP5 to further improve their capacity of cell-penetration, since Trp has high propensity to be inserted into membranes [7-8], yielding three novel hexapeptides: CPP6-1 (WKLPVM), CPP6-2 (KLPVMW), and CPP6-3 (WVPMLK). These conjugates were designed to facilitate intracellular delivery of this drug and even overcome the problem of transporter deficiency related drug resistance, as CPPs are non-cytotoxic vectors and drug delivery vehicles. Additionally, gemcitabine is protected from CDA enzymatic deamination since its 4-N amine was modified. The bioactivity of these new prodrugs was previously evaluated in different cell lines and showed promising results [5].

In this work, we have evaluated the absorption and permeability of gemcitabine, three CPP6 and the respective Gem-CPP6 conjugates across Caco-2 monolayers. The single layer of epithelial cells that covers the inner intestinal wall forms the rate-limiting barrier to the absorption of dissolved compounds administered orally. Consequently, proper reconstitution of a human differentiated epithelial cell monolayer *in vitro* can be used to predict the absorption and permeability coefficients of orally administered drugs. The human colon carcinoma cell line Caco-2 has been successfully used to fulfill this purpose and monolayers grown on permeable filters have become the in vitro golden standard for these predictions [9]. This method is recognized by the American Food and Drug Administration (FDA) [10].

Experimental

Cell culture

Human colon adenocarcinoma cell line Caco-2 (passage 25-47, kindly provided by the Department of Biomedicine of the Faculty of Medicine of University of Porto, and previously acquired via ATCC) was routinely maintained in Dulbecco's Modified Eagle's Medium (DMEM) supplemented with 10 % fetal bovine serum (FBS), L-glutamine and antibiotics penicillin and streptomycin. Cells were cultured at 37 °C in a 5 % CO_2 humidified atmosphere. Culturing medium was replaced every 2-3 days and cell subculture was conducted once a week by trypsinization (0.25 % trypsin-EDTA wt/vol, 5 min, 37 °C).

Cytotoxicity assay

The cell growth inhibitory activity of gemcitabine in Caco-2 cells was assessed with the MTT assay. Briefly, a growth curve was traced to determine the best cell density for the assay. Cells were seeded in 96-well plates (growth surface 0.322 cm^2, from TPP®, Product No. 92696) with an initial cell density of 9.3 x 10^3 cells/mL (200 µL per well). Cells were allowed to attach for 24 h and were then either left untreated (culture medium was replaced for fresh medium) or treated with gemcitabine (0.1, 1, 5, 10, 20, 50, 100, 1000, 10000 and 100000 µM). Following 72 h incubation, cell medium was removed and 100 µL of MTT (3-(4,5-dimethylthiazol-2-yl)-2,5-diphenyltetrazolium bromide) solution were added per well. Cells were then incubated for another 4 h protected from light. Finally, MTT solution was removed, DMSO (100 µL per well) was added to solubilize the formazan crystals formed by viable cells and absorbance was measured at 570 nm in an automated microplate reader (Sinergy HT, Biotek Instruments Inc, Vermont, USA). All conditions were performed in triplicate.

Gemcitabine cytotoxicity results were compared with the untreated control (mean of values was set to 100 %) and expressed as mean ± SEM. The statistical significance between different gemcitabine concentrations was analyzed in GraphPad Prism 7 (San Diego, EUA) using one-way ANOVA ($p<0.05$).

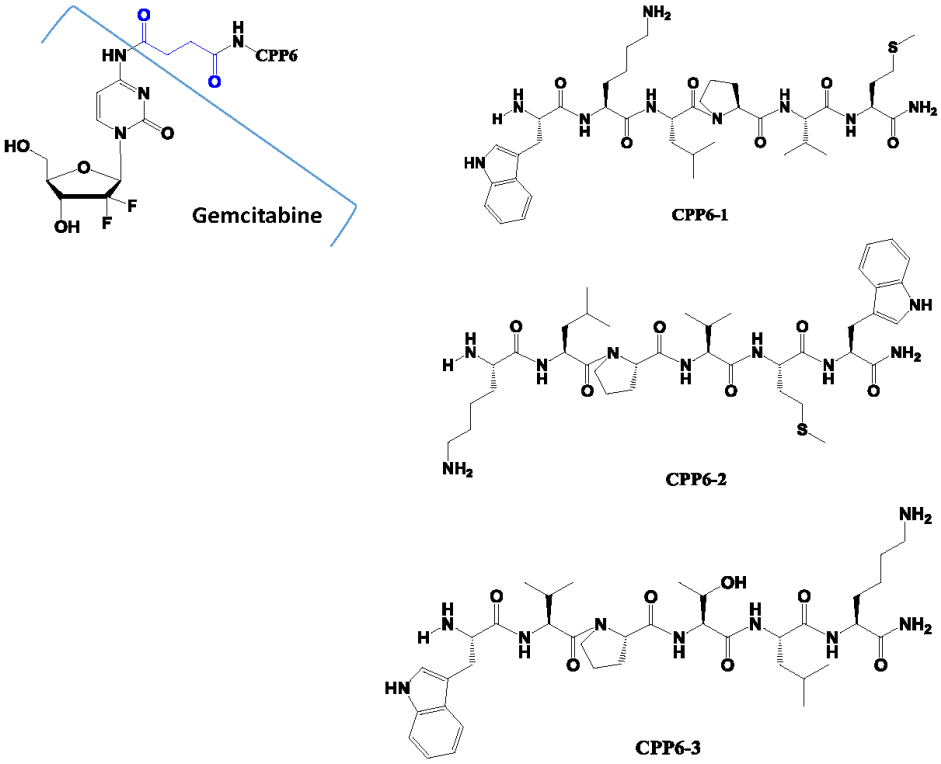

Scheme 1. Chemical structure of gemcitabine (before and after modification and conjugation with CPP6) and of the three CPP6 studied, CPP6-1 (WKLPVM), CPP6-2 (KLPVMW) and CPP6-3 (WVPMLK).

Preparation of CPPs and gemcitabine-CPP6 conjugates

All the compounds evaluated in this work (except for Gemcitabine, that was purchase from Sigma-Aldrich as Gemcitabine hydrochloride, G6423) had been previously synthesized by our research group [5]. Briefly, CPP6-1 (WKLPVM), CPP6-2 (KLPVMW) and CPP6-3 (WVPTLK) were manually synthesized using

standard solid phase peptide synthesis (SPPS) and Fmoc chemistry. Gemcitabine was modified to allow conjugation with CPP6. First, the two hydroxyl groups of gemcitabine were selectively protected with Boc groups; then, succinic anhydride was linked to the 4-N amine and lastly a CPP6 was conjugated to this anticancer drug. Some properties of these new conjugates are presented in Table 1.

Permeability assay

A monolayer of Caco-2 cells was established in a 12-well plate [11]. Each well contains a permeable filter insert, a transparent collagen treated (equimolar mixture of types I and III collagen) polytetrafluoroethylene (PTFE) membrane, with 12 mm diameter and 0.4 μm pore (Corning Inc, Corning Transwell COL collagen coated membrane inserts, NY, USA, Cat. No. 3493). Firstly, filters were pre-wet with 0.1 mL of culture medium for 2 minutes. Cells were seeded in the apical side (0.5 mL of cells per well, cell density of 4.0×10^5 cells/mL). The basolateral compartment was filled with 1.5 mL of culture medium and plates were incubated for 6 h (5 % CO_2 humidified atmosphere at 37 °C). Then, to remove non-adherent cells and reduce the risk of multilayer formation, the medium in the apical side was removed and replaced with fresh medium. Cells were maintained for 29 days, replacing the culture medium from both compartments every other day.

Transport across Caco-2 monolayer assay

All the solutions used were pre-warmed to 37 °C. Culture medium was replaced with fresh medium 24 h prior the beginning of the experiment. Next, this culture medium was removed first from the basolateral and then from the apical compartment. The apical compartment was carefully washed and then filled with 0.5 mL of Hank's Balanced Salt Solution (HBSS, pH 7.4) and the basolateral compartment was also filled with 1.5 mL of HBSS. The plates were incubated for 17 min at 37 °C under gentle shaking (190 rpm, GFL® Orbital Shaker 3015). All tested compounds were prepared in HBBS (60 μM) and added to the apical compartment. Throughout this assay, the final volume was 0.4 mL in the apical compartment and 1.2 mL in the basolateral chamber. At t = 0 min, 0.45 mL of the donor solution was added to the apical compartment and a sample (0.05 mL) was immediately taken. The plate was incubated (lid-covered) at 37 °C under gentle shaking (190 rpm). Every 30 min for the next 2 h, a sample of 0.6 mL was taken from the basolateral compartment and replaced with the same volume of HBSS. After 120 min, a sample of 0.05 mL was taken from the apical side.

HPLC quantification

The concentrations of the evaluated compound in the basolateral and apical compartments were determined by high-performance liquid chromatography (HPLC) (VWR International LCC, LaChrom Ultra, Pennsylvania, USA). Elution was performed with a variable gradient of acetonitrile (ACN) in water containing 0.05 % trifluoroacetic acid (TFA), at a 0.7 mL/min flow and detection at variable wavelength (243 nm for gemcitabine and 220 nm for peptides and conjugates). All chemicals were either analytical or HPLC grade.

Results and discussion

Gemcitabine cytotoxicity

Every concentration of gemcitabine tested caused a statistically significant inhibition of cell growth in Caco-2 cells compared to untreated cells (Figure 1). The maximum inhibition was observed after treatment with the highest concentration of gemcitabine evaluated (100000 μM). The IC_{50} was calculated as 52.4 μM.

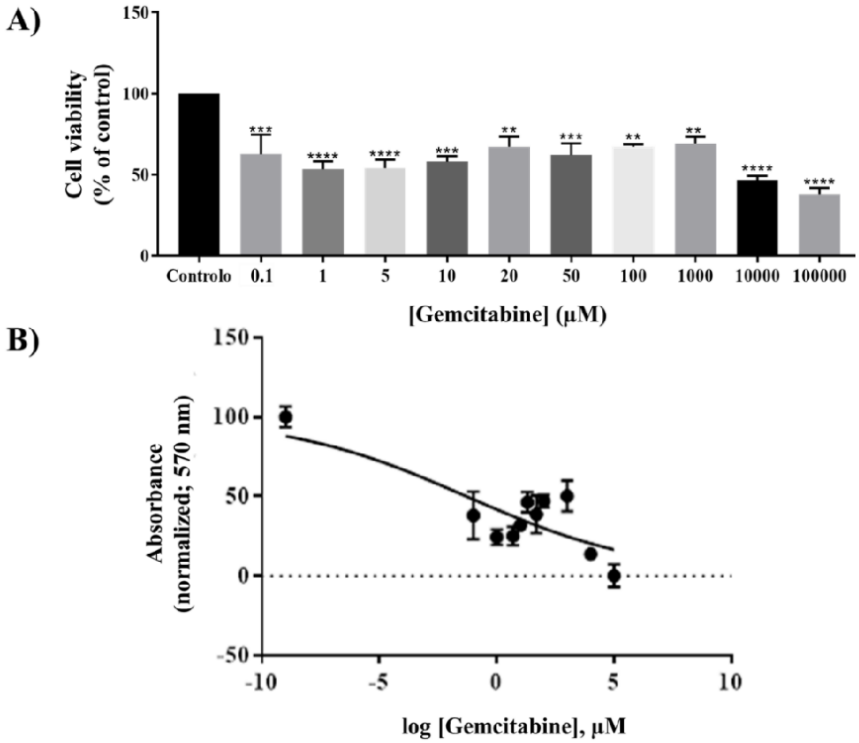

Figure 1. Concentration-dependent cytotoxicity of gemcitabine in Caco-2 cells (Abs 570 nm). Results are presented as (**A**) the percentage of inhibition compared to control untreated cells and (**B**) plotted as the log [gemcitabine] against the percentage of control untreated cells. Results are expressed as mean ± SEM (n=3; $p<0.05$, one-way ANOVA).

Caco-2 monolayer and permeability of Gemcitabine

Microscopic analysis of the filter revealed a uniformly formed monolayer, with no detection of anomalies or areas without cells. A Caco-2 monolayer was successfully established and this is a reliable indicator for proceeding with the permeability study.

After 30 minutes, just 3 % of Gemcitabine was found in the basolateral side. At the 90 min time point, a plateau was reached and only an additional 1 % of the drug crossed the membrane until the end of assay (120 min), with a total of 18 % of the amount of Gemcitabine initially applied in the apical side having crossed into the basolateral compartment.

Permeability of CPP6

Comparable amounts of the 3 CPP6 crossed the monolayer of Caco-2 cells after 120 minutes. Still, CPP6-2 exhibited the highest permeability, with 40 % being recovered in the basolateral chamber, followed by CPP6-3 (37 %) and CPP6-1 (33 %). During the first 30 minutes, only 4 to 5 % of all CPPs reached the basolateral side; the rate of permeation was highest between 30 and 90 minutes. CPP6-2 and CPP6-3 registered a decrease in this rate for the last 30 minutes of this assay. Throughout the experiment, a slower rate of permeation was observed for CPP6-1 (Figure 2).

By the end of the experiment, the sum of the CPP absorbed from the apical side and found in the basolateral chamber was 84 % for CPP6-2, 75 % for CPP6-3 and 50 % for CPP6-1. This indicates that some

peptide is retained inside the cells or was degraded.

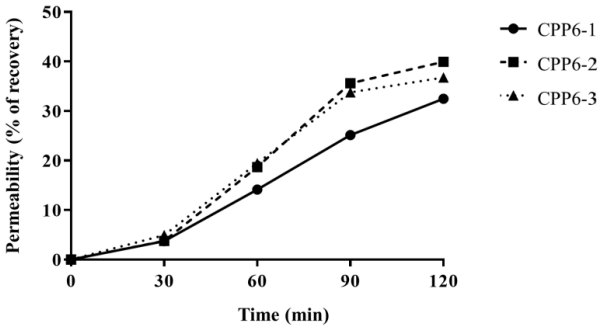

Figure 2. Concentration of CPP6 in the basolateral compartment after incubation with 60 µM in the apical compartment and fitted curves.

Permeability of Gem-CPP6 conjugates

As for the Gem-CPP6 conjugates, the conjugate of gemcitabine with CPP6-2 clearly stands out as the most permeable across the Caco-2 cell monolayer. The extent of permeation of this conjugate was about 3-fold the observed for the Gem-CPP6-1 and Gem-CPP6-3 conjugates. Approximately 31 % of the Gem-CPP6-2 conjugate was found in the basolateral chamber, while only 9 % of Gem-CPP6-1 and Gem-CPP6-3 conjugates were able to cross the monolayer of Caco-2 cells and was quantified in this compartment (Figure 3).

The higher permeability of the Gem-CPP6-2 conjugate is in agreement with the previous evaluation of the permeability of the isolated CPP6, with CPP6-2 being the most permeable peptide. Of the three studied CPP6, CPP6-2 is the only one that has a Trp residue in its C-terminal (CPP6-1 and CPP6-3 have a Trp residue in the N-terminal position). Additionally, the only difference between CPP6-1 and CPP6-2 is the position of this amino acid residue (N-terminal versus C-terminal).

Tryptophan can be considered hydrophobic due to its uncharged side chain. Given its aromatic character, it can form hydrogen bonds and strongly interact with cellular membranes, disrupting the stability of the membrane lipidic chains. These properties grant this amino acid residue a great tendency to insert into membranes [12-15]. It has been shown that the replacement of the 2 Trp residues of the known CPP Penetratin for phenylalanine residues completely eliminates the penetration ability of this peptide [16]. Furthermore, Rydberg et al. have reported that the number of Trp residues in a CPP is relevant, with a higher number of Trp residues in a CPP corresponding to greater penetration ability [12]. These authors have also demonstrated that the position of this residue is another factor influencing permeability; in this case, CPPs with Trp residues in the N-terminal position were less absorbed.

Some properties of these new Gem-CPP6 conjugates were predicted using in silico tools and are presented in Table 1. Gem-CPP6-2 has the highest calculated P_{app} and is also predicted as the most permeable conjugate by GastroPlus™, a mechanistically based pharmacokinetics and pharmacodynamics simulation software.

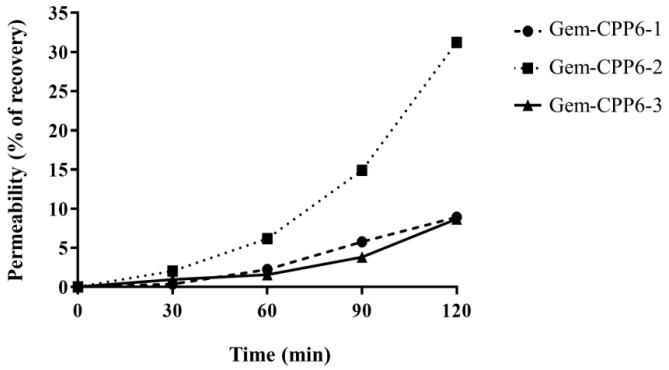

Figure 3. Permeability of the Gem-CPP6 conjugates, expressed as the percentage recovered in the basolateral compartment.

Table 1. Physicochemical and in silico pharmacokinetic data of CPP6-Gemcitabine conjugates.

Peptide/Conjugate	M_W (g/mol)	PSA [a] (Å^2)	HBD	P_{eff} (cm/s) [b] (x10^{-6})	P_{eff} (cm/s) [c] (x10^{-9})	P_{app} (cm/s) (x10^{-8})
Gem-CPP6-1	1117.29	247.63	13	3.19	1.31	1.326
Gem-CPP6-2	1117.29	247.63	13	3.82	1.31	4.568
Gem-CPP6-3	1087.20	267.86	14	2.47	0.412	1.326

[a] Polar surface area, predicted by MedChem Designer (version 3.1.0.30, Simulations Plus, Inc., Lancaster, California, USA);
[b] Effective permeability, predicted by GastroPlus™ (version 9.5, Simulations Plus, Inc., Lancaster, California, USA);
[c] Effective permeability, calculated from Winiwarter equation: Log P_{eff} = (-2.546) – (0.011 x PSA) – (0.278 x HBD); HBD: hydrogen bond donors; [17].

Conclusions

The monolayer of Caco-2 cells was a suitable method to study the permeability of the anticancer drug gemcitabine, the cell-penetrating hexapeptides (CPP6) and the new prodrug conjugates Gem-CPP6. Every CPP6 and Gem-CPP6 conjugate was able to cross this monolayer, suggesting their potential as drug delivery systems. In agreement with previous reports, the position of the Trp residue was a determinant factor influencing the permeability of the CPP6 and Gem-CPP6 conjugates. Amongst the evaluated compounds, CPP6-2 and the respective Gem-CPP6-2 conjugate showed the highest permeability, crossing the cell monolayer to a greater extent. This data puts forward this conjugate as a lead for further studies and as the most promising for potential clinical application.

Acknowledgements

This work was financed by FEDER – Fundo Europeu de Desenvolvimento Regional through the COMPETE 2020 – Operational Programme for Competitiveness and Internationalization (POCI), Portugal 2020, and by Portuguese funds through FCT – Fundação para a Ciência e a Tecnologia, in a framework of CINTESIS, R&D Unit (reference UIDB/4255/2020). N.V. also thanks support FCT and FEDER (European Union), award number IF/00092/2014/CP1255/CT0004. RL thanks FCT through grant UID/QUI/50006/2019 (LAQV-REQUIMTE). AF thanks FCT for a doctoral fellowship (PD/BD/135120/2017). The contents of this article are solely the responsibility of the authors and do not necessarily represent the official view of the FCT.

Conflict of interest: On behalf of all authors, the corresponding author states that there is no conflict of interest.

References

[1] Global cancer burden in 2018 (GLOBOCAN 2018 database, International Agency for Research on Cancer). https://gco.iarc.fr/today/data/factsheets/populations/900-world-fact-sheets.pdf (accessed June 10, 2020).

[2] A. Wong, R.A. Soo, W.-P. Yong, F. Innocenti. Clinical pharmacology and pharmacogenetics of gemcitabine. *Drug Metabolism Reviews* **41** (2009) 77-88.

[3] E. Mini, S. Nobili, B. Caciagli, I. Landini, T. Mazzei. Cellular pharmacology of gemcitabine. *Annals of Oncology* **17** (2006) 7-12.

[4] E. Moysan, G. Bastiat, J.-P. Benoit. Gemcitabine versus modified gemcitabine: a review of several promising chemical modifications. *Molecular Pharmaceutics* **10** (2013) 430-444.

[5] C. Correia, C.P.R. Xavier, D. Duarte, A. Ferreira, S. Moreira, M.H. Vasconcelos, N. Vale. Development of potent CPP6-gemcitabine conjugates against human prostate cancer cell line (PC-3). *RSC Medicinal Chemistry* **11** (2020) 268-273.

[6] N. Vale, A. Ferreira, I. Fernandes, C. Alves, M.J. Araujo, N. Mateus, P. Gomes. Gemcitabine anti-proliferative activity significantly enhanced upon conjugation with cell-penetrating peptides. *Bioorganic and Medicinal Chemistry* **27** (2017) 2898-2901.

[7] K. Kachel, E. Asuncion-Punzalan, E. London. Anchoring of tryptophan and tyrosine analogs at the hydrocarbon-polar boundary in model membrane vesicles. *Biochemistry* **34** (1995) 15475-15479.

[8] D.J. Schibli, R.F. Epand, H.J. Vogel, R.M. Epand. Tryptophan-rich antimicrobial peptides: comparative properties and membrane interactions. *Biochemistry Cell Biology* **80** (2002) 667-677.

[9] I.D. Angelis, L. Turco. Caco-2 cells as a model for intestinal absorption. *Current Protocols in Toxicology* **47** (2011) 20.6.1-20.6.15.

[10] U.S. Department of Health and Human Services, Food and Drug Administration, Center for Drug Evaluation and Research (CDER). Waiver of in vivo bioavailability and bioequivalence studies for immediate-release solid oral dosage forms based on a biopharmaceutics classification system. December 2017, Biopharmaceutics.

[11] I. Hubatsch, E.G. Ragnarsson, P. Artursson. Determination of drug permeability and prediction of drug absorption in Caco-2 monolayers. *Nature Protocols* **2** (2007) 2111-2119.

[12] H.A. Rydberg, M. Matson, H.L. Åmand, E.K. Esbjorner, B. Nordén. Effects of tryptophan content and backbone spacing on the uptake efficiency of cell-penetrating peptides. *Biochemistry* **51** (2012) 5531-5539.

[13] D.I. Chan, E.J. Prenner, H.J. Vogel. Tryptophan-and arginine-rich antimicrobial peptides: structures and mechanisms of action. *Biochimica et Biophysica Acta (BBA)-Biomembranes* **1758** (2006) 1184-1202.

[14] G. Trinquier, Y.-H. Sanejouand. Which effective property of amino acids is best preserved by the genetic code? *Protein Engineering* **11** (1998) 153-169.

[15] W.-M. Yau, W.C. Wimley, K. Gawrisch, S.H. White. The preference of tryptophan for membrane interfaces. *Biochemistry* **37** (1998) 14713-14718.

[16] M.-L. Jobin, M. Blanchet, S. Henry, S. Chaignepain, C. Manigand, S. Castano, S. Lecomte, F. Burlina, S. Sagan, I.D. Alves. The role of tryptophans on the cellular uptake and membrane interaction of arginine-rich cell-penetrating peptides. *Biochimica et Biophysica Acta (BBA)-Biomembranes* **1848** (2015) 593-602.

[17] S. Winiwarter, N.M. Bonham, F. Ax, A. Hallberg, H. Lennernäs, A. Karlén. Correlation of human jejunal permeability (in vivo) of drugs with experimentally and theoretically derived parameters. A multivariate data analysis approach. *Journal of Medicinal Chemistry* **41** (1998) 4939-4949.

CHAPTER 3

Permeability of Gemcitabine and PBPK Modeling to Assess Oral Administration

Abigail Ferreira, Rui Lapa, Nuno Vale

Current Issues in Molecular Biology, **2021**, 43(3), pp. 2189-2198.
DOI: 10.3390/cimb43030153 (registering DOI).

As the most frequently employed chemotherapy treatment involves intravenous infusions, an invasive and unpleasant procedure, an alternative administration route was proposed and evaluated regarding the pharmacokinetic profile and feasibility. In this work, an oral administration via tablet was proposed and analyzed using GastroPlus™, revealing this is a promising treatment option. Despite maximum concentration reached in plasma was predicted to be lower following oral administration, the estimated area under the curve (AUC) was greater for three of the studied oral regimens following tablet administration, providing enhanced drug exposure. Importantly, although studied doses were higher than conventionally used, no drug accumulation was predicted over time and with prolonged treatment.

current issues in molecular biology

MDPI

Article

Permeability of Gemcitabine and PBPK Modeling to Assess Oral Administration

Abigail Ferreira [1,2], Rui Lapa [2] and Nuno Vale [1,3,*]

[1] OncoPharma Research Group, Center for Health Technology and Services Research (CINTESIS), Rua Doutor Plácido da Costa, 4200-450 Porto, Portugal; abigail.ferreira@fc.up.pt
[2] LAQV/REQUIMTE, Laboratory of Applied Chemistry, Department of Chemical Sciences, Faculty of Pharmacy, University of Porto, Rua de Jorge Viterbo Ferreira 228, 4050-313 Porto, Portugal; ruilapa@ff.up.pt
[3] Faculty of Medicine, University of Porto, Alameda Professor Hernâni Monteiro, 4200-319 Porto, Portugal
* Correspondence: nunovale@med.up.pt

Abstract: Gemcitabine is a nucleoside analog effective against several solid tumors. Standard treatment consists of an intravenous infusion over 30 min. This is an invasive, uncomfortable and often painful method, involving recurring visits to the hospital and costs associated with medical staff and equipment. Gemcitabine's activity is significantly limited by numerous factors, including metabolic inactivation, rapid systemic clearance of gemcitabine and transporter deficiency-associated resistance. As such, there have been research efforts to improve gemcitabine-based therapy efficacy, as well as strategies to enhance its oral bioavailability. In this work, gemcitabine in vitro and clinical data were analyzed and in silico tools were used to study the pharmacokinetics of gemcitabine after oral administration following different regimens. Several physiologically based pharmacokinetic (PBPK) models were developed using simulation software GastroPlus™, predicting the PK parameters and plasma concentration–time profiles. The integrative biomedical data analyses presented here are promising, with some regimens of oral administration reaching higher AUC in comparison to the traditional IV infusion, supporting this route of administration as a viable alternative to IV infusions. This study further contributes to personalized health care based on potential new formulations for oral administration of gemcitabine, as well nanotechnology-based drug delivery systems.

Keywords: gemcitabine; cancer therapy; in silico study; PBPK modeling; GastroPlus™

Citation: Ferreira, A.; Lapa, R.; Vale, N. Permeability of Gemcitabine and PBPK Modeling to Assess Oral Administration. *Curr. Issues Mol. Biol.* **2021**, *43*, 2189–2198. https://doi.org/10.3390/cimb43030153

Academic Editor: Hidayat Hussain

Received: 17 November 2021
Accepted: 2 December 2021
Published: 7 December 2021

1. Introduction

Cancer is one of the most prevalent and mortal diseases and still has an increasing incidence rate. Globally, about one in six deaths is due to cancer [1]. Treatment options include chemotherapy, radiotherapy and/or surgery. Although surgical removal and/or radiotherapy is typically the first recommendation for well-defined solid tumors with a promising prognosis, chemotherapy is administered to almost all cancer patients, even if as an adjuvant treatment. There has been continuous research to improve overall treatment efficacy and reduce associated adverse side effects, as there are several shortcomings in the currently available treatments.

Gemcitabine (2′,2′-difluoro-2′-deoxycytidine or dFdC) is a nucleoside analog and pyrimidine antimetabolite with proven efficacy against a variety of solid tumors, being the first-line treatment for pancreatic cancer and also used in the therapy of ovarian, breast and non-small-cell lung cancer [2,3]. Combinations of gemcitabine with other anticancer agents, such as paclitaxel and platinum analogs oxaliplatin, carboplatin and cisplatin, are also employed [4–6]. However, multiple factors limit the efficacy of gemcitabine-based treatments. Gemcitabine is rapidly inactivated in the serum through metabolic deamination by cytidine deaminase (CDA). Additionally, this drug's binding to plasma proteins is negligible (<10%, [7]), leaving the majority of circulating gemcitabine unbound

and available for metabolic modification and inactivation. Gemcitabine is thus very rapidly cleared from the body, having a short half-life (8–17 min). Another drawback limiting the efficacy of this drug is the resistance related to nucleoside transporter deficiency. The human equilibrative nucleoside transporter 1 (hENT1) is primarily responsible for the cellular uptake of gemcitabine, but an underexpression of this transporter is developed in some tumor cells after initial tumor regression [3]. Thus, much higher doses may be required to reach an effective plasma concentration.

Currently, standard treatment with gemcitabine is an intravenous (IV) infusion of 1000 or 1250 mg/m^2 over 30 min once a week and then follows different treatment cycle schedules [7]. This is an invasive and very uncomfortable method. As previously mentioned, numerous strategies have been developed to improve treatment efficacy and reduce side effects, including the study of drug combinations, chemical modifications and the development of prodrugs. Some strategies aim at surpassing some of the unfavorable physicochemical properties of gemcitabine and improving this drug's oral bioavailability, to avoid IV administration.

The oral route of administration presents some limitations, the most impactful being the first-pass effect, which significantly diminishes the amount of drug that reaches systemic circulation (in the case of gemcitabine, CDA is present in high levels in the liver and metabolizes gemcitabine to the inactive metabolite 2′,2′-difluorodeoxyuridine, dFdU). Nevertheless, this is undoubtedly a much more convenient and comfortable form of administering drugs. We were encouraged by promising previous results reported for various prodrugs of gemcitabine developed to enhance oral bioavailability [8–10], including some studies carried out by our research group regarding gemcitabine conjugates with cell-penetrating peptides (CPPs) [11–13].

In this work, the oral route of administration was preliminarily assessed as an alternative to IV infusions, and the pharmacokinetics of gemcitabine after oral administration via a tablet following different treatment regimens with varying doses and dosing intervals were studied and compared to the IV form. Since the single layer of epithelial cells covering the inner intestinal wall is the rate-limiting barrier to the absorption of dissolved compounds administered orally, the permeability of gemcitabine through a monolayer of Caco-2 cells was also evaluated, using a method recognized by the American Food and Drug Administration (FDA) [14]. Several physiologically based pharmacokinetic (PBPK) models were then developed, and the main PK parameters were predicted using simulation software GastroPlus™. This software integrates an advanced compartmental absorption and transit model (ACAT) and uses a set of differential equations to model the amount of drug that is released, dissolved and absorbed for all physiologically predefined compartments. The plasma concentration–time profiles and the regional absorption throughout the different compartments of the gastrointestinal tract were also evaluated and are presented here.

2. Materials and Methods

2.1. Cell Culture

Human colon adenocarcinoma cells, from cell line Caco-2 (passage 25–47, kindly provided by the Department of Biomedicine of the Faculty of Medicine of University of Porto (Professor Fátima Martel), and previously acquired via ATCC) were routinely maintained in Dulbecco's modified Eagle's medium (DMEM), supplemented with 10% fetal bovine serum (FBS), L-glutamine and antibiotics penicillin and streptomycin. Cells were cultured at 37 °C in a 5% CO_2 humidified atmosphere. Culturing medium was replaced every 2–3 days, and cell subculture was conducted once a week by trypsinization.

2.2. Permeability Assay

2.2.1. Establishment of a Caco-2 Monolayer

A monolayer of Caco-2 cells was established in a 12-well plate. Each well contains a permeable filter insert, a transparent collagen-treated (equimolar mixture of types I and III collagen) polytetrafluoroethylene (PTFE) membrane, 12 mm in diameter with a

0.4 μm pore size (Corning Transwell®-COL collagen-coated membrane inserts, Corning Inc, Corning, NY, USA, Cat. No. 3493) (Figure 1).

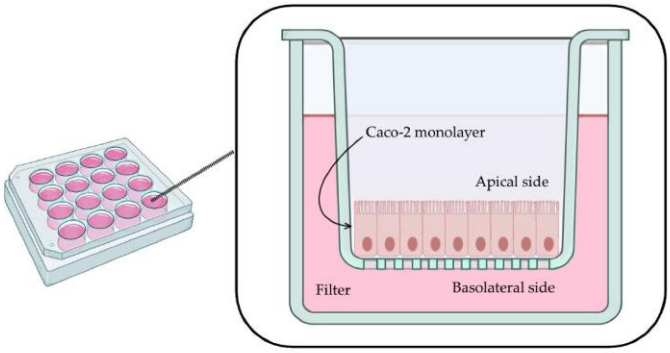

Figure 1. Caco-2 monolayer in permeable filter (illustration created with BioRender [15] for this project).

Firstly, filters were pre-wet with 0.1 mL of culture medium for 2 min. Cells were seeded on the apical side (0.5 mL of cells per well, cell density of 4.0×10^5 cells/mL). The basolateral compartment was filled with 1.5 mL of culture medium, and plates were incubated for 6 h (5% CO_2 humidified atmosphere at 37 °C). Then, to remove nonadherent cells and reduce the risk of multilayer formation, the medium on the apical side was removed and replaced with fresh medium. Cells were maintained for 29 days, replacing the culture medium from both compartments every other day (aspiration from the basal chamber first, followed by careful aspiration from the apical compartment and replacement with the same volume of fresh medium first in the apical compartment and finally in the basal compartment).

2.2.2. Transport across Caco-2 Monolayer Assay

All the solutions used were pre-warmed to 37 °C. Culture medium was replaced with fresh medium 24 h prior to the beginning of the experiment. Then, the culture medium was removed from both compartments, and the apical compartment was carefully washed and filled with 0.5 mL of Hank's balanced salt solution (HBSS, pH 7.4). The basolateral compartment was also filled with 1.5 mL of HBSS, and the plates were incubated for 17 min at 37 °C under gentle shaking (190 rpm, GFL® Orbital Shaker 3015).

Gemcitabine (purchased from Sigma-Aldrich as gemcitabine hydrochloride, G6423, Algés, Portugal) was prepared in HBBS and added to the apical compartment (final concentration of 60 μM). Throughout this assay, the final volume was 0.4 mL in the apical compartment and 1.2 mL in the basolateral chamber. At t = 0 min, 0.45 mL of the donor solution was added to the apical compartment, and a sample of 0.05 mL was immediately taken. Plates were incubated (lid covered) at 37 °C under gentle shaking (190 rpm). Every 30 min for the next 2 h, a sample of 0.6 mL was taken from the basolateral compartment and replaced with the same volume of HBSS. After 120 min, a sample of 0.05 mL was taken from the apical side. Results are expressed as mean SEM (n = 4).

2.2.3. HPLC Quantification

The concentration of gemcitabine in the basolateral and apical compartments was determined by high-performance liquid chromatography (HPLC) (VWR International LCC, LaChrom Ultra, Alfragide, Portugal). Elution was performed with a variable gradient of acetonitrile (ACN) in water containing 0.05% trifluoroacetic acid (TFA) at 0.7 mL/min flow and detection at 243 nm. All chemicals were either analytical or HPLC grade.

2.3. PBPK Modeling

GastroPlus™ software version 9.5 (Simulations Plus Inc., Lancaster, CA, USA) was used for absorption modeling and simulation (PBPK modeling), prediction of PK parameters and generation of simulated human plasma concentration profiles. The absorption of oral formulations from the GI tract was modeled by the advanced compartmental absorption and transit (ACAT™) model implemented in GastroPlus™. All simulations were modeled with a compartmental model considering a fasted state. Gemcitabine clearance was inputted as 120 L/h (according to this drug's FDA label and information deposited on DrugBank) [7,16,17], and the simulation time was set to 24 h for all conditions. The intravenous administration was set as a 30 min infusion of 1800 mg of gemcitabine (standard treatment is 1000 mg/m^2). For the oral route of administration, an immediate-release tablet was selected, and different treatment regimens were studied: a tablet of 1000 mg once, twice and three times a day and a tablet of 1500 mg twice and three times a day. These dosages were selected as an approximation to the standard treatments. A dose volume of 250 mL was set for all simulations.

3. Results and Discussion

3.1. Gemcitabine Permeability

The successful formation of a monolayer of Caco-2 cells was verified by observation under an optical microscope, with no detection of anomalies or areas without cells, a reliable indicator for proceeding with the permeability study. The integrity of the cells was not compromised by the concentration of gemcitabine used in the permeability assay (60 µM), since the IC50 of this drug is far greater (approximately 50 mM, as determined experimentally via MTT assay and previously reported by Lim et al. [18]). Results are presented in Figure 2 as a percentage of recovery from the basolateral compartment.

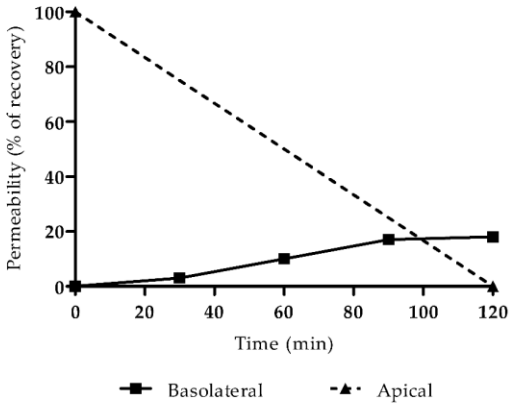

Figure 2. Permeability of gemcitabine, expressed as the percentage recovered in the basolateral and apical compartments.

The apparent permeability was then calculated as 5.8×10^{-6} cm/s using Equation (1),

$$P_{app} = \left(\frac{dQ/dt}{C_0 \times A} \right) \quad (1)$$

where *dQ/dt* is the amount of compound in the basolateral compartment as a function of time, C_0 is the initial concentration in the donor (apical) compartment and A is the area of the transwell filter (cm^2). This value was inputted in GastroPlus™ and used in all simulations.

3.2. PBPK Modeling

Some properties of gemcitabine predicted by GastroPlus™ and parameters used in the simulations are presented in Table 1. The PK parameters predicted from the simulations carried out in this study are presented in Table 2.

Table 1. Structure, parameters and gemcitabine properties predicted by GastroPlus™ used in the simulations.

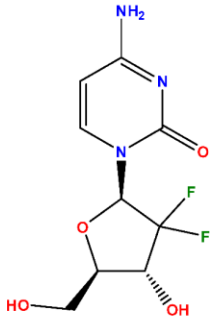

Parameter	Value	Source
Molecular weight	263.2	GastroPlus™
logP (neutral)	−1.32	
Solubility	5.01 mg/mL (at pH 7.92)	
Mean precipitation time	900 s	
Drug particle density	1.2 g/mL	
Diffusion coefficient	0.93×10^5 cm^2/s	
Blood/plasma concentration ratio	1.12	
Human jejunal permeability	0.59×10^{-4} cm/s	GastroPlus™ and experimental determination
F_{up}	84.60%	GastroPlus™ (>90% in [7,16])
V_c	1.45 L/kg	GastroPlus™ (1.3 L/kg in [7,16])
$T_{1/2}$	0.59 h	GastroPlus™ (0.7 to 1.57 h in [7,16])

Table 2. Predicted pharmacokinetic properties of gemcitabine determined with GastroPlus™ for different treatment conditions.

Posology			Fa (%) [1]	FDp (%) [2]	F (%) [3]	C_{max} (mg/L) [4]	T_{max} (h) [5]	$AUC_{0\text{-}inf}$ (µg·h/mL) [6]	$AUC_{0\text{-}t}$ (µg·h/mL) [7]	$C_{max\ liver}$ (mg/L) [8]
Admin. Route	**Dose (mg)**	**Interval**								
IV	1800	—	99.929	99.929	99.929	13.132	0.50	14.990	14.989	12.5610
Tablet (Immediate release)	1000	24 h (1×/day)	68.026	68.013	68.013	1.656	1.68	5.732	5.663	3.9916
		12 h (2×/day)	67.411	67.387	67.387	1.668	13.68	11.458	11.214	4.0185
		8 h (3×/day)	67.051	67.020	67.020	1.684	17.68	16.807	16.711	4.0517
	1500	12 h (2×/day)	66.945	66.925	66.925	2.493	13.68	17.095	16.711	6.0148
		8 h (3×/day)	66.460	66.433	66.433	2.506	17.68	24.965	24.855	6.0435

[1] Fraction absorbed as a percent of the dose (crossing the lumen and entering enterocytes). [2] Percent of the dose that has reached the portal vein. [3] Bioavailability. [4] Maximum plasma concentration reached in the central compartment, in mg/L. [5] Time to reach maximum plasma concentration, in hours. [6] Area under the plasma concentration–time curve, in µg·h/mL, extrapolated to infinity. [7] Area under the plasma concentration–time curve, in µg·h/mL, for the time of the simulation. [8] Maximum concentration reached in the liver, in mg/L.

In cancer therapy, there are several drugs that are given orally, with dosages of 1000 mg and 1500 mg for the active ingredient. These values were used by us in the simulations to ensure that we had a high dose of the drug for assessing the accumulation and clearance factor when compared to the IV form of gemcitabine administration (Table 2). It is possible to derive a rough estimate of the dose starting from the IV dose (reference) and dividing by the F value of the drug.

The simulation of the standard treatment via IV infusion provided a prediction of PK parameters approximate to values calculated in studies with cancer patients [19–21]. The maximum concentration was estimated as 13.132 mg/L, reached at the end of the infusion

(30 min). The C_{max} values predicted for all studied regimens of oral administration were always lower compared to the IV infusion (highest C_{max} predicted was 2.506 mg/L after a tablet of 1500 mg three times a day). However, despite reaching lower gemcitabine concentrations in the plasma, the estimated $AUC_{0\text{-}inf}$ was higher for three of the studied oral regimens following tablet administration (16.807 µg·h/mL for 1000 mg tablet 3×/day, 17.095 µg·h/mL for 1500 mg tablet 2× and 24.965 µg·h/mL for 1500 mg tablet 3×/day) compared to the IV administration (14.99 µg·h/mL). This is plausible, since the total daily dose administered is higher. A comparison is depicted and highlighted in Figure 3.

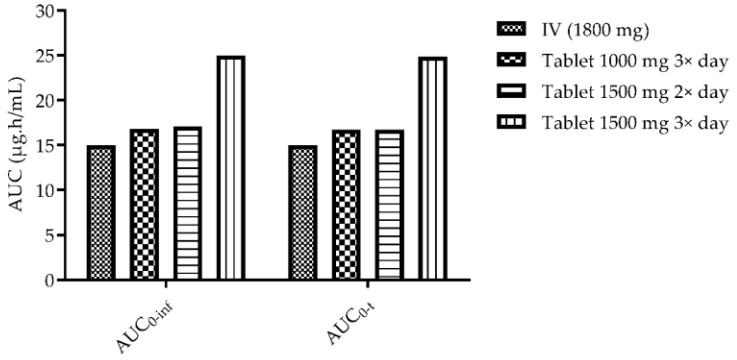

Figure 3. Comparison of AUC between IV infusion (1800 mg), 1000 tablet 3× a day and 1500 mg tablet 2× and 3× a day.

The simulated plasma concentration–time profiles for all studied conditions are presented in Figure 4. The profile simulated for the IV administration is also consistent with reports from the literature and studies in human patients. Wang et al. studied the PK of gemcitabine in patients with non-small-cell lung cancer (NSCLC) and presented the plasma concentration–time profile for six patients receiving 1200 mg/m^2 of gemcitabine as a 30 min infusion [19]. A comparison of the profile reported by this group of researchers and the one predicted here is presented in Figure 5. Additionally, it is important to note that there is no drug accumulation in the plasma, even with multiple doses being administered throughout the day and the combined total dose of gemcitabine in some of the studied regimens being higher than 1800 mg (2000 mg, 3000 mg and 4500 mg). The regional absorption of gemcitabine was also analyzed and is presented in Figure 6. These results show that there is no significant difference in the distribution of absorbed gemcitabine between different regimens of oral administration.

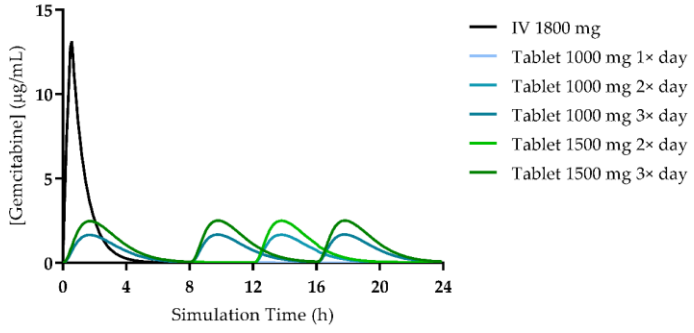

Figure 4. Plasma concentration—time profiles for gemcitabine following 30 min IV infusion and different oral (tablet) treatment regimens.

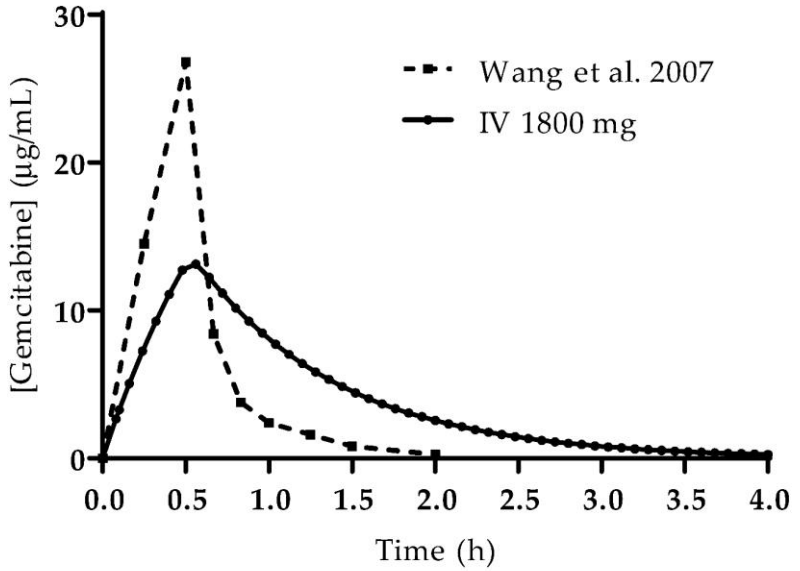

Figure 5. Comparison of the plasma concentration–time profiles from Wang et al. [19] (1200 mg/m^2 by 30 min IV infusion) and the profile acquired in the simulation carried out in this study (1800 mg by 30 min infusion).

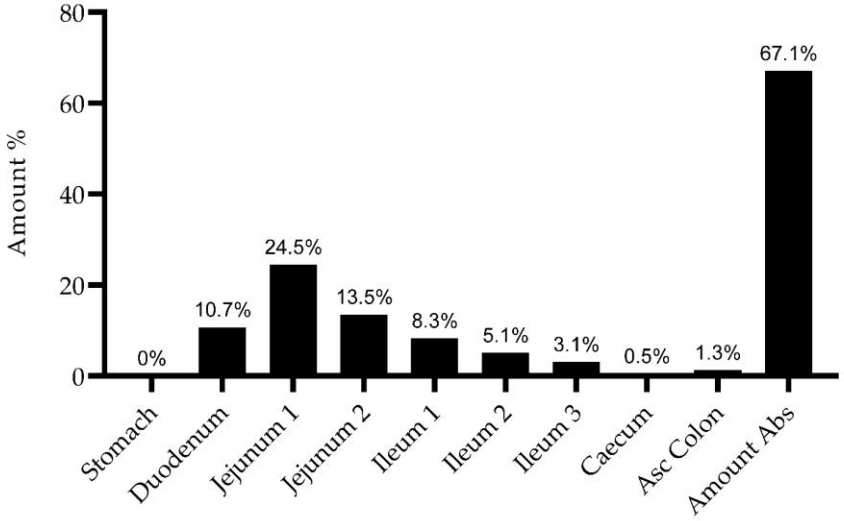

Figure 6. Simulated distribution of gemcitabine absorbed by different compartments after administration of a 1000 mg tablet three times a day.

4. Discussing the Limitations of the Present Study

Despite the convenience of the oral route of administration, there are many aspects to take into consideration regarding this route. As mentioned in the Introduction (Section 1), gemcitabine is significantly metabolized by CDA, present in high levels in the plasma and liver, and is rapidly cleared from the body upon its enzymatic conversion [22,23]. Other enzymes will further contribute to the metabolic transformation and degradation of gemcitabine, including nucleosidase enzymes in the intestinal lumen. Additionally,

gemcitabine's entry into cells is transporter dependent. Not only are equilibrative and concentrative nucleoside transporters required for the perfusion into tissues, gemcitabine will also be a substrate for intestinal nucleoside transporters [24,25].

Regarding another considerable factor, gemcitabine's permeability has been previously assessed in in vitro and in vivo mouse models [24] and has been evaluated here in a Caco-2 monolayer of cells to mimic the intestinal epithelium. Although Caco-2 permeability values do not directly translate in vivo permeability, in this project, this was used to help parametrize the PBPK models.

The oral administration of gemcitabine was previously evaluated in patients with refractory tumors by Veltkamp et al., in much lower doses than the ones evaluated here, ranging from 2 to 20 mg [26]. However, in this preliminary work, the chosen doses were closer to the ones intravenously administered in conventional therapy, to assess the exposure via the oral route of administration.

In sum, this work intended to analyze the pharmacokinetic viability of the oral route of administration for gemcitabine. Taking the results observed, progressing with this study will imply acquiring more data relating to the metabolism, transport and, later, the pharmacodynamic aspects of this drug.

5. Conclusions

Given the major drawbacks of chemotherapy, we were interested in studying an alternative to the standard treatment regimen for gemcitabine that includes IV infusions. Here, we developed several PBPK models and studied the PK of this drug after different regimens of oral administration via tablet, an easier and more comfortable route of administration for patients. The results from our simulations showed that despite the estimated C_{max} being lower for all regimens of oral administration, the predicted AUC is higher for three of the studies conditions (1000 mg tablet 3×/day, 1500 mg tablet 2×–3×/day) compared to the IV administration. This can indicate an enhanced exposure to this drug, retaining the therapeutic effect despite the lower concentration in the plasma. Furthermore, there was no drug accumulation even with multiple doses a day and a total dose higher than 1800 mg (maximum daily dose of 4500 mg). Taking together the results from the present study, we believe that oral administration of gemcitabine is a promising and viable alternative to the current standard IV regimen, since it can allow high drug exposure, and that other therapeutic options are worthy of further study. It would also be important to note that the distribution remains the same because it can be influenced by the physicochemical properties of gemcitabine and not by the route of absorption. In addition, the absence of accumulation may also be expected as the daily dose administered is not significantly different from that of the IV infusion.

This study involving physiologically based pharmacokinetic modeling combines the system-dependent physiological, anatomical and biochemical properties, specific properties of gemcitabine, as well as the formulation parameters, providing an approach to predict the plasma concentration–time profiles. We believe these can be important to support decision making throughout the drug research and development. Additionally, it is possible to use this information to determine the best dosing regimen for an effective and safe concentration, using the patient covariate values. This can be an example of personalized medicine based on potential new formulations for oral administration of gemcitabine, as well as nanotechnology-based drug delivery systems.

Switching from IV to the oral route (and vice versa) may be based not only on a comparison of C_p-time profiles but also on PBPK modeling. Therefore, joint PBPK simulations can be performed to examine the simulated PD effect (which may serve as a surrogate for the clinical effect). A robust gemcitabine PBPK model has not been developed yet. PBPK model evaluation can be performed using several methods. Model predictions of plasma concentration–time profiles can be graphically compared to observed profiles from the respective clinical studies. Subsequently, predicted plasma concentrations from all studies will be plotted against their corresponding observed values in goodness-of-fit plots.

Author Contributions: Conceptualization, N.V.; methodology, A.F. and N.V.; software, A.F.; validation, N.V., A.F. and R.L.; investigation, A.F. and N.V.; resources, N.V. and R.L.; writing—original draft preparation, A.F.; writing—review and editing, R.L. and N.V.; super-vision, N.V.; project administration, N.V.; funding acquisition, R.L. and N.V. All authors have read and agreed to the published version of the manuscript.

Funding: This work was financed by Fundo Europeu de Desenvolvimento Regional through the COMPETE 2020 (FEDER) Operational Programme for Competitiveness and Internationalization (POCI), Portugal 2020, and by Portuguese funds through Fundação para a Ciência e a Tecnologia (FCT), in the framework of CINTESIS, R&D Unit (Reference UIDB/4255/2020). N.V. also thanks the support of FCT and FEDER (European Union), Award Number IF/00092/2014/CP1255/CT0004. R.L. thanks FCT through Grant UID/QUI/50006/2019 (LAQV-REQUIMTE).

Institutional Review Board Statement: Not applicable.

Informed Consent Statement: Not applicable.

Data Availability Statement: Not applicable.

Acknowledgments: A.F. thanks FCT for the doctoral fellowship (PD/BD/135120/2017). The contents of this article are solely the responsibility of the authors and do not necessarily represent the official view of the FCT.

Conflicts of Interest: On behalf of all authors, the corresponding author states that there are no conflicts of interest.

References

1. Bray, F.; Ferlay, J.; Soerjomataram, I.; Siegel, R.L.; Torre, L.A.; Jemal, A. Global cancer statistics 2018: GLOBOCAN estimates of incidence and mortality worldwide for 36 cancers in 185 countries. *CA Cancer J. Clin.* **2018**, *68*, 394–424. [CrossRef]
2. Wong, A.; Soo, R.A.; Yong, W.-P.; Innocenti, F. Clinical pharmacology and pharmacogenetics of gemcitabine. *Drug Metab. Rev.* **2009**, *41*, 77–88. [CrossRef]
3. Mini, E.; Nobili, S.; Caciagli, B.; Landini, I.; Mazzei, T. Cellular pharmacology of gemcitabine. *Ann. Oncol.* **2006**, *17* (Suppl. 5), v7–v12. [CrossRef] [PubMed]
4. Jin, J.; Teng, C.; Li, T. Combination therapy versus gemcitabine monotherapy in the treatment of elderly pancreatic cancer: A meta-analysis of randomized controlled trials. *Drug Des. Devel. Ther.* **2018**, *12*, 475. [CrossRef]
5. Ciliberto, D.; Botta, C.; Correale, P.; Rossi, M.; Caraglia, M.; Tassone, P.; Tagliaferri, P. Role of gemcitabine-based combination therapy in the management of advanced pancreatic cancer: A meta-analysis of randomised trials. *Eur. J. Cancer* **2013**, *49*, 593–603. [CrossRef]
6. Louvet, C.; Labianca, R.; Hammel, P.; Lledo, G.; Zampino, M.G.; Andre, T.; Zaniboni, A.; Ducreux, M.; Aitini, E.; Taieb, J. Gemcitabine in combination with oxaliplatin compared with gemcitabine alone in locally advanced or metastatic pancreatic cancer: Results of a GERCOR and GISCAD phase III trial. *J. Clin. Oncol.* **2005**, *23*, 3509–3516. [CrossRef] [PubMed]
7. USA Food and Drug Admistration. GEMZAR®(Gemcitabine HCl) for Injection. FDA Label. Available online: https://www.accessdata.fda.gov/drugsatfda_docs/label/2011/020509s069lbl.pdf (accessed on 10 April 2021).
8. Yamamoto, N.; Nokihara, H.; Yamada, Y.; Uenaka, K.; Sekiguchi, R.; Makiuchi, T.; Slapak, C.A.; Benhadji, K.A.; Tamura, T. Phase I study of oral gemcitabine prodrug (LY2334737) in Japanese patients with advanced solid tumors. *Cancer Chemother. Pharmacol.* **2013**, *71*, 1645–1655. [CrossRef] [PubMed]
9. Hao, W.H.; Wang, J.J.; Hsueh, S.P.; Hsu, P.J.; Chang, L.C.; Hsu, C.S.; Hsu, K.Y. In vitro and in vivo studies of pharmacokinetics and antitumor efficacy of D07001-F4, an oral gemcitabine formulation. *Cancer Chemother. Pharmacol.* **2013**, *71*, 379–388. [CrossRef]
10. Wickremsinhe, E.; Bao, J.; Smith, R.; Burton, R.; Dow, S.; Perkins, E. Preclinical absorption, distribution, metabolism, and excretion of an oral amide prodrug of gemcitabine designed to deliver prolonged systemic exposure. *Pharmaceutics* **2013**, *5*, 261–276. [CrossRef]
11. Ferreira, A.; Lapa, R.; Vale, N. Combination of Gemcitabine with Cell-Penetrating Peptides: A Pharmacokinetic Approach Using in Silico Tools. *Biomolecules* **2019**, *9*, 693. [CrossRef]
12. Correia, C.; Xavier, C.P.R.; Duarte, D.; Ferreira, A.; Moreira, S.; Vasconcelos, M.H.; Vale, N. Development of potent CPP6-gemcitabine conjugates against human prostate cancer cell line (PC-3). *RSC Med. Chem.* **2020**, *11*, 268–273. [CrossRef]
13. Vale, N.; Ferreira, A.; Fernandes, I.; Alves, C.; Araujo, M.J.; Mateus, N.; Gomes, P. Gemcitabine anti-proliferative activity significantly enhanced upon conjugation with cell-penetrating peptides. *Bioorg. Med. Chem. Lett.* **2017**, *27*, 2898–2901. [CrossRef] [PubMed]
14. Food and Drug Administration. *Waiver of In Vivo Bioavailability and Bioequivalence Studies for Immediate-Release Solid Oral Dosage Forms Based on a Biopharmaceutics Classification System: Guidance for Industry*; Food and Drug Administration, Center for Drug Evaluation and Research, Department of Health and Human Services: Washington, DC, USA, 2000.
15. BioRender™. Available online: https://app.biorender.com/ (accessed on 10 April 2021).

16. DrugBank. Gemcitabine on DrugBank Database. Available online: https://www.drugbank.ca/drugs/DB00441 (accessed on 10 April 2021).
17. Wishart, D.S.; Feunang, Y.D.; Guo, A.C.; Lo, E.J.; Marcu, A.; Grant, J.R.; Sajed, T.; Johnson, D.; Li, C.; Sayeeda, Z.; et al. DrugBank 5.0: A major update to the DrugBank database for 2018. *Nucleic Acids Res.* **2018**, *46*, D1074–D1082. [CrossRef]
18. Lim, J.H.; You, S.K.; Baek, J.S.; Hwang, C.J.; Na, Y.G.; Shin, S.C.; Cho, C.W. Preparation and evaluation of polymeric microparticulates for improving cellular uptake of gemcitabine. *Int. J. Nanomed.* **2012**, *7*, 2307–2314. [CrossRef]
19. Wang, L.R.; Liu, J.; Huang, M.Z.; Xu, N. Comparison of pharmacokinetics, efficacy and toxicity profile of gemcitabine using two different administration regimens in Chinese patients with non-small-cell lung cancer. *J. Zhejiang Univ. Sci. B* **2007**, *8*, 307–313. [CrossRef] [PubMed]
20. Nieto, Y.; Aldaz, A.; Rifón, J.; Pérez-Calvo, J.; Zafra, A.; Zufia, L.; Viúdez, A.; Viteri, S.; Aramendía, J.M.; Aristu, J.; et al. Phase I and pharmacokinetic study of gemcitabine administered at fixed-dose rate, combined with docetaxel/melphalan/carboplatin, with autologous hematopoietic progenitor-cell support, in patients with advanced refractory tumors. *Biol. Blood Marrow Transpl.* **2007**, *13*, 1324–1337. [CrossRef]
21. Faivre, S.; Le Chevalier, T.; Monnerat, C.; Lokiec, F.; Novello, S.; Taieb, J.; Pautier, P.; Lhommé, C.; Ruffié, P.; Kayitalire, L.; et al. Phase I-II and pharmacokinetic study of gemcitabine combined with oxaliplatin in patients with advanced non-small-cell lung cancer and ovarian carcinoma. *Ann. Oncol.* **2002**, *13*, 1479–1489. [CrossRef]
22. Bjånes, T.K.; Jordheim, L.P.; Schjøtt, J.; Kamceva, T.; Cros-Perrial, E.; Langer, A.; Ruiz de Garibay, G.; Kotopoulis, S.; McCormack, E.; Riedel, B. Intracellular Cytidine Deaminase Regulates Gemcitabine Metabolism in Pancreatic Cancer Cell Lines. *Drug Metab. Dispos.* **2020**, *48*, 153–158. [CrossRef]
23. Tibaldi, C.; Camerini, A.; Tiseo, M.; Mazzoni, F.; Barbieri, F.; Vittimberga, I.; Brighenti, M.; Boni, L.; Baldini, E.; Gilli, A.; et al. Cytidine deaminase enzymatic activity is a prognostic biomarker in gemcitabine/platinum-treated advanced non-small-cell lung cancer: A prospective validation study. *Br. J. Cancer* **2018**, *119*, 1326–1331. [CrossRef]
24. Thompson, B.R.; Hu, Y.; Smith, D.E. Mechanisms of gemcitabine oral absorption as determined by in situ intestinal perfusions in mice. *Biochem. Pharmacol.* **2019**, *168*, 57–64. [CrossRef]
25. Pastor-Anglada, M.; Urtasun, N.; Pérez-Torras, S. Intestinal nucleoside transporters: Function, expression, and regulation. *Compr. Physiol.* **2011**, *8*, 1003–1017.
26. Veltkamp, S.A.; Jansen, R.S.; Callies, S.; Pluim, D.; Visseren-Grul, C.M.; Rosing, H.; Kloeker-Rhoades, S.; Andre, V.A.M.; Beijnen, J.H.; Slapak, C.A.; et al. Oral Administration of Gemcitabine in Patients with Refractory Tumors: A Clinical and Pharmacologic Study. *Clin. Cancer Res.* **2008**, *14*, 3477–3486. [CrossRef] [PubMed]

CHAPTER 4

New *in vitro-in silico* approach for the prediction of *in vivo* performance of drug combinations

Cristiana Correia, **Abigail Ferreira**, Joana Santos, Marjo Yliperttula, Arto Urtti, Nuno Vale

Molecules, **2021**, 26(14), pp. 4257. DOI: 10.3390/molecules26144257

Combination therapy of conventional anticancer drugs with repurposed drugs is a very promising approach that has demonstrated encouraging results. This work evaluated the combinations of anticancer drugs gemcitabine and 5- fluorouracil (5-FU) with repurposed drugs itraconazole, verapamil or tacrine *in vitro*, for their activity against cancer cell lines. Subsequently, these results were analyzed using multiple pharmacokinetic compartmental models developed in this work. This research has coupled *in vitro* bioactivity data and *in silico* tools to study the relationship between tissue drug concentration and inhibition of cell growth. Of the investigated combinations, itraconazole was the most effective in combination with either reference anticancer drugs, showing dose-dependent cell growth inhibition, and an increase in effect was predicted if itraconazole administration was continued.

molecules

MDPI

Article

New In Vitro-In Silico Approach for the Prediction of In Vivo Performance of Drug Combinations

Cristiana Correia [1,2], Abigail Ferreira [1,3], Joana Santos [1], Rui Lapa [3], Marjo Yliperttula [4], Arto Urtti [4] and Nuno Vale [1,5,*]

[1] OncoPharma Research Group, Center for Health Technology and Services Research (CINTESIS), Rua Dr. Plácido da Costa, 4200-450 Porto, Portugal; cristianacorreia95@gmail.com (C.C.); abigail.ferreira@fc.up.pt (A.F.); jmdmsantos@hotmail.com (J.S.)
[2] Faculty of Sciences, University of Porto, Rua do Campo Alegre, s/n, 4169-007 Porto, Portugal
[3] LAQV/REQUIMTE, Laboratory of Applied Chemistry, Department of Chemical Sciences, Faculty of Pharmacy, University of Porto, Rua de Jorge Viterbo Ferreira, 228, 4050-313 Porto, Portugal; ruilapa@ff.up.pt
[4] Division of Pharmaceutical Biosciences, Faculty of Pharmacy, University of Helsinki, P.O. Box 56, 00014 Helsinki, Finland; marjo.yliperttula@helsinki.fi (M.Y.); arto.urtti@helsinki.fi (A.U.)
[5] MEDCIDS—Department of Community Medicine, Health Information and Decision, Faculty of Medicine, University of Porto, Alameda Prof. Hernâni Monteiro, 4200-319 Porto, Portugal
* Correspondence: nunovale@med.up.pt; Tel.: +351-220-426-537

Abstract: Pharmacokinetic (PK) studies improve the design of dosing regimens in preclinical and clinical settings. In complex diseases like cancer, single-agent approaches are often insufficient for an effective treatment, and drug combination therapies can be implemented. In this work, in silico PK models were developed based on in vitro assays results, with the goal of predicting the in vivo performance of drug combinations in the context of cancer therapy. Combinations of reference drugs for cancer treatment, gemcitabine and 5-fluorouracil (5-FU), and repurposed drugs itraconazole, verapamil or tacrine, were evaluated in vitro. Then, two-compartment PK models were developed based on the previous in vitro studies and on the PK profile reported in the literature for human patients. Considering the quantification parameter area under the dose-response-time curve (AUC_{effect}) for the combinations effect, itraconazole was the most effective in combination with either reference anticancer drugs. In addition, cell growth inhibition was itraconazole-dose dependent and an increase in effect was predicted if itraconazole administration was continued (24-h dosing interval). This work demonstrates that in silico methods and AUC_{effect} are powerful tools to study relationships between tissue drug concentration and the percentage of cell growth inhibition over time.

Keywords: in vitro-in silico approach; pharmacokinetics; drug repurposing; drug combination; cell growth inhibition

Citation: Correia, C.; Ferreira, A.; Santos, J.; Lapa, R.; Yliperttula, M.; Urtti, A.; Vale, N. New In Vitro-In Silico Approach for the Prediction of In Vivo Performance of Drug Combinations. *Molecules* **2021**, *26*, 4257. https://doi.org/10.3390/molecules26144257

Academic Editor: Sérgio F. Sousa

Received: 6 May 2021
Accepted: 9 July 2021
Published: 13 July 2021

1. Introduction

The process of research and development (R&D) of new drugs is very time consuming and expensive. New drugs approval takes on average seven to nine years and the cost of introducing a new drug can range from 600 million to 1 billion euros [1,2]. Pharmacokinetic (PK) models describe the absorption, distribution, metabolism, and the elimination of molecules (drugs, compounds under development, etc.) in an organism, thus providing useful information to foster efficient and informative drug development. These models not only improve decision making throughout clinical drug development, but also enable the design and optimization of dosing regimens, increasing the chances of the drug to reach its target with the desired concentration and drug plasma concentration to be maintained within the therapeutic window [3–5]. The study of PK involves both theoretical and experimental approaches. Theoretical approaches aim at the development of PK models to predict drug disposition, which includes drugs distribution and elimination

after its administration. These models can be divided into three categories, empirically, physiologically, and compartmentally based PK models [6]. The most used PK model is the compartmentally based, which represents a very simple and useful tool in PK. In this model type, tissues are grouped into compartments, depending on their blood flow and drug binding (tissues with similar blood flow and drug tissue binding are grouped in the same compartment) [3–5,7–9].

STELLA® (ISEE Systems Inc., Lebanon, PA, USA) is a simulation software application that enables the study of systems through its graphical representation. The program uses Compartments, Flows, Converters, and Connectors as building blocks. "Compartments" accumulate whatever flows into them, net of whatever flows out of them, with "Flows" filling and draining accumulations. The Converter serves a utilitarian role in the software. It holds values for constants, defines external inputs to the model and calculates algebraic relationships. In general, it converts inputs into outputs. Connectors, as its name suggests, connect model elements. Moreover, the use of built-in time functions in converters, such as AND, OR, IF . . . THEN . . . ELSE or PULSE, allows a set of rules to be established, which are used by the program to control flow through the model, enabling the construction of more complex models. When the model is complete, the user has only to establish a simulation time period and a time increment (h). Each value calculation can be made using either Euler's, 2nd, 3rd, or 4th order Runge-Kutta methods, being Euler's the simplest version of the Runge-Kutta method. These are integration methods that estimate a new value (y_{i+1}) through the extrapolation of an old value (y_i) following Equation (1). In Euler's method, φ is the slope in x_i (first derivate in x_i). In the Runge-Kutta method, instead of one single derivation, one or more representative slopes (depending on the order of the method) are determined during an interval, h, to estimate the new value. This equation can be applied step by step and trace out the trajectory of the solution (Figure 1) [10–13].

$$y_{i+1} = y_i + \varphi h \quad (1)$$

GastroPlus™ (Simulations Plus, Inc., Lancaster, CA, USA) is an advanced technology computational program used in drug R&D. Contrary to STELLA®, GastroPlus™ is specifically designed for PK studies, particularly physiologically based pharmacokinetics (PBPK) and physiologically based biopharmaceutics modeling (PBBM). Additionally, its incorporated absorption model, ACAT (Advanced Compartmental Absorption and Transit model), allows the simulation of intravenous, gastrointestinal, ocular, nasal, and pulmonary absorption of molecules. This enables the user to obtain a detailed absorption profile of the molecules in study, since it considers several physiological variables. GastroPlus™ simulations rely on the numerical integration of differential equations that coordinate a set of well-characterized physical events that occur and are interconnected as a result of diverse physicochemical and biologic phenomena. Furthermore, GastroPlus™ has additional modules, including ADMET Predictor™ module for the prediction of physicochemical and pharmacokinetic parameters of compounds, and other modules for deeper insight into the pharmacokinetics of a drug, such as PKPlus™ and PBPKPlus™. Despite its sophistication, GastroPlus™ is relatively easy for someone with a background in ADME to learn and use because it incorporates an intuitive and modern graphical user interface that enables a rapid and smooth transition from setting up inputs to evaluating results [14].

The lack of satisfactory results with single-agent therapy in patients led to the introduction of drug combination therapies in health care. The use of drugs with different mechanisms of action enables multiple targeting, either within the same cell or in multiple cell subpopulations, or the targeting of multiple diseases simultaneously, providing more effective treatment. This strategy's possible favorable outcome includes the enhancement of the efficacy of the therapeutic effect, reducing the dosage, but increasing or maintaining the efficacy, minimizing or avoiding possible toxicity, and reducing or slowing down the development of drug resistance. Due to these therapeutic benefits, drug combinations have been widely used and became the leading choice for treating complicated and complex diseases, such as cancer and infectious diseases, including AIDS [15–17].

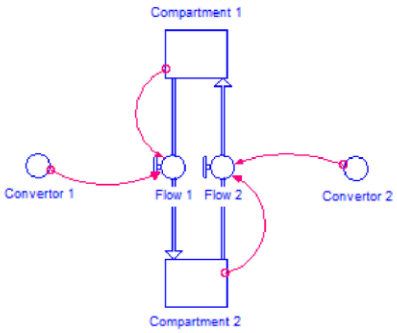

Figure 1. Schematic representation of a model built in STELLA® modeling program. In this model, mass flows from compartment 1 to compartment 2 and from compartment 2 to compartment 1. Flow rates 1 and 2 are determined by convertor 1 and 2 respectively.

Several in silico tools have been developed for theoretical drug combination studies. Some research areas are more focused on predicting whether the combined effect may be synergistic, additive or antagonistic, while others are more interested in predicting drug-drug interactions. For this, several PK modeling programs, such as Simcyp® (Certara UK Limited, Sheffield, UK) or GastroPlus™, now have specific modules to predict drug-drug interaction, using previous knowledge on main metabolizing enzymes of each drug in study [18–20]. Although a wide variety of in silico tools is already available for drug combination studies, new approaches can be proposed, and drug combination effect coupled with drug disposition simulation is an example of a gap in the existing resources.

Cancer treatment by chemotherapy is one of the most used methodologies in cancer therapy, either as primary treatment or as an adjuvant to other treatment modalities, such as surgery, radiotherapy or immunotherapy. This approach involves the use of low-molecular-weight drugs to destroy or reduce the proliferation of cancer cells [21]. This work evaluated the activity of two traditional anticancer drugs (ACDs), gemcitabine and 5-fluorouracil (5-FU), and the effect of the combination of these ACDs with repurposed drugs itraconazole, verapamil and tacrine, based on and extending previous research carried out by our group [22].

The goal of the present study was to evaluate, model and predict the performance of anticancer drugs and drug combinations in humans, through in vitro and in silico approaches. In short, the drug combinations effect was evaluated through in vitro methodologies and the results were then modeled and analyzed in silico in more detail. Inhibition of cell growth was assessed with the MTT cell viability assay in healthy and cancer human prostate cell lines (PNT2 and PC-3, respectively), and in NSCLC human cell line A549. Six different drug combinations were tested, where one of the drugs is a clinically used anticancer drug (ACD) (gemcitabine or 5-fluorouracil) and the other is a repurposed drug (RD) with promising qualities for cancer treatment (itraconazole, verapamil and tacrine). At this stage in our research, the main goal was to understand if ACDs' activity is enhanced in the presence of one of the RD in these cell lines. Then, the aim of the in silico approach was the development of two-compartment PK models that mimic the drug combination effect previously assessed in vitro and to couple it to drug's human PK. In sum, using multiples approaches, this work provides a better general comprehension of drug combinations' performance in the context of cancer therapy, allowing the assessment of the PK behavior in the human body over time, and the evaluation of varying doses and its influence.

2. Materials and Methods

2.1. Chemicals

Gemcitabine, 5-FU, itraconazole, tacrine, and verapamil were obtained from Sigma-Aldrich®/Merck© (2021 Merck KGaA, Darmstadt, Germany) and dissolved in sterile

dimethyl sulfoxide (DMSO) at 100, 50, 17, 10 and 10 μM, respectively, as stock solutions. The drugs were stored at −20 °C and diluted with culture medium prior to use.

2.2. Cell Culture

The normal human prostate epithelium cell line PNT-2, human prostate adenocarcinoma cell line PC-3 and human lung carcinoma cell line A549 were obtained from the American Type Culture Collection and maintained in RPMI-1640 medium with 2 mM L-glutamine (Gibco™, Thermo Fisher Scientific, Inc., Waltham, MA, USA) supplemented with 10% heat-inactivated fetal bovine serum (FBS) (Gibco™) at 37 °C in a 5% CO_2 atmosphere.

All the cell culture procedures were carried out under sterile conditions in biological safety cabinets, using sterile reagents and materials. Cells were routinely kept exponentially growing and were sub-cultured by trypsinization twice a week. Cell viability of the cell cultures was routinely evaluated using the trypan blue exclusion assay. All experiments were carried out with exponentially growing cells having over 90% of cell viability.

2.3. Evaluation of Cell Growth Inhibition with the MTT Assay

2.3.1. Dose-Response Curve Determination for ACDs and ACD-RD Combinations

The optimal cell concentration determined was 4×10^4 cells/mL (for all the cells lines) and was then used in the MTT assays. The cells were incubated for 72 h with different concentrations of ACD or ACD-RD combination. Cells were allowed to adhere to the plate for 24 h and then 100 μL/well of drug solution were added. The multiple serial dilutions tested of each drug solution were prepared in culture medium (RPMI-1640 medium + 10% FBS). The concentrations tested ranged from 0.01 to 50 μM for gemcitabine and from 0.05 to 100 μM for 5-FU. When evaluating drug combinations, 50 μL/well of different concentrations of the ACD (gemcitabine or 5-FU) were added to the cells along with 50 μL/well of a fixed concentration of RD. The same ranges of concentrations for gemcitabine and 5-FU were tested and the chosen concentration of each RD was based on the maximum plasma concentration (C_{max}) found in the literature. Since gemcitabine is a prodrug, which is phosphorylated into an active drug inside the cells, we assume this conversion is complete, and something similar for 5-FU as well. As such, verapamil, itraconazole and tacrine solutions were prepared and used in this assay with the concentrations of 1, 8.5 and 0.24 μM, respectively [23–26]. A DMSO control was also included in the experiments (maximum concentration used, 0.2%, was previously considered non-toxic to the cells). After 72-h incubation, the media was removed by aspiration, 100 μL/well of MTT solution (0.5 mg/mL in media) was added to each well and cells were incubated for another 3 h. The MTT solution was then removed by aspiration, cells were washed with 100 μL/well of PBS and 100 μL/well of DMSO were added to dissolve the formazan crystals. Absorbance was read in a spectrometer (Varioskan™ LUX multimode microplate reader) at 540 nm. Results were treated in Microsoft Excel and GraphPad Prism 6. The dose-response curves for each treatment were then plotted in appropriate graphs, differences between treatments were compared and the IC50 value, indicating the concentration resulting in inhibition of 50% of the maximal cell growth, was determined. The percentage of cell growth inhibition resulting from each drug was calculated as: [(OD 540 control cells—OD 540 treated cells)/OD 540 control cells] × 100. These assays were repeated in at least three independent experiments.

2.3.2. Further Studies with Itraconazole in Combination with Gemcitabine or 5-FU

The results from the previous assay demonstrated itraconazole had the greatest ability to enhance ACDs' activity. To study how the drug combination response is affected by itraconazole concentration, additional studies were performed. For these, only the human lung carcinoma cell line A549 was used for simplification purposes. Two studies were then performed:

1. Range of itraconazole concentrations + fixed concentration of ACD (Gem or 5-FU); itraconazole's concentrations ranged from 0.07 to 4.25 μM, since the concentration

used in the previous experiments was 8.5 μM (note dilution factor of 2 in the well). The concentration chosen for Gem and 5-FU was the one that showed the lowest effect in the previous experiments: 0.01 and 1 μM, respectively. The ACDs were also tested alone for control purposes;

2. Range of ACD (Gem or 5-FU) concentrations + fixed concentration of itraconazole (three different concentrations were tested). Different concentrations of ACD (Gem or 5-FU) were added to the wells, as well as a fixed concentration of itraconazole. The multiple serial dilutions tested for ACD ranged from 0.005 to 10 μM for Gem (since in the previous experiments the resulting dose-response curve did not have the ideal shape), and the range was maintained for 5-FU. The concentrations for itraconazole were 2, 4 and 6 μM (concentrations within the range that showed an effect when administered with a very low concentration of ACD). Itraconazole was also tested alone for control purposes.

As previously mentioned, following the 72-h cellular treatment, MTT assay was performed. These assays were repeated in at least three independent experiments each.

2.4. Model Development

From data available in the literature and the results of the experimental work, pharmacokinetic models were built in the simulation software STELLA® 10.0.3 (ISEE Systems Inc., Lebanon, PA, USA). The structure of the model, as well as all the equations, variables and constants used for this purpose, are described in detail in the following sections.

2.4.1. WinNonlin: PK Analysis

Compartmentally based PK STELLA® models require the input of PK parameters of each drug, such as the volume of distribution in central and tissue compartment (V_{d1} and V_{d2}, respectively), clearance (CL) and transfer rate constants from central compartment to tissue compartment and from tissue compartment to central compartment (k_{12} and k_{21}, respectively). Ideally, all parameters would belong to the same source: human plasma concentration versus time data (C_p-time data) belonging to the same ethnicity, gender, and age. Due to lack of data available in the literature concerning this issue, the only mandatory conditions were that collected data for this study was from human patients and that all the PK data for each drug belonged to the same literature source.

Phoenix WinNonlin (Certara UK Limited, Sheffield, UK) is a pharmacokinetic/ pharmacodynamic (PK/PD) modeling software that, through the analysis of the C_p-time data of a certain drug, can generate its PK parameters.

For gemcitabine, the C_p-time data collected were from NSCLC Chinese patients [27]. Briefly, gemcitabine was intravenously infused for 120 min at a rate of 15.7 mg·min^{-1} and plasma samples were collected until 210 min after infusion start. In relation to 5-FU, C_p-time data collected belonged to English cancer patients [28]. 5-FU was administered over 1 min, by intravenous bolus injection, at a dose of 900 mg. Plasma samples were collected for 90 min. For itraconazole, the data is relative to healthy subjects from The Netherlands, who received 100 mg administered intravenously, over 1 h, and plasma samples were collected for 96 h [29].

2.4.2. Model Structure

Several models were built depending on the case study, since each drug has a specific route of administration and particular properties. The model structure differs according to the variables, constants and some equations corresponding to each case. Moreover, the drugs in each drug combination do not share metabolic pathways or transporters and only one has high protein binding. Therefore, it can be assumed that no drug interaction will occur, and each drug disposition will not be affected. Therefore, the compartmental models are developed for each drug separately, but they are connected in the same human model. The layout of each model will be detailed for each case.

2.4.3. Determination of the AUC for Each Drug Combination Effect in Humans

AUC is usually calculated when bioavailability is concerned, to compare two different drug formulations, routes of administration or the effect of food on the bioavailability of a certain drug, for example [30,31]. In the models developed in this work, "AUC plasma concentration" was calculated for model validation purposes. "AUC_{effect}" was determined to evaluate the overall effect of each drug combination tested in the NSCLC cell line A549. In current STELLA® models, AUC is recorded using a separate compartment, but it follows a principle which is mathematically expressed in Equation (2):

$$AUC = AUC(t - dt) + \text{"variable in study"} * dt \quad (2)$$

The model built for gemcitabine and 5-FU is a two-compartmental model since their C_p-time profile has a two-compartment distribution. Using gemcitabine and 5-FU C_p-time data for intravenous infusion obtained from literature and the PK/PD modeling program Phoenix WinNonlin (64-bit, version 7.00), the curve that best fitted the experimental values obtained in the experimental in vitro approach was traced and the values for each PK parameter (V_{d1}, V_{d2}, CL, k_{12} and k_{21}) were obtained. Therefore, with the input of the parameters obtained through WinNonlin, the models developed in STELLA® describe the disposition of each drug over time, after intravenous infusion. The input dose is also the same as the one reported in the literature source used (infusion of 15.7 $mg \cdot min^{-1}$ for 120 min for gemcitabine, and bolus injection of 900 mg for 5-FU).

The gemcitabine and 5-FU concentration-dependent percentage of cell growth inhibition was determined by the previous in vitro studies, where a range of concentrations of either gemcitabine or 5-FU was tested. Therefore, in the models, gemcitabine/5-FU tissue concentration was linked to percentage of cell growth inhibition in cancer cells, i.e., the percentage of cell growth inhibition depends on the concentration of anticancer drug in the tissue compartment over time. Although tumor microenvironments have different characteristics from healthy tissues, including vascularization and permeability, for simplification purposes, in the developed models it was assumed that tumor tissue behaves the same way as other tissues grouped in tissue compartments.

Dose-response curves were obtained from the in vitro studies in the A549 cell line as reported above. With the constants obtained from those curves, such as the lowest and highest effect achieved ("Bottom" and "Top" respectively), the steepness of the curve ("Steepness factor") and the drug concentration at which 50% of the maximum effect was obtained ("EC_{50}"), the effect over time can be determined through a Hill Equation (3) (because tissue concentration will vary over time):

$$\%\ \text{of effect} = (\text{Bottom}) + \frac{(\text{Top}) - (\text{Bottom})}{1 + \left(\frac{\text{tissue concentration}}{EC_{50}}\right)^{-\text{steepness factor}}} \quad (3)$$

The parameters from all the 8 dose-response curves were used in this model (one at a time) and for each, the AUC_{effect} was evaluated: Gemcitabine alone; gemcitabine + itraconazole 2 μM; gemcitabine + itraconazole 4 μM and gemcitabine + itraconazole 6 μM; 5-FU alone; 5-FU + itraconazole 2 μM; 5-FU + itraconazole 4 μM and 5-FU + itraconazole 6 μM. All the variables, such as drug plasma concentration, drug tissue concentration, drug amount eliminated, and percentage of effect can be plotted in graphs or tables and evaluated over time.

For the simulations, Runge-Kutta 4th order integration method was used since it is the most accurate integration method available in STELLA®. Simulation length and step size (h) were chosen in a way that h was low enough to give accurate results without compromising the speed of the simulation and simulation length was long enough to allow the lower effect value to be reached. Therefore, $h = 0.02$ and 400 min of simulation length were used for gemcitabine and $h = 0.02$ and 200 min of simulation length were used for 5-FU.

Figures 2 and 3 show the models for gemcitabine and 5-FU, respectively, without itraconazole (I = 0 μM). For the combinations of gemcitabine or 5-FU with itraconazole, the exact same layout was used and only the "Bottom", "Top", "Steepness factor" and "EC_{50}" variables were changed, according to each situation.

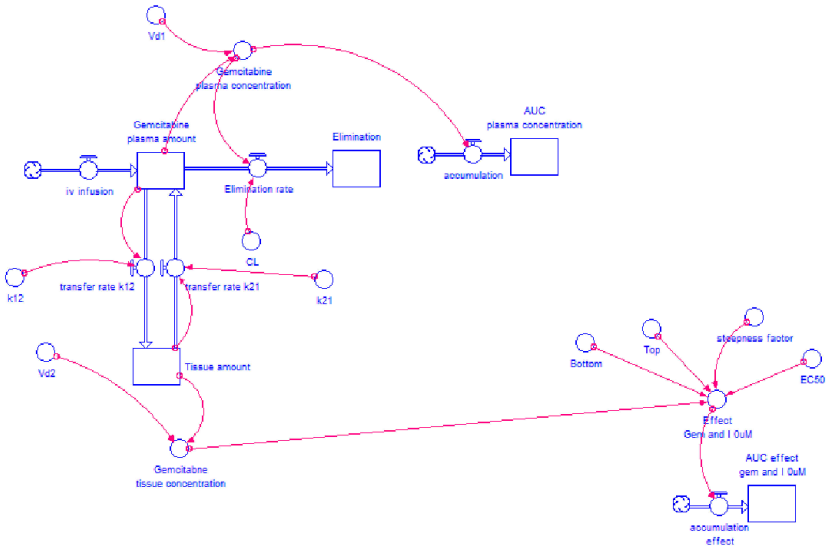

Figure 2. Two-compartment model of gemcitabine intravenous infusion administration. The drug is infused to plasma compartment at a rate of 15.7 mg·min^{-1} for 120 min. The drug is transferred from plasma compartment to tissue compartment and vice versa at a rate defined by "k_{12}" × "gemcitabine plasma amount" and "k_{21}" × "Tissue amount", respectively, where "k_{12}" and "k_{21}" are transfer rate constants. The drug is eliminated from plasma compartment to elimination compartment at a rate defined by "CL" × "gemcitabine plasma concentration" where "CL" is a constant and "gemcitabine plasma concentration" is a variable that changes over time. "Gemcitabine plasma concentration" is the result of "gemcitabine plasma amount" divided by "V_{d1}", while "gemcitabine tissue concentration" results from "Tissue amount" divided by "V_{d2}". "Gemcitabine plasma amount" is the net result of the amount of drug that leaves plasma compartment (to elimination and tissue compartment) and the amount that enters in this compartment (coming from the infusion and tissue compartment). "AUC plasma concentration" is generated through Equation (2), where the variable in study is "gemcitabine plasma concentration". Considering Equation (3), "gemcitabine tissue concentration" and the four parameters obtained from gemcitabine without itraconazole dose-response curve ("Bottom", "Top", "Steepness factor" and "EC_{50}"), the effect of gemcitabine alone is modelled over time.

2.4.4. Itraconazole's Dose-Dependent Effect, when Combined with Gemcitabine or 5-FU

After quantification of each drug combination effect (through the determination of their AUC_{effect}), where the main variable was ACD tissue concentration, itraconazole's dose-dependent effect was evaluated. At this stage, the exact same 8 dose-response curves were considered: ACD alone; ACD + itraconazole 2 μM; ACD + itraconazole 4 μM and ACD + itraconazole 6 μM. The difference from the previous study lies in the addition of a second two-compartment model (this time for itraconazole) and the itraconazole dose-dependent effect evaluation. For this purpose, three different itraconazole doses were evaluated in the simulations (100, 300 and 500 mg). ACD doses remained the same as in the previous study (1884 mg of gemcitabine and 900 mg of 5-FU).

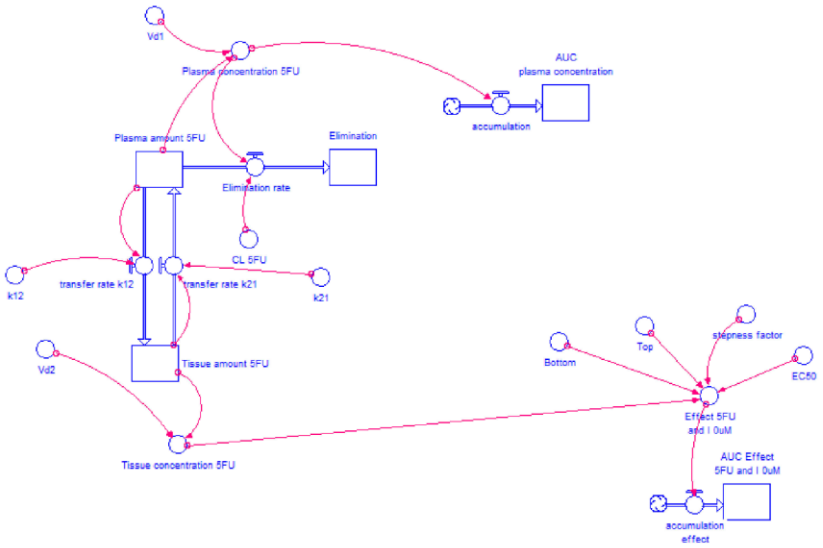

Figure 3. Two-compartment model of 5-FU intravenous injection administration. The drug is injected into plasma compartment at a dose of 900 mg. The drug is transferred from plasma compartment to tissue compartment and vice versa at a rate defined by "k_{12}" × "Plasma amount 5-FU" and "k_{21}" × "Tissue amount 5-FU", respectively, where "k_{12}" and "k_{21}" are transfer rate constants. The drug is eliminated from plasma compartment to elimination compartment at a rate defined by "CL" × "Plasma concentration 5-FU", where "CL" is a constant and "Plasma concentration 5-FU" is a variable that changes over time. "Plasma concentration 5-FU" is the result of "Plasma amount 5-FU" divided by "V_{d1}" while "Tissue concentration 5-FU" results from "Tissue amount 5-FU" divided by "V_{d2}". "Plasma amount 5-FU" is the net result of the amount of drug that leaves plasma compartment (to elimination" or tissue compartment) and the amount that enters in this compartment (coming from tissue compartment). "AUC plasma concentration" is generated through Equation (2) where the variable in study is "Plasma concentration 5-FU". Considering Equation (3), "Tissue concentration 5-FU" and the four parameters obtained from 5-FU without itraconazole dose-response curve ("Bottom", "Top", "Steepness factor" and "EC_{50}"), the effect of 5-FU alone is modeled over time.

Two-compartment PK models were built for each ACD in study, in accordance with the literature information about the model that best fits their C_p-time data. Although itraconazole is most frequently administered orally, the intravenous infusion was selected to avoid the low oral bioavailability characteristic of this drug. Therefore, based on the literature human C_p-time data for intravenous infusion of itraconazole and using the WinNonlin program, all PK parameters needed for two-compartment model construction were collected and the model was built.

Only the "Bottom" value of the ACD dose-response curve was found to be significantly affected by itraconazole concentration. Therefore, equations that relate the change of "Bottom" value with the concentration of itraconazole were included in "Bottom" Converter, i.e., the percentage of cell growth inhibition is given taking into account not only ACD concentration (Equation (3), but also the influence of itraconazole concentration on "Bottom" value. Equation (4) describes the change of "Bottom" value in gemcitabine + itraconazole dose-response curves and Equation (5) describes it for the 5-FU + itraconazole combination. x is itraconazole tissue concentration, in $\mu g \cdot mL^{-1}$. In relation to the other variables that describe dose-response curve ("Top", "Steepness factor" and "EC_{50}"), the average of the three values (relative to ACD + itraconazole 2, 4 and 6 μM dose-response curves) were used. The model for gemcitabine + itraconazole combination is shown in Figure 4. 5-FU + itraconazole combination model is shown in Figure 5. Again, the exact same layout was used to test three different doses of itraconazole, and 5-FU dose remained the same. All

the variables, such as drug plasma concentration, drug tissue concentration, drug amount eliminated, and percentage of effect can be plotted in graphs or tables and evaluated over time. Similar Runge-Kutta 4th order integration methods were used.

$$\text{Bottom} = 2.44x^2 - 1.95x - 1.06 \quad (4)$$

$$\text{Bottom} = 2.15x^2 - 1.15x - 0.47 \quad (5)$$

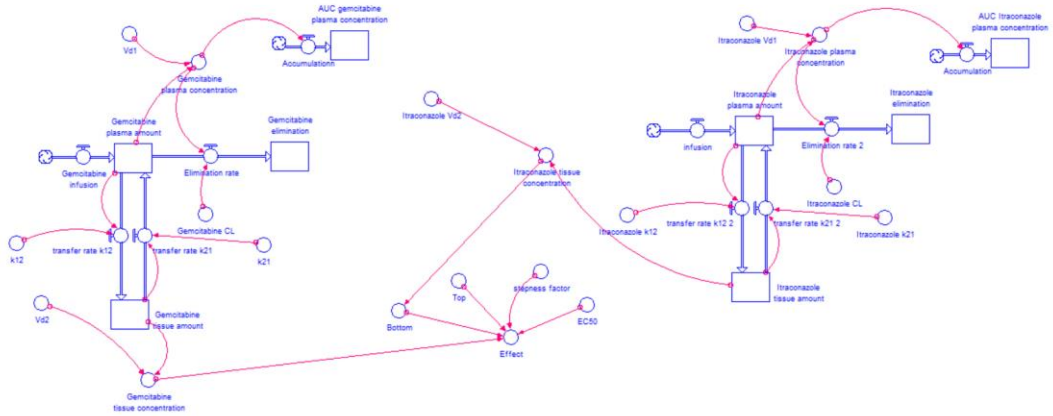

Figure 4. Two-compartment PK model for gemcitabine with IV infusion, two-compartment PK model for itraconazole with IV infusion and the relation of their tissue concentration with percentage of cell growth inhibition in A549 cancer cell line. Gemcitabine's model has been described in Figure 2. For itraconazole compartmental model, drug is infused to plasma compartment at a rate of 8.3, 5 or 1.7 mg·min^{-1} during 1 h (500, 300 or 100 mg doses, respectively). It is transferred from plasma compartment to tissue compartment and vice versa at a rate defined by "k_{12}" × "Itraconazole plasma amount" and "k_{21}" × "Itraconazole tissue amount", respectively, where "k_{12}" and "k_{21}" are transfer rate constants. The drug is eliminated from plasma compartment to elimination compartment at a rate defined by "CL" × "Itraconazole plasma concentration", where "CL" is a constant and "Itraconazole plasma concentration" is a variable that changes over time. "Itraconazole plasma concentration" is the result of "Itraconazole plasma amount" divided by "V_{d1}" while "Itraconazole tissue concentration" results from "Itraconazole tissue amount" divided by "V_{d2}". "Itraconazole plasma amount" is the net result of the amount of drug that leaves plasma compartment (to elimination and tissue compartment) and the amount that enters in this compartment (coming from infusion and tissue compartment). "AUC plasma concentration" is generated through Equation (2), where variable in study is "Itraconazole plasma concentration". Considering Equation (3), "Gemcitabine tissue concentration", the average of gemcitabine + itraconazole dose-response curve parameters "Top", "Steepness factor" and "EC_{50}", and Equation (4), itraconazole dose-dependent effect was modelled.

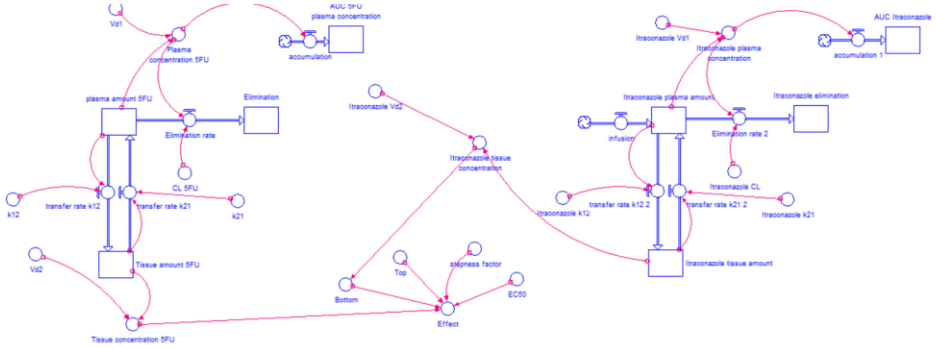

Figure 5. Two-compartment PK model for 5-FU with IV injection (described in Figure 3), two-compartment model for itraconazole with IV infusion and the relation of their tissue concentration with percentage of cell growth inhibition in A549 cancer cell line. For itraconazole, compartment model drug is infused to plasma compartment at a rate of 8.3, 5 or 1.7 mg·min^{-1} during 1 h (500, 300, or 100 mg doses, respectively). It is transferred from plasma compartment to tissue compartment and vice versa at a rate defined by "k_{12}" × "Itraconazole plasma amount" and "k_{21}" × "Itraconazole tissue amount", respectively, where "k_{12}" and "k_{21}" are transfer rate constants. The drug is eliminated from plasma compartment to elimination compartment at a rate defined by "CL" × "Itraconazole plasma concentration", where "CL" is a constant and "Itraconazole plasma concentration" is a variable that changes over time. "Itraconazole plasma concentration" is the result of "Itraconazole plasma amount" divided by "V_{d1}", while "Itraconazole tissue concentration" results from "Itraconazole tissue amount" divided by "V_{d2}". "Itraconazole plasma amount" is the net result of the amount of drug that leaves plasma compartment (to elimination and tissue compartment) and the amount that enters in this compartment (coming from infusion and tissue compartment). "AUC plasma concentration" is generated through Equation (2) where variable in study is "Itraconazole plasma concentration". Considering Equation (3), "Tissue concentration 5-FU", the average of 5-FU + itraconazole dose-response curve parameters "Top", "Steepness factor" and "EC_{50}", and Equation (5), itraconazole dose-dependent effect was modelled.

2.5. Model Validation

Two assessments were carried out to establish whether two-compartment models were well-constructed and that there were no errors in parameter inputs. First, STELLA® generated C_p-time curves were plotted against literature C_p-time data and general shape of the curve and fitting was evaluated. AUC plasma concentration was another parameter used to evaluate the accuracy of the models. Therefore, using the exact same dosages and routes of administration as the ones used in the literature experiments, C_p-time curve and AUC plasma concentration were determined and compared with literature data.

The results of the present study provide new insight in ACD and RD combinations evaluated for lung and prostate cancer treatment and a new tool to quantify drug combinations effect, as the area under the dose-response-time curve, or AUC_{effect}. Furthermore, the innovative idea developed in this work resides in an in silico study that enables the coupling of cell viability assay data with human drug disposition.

3. Results and Discussion

3.1. In Vitro Experiments—Evaluation of Inhibition of Cell Growth

To evaluate the effect of six drug combinations (ACD gemcitabine or 5-FU with RD itraconazole, verapamil or tacrine) in cell proliferation, MTT assay was performed following 72-h treatment in human lung carcinoma A549 cell line, human prostate adenocarcinoma PC-3 cell line and normal human prostate epithelium PNT2 cell lines.

3.1.1. Range of ACD Concentrations + Fixed Concentration of RD

Firstly, several ACD concentrations (gemcitabine or 5-FU) were tested with or without RD (itraconazole, verapamil or tacrine) at a fixed concentration. The dose-response curves are represented in Figures 6 and 7.

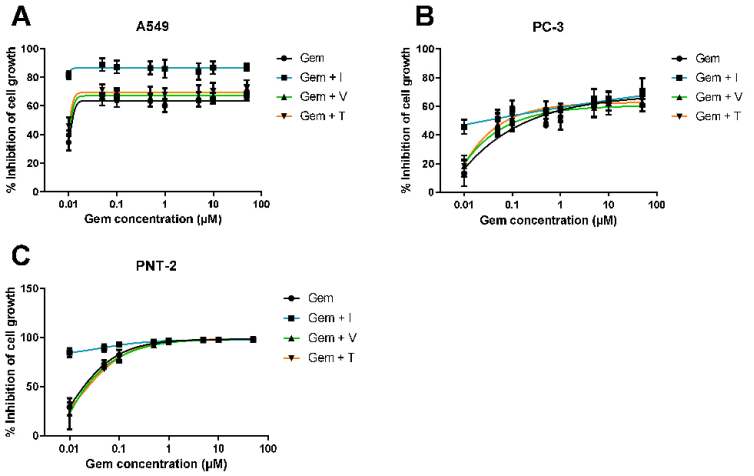

Figure 6. Dose-response curve of gemcitabine in combination with RD. Percentage of cell growth inhibition of human lung carcinoma A549 cell line ((**A**)—top left), human prostate adenocarcinoma PC-3 cell line ((**B**)—right top) and normal human prostate epithelium PNT2 cell line ((**C**)— bottom left), treated with a wide range of concentrations of gemcitabine (Gem) alone (black line) or Gem in combination with a fixed concentration of RD (verapamil, V, green line; itraconazole, I, blue line; or tacrine, T, orange line), during 72 h, determined with MTT assay. The results are the mean of at least three independent experiments. The DMSO control did not present toxicity to the cells (data not shown).

These results show all tested cell lines are sensitive to gemcitabine and 5-FU but to different degrees. The dose-response curve for gemcitabine and 5-FU alone is approximate to gemcitabine and 5-FU in combination with verapamil or tacrine, in all cell lines. On the other hand, itraconazole combination substantially improved the overall effect, comparing to ACD alone. In healthy and cancer prostate cell lines (PNT2 and PC-3, respectively), itraconazole effect is more noticeable when gemcitabine concentration is low (<0.5 μM in PNT2 and <0.1 μM in PC-3 cell lines). At higher concentrations, Gem + I curve matches the control line, suggesting that the overall effect is due to gemcitabine. In the A549 cell line, itraconazole considerably enhanced cell growth inhibition in all gemcitabine concentrations tested. However, the overall effect of 5-FU + I combination is almost independent on 5-FU concentration, suggesting that the observed response is mostly due to itraconazole. Yet, this conclusion cannot be validated due to the lack of itraconazole alone control.

The three selected repurposed drugs were expected to show noticeable improvement in cell growth inhibition when combined with gemcitabine or 5-FU. However, tacrine and verapamil did not reveal promising activity. Tacrine has been reported to enhance tumor suppressor's activity, such as caspase, Bax, and p53 expression in mouse hepatocytes [32]; though, when used in combination with gemcitabine or 5-FU at a concentration of 1 μM in the cell lines tested here, it did not reveal significant improvement in cell growth inhibition comparing to the control (ACD alone). Verapamil is known to promote intracellular accumulation of chemotherapeutic drugs. It has been studied in multiple types of cancer cell lines and in combination with multiple ACDs and has proven efficacy in reversing multidrug resistance through inhibition of P-gp, one of the main proteins responsible for

drug extrusion in cancer [31,33–37]. A recent study has also evaluated the combination of verapamil with gemcitabine in chemotherapy-resistant pancreatic cancer side population (SP) cells, showing enhancement in cytotoxicity when used in combination with this chemotherapeutic agent, as well as apoptosis induction of stem-like SP cells in L3.6pl and AsPC-1 pancreatic carcinoma models and significant inhibition of pancreatic cancer tumor growth in vivo, potentially by targeting stem-like side population cells [38]. However, in this work, verapamil did not show significant improvement of cell growth inhibition when in combination with gemcitabine or 5-FU.

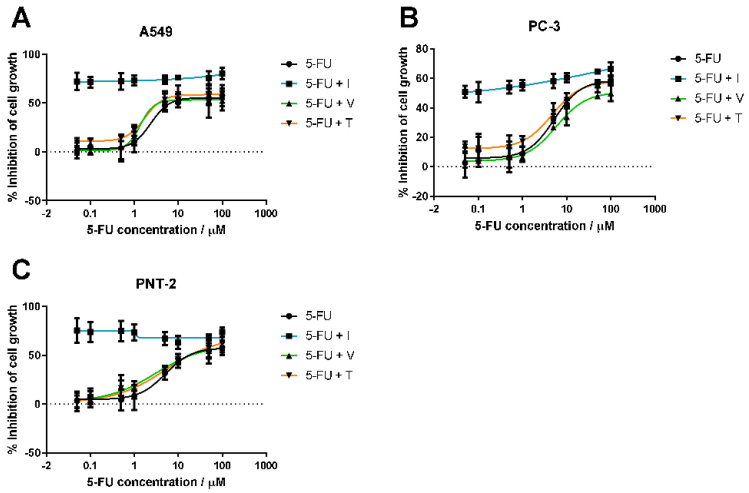

Figure 7. Dose-response curve of 5-FU in combination with RD. Percentage of cell growth inhibition of human lung carcinoma A549 cell line ((**A**)—top left), human prostate adenocarcinoma PC-3 cell line ((**B**)—top right) and normal human prostate epithelium PNT2 cell line ((**C**)—bottom left), treated with wide range of concentrations of 5-fluorouracil (5-FU) alone (black line) or 5-FU in combination with a fixed concentration of RD (verapamil, V, green line; itraconazole, I, blue line; or tacrine, T, orange line), during 72 h, determined with MTT assay. Results are the mean of at least three independent experiments. The DMSO control did not present toxicity to the cells (data not shown).

As shown in the results above, itraconazole was the only RD that significantly increased the cell growth inhibition when combined with an ACD (gemcitabine or 5-FU). Itraconazole has been extensively studied in cancer research and several anticancer mechanisms of action have been identified, which include the ability to inhibit Hedgehog pathway and angiogenesis, both mechanisms related to cancer development, autophagy induction and reversal of multidrug resistance [39–44]. Therefore, the enhancement of cell growth inhibition may be explained by the targeting of an additional pathway in cell division. To better understand how the itraconazole concentration affected cell growth inhibition, lower itraconazole concentrations were tested, since the concentration tested in the previous experiments was the maximum plasma concentration recommended.

3.1.2. Range of Itraconazole Concentrations + Fixed Concentration of ACD

A range of concentrations of itraconazole was either tested alone (control) or in combination with a fixed concentration of ACD. ACDs were also tested alone as a control. Itraconazole dose-response curve is represented in Figure 8, demonstrating no cell growth inhibition is achieved at concentrations lower than 2 µM. Concentrations higher than this value drove cell growth inhibition in a dose-dependent manner. However, the dose-response curve of itraconazole + 5-FU overlaps itraconazole alone dose-response curve. Hence, this data is not enough to understand if itraconazole is improving 5-FU effect or if

the result is only due to itraconazole itself. For the itraconazole + gemcitabine combination, at higher concentrations of itraconazole the effect is higher than itraconazole or gemcitabine effect alone. As stated, only itraconazole concentrations above 2 μM enhanced the cell growth inhibition when in combination with an ACD. Thus, to evaluate the itraconazole concentration effect in ACD dose-response curve, further experiments were done.

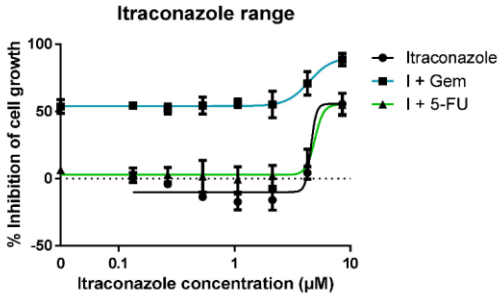

Figure 8. Dose-response curve of itraconazole in combination with ACD. Percentage of cell growth inhibition of human lung carcinoma A549 cell line treated with a range of concentrations of itraconazole alone (black line) or itraconazole in combination with a fixed concentration of ACD (Gem (blue line) or 5-FU (green line)), during 72 h, determined with MTT assay. The results are mean of at least three independent experiments. The DMSO control did not present toxicity to the cells (data not shown).

3.1.3. Range of ACD Concentrations + Fixed Concentration of Itraconazole

ACD range of concentrations was tested with or without a fixed concentration of itraconazole. Three different concentrations of itraconazole were tested: 2, 4 and 6 μM. Itraconazole was also tested alone as a control. Figure 9 shows gemcitabine + itraconazole (A) and 5-FU + itraconazole (B) dose-response curves. According to the results, itraconazole concentration does not significantly affect the highest percentage of cell growth inhibition ("Top" value), but it strongly affects the lowest value of the curve ("Bottom" value), meaning the highest effect ("Top" value) achieved with gemcitabine or 5-FU alone is approximately the same as drug combinations, values rounding 73% and 59%, respectively (Tables 1 and 2). On the other hand, the lowest percentage of cell growth inhibition ("Bottom" value) strongly depends on itraconazole concentration, varying in a dose-dependent manner. Increasing itraconazole concentration to 4 and 6 μM increases "Bottom" value from 0 (control) to about 13%, and 33%, respectively, in both combination groups (Figure 9A,B).

Table 1. Dose-response curve parameters for gemcitabine and itraconazole combinations, obtained from GraphPad. (N.A.: non-applicable.).

Gem + I [a]	Bottom (%)	Top (%)	Steepness Factor	EC_{50} ($\mu g \cdot mL^{-1}$)
I = 6 μM	34.33 ± 2.43	80.39 ± 1.71	4.30 ± 1.30	$0.0016 \pm 3.2 \times 10^{-7}$
I = 4 μM	12.83 ± 2.79	73.07 ± 1.97	4.37 ± 0.99	$0.0018 \pm 3.1 \times 10^{-7}$
I = 2 μM	−5.51 ± 1.83	67.47 ± 1.29	5.35 ± 1.12	$0.0022 \pm 1.6 \times 10^{-7}$
I = 0 μM	−1.06 ± 2.35	70.12 ± 1.67	$23.14 \pm 4.20 \times 10^{5}$	$0.0026 \pm 2.2 \times 10^{5}$
Average	N.A.	72.76	4.67	0.0021

[a] I is the drug itraconazole. Gem + I = 2 μM for "Bottom (%)" and Gem + I = 0 μM for "Steepness factor" were not included in the calculation of the average.

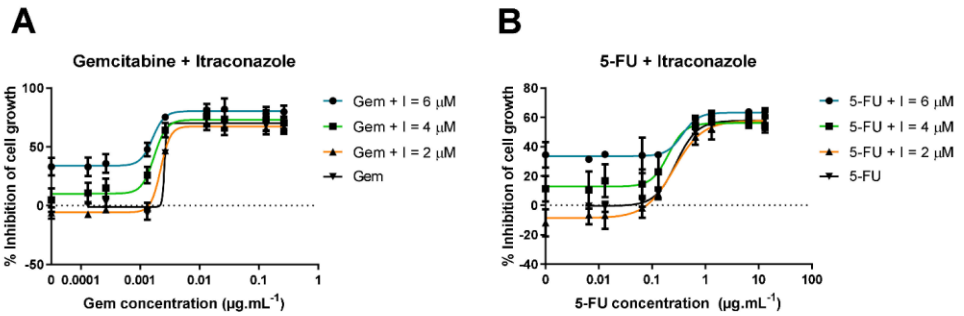

Figure 9. Dose-response curves of ACD in combination with itraconazole. (**A**): Percentage of cell growth inhibition of human lung carcinoma A549 cell line treated with wide range of concentrations of gemcitabine (Gem) alone (control) or Gem in combination with a fixed concentration of itraconazole (I), during 72 h, determined with MTT assay; (**B**): Percentage of cell growth inhibition of human lung carcinoma A549 cell line, treated with wide range of concentrations of 5-FU alone (control) or 5-FU in combination with a fixed concentration of I, during 72 h, determined with MTT assay. The results are the mean of at least three independent experiments. The DMSO control did not present toxicity to the cells (data not shown).

Table 2. Dose-response curve parameters for 5-FU and itraconazole combinations, obtained from GraphPad. (N.A.: non applicable.).

5-FU + I [a]	Bottom (%)	Top (%)	Steepness Factor	EC_{50} (µg·mL^{-1})
I = 6 µM	33.22 ± 1.58	63.24 ± 1.62	2.77 ± 1.23	0.36 ± 0.01
I = 4 µM	13.42 ± 3.09	56.05 ± 2.87	2.90 ± 2.40	0.20 ± 0.0071
I = 2 µM	−6.99 ± 2.14	57.52 ± 2.11	1.70 ± 0.26	0.27 ± 0.002
I = 0 µM	−0.47 ± 1.32	57.80 ± 1.32	2.19 ± 0.27	0.28 ± 0.001
Average	N.A.	58.65	2.39	0.28

[a] I is the drug itraconazole. 5-FU + I = 2 µM for "Bottom (%)" was not included in the calculation of the average.

3.2. WinNonlin: PK Analysis

The concentration-time curves of gemcitabine in plasma from the literature were evaluated by compartmental analysis (Phoenix WinNonlin (64-bit, version 7.00)). The best fitting was achieved with a two-compartmental model (Figure 10) and PK parameters were obtained through PK analysis (Table 3). Although WinNonlin prediction (blue line) did not fit all experimental values (red circles), k_{10}, AUC, C_{max} and CL values obtained are in accordance with the literature. However, transfer rate constants k_{12} and k_{21} and tissue compartment volume of distribution (V_{d2}) measurements are not very precise, but since no more accurate data was available, the values were included in the STELLA® model.

Table 3. Gemcitabine PK parameters obtained from WinNonlin.

Gemcitabine Parameters	Estimate	CV (%)	Literature Values [27]
k_{10} (min^{-1})	5.54×10^{-2}	144.9	7.00×10^{-2}
k_{12} (min^{-1})	6.64×10^{-4}	45,998.6	-
k_{21} (min^{-1})	1.02×10^{-1}	29,203.6	-
AUC (µg·mL^{-1}·min)	499.58	10.3	453.00
C_{max} (µg·mL^{-1})	4.16	10.5	4.92
CL (mL·min^{-1})	3771.20	10.3	3940.05
V_{ss} (mL)	68,464.40	37.4	-
V_{d1} (mL)	68,019.62	148.8	-
V_{d2} (mL)	444.79	19,137.5	-

k_{10}: elimination rate constant; k_{12}: transfer rate constant from central compartment to tissue compartment; k_{21}: transfer rate constant from tissue compartment to central compartment; AUC: area under the plasma concentration-time curve; C_{max}: maximum plasma concentration; CL: clearance; V_{ss}: steady state volume of distribution; V_{d1}: volume of distribution of central compartment; V_{d2}: volume of distribution of tissue compartment.

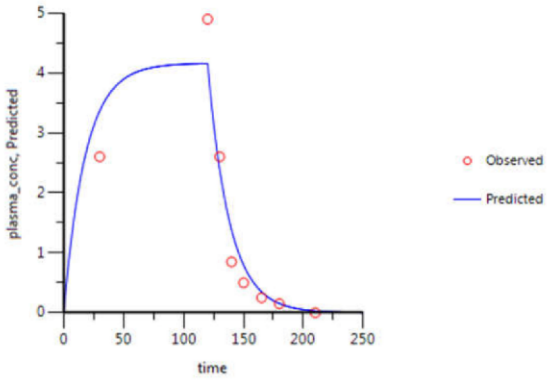

Figure 10. Gemcitabine C_p-time curve prediction through two-compartment model fitting of its observed C_p-time data. Red circles correspond to the experimental data, obtained from the literature, and the continuous blue line corresponds to the in silico C_p-time curve prediction. Plasma concentration is given in $\mu g \cdot mL^{-1}$ and time in minutes.

The concentration-time curves of 5-FU in plasma from the literature were also evaluated by compartmental analysis and the best fitting was achieved with a two-compartment model (Figure 11). PK parameters were obtained through PK analysis (Table 4). As shown in Figure 11, WinNonlin prediction (blue line) fits all experimental values (red circles) almost perfectly. All PK parameters obtained are also in accordance with literature values.

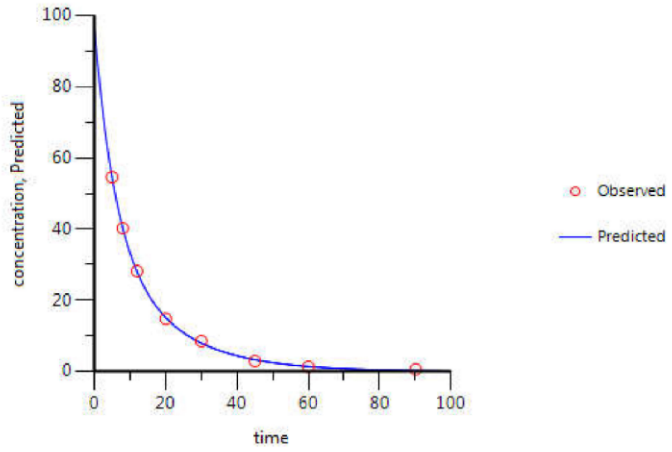

Figure 11. 5-FU C_p-time curve prediction through two-compartment model fitting of its observed C_p-time data. Red circles correspond to the experimental data, obtained from the literature, and the continuous blue line corresponds to the in silico C_p-time curve prediction. Plasma concentration is given in $\mu g \cdot mL^{-1}$ and time in minutes.

Finally, concentration-time curves of itraconazole in plasma were also evaluated and best-fitted to a two-compartmental model (Figure 12 and Table 5). Although the predicted steady-state volume of distribution (V_{ss}) is quite lower than the volume of distribution reported in literature source, WinNonlin prediction (blue line) fits all experimental values (red circles) almost perfectly and % CV is fairly small in all parameters determined. Therefore, WinNonlin prediction was assumed to be reliable. In fact, the volume of distribution parameter determined in the literature is V_{darea} [28], which means that it was determined

during the elimination phase and not at steady-state, as in WinNonlin prediction [45]. Therefore, the parameters cannot be compared.

Table 4. 5-FU PK parameters obtained from WinNonlin.

5-FU Parameters	Estimate	CV (%)	Literature Values [29]
k_{10} (min^{-1})	9.17×10^{-2}	4.9	-
k_{12} (min^{-1})	3.21×10^{-2}	29.5	-
k_{21} (min^{-1})	1.07×10^{-1}	28.1	-
AUC ($\mu g \cdot mL^{-1} \cdot min$)	1058.81	1.6	926.80
C_{max} ($\mu g \cdot mL^{-1}$)	97.14	5.1	-
CL ($mL \cdot min^{-1}$)	850.01	1.6	1069.20
V_{ss} (mL)	12,056.99	4.9	15,912.00
V_{d1} (mL)	9265.14	5.1	-
V_{d2} (mL)	2791.84	14.2	-

k_{10}: elimination rate constant; k_{12}: transfer rate constant from central compartment to tissue compartment; k_{21}: transfer rate constant from tissue compartment to central compartment; AUC: area under the plasma concentration-time curve; C_{max}: maximum plasma concentration; CL: clearance; V_{ss}: steady state volume of distribution; V_{d1}: volume of distribution of central compartment; V_{d2}: volume of distribution of tissue compartment.

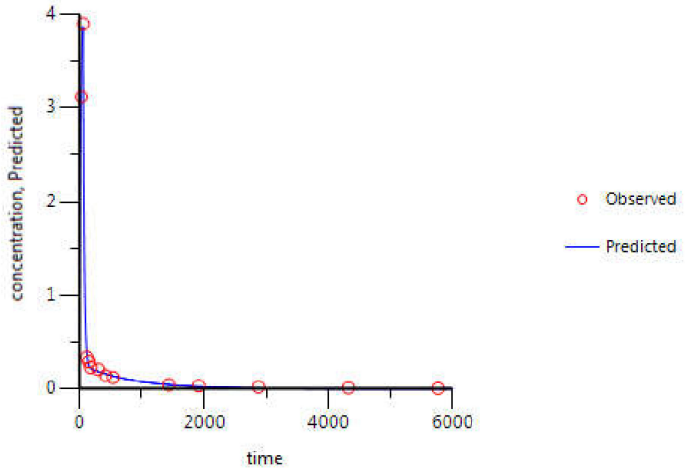

Figure 12. Itraconazole C_p-time curve prediction through two-compartmental model fitting of its observed C_p-time data. Red circles correspond to the experimental data, obtained from the literature, and the continuous blue line corresponds to the in silico Cp-time curve prediction. Plasma concentration is given in $\mu g \cdot mL^{-1}$ and time in minutes.

Table 5. Itraconazole PK parameters obtained from WinNonlin.

Itraconazole Parameters	Estimate	CV (%)	Literature Values [28]
k_{10} (min^{-1})	2.80×10^{-2}	8.8	2.66×10^{-2}
k_{12} (min^{-1})	2.38×10^{-2}	9.4	-
k_{21} (min^{-1})	2.34×10^{-3}	15.3	-
AUC ($\mu g \cdot mL^{-1} \cdot min$)	437.73	7.9	449.88
C_{max} ($\mu g \cdot mL^{-1}$)	3.88	0.6	-
CL ($mL \cdot min^{-1}$)	228.45	7.9	246.67
V_{ss} (mL)	90,922.24	20.9	558,000.00
V_{d1} (mL)	8145.37	2.6	-
V_{d2} (mL)	82,776.88	22.9	-

k_{10}: elimination rate constant; k_{12}: transfer rate constant from central compartment to tissue compartment; k_{21}: transfer rate constant from tissue compartment to central compartment; AUC: area under the plasma concentration-time curve; C_{max}: maximum plasma concentration; CL: clearance; V_{ss}: steady state volume of distribution; V_{d1}: volume of distribution of central compartment; V_{d2}: volume of distribution of tissue compartment.

3.3. STELLA® Models

3.3.1. Input Data for the Model

For the models described in the experimental section, two types of parameters were used: (1) the parameters related with the drug in focus obtained through WinNonlin (Tables 3–5), which were used as constants without further modification, and (2) the parameters obtained from the in vitro studies.

3.3.2. Model Validation

To evaluate the model accuracy, C_p-time curve was determined through STELLA® models and compared with the experimental values. Figure 13 shows that gemcitabine STELLA® model (Figure 2) is quite accurate in predicting gemcitabine's plasma concentration over time. Since the input values came from WinNonlin, and WinNonlin C_p-time curve prediction did not fit all experimental values, then C_p-time curve predicted through STELLA® will not fit them all either. For the 5-FU STELLA® model, Figure 14 demonstrates C_p-time curve predicted with STELLA® (blue line) fitting all the experimental values (orange circles). Thus, model accuracy predicting 5-FU's plasma concentration over time can be assumed. Similarly, itraconazole C_p-time curve predicted with STELLA® (blue line) is also fitting all the experimental values (orange circles) (Figure 15). Once more, model accuracy predicting itraconazole plasma concentration over time can be assumed. Besides C_p-time curve graphical analysis, to validate STELLA® models, AUC values were determined and compared with literature sources. In Figure 16, three AUC values are depicted for each drug: AUC calculated from experimental data (literature value), WinNonlin PK analysis, and STELLA® model simulation prediction. As expected, for each drug, STELLA® prediction is in perfect accordance with WinNonlin PK analysis, showing the exact same AUC value. Literature values are slightly different from STELLA® and WinNonlin predictions, probably due to differences in the integration method used for AUC calculation (all literature sources used trapezoidal rule, while STELLA® and WinNonlin predictions resorted to 4th order Runge-Kutta method).

3.3.3. AUC_{effect}: Drug Combination Effect Comparison

To compare drug combination effect in A549 cancer cell line, AUC_{effect} was determined in STELLA®. The effect is calculated through Equation (3), where the only variable is ACD tissue concentration. All the other parameters are constants and characterize the dose-response curve obtained from the in vitro studies, i.e., depending on ACD tissue concentration and the parameters introduced in model converters, "Effect" gets a certain value over time. AUC_{effect} quantifies the overall effect during simulation. According to the simulations (Figure 17), and in accordance with the in vitro experimental results (Figure 9), the higher the itraconazole concentration, the higher is the AUC_{effect} value. In gemcitabine combinations, when itraconazole tissue concentration is 4 μM and 6 μM, AUC_{effect} is about 9% and 22% higher than control (gemcitabine without itraconazole), respectively. In 5-FU combinations, these values reach 12% and 34% improvement relative to control (5-FU without itraconazole), respectively. However, for unknown reasons, when itraconazole concentration is 2 μM, AUC_{effect} is lower than control, in both combination groups.

Although gemcitabine and 5-FU elimination half-life ($t_{1/2}$) is identical (10 and 12 min, respectively) [27,29], the former is infused at a rate of 15.7 mg per minute, over 2 h, which represents a total dose of 1884 mg, while the latter is administered through a bolus IV injection at a dose of 900 mg. Therefore, the AUC_{effect} of 5-FU is expected to be much smaller than gemcitabine's, due to the lower dose and overall reduced exposure time of 5-FU in tissue. Besides the $AUC_{effect,}$ further analysis was done regarding itraconazole dose-dependent effect. This time, instead of only one variable (ACD concentration), as in the previous study, the percentage of effect will also depend on itraconazole tissue concentration over time. "% Effect" is still calculated through Equation (3), where ACD tissue concentration is the main variable, but "Bottom" parameter is now an equation dependent on itraconazole tissue concentration, instead of being a constant (Equations (4) and (5)).

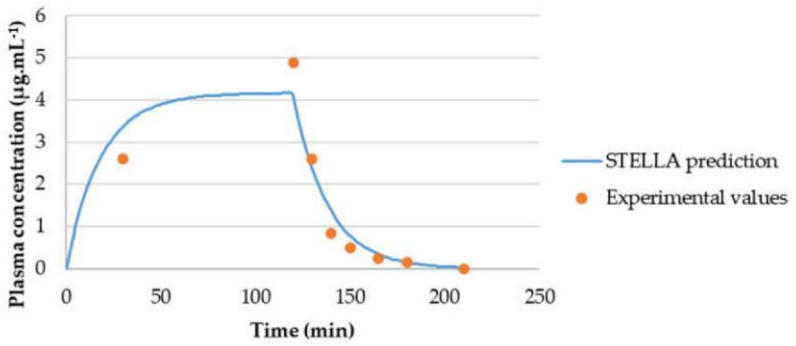

Figure 13. Graphical representation of experimental C_p-time data of gemcitabine and C_p-time curve generated in silico for this drug over 210 min.

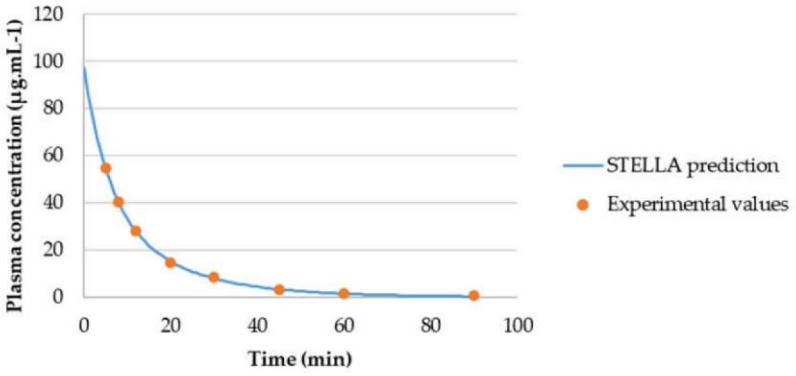

Figure 14. Graphical comparison between experimental C_p-time data of 5-FU and C_p-time curve generated in silico for this drug over 90 min.

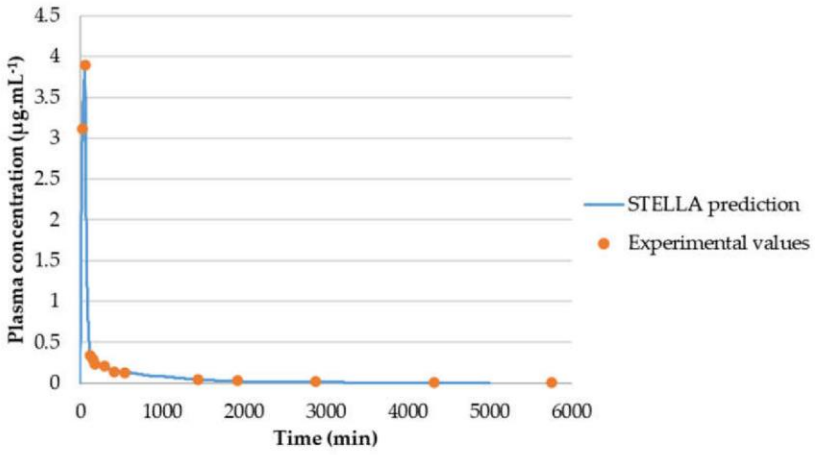

Figure 15. Graphical comparison between experimental C_p-time data of itraconazole and C_p-time curve generated in silico for this drug over 5000 min.

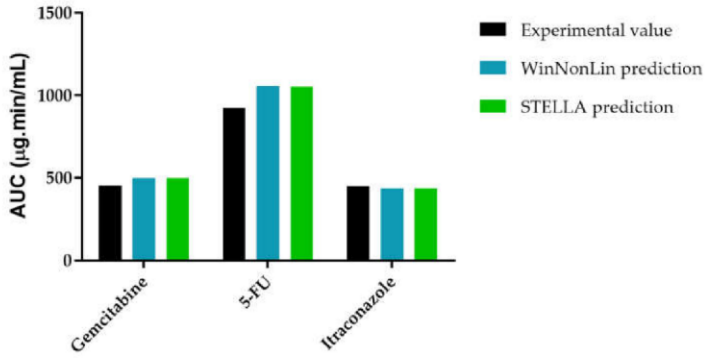

Figure 16. Graphical representation of AUC plasma concentration of gemcitabine, 5-FU, and itraconazole when determined experimentally, through WinNonlin or STELLA® models.

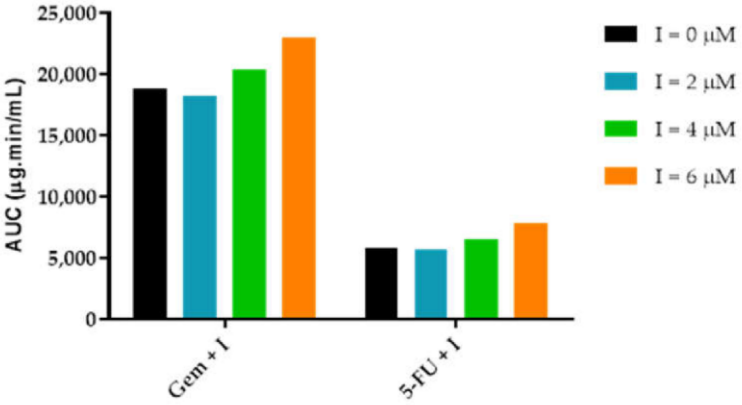

Figure 17. Graphical representation of AUC_{effect} for gemcitabine + itraconazole and 5-FU + itraconazole combinations.

Figure 18 presents five different graphs that enable the evaluation of drug concentration in the tissue compartment and its relationship with % effect over time. Graphs A and B show effect-time curve of ACD and itraconazole drug combination. Using constant ACD dose administration and three different doses of itraconazole, differences between effect-time curves can be observed. According to Figure 18A,B, depending on itraconazole dose administration, the final part of the curve is different.

For gemcitabine + itraconazole drug combination (Figure 18A), first the "% Effect" remains constant, at a level of 73% of cell growth inhibition. Then, at minute 260, the effect starts dropping abruptly. This drop can be explained with a deeper analysis of Equation (3). Gemcitabine concentration affects "% Effect" through exponential function described by Equation (6), where x is gemcitabine tissue concentration. According to this equation, at very high concentrations, gemcitabine tissue concentration influence on "% Effect" can be despised because f(x) will result in a very low value (Equation (6). Then, this value will be summed to 1 and divided to ("Top"-"Bottom") values. When this concentration is reduced to a value lower than 0.008 $\mu g \cdot mL^{-1}$, f(x) increases exponentially, reducing "% Effect" abruptly. Figure 18C shows gemcitabine tissue concentration-time curve:

$$f(x) = \left(\frac{x}{0.0019}\right)^{-4.67}. \quad (6)$$

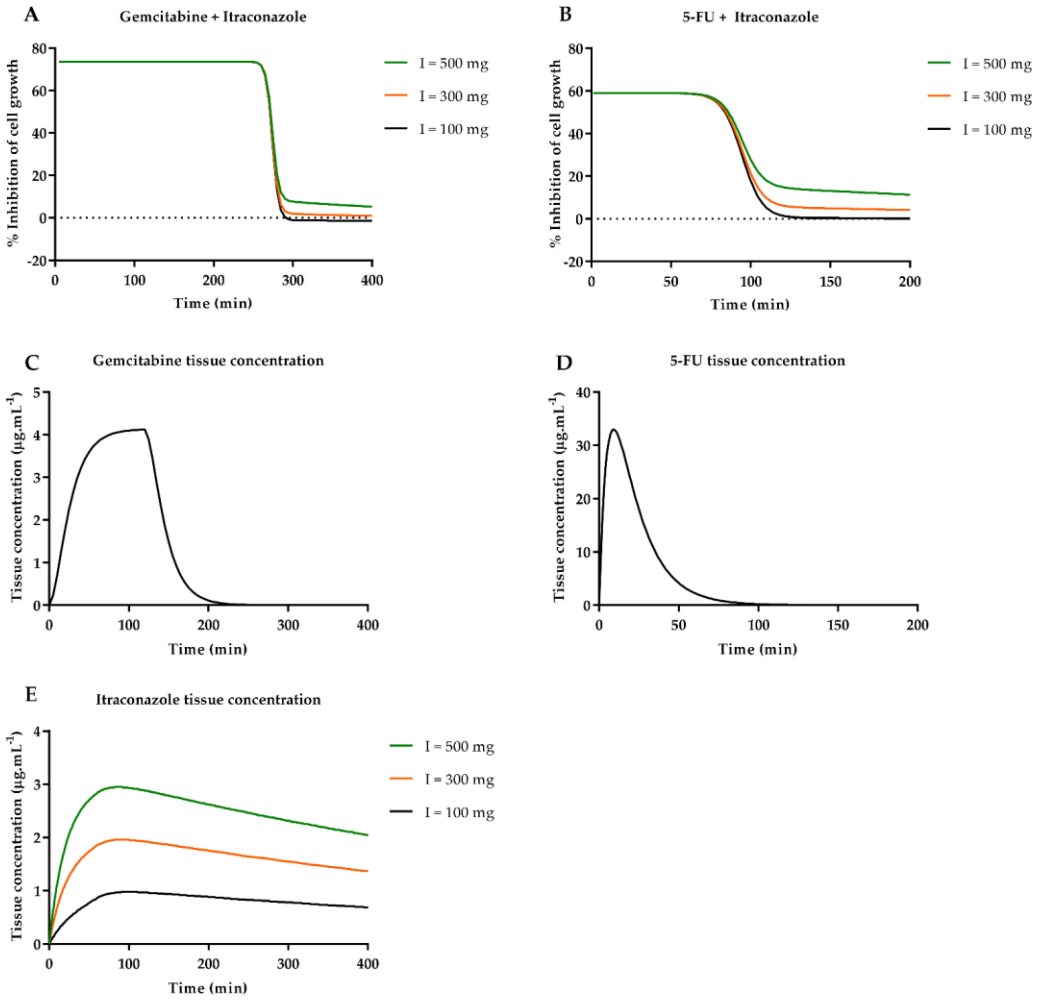

Figure 18. ACD + itraconazole (I) combination STELLA® simulation. (**A**,**B**): Effect curves for gemcitabine + itraconazole and 5-FU + itraconazole combinations, respectively. Three itraconazole doses were tested, (**C**,**D**): Tissue concentration-time curves of gemcitabine and 5-FU, when intravenously administered at a dose of 1884 mg (infusion), and 900 mg (injection), respectively; (**E**): Tissue concentration-time curve of itraconazole for three different doses of intravenous infusion.

After the drop in "% Effect" value, slight differences between effect-time curves start to be noticed. At this point, itraconazole tissue concentration plays the main role in the overall effect, since "% Effect" equals "Bottom" value (Equation (3), which is directly dependent on itraconazole tissue concentration. In Figure 18E, itraconazole tissue concentration is shown for the three studied doses. According to the results, itraconazole is slowly eliminated from the tissue compartment and will maintain % of cell growth inhibition relatively constant while it is being eliminated from the tissue compartment. In fact, if higher values of itraconazole tissue concentration were considered, "% Effect" would be equally higher. This can be mathematically explained through Equation (4) analysis. Itraconazole multiple dosing simulation was attempted in the STELLA® simulation program, with the objective

of increasing itraconazole tissue concentration, but limitations in the software's built-in functions did not allow the study.

For 5-FU + itraconazole drug combination (Figure 18B), first "% Effect" remains constant, at a level of 59% of cell growth inhibition. Then, at minute 70, effect starts dropping abruptly. This drop can be explained with the same reasoning as presented above for gemcitabine (Equation (7). When 5-FU concentration is reduced to a value lower than 0.5 $\mu g \cdot mL^{-1}$, f(x) increases exponentially reducing "% Effect" abruptly. Figure 18D shows 5-FU tissue concentration-time curve. When the drop in "% Effect" value starts, slight differences between effect-time curves start to be noticed. At this point, itraconazole tissue concentration plays the main role in the overall effect, since "% Effect" equals "Bottom" value (Equation (3), which is directly dependent on itraconazole tissue concentration. As stated above, if higher values of itraconazole tissue concentration were considered, "% Effect" would be equally higher. This can be mathematically explained through Equation (5) analysis:

$$f(x) = \left(\frac{x}{0.28}\right)^{-2.62} \quad (7)$$

While drug dose-response curves enable the establishment of a relationship between drug concentration and % of cell growth inhibition, this kind of approach facilitates the study of drug concentration-% of cell growth inhibition relationship over time, providing a better understanding about for how long a drug will exert its effect when administered at a certain dose until metabolization reduces drug concentration to a non-therapeutic level.

4. Discussing the Limitations in Pharmacokinetics Modeling

Despite the overall success of this project, some difficulties were detected during its development, particularly regarding STELLA® simulation program, namely the impossibility to make multiple dosing regimens (for IV infusion). As mentioned in Section 3.3.3., itraconazole concentration in the tissue compartment was not high enough to significantly influence the overall "% Effect". The idea of using multiple dosing regimen was to reach steady-state plasma concentration (C_{ss}), increasing itraconazole accumulation in tissue compartment, and thus, to predict the influence of itraconazole in cell growth inhibition. Thus, alternatives to the STELLA® simulation program were explored to overcome this problem, which included the use of GastroPlus™ PBPK simulation software and Microsoft Excel.

In this project, an attempt to replicate experimental C_p-time data of itraconazole in GastroPlus™ was made, but neither uploading itraconazole molecular structure nor inputting experimental parameters could replicate the concentration plasma profile reported in the literature. As shown in Figure 19, itraconazole C_{max} predicted through this program, for 100 mg, 1 h IV infusion, is about 0.095 $\mu g \cdot mL^{-1}$, while the equivalent value reported in the literature, for the same dosing regimen, is 3.9 $\mu g \cdot mL^{-1}$. GastroPlus™ is a complex software and it is not solely ruled by simple pharmacokinetics equations. To run a simulation in this program, the input of a few parameters is needed. Apart from common parameters input as dose, dosage form, solubility and the pH at which it was measured, logP and pKa's (if any), it also requires some knowledge about particle radius, particle density and diffusion coefficient. In the simulation presented in Figure 19, most of the parameters used were predicted through itraconazole structure upload. Even with the input of some experimental values, itraconazole C_p-time is quite different from the reported one. Thus, it was impossible to validate the model and multiple dosing regimen could not be evaluated.

Given the circumstances, the study of itraconazole's multiple dosing regimen was done in Microsoft Excel. The literature C_{ss} value was used as the itraconazole plasma concentration. The transfer rate constants k_{12} and k_{21} previously obtained through WinNonlin were used to simulate itraconazole flow between plasma and tissue compartment. Then, the "Bottom" value was calculated at every time point, which is dependent on itraconazole tissue concentration on that specific time point (Equation (4) or Equation (5)). Finally, "% Effect" was calculated through Equation (3).

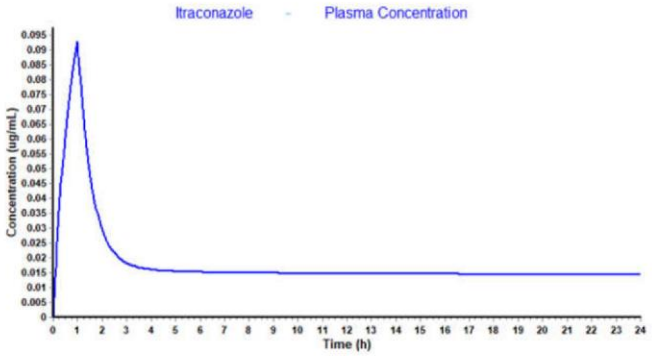

Figure 19. Itraconazole C_p-time profile predicted through GastroPlus™ simulation software.

There are several potential benefits in employing in silico models in the process of drug R&D. However, reliable results require complex and data-intensive models. Furthermore, the use of complex models in drug development requires adequate resources and well-qualified researchers with a good understanding of the ADME data required to drive the models.

STELLA® models developed in this work are simple but innovative, and provided insight on the PK and effect of combinations of anticancer drugs with repurposed drugs. Ideally, parameters used in the model structure should be more consistent, but for a first idea of the general behavior of the drug combinations in human body, the data used is fairly appropriate. There is variability in the populations originating the data, and moreover, the tumor is assumed to behave like the tissues grouped into a tissue compartment, but no such assumption was confirmed or validated. Although in vitro results do not correlate directly with in vivo effect, these preliminary studies might be useful for comparative effect purposes and to provide mechanistic predictions of dosing regimens.

5. Conclusions

We know that the interaction of two drugs in a combination can generate distinct but complementary cellular responses, but the outcome of this study suggests an interesting hypothesis to be tested in the clinic, and the preclinical model developed in our study might provide a reference for the dose selection in the combination therapy of cancer treatment. Therefore, it is now possible to study tissue drug concentration—% of cell growth inhibition relationships over time. This provides a better understanding regarding how long a drug will exert its effect when administered at a certain dose until metabolization reduces drug concentration to a non-therapeutic level.

In the future, other drug combinations can be tested in cell models, and % effect can be evaluated over time through similar models. However, due to some limitations and inconsistencies found in the models developed here, some upgrading/alterations may be required. Furthermore, future experiments may need different model construction, depending on the context in which they are inserted, but understanding how STELLA® modeling program works, one can collect and analyze the necessary data and build the most convenient model. Additionally, the effect of these combinations must be studied using appropriate in vivo models.

Author Contributions: Conceptualization, A.U. and N.V.; methodology, C.C., A.F., J.S. and N.V.; software, C.C., A.F., J.S.; validation, M.Y., A.U., R.L. and N.V.; investigation, C.C., A.F., J.S. and N.V.; resources, N.V. and R.L.; writing—original draft preparation, C.C., A.F. and J.S.; writing—review and editing, R.L. and N.V.; super-vision, N.V.; project administration, N.V.; funding acquisition, R.L., M.Y., A.U. and N.V. All authors have read and agreed to the published version of the manuscript.

Funding: This work was financed by FEDER—Fundo Europeu de Desenvolvimento Regional through the COMPETE 2020—Operational Programme for Competitiveness and Internationalization (POCI), Portugal 2020, and by Portuguese funds through FCT—Fundação para a Ciência e a Tecnologia, in a framework of CINTESIS, R&D Unit (reference UIDB/4255/2020). N.V. also thanks support FCT and FEDER (European Union), award number IF/00092/2014/CP1255/CT0004. RL thanks FCT through grant UID/QUI/50006/2019 (LAQV-REQUIMTE).

Institutional Review Board Statement: Not Applicable.

Informed Consent Statement: Not Applicable.

Data Availability Statement: Not Applicable.

Acknowledgments: A.F. thanks FCT for a doctoral fellowship (PD/BD/135120/2017). The contents of this article are solely the responsibility of the authors and do not necessarily represent the official view of the FCT.

Conflicts of Interest: The authors declare no conflict of interest.

Sample Availability: Not Applicable.

References

1. Jambhekar, S.S.; Breen, P.J. *Basic Pharmacokinetics*; Pharmaceutical Press: London, UK, 2009; Volume 76.
2. DiMasi, J.A.; Hansen, R.W.; Grabowski, H.G. The price of innovation: New estimates of drug development costs. *J. Health Econ.* **2003**, *22*, 151–185. [CrossRef]
3. Box, G.E.; Draper, N.R. *Empirical Model-Building and Response Surfaces*; Wiley: New York, NY, USA, 1987; Volume 424.
4. Rooney, K.F.; Snoeck, E.; Watson, P.H. Modelling and simulation in clinical drug development. *Drug Discov. Today* **2001**, *6*, 802–806. [CrossRef]
5. Gieschke, R.; Steimer, J. Pharmacometrics: Modelling and simulation tools to improve decision making in clinical drug development. *Eur. J. Metabol. Pharmacokinet.* **2000**, *25*, 49–58. [CrossRef]
6. Shargel, L.; Wu-Pong, S.; Yu, A.B. *Applied Biopharmaceutics & Pharmacokinetics*; Mcgraw-Hill: New York, NY, USA, 2007.
7. Zhuang, X.; Lu, C. PBPK modeling and simulation in drug research and development. *Acta Pharm. Sin. B* **2016**, *6*, 430–440. [CrossRef]
8. De Biasi, J.; Rekik, L. Four compartment mammillary model applied to the pharmacokinetics of a spiroarsorane administered orally to rabbits. *J. Biomed. Eng.* **1991**, *13*, 439–440. [CrossRef]
9. Gabrielsson, J.; Weiner, D. *Pharmacokinetic and Pharmacodynamic Data Analysis: Concepts and Applications*; CRC Press: Boca Raton, FL, USA, 2001.
10. Chapra, S.C.; Canale, R.P. *Numerical Methods for Engineers*; McGraw-Hill Higher Education: Boston, MA, USA, 2010.
11. Otsuka, K.; Wagner, C.; Selen, A.; Dressman, J. Prediction of in-vivo pharmacokinetic profile for immediate and modified release oral dosage forms of furosemide using an in-vitro–in-silico–in-vivo approach. *J. Pharm. Pharmacol.* **2015**, *67*, 651–665. [CrossRef]
12. Vellonen, K.-S.; Soini, E.-M.; Del Amo, E.M.; Urtti, A. Prediction of ocular drug distribution from systemic blood circulation. *Mol. Pharm.* **2016**, *13*, 2906–2911. [CrossRef] [PubMed]
13. Hargrove, J.; Hulsey, M.; Summers, A. From genotype to phenotype: Computer-based modeling of gene expression with STELLA II. *BioTechniques* **1993**, *15*, 1096–1101. [PubMed]
14. Miller, N.A.Y.; Reddy, M.B.; Heikkinen, A.T.; Lukacova, V.; Parrott, N. Physiologically Based Pharmacokinetic Modelling for First-In-Human Predictions: An Updated Model Building Strategy Illustrated with Challenging Industry Case Studies. *Clin. Pharmacokinet.* **2019**, *58*, 727–746. [CrossRef] [PubMed]
15. DeVita, V.T., Jr. Single agent versus combination chemotherapy. *CA Cancer J. Clin.* **1975**, *25*, 152–158.
16. Perelson, A.S.; Essunger, P.; Cao, Y.; Vesanen, M.; Hurley, A.; Saksela, K.; Markowitz, M.; Ho, D.D. Decay characteristics of HIV-1-infected compartments during combination therapy. *Nature* **1997**, *387*, 188–191. [CrossRef]
17. Armand, J.; Dormont, J.; Schwebig, A. Recommendations for the study of drug combination therapy for the treatment of AIDS and cancer. Round Table No 7 at Giens XIII. *Therapie* **1998**, *53*, 385–389.
18. Ai, N.; Fan, X.; Ekins, S. In silico methods for predicting drug–drug interactions with cytochrome P-450s, transporters and beyond. *Adv. Drug Deliv. Rev.* **2015**, *86*, 46–60. [CrossRef] [PubMed]
19. Tallarida, R.J. An overview of drug combination analysis with isobolograms. *J. Pharmacol. Exp. Ther.* **2006**, *319*, 1–7. [CrossRef] [PubMed]
20. Chou, T.-C. Drug combination studies and their synergy quantification using the Chou-Talalay method. *Cancer Res.* **2010**, *70*, 440–446. [CrossRef]
21. Skeel, R.T.; Khleif, S.N. *Handbook of Cancer Chemotherapy*; Lippincott Williams & Wilkins: Philadelphia, PA, USA, 2011.
22. Correia, A.; Silva, D.; Correia, A.; Vilanova, M.; Gärtner, F.; Vale, N. Study of new therapeutic strategies to combat breast cancer using drug combinations. *Biomolecules* **2018**, *8*, 175. [CrossRef]

23. Hamann, S.R.; Blouin, R.A.; McAllister, R. Clinical pharmacokinetics of verapamil. *Clin. Pharmacokinet.* **1984**, *9*, 26–41. [CrossRef] [PubMed]
24. Heykants, J.; Van Peer, A.; Van de Velde, V.; Van Rooy, P.; Meuldermans, W.; Lavrijsen, K.; Woestenborghs, R.; Van Cutsem, J.; Cauwenbergh, G. The clinical pharmacokinetics of itraconazole: An overview. *Mycoses* **1989**, *32*, 67–87. [CrossRef]
25. Madden, S.; Spaldin, V.; Park, B.K. Clinical pharmacokinetics of tacrine. *Clin. Pharmacokinet.* **1995**, *28*, 449–457. [CrossRef]
26. Milroy, R. A randomised clinical study of verapamil in addition to combination chemotherapy in small cell lung cancer. *Br. J. Cancer* **1993**, *68*, 813–818. [CrossRef] [PubMed]
27. Wang, L.R.; Huang, M.Z.; Xu, N.; Shentu, J.Z.; Liu, J.; Cai, J. Pharmacokinetics of gemcitabine in Chinese patients with non-small-cell lung cancer. *J. Zhejiang Univ. Sci. B* **2005**, *6*, 446–450. [CrossRef] [PubMed]
28. Mouton, J.W.; van Peer, A.; de Beule, K.; Van Vliet, A.; Donnelly, J.P.; Soons, P.A. Pharmacokinetics of itraconazole and hydroxyitraconazole in healthy subjects after single and multiple doses of a novel formulation. *Antimicrob. Agents Chemother.* **2006**, *50*, 4096–4102. [CrossRef] [PubMed]
29. Heggie, G.D.; Sommadossi, J.P.; Cross, D.S.; Huster, W.J.; Diasio, R.B. Clinical pharmacokinetics of 5-fluorouracil and its metabolites in plasma, urine, and bile. *Cancer Res.* **1987**, *47*, 2203–2206. [PubMed]
30. Soria, I.; Myhre, P.; Horton, V.; Ellefson, P.; McCarville, S.; Schmitt, K.; Owens, M. Effect of food on the pharmacokinetics and bioavailability of oral imiquimod relative to a subcutaneous dose. *Int. J. Clin. Pharmacol. Ther.* **2000**, *38*, 476–481. [CrossRef]
31. Ince, P.; Appleton, D.; Finney, K.; Sunter, J.; Watson, A. Verapamil increases the sensitivity of primary human colorectal carcinoma tissue to vincristine. *Br. J. Cancer* **1986**, *53*, 137. [CrossRef]
32. Mansouri, A.; Haouzi, D.; Descatoire, V.; Demeilliers, C.; Sutton, A.; Vadrot, N.; Fromenty, B.; Feldmann, G.; Pessayre, D.; Berson, A. Tacrine inhibits topoisomerases and DNA synthesis to cause mitochondrial DNA depletion and apoptosis in mouse liver. *Hepatology* **2003**, *38*, 715–725. [CrossRef]
33. Merry, S.; Fetherston, C.; Kaye, S.; Freshney, R.; Plumb, J. Resistance of human glioma to adriamycin in vitro: The role of membrane transport and its circumvention with verapamil. *Br. J. Cancer* **1986**, *53*, 129–135. [CrossRef] [PubMed]
34. Morrow, M.; Wait, R.; Rosenthal, R.; Gamelli, R. Verapamil enhances antitumor activity without increasing myeloid toxicity. *Surgery* **1987**, *101*, 63–68.
35. Tsuruo, T.; Iida, H.; Tsukagoshi, S.; Sakurai, Y. Overcoming of vincristine resistance in P388 leukemia in vivo and in vitro through enhanced cytotoxicity of vincristine and vinblastine by verapamil. *Cancer Res.* **1981**, *41*, 1967–1972.
36. Ambudkar, S.V.; Dey, S.; Hrycyna, C.A.; Ramachandra, M.; Pastan, I.; Gottesman, M.M. Biochemical, cellular, and pharmacological aspects of the multidrug transporter. *Annu. Rev. Pharmacol. Toxicol.* **1999**, *39*, 361–398. [CrossRef]
37. Wang, F.; Zhang, D.; Zhang, Q.; Chen, Y.; Zheng, D.; Hao, L.; Duan, C.; Jia, L.; Liu, G.; Liu, Y. Synergistic effect of folate-mediated targeting and verapamil-mediated P-gp inhibition with paclitaxel-polymer micelles to overcome multi-drug resistance. *Biomaterials* **2011**, *32*, 9444–9456. [CrossRef]
38. Zhao, L.; Zhao, Y.; Schwarz, B.; Mysliwietz, J.; Hartig, R.; Camaj, P.; Bao, Q.; Jauch, K.-W.; Guba, M.; Ellwart, J.W. Verapamil inhibits tumor progression of chemotherapy-resistant pancreatic cancer side population cells. *Int. J. Oncol.* **2016**, *49*, 99–110. [CrossRef]
39. Chong, C.R.; Xu, J.; Lu, J.; Bhat, S.; Sullivan Jr, D.J.; Liu, J.O. Inhibition of angiogenesis by the antifungal drug itraconazole. *ACS Chem. Biol.* **2007**, *2*, 263–270. [CrossRef] [PubMed]
40. Kim, J.; Tang, J.Y.; Gong, R.; Kim, J.; Lee, J.J.; Clemons, K.V.; Chong, C.R.; Chang, K.S.; Fereshteh, M.; Gardner, D. Itraconazole, a commonly used antifungal that inhibits Hedgehog pathway activity and cancer growth. *Cancer Cell* **2010**, *17*, 388–399. [CrossRef] [PubMed]
41. Nacev, B.A.; Grassi, P.; Dell, A.; Haslam, S.M.; Liu, J.O. The antifungal drug itraconazole inhibits vascular endothelial growth factor receptor 2 (VEGFR2) glycosylation, trafficking, and signaling in endothelial cells. *J. Biol. Chem.* **2011**, *286*, 44045–44056. [CrossRef]
42. Kim, J.; Aftab, B.T.; Tang, J.Y.; Kim, D.; Lee, A.H.; Rezaee, M.; Kim, J.; Chen, B.; King, E.M.; Borodovsky, A. Itraconazole and arsenic trioxide inhibit Hedgehog pathway activation and tumor growth associated with acquired resistance to smoothened antagonists. *Cancer Cell* **2013**, *23*, 23–34. [CrossRef] [PubMed]
43. Liu, R.; Li, J.; Zhang, T.; Zou, L.; Chen, Y.; Wang, K.; Lei, Y.; Yuan, K.; Li, Y.; Lan, J. Itraconazole suppresses the growth of glioblastoma through induction of autophagy: Involvement of abnormal cholesterol trafficking. *Autophagy* **2014**, *10*, 1241–1255. [CrossRef]
44. Wang, E.-j.; Lew, K.; Casciano, C.N.; Clement, R.P.; Johnson, W.W. Interaction of common azole antifungals with P glycoprotein. *Antimicrob. Agents Chemother.* **2002**, *46*, 160–165. [CrossRef]
45. Toutain, P.-L.; Bousquet-Mélou, A. Volumes of distribution. *J. Vet. Pharmacol. Ther.* **2004**, *27*, 441–453. [CrossRef]

PART II

PART II

CHAPTER 5

In silico pharmacokinetic study of vancomycin using PBPK modeling and therapeutic drug monitoring

Abigail Ferreira, Helena Martins, José C Oliveira, Rui Lapa, Nuno Vale

Current Drug Metabolism, **2021**; 22(2), pp. 150-162.

DOI: 10.2174/1389200221999210101232417

Antibiotics are one of the most prescribed drugs worldwide. However, it is crucial to optimize their use to ensure a successful clinical outcome and to prevent the widespread of resistance to these drugs, dangerously threatening to render them ineffective. Vancomycin has been used for over five decades to treat serious infections, including those caused by methicillin-resistant *Staphylococcus aureus* (MRSA).

As a result of a collaboration with *Centro Hospitalar Universitario do Porto* (CHUP), clinical and demographic data from inpatients was analyzed and the influence of different treatment regimens, as well as patients' age, weight, and renal function on the biodistribution of this antibiotic was investigated. The main pharmacokinetic parameters and the plasma concentration-time profiles were estimated using GastroPlus™.

The main factors impacting the PK of vancomycin were renal function and total body weight, and a direct proportionality was observed between dose and plasma levels of vancomycin.

Current Drug Metabolism, 2021, *22*, 150-162

RESEARCH ARTICLE

In Silico Pharmacokinetic Study of Vancomycin Using PBPK Modeling and Therapeutic Drug Monitoring

Abigail Ferreira[1,2], Helena Martins[3], José C. Oliveira[3], Rui Lapa[2] and Nuno Vale[1,4,*]

[1]*OncoPharma Research Group, Center for Health Technology and Services Research (CINTESIS), Rua Dr. Plácido da Costa, 4200-450 Porto, Portugal;* [2]*LAQV/REQUIMTE, Laboratory of Applied Chemistry, Department of Chemical Sciences, Faculty of Pharmacy, University of Porto, Rua de Jorge Viterbo Ferreira, 228, 4050-313 Porto, Portugal;* [3]*Departament of Pathology, Clinical Chemistry Service, Centro Hospitalar Universitário do Porto (CHUP), Largo Prof. Abel Salazar 4099-001, Porto, Portugal;* [4]*Faculty of Medicine, University of Porto, Al. Prof. Hernâni Monteiro, 4200-319 Porto, Portugal*

ARTICLE HISTORY

Received: June 26, 2020
Revised: August 19, 2020
Accepted: September 16, 2020

DOI:
10.2174/1389200221999210101232417

Abstract: ***Background*:** Vancomycin has been in clinical use for nearly 50 years and remains the first-line treatment option for Gram-positive infections, including methicillin-resistant *Staphylococcus aureus* (MRSA). There are multiple strategies to monitor therapy and adjust the dose of this antibiotic. AUC24/MIC ratio has been demonstrated to be the best parameter to predict the effectiveness and safety of vancomycin, and a target ratio of ≥400 is recommended. Still, trough and peak serum levels at steady-state conditions have been used in clinical settings as an accurate and practical method to monitor vancomycin.

***Methods*:** In this work, we collected and analyzed clinical information of patients being treated in a hospital center in Porto (Portugal) and studied the pharmacokinetics of vancomycin *in silico*, developing several physiologically based pharmacokinetic (PBPK) models using simulation software GastroPlus™. Different dosages and treatment regimens were studied, and the influence of patients' age, weight and renal function was evaluated; a simulation population was also performed.

***Results*:** A linear effect of dose and a significant influence of weight and renal function in plasmatic levels of vancomycin was observed.

***Conclusion*:** The results of this work corroborate the accumulation of vancomycin in plasma and identify some parameters that influence the pharmacokinetics of this antibiotic. The importance of therapeutic monitoring of vancomycin is highlighted, and the usefulness of *in silico* tools, namely PBPK modeling, is demonstrated.

Keywords: Vancomycin, therapeutic drug monitoring, renal function, drug metabolism, PBPK, Gastroplus™.

1. INTRODUCTION

Glycopeptide antibiotic vancomycin has been used for decades, and is an important penicillin alternative to treat penicillinase-producing strains of *Staphylococcus aureus*. It is still one of the most widely used antibiotics in the United States for the treatment of serious gram-positive infections involving methicillin-resistant *S. aureus* (MRSA), being the first-line treatment option for these infections [1-3].

International guidelines for the clinical application of this antibiotic recommend the administration of 15 to 20 mg/kg of body weight every 8 to 12 h to achieve therapeutic efficacy [4-6]. There are some adverse events that have been associated with vancomycin, with nephrotoxicity causing the most concern, although this is usually mild to moderate and reversible [7]. There is debate regarding the cause of this toxic effect since it is not clear whether high vancomycin levels are a cause or an effect of renal function impairment [8, 9]. Due to great inter-individual variability and to avoid serious deterioration of renal function associated with accumulation of vancomycin and increased plasmatic levels while aiming at improving clinical outcome, patients must be monitored, and vancomycin posology must be adjusted throughout the duration of the treatment. Different approaches can be adopted for this purpose. The area under the curve to minimum inhibitory concentration ratio AUC24/MIC has been established as the best marker of vancomycin therapeutic efficacy as well as of treatment safety. The target consensus of an AUC24/MIC ratio of ≥400 for MRSA infections is supported by *in vitro* data, animal models, and clinical studies that have related an AUC24/MIC ratio of 350 to 400 to a successful clinical outcome [10, 4, 7]. For pathogens with an MIC of 1 mg/L, an AUC/MIC of approximately 250 can be achieved in most patients with 1000 mg every 12 hours (based on a patient with 80 kg and normal renal function) [4].

The determination of trough serum levels at steady-state conditions is most frequently used to monitor vancomycin as it is difficult to calculate AUC in a clinical setting. This has been shown to be not only a practical but also an accurate method. As indicated by the guidelines for the treatment with this antibiotic, the monitoring of vancomycin trough concentration should start before the fourth dose and achieve target levels of 15 to 20 mg/L [4, 11]. Although peak vancomycin serum levels do not correlate to toxicity or efficacy, this concentration is often determined when utilizing Bayesian estimation procedures for dose optimization of vancomycin.

Nevertheless, guiding vancomycin dosing exclusively based on trough levels may be insufficient. A more accurate approach has been provided by linear regression analysis, population PK models and Bayesian estimation procedures. Of these methods, the Bayesian approach is the most accurate procedure when correctly used. It combines optimized population data with information from the

* Address correspondence to this author at the OncoPharma Research Group, Center for Health Technology and Services Research (CINTESIS), Rua Dr. Plácido da Costa, 4200-450 Porto, Portugal; E-mail: nunovale@med.up.pt

1875-5453/21 $65.00+.00

patient to determine the appropriate posology to achieve a target AUC24/MIC [12, 13]. These estimations require exact information such as age, weight, renal function, and previous therapeutic regimen, among others. This presents a hindrance to the use of Bayesian methods in research as this information is usually not available in this context. However, in clinical settings, Bayesian estimation procedures can be used to assist in the adjustment of posology, provided there are trained personnel with specialized pharmacokinetics (PK) knowledge.

In this study, clinical data from patients receiving vancomycin for the treatment of 84 serious infections of diverse etiologies was examined. These patients were hospitalized in *Centro Hospitalar Universitário do Porto* (Portugal). This data was analyzed, and the pharmacokinetics of vancomycin was studied *in silico* with physiologically based pharmacokinetic (PBPK) models using GastroPlus™. This mechanistically based simulation and modeling software for pharmaceutical research builds PBPK models based on preinstalled human physiological parameters. It is a powerful tool, with features and capabilities to support model-based drug development in all phases of drug discovery, translational research and clinical development, and has been used in numerous academic studies and by pharmaceutical companies of excellence, along with the U.S. Food and Drug Administration (FDA), the Centers for Disease Control and Prevention (CDC), the National Institutes of Health (NIH), and the National Cancer Institute (NCI) [14-16]. Based on a drug's structure and inputted data, the most important parameters in pharmacokinetics can be predicted.

Bioavailability and fraction absorbed, maximum concentration reached in plasma and necessary time to reach this concentration, AUC (extrapolated to infinity and over the time of the simulations), and maximum concentration reached in the liver were predicted and are presented here. The influence of vancomycin administered dose, as well as patients' age, weight and renal function, were evaluated. A population simulation was also performed. Together, the results from this work demonstrate that therapeutic monitoring of vancomycin is of critical importance and that patients with impaired renal function must be closely monitored to avoid the plasmatic accumulation of vancomycin. *In silico* tools, namely PBPK modeling, play an important role in this process and can assist clinical staff.

2. METHODS

2.1. Study Population

Clinical information was gathered from a total of 47 patients hospitalized in CHUP, receiving vancomycin for the treatment of serious infections. This data includes posology, observed vancomycin and creatinine plasma concentrations, as well as demographic information such as gender, age, total body weight, and height. Renal function is estimated from creatinine concentration using the Cockcroft-Gault formula to calculate clearance (CL) [17]. Trough concentrations were determined from samples collected right before a vancomycin administration (maximum of 30 minutes before infusion); the concentration of vancomycin is determined in the plasma 3 hours after a dose and is considered the C_{max}. The collected information is presented in Table **1** and summarized in Table **2**.

2.2. Software Used for the *In Silico* Study

GastroPlus™ software version 9.5 (Simulations Plus Inc., Lancaster, California, USA) was used for absorption modeling and simulation (PBPK modeling), prediction of PK parameters and generation of simulated human plasma concentration profiles. Physicochemical properties of vancomycin and input parameters used in the simulations are presented in Table **3**.

2.3. Vancomycin PK *In Silico* Study

2.3.1. Influence of Dose Regimen

Simulations were performed to predict the pharmacokinetics of vancomycin after intravenous administration (over a 1-h infusion). Different doses and intervals between doses were studied: the administration of 1000 mg, 850 mg and 500 mg of vancomycin once daily (every 24 h) and twice daily (every 12 h) for 24 h and 72 h was simulated. PBPK model was customized to represent a patient with age, total body weight, height, and renal clearance equal to the study population average (63 years old, 69 kg, 163 cm, CL = 5.7936 L/h).

2.3.2. Influence of Inter-individual Variability

In a clinical setting and since vancomycin is used to treat serious infections with different etiologies, patients receiving treatment with this antibiotic are demographically diverse. In order to study the influence of patients' age, weight and renal function, the PBPK setup was altered and the lower and upper limit of each of these parameters was used as input to create separate models and simulate the administration of 1000 mg of vancomycin twice daily over 24 h and 72 h. Due to a software restriction, the maximum age was considered 85 years old (the oldest patient in the study population was 93 years old).

2.3.3. Population Simulation

A population of 2500 subjects (randomly generated by Monte Carlo methods; maximum number of subjects allowed by the software) was set to resemble the study population: 55.3% of male subjects, between 19 and 93 years old, and an average clearance of 5.7936 L/h. The end time of the simulation was 72 h and 300 output data points were saved for each virtual subject.

3. RESULTS AND DISCUSSION

3.1. $C_{vancomycin}$ is Proportional to the Administered Dose

PK parameters from simulations developed to study the influence of dose regimen are presented in Table **4**. As expected for an intravenous administration, predicted bioavailability and fraction absorbed were >99% for all simulations. A peak in $C_{vancomycin}$ is always predicted to be reached at the end of each infusion. GastroPlus™ predicted a direct proportionality between dose and predicted C_{max}, and AUC increases by 2-fold with the increase of dosage from 500 mg to 1000 mg. Fig. **1** shows the plasma concentration-time profiles for the studied doses (1000 mg, 850 mg, and 500 mg twice daily).

Predicted plasma concentrations were slightly below expected for these doses and observed data in patients. In the study population, some patients presented very elevated trough concentrations due to impaired and/or aggravation of renal function and accumulation of vancomycin in plasma with continued treatment.

Despite the underprediction of plasmatic concentrations, the vancomycin distribution profile over time is in agreement with the literature and is similar to previously described by Avent *et al.* [12]. These authors reported a vancomycin plasma concentration-time profile for a simulation of a 60-year-old male weighing 70 kg and with a creatinine of 0.90 mg/dL (calculated clearance of 5.16 L/h) following a 2000 mg loading dose and 1000 mg every 12 h.

Table 1. Demographic information and clinical data of the study population.
A population of 47 patients was studied, and the collected data is presented below. Blood samples were typically collected prior to the following vancomycin administration to measure C_{min} (at most 30 minutes before infusion) and 3 h after the end of an infusion to measure C_{max}. When an occasional sample was collected, the concentration is presented in the C_{max} column with the indication of the time of blood sample collection. In some cases, it was not possible to determine vancomycin concentration and a calculated range is presented (estimation of PKS software, used in the clinical setting, ABBOTTBASE® Pharmacokinetic Systems, version 1.10, Abbott Laboratories, Texas, USA). The considered normal range of creatinine concentration in plasma is 0.7 - 1.2 mg/dL for male patients and 0.5 - 0.9 mg/dL for female patients. Clearance was calculated from creatinine concentration using Cockcroft-Gault formula: CL = ((141-age) x weight)/(72 x [creatinine]); multiply by 0.85 in women; CL in mL/min, weight in kg, [creatinine] in mg/dL.

#ID	Sex	Age (Years)	Weight (kg)	Height (cm)	Date	Recommended Posology		C_{min} (mg/L)	C_{max} (mg/L)	[creatinine] (mg/dL)	Clearance (L/h)
						Dose (mg)	Interval				
1	Fem	88	66	155	Day 1	-	-	-	-	0.95	2.56
					Day 4	1000	12 h	-	-	0.90	2.70
					Day 6	750	12 h	17.7	31.0	0.80	3.04
					Day 8	Susp 1 dose > 500 mg 12/12 h		23.4	34.1	0.81	3.00
					Day 12	Susp 1 dose > 750 mg 24/24 h		22.1	27.3	1.04	2.34
					Day 20	500	24 h	21.2	34.7	1.18	2.06
2	Fem	51	90	165	Day 1	1000	12 h	-	-	-	-
					Day 3	800	8 h	9.3	19.8	0.86	6.60
					Day 4	-	-	-	-	0.72	7.88
					Day 6	800	8 h	10.2	19.1	0.55	10.32
					Day 9	-	-	-	-	0.74	7.67
					Day 10	-	-	-	-	0.79	7.18
					Day 11	950	8 h	12.2	21.2	0.60	9.46
3	Fem	50	90	160	Day 1	1000	12 h	-	-	-	-
					Day 8	Susp 1 dose > 600 mg 12/12 h		26.0	36.1	1.05	5.46
					Day 11	600	12 h	15.6	24.3	1.12	5.12
					Day 16	700	12 h	12.5	23.9	0.90	6.38
					Day 19	600	12 h	18.6	(occas 4 h) 29.7	1.02	5.63
4	Fem	61	68	160	Day 1	-	-	-	-	0.72	5.28
					Day 2	1000	12 h	-	-	0.63	6.04
					Day 3	1000	8 h	6.6	16.1	0.52	7.32
					Day 4	-	-	-	-	0.58	6.56
					Day 5	-	-	-	-	0.49	7.77
			75		Day 6	Susp 1 dose > 700 mg 8/8 h		23.8	36.2	0.45	8.46
					Day 9	700	8 h	7.8	18.9	0.56	6.79
5	Male	58	87	185	Day 1	1000	12 h	-	-	-	-
					Day 3	-	-	-	-	0.71	8.37
					Day 4	1000	8 h	7.3	16.8	0.72	8.26
					Day 6	Susp vancomycin administration		16.7	23.7	1.32	4.50
6	Male	62	70	172	Day 1	1000	12 h	-	-	-	-
					Day 2	-	-	-	-	0.57	7.98
					Day 3	650	6 h	8.5	17.1	0.52	8.75
					Day 5	700	6 h	10.8	15.2	0.53	8.58
7	Male	53	65	165	Day 1	-	-	-	-	0.97	4.86
					Day 2	1000	12 h	-	-	1.16	4.06
					Day 5	850	12 h	calc 19-21	(occas 4 h) 30.2	0.88	5.36
					Day 6	850	12 h	15.4	27.3	1.10	4.28
					Day 7	850	12 h	14.9	28.4	1.01	4.67
					Day 9	-	-	-	-	1.23	3.83
					Day 13	600	12 h	22.3	34.0	1.13	4.17
8	Fem	66	140	163	Day 1	1000	12 h	-	-	-	-
					Day 3	Susp 1 dose > 500 mg 12/12 h		19.6	28.3	-	-
					Day 7	Susp 1 dose > 950 mg 24/24 h		17.4	22.9	0.84	8.74
					Day 13	800	24 h	14.1	(occas 4 h) 23.7	-	-
9	Male	64	70	168	Day 1	1000	12 h	-	-	-	-
					Day 5	1000	12 h	14.7	28.0	-	-

(Table 1) contd....

#ID	Sex	Age (Years)	Weight (kg)	Height (cm)	Date	Recommended Posology		C_{min} (mg/L)	C_{max} (mg/L)	[creatinine] (mg/dL)	Clearance (L/h)
						Dose (mg)	Interval				
-	-	-	-	-	Day 7	850	12 h	19.3	21.1	1.17	3.79
					Day 12	Susp 1 dose > 1000 mg 24/24 h		28.0	33.4	1.29	3.44
					Day 15	500	12 h	10.7	calc 27-29	1.35	3.28
10	Fem	47	65	147	Day 1	1000	12 h	-	-	-	-
					Day 3	Susp 1 dose > 750 mg 12/12 h		17.3	42.5	1.10	3.89
					Day 7	500	8 h	10.5	23.0	-	-
					Day 10	500	8 h	13.1	22.4	0.70	6.12
11	Fem	73	80	160	Day 1	1000	12 h	-	-	-	-
					Day 6	Susp 1 dose > 650 mg 12/12 h		26.4	32.6	0.53	7.16
					Day 14	600	12 h	19.1	25.3	-	-
					Day 19	600	12 h	15.5	23.7	-	-
					Day 23	650	12 h	16.5	-	-	-
					Day 25	-	-	-	-	0.47	8.08
					Day 27	600	12 h	20.9	26.6	0.45	8.44
					Day 30	500	12 h	22.4	31.0	0.41	9.26
12	Male	59	85	174	Day 1	500	6 h	-	-	-	-
					Day 3	700	6 h	10.7	11.8	-	-
					Day 4	-	-	-	-	0.48	11.95
					Day 5	800	6 h	11.4	14.8	-	-
13	Fem	20	29	155	Day 1	1000	12 h	-	-	-	-
					Day 3	500	6 h	5.8	-	0.35	7.04
					Day 5	300	4 h	8.1	15.0	0.35	7.04
					Day 8	300	4 h	13.2	-	0.41	6.01
					Day 11	300	4 h	1.6[a]; calc 12-14	-	0.40	6.16
14	Male	80	60	160	Day 1	-	-	-	-	4.78	0.63
					Day 2	900	12 h	-	-	-	-
					Day 3	-	-	-	-	4.46	0.67
					Day 4	-	-	-	-	4.43	0.68
					Day 5	Susp vancomycin administration		22.3	(occas 4 h) 39.6	3.99	0.75
					Day 6	-	-	-	-	2.98	1.01
					Day 7	-	-	24.3	-	3.32	0.90
					Day 8	500	24 h	-	-	2.83	1.06
					Day 9	-	-	-	-	2.24	1.34
					Day 11	-	-	-	-	1.78	1.69
					Day 12	400	24 h	21.4	27.5	1.95	1.54
15	Fem	82	70	165	Day 1	-	-	-	-	0.93	3.09
					Day 2	-	-	-	-	0.80	3.59
					Day 3	-	-	-	-	0.89	3.23
					Day 4	-	-	-	-	0.78	3.69
					Day 5	1000	12 h	-	-	-	-
					Day 6	1000	12 h	10.6	23.0	0.80	3.59
					Day 9	-	-	-	-	1.01	2.85
					Day 11	900	12 h	17.2	32.5	0.96	3.00
					Day 13	Susp 1 dose > 500 mg 12/12 h		27.2	36.5	0.92	3.13
16	Male	53	70	170	Day 1	1000	12 h	-	-	0.50	10.15
					Day 3	-	-	-	-	0.40	12.69
					Day 4	850	6 h	4.8	11.2	0.40	12.69
					Day 6	850	6 h	9.6	14.2	0.54	9.40
					Day 7	900	6 h	9.5	13.0	0.40	12.69
					Day 9	-	-	-	-	0.68	7.46
					Day 10	-	-	-	-	0.78	6.51
					Day 11	850	6 h	18.5	28.1	0.68	7.46
17	Male	93	50	170	Day 1	-	-	-	-	3.32	0.59
					Day 2	-	-	-	-	2.85	0.69

(Table 1) contd....

#ID	Sex	Age (Years)	Weight (kg)	Height (cm)	Date	Recommended Posology		C_{min} (mg/L)	C_{max} (mg/L)	[creatinine] (mg/dL)	Clearance (L/h)
						Dose (mg)	Interval				
-	-	-	-	-	Day 4	1000	12 h	-	-	-	-
					Day 8	Susp 3 days > 900 mg 24/24 h		44.5	60.1	2.04	0.96
					Day 13	Susp vancomycin administration		31.4	45.3	2.06	0.95
18	Male	65	65	170	Day 1	1000	12 h	-	-	-	-
					Day 6	750	6 h	7.9	15.6	0.61	6.66
					Day 9	850	6 h	12.9	17.7	0.69	5.89
					Day 13	Susp 2 doses > 650 mg 6/6 h		21.1	27.9	0.74	5.49
					Day 22	1000	12 h	-	-	-	-
					Day 26	600	6 h	11.0	21.3	-	-
19	Male	54	70	172	Day 1	1000	8 h	-	-	-	-
					Day 2	850	6 h	10.7	19.8	-	-
					Day 4	800	6 h	13.7	21.9	-	-
					Day 6	-	-	-	-	0.47	10.67
					Day 7	-	-	-	-	0.41	12.24
					Day 8	800	8 h	5.4	-	0.49	10.24
					Day 9	-	-	-	-	0.61	8.22
					Day 10	700	8 h	21.5[a]	-	0.53	9.47
					Day 11	-	-	9.5	14.2	-	-
					Day 12	-	-	-	-	0.47	10.67
					Day 14	-	-	-	-	0.37	13.56
					Day 15	-	-	14.7	-	0.45	11.15
20	Male	61	90	175	Day 1	1000	12 h	-	-	-	-
					Day 3	-	-	-	-	1.01	5.87
					Day 4	-	-	-	-	0.93	6.37
					Day 7	Susp vancomycin administration		14.9	30.2	0.81	7.31
21	Fem	70	61	158	Day 1	1000	12 h	-	-	0.77	3.93
					Day 3	-	-	-	-	0.74	4.09
					Day 6	700	12 h	20.5	35.6	0.76	3.98
22	Male	79	60	150	Day 1	-	-	-	-	1.98	1.54
					Day 3	-	-	-	-	1.98	1.54
					Day 4	1000	24 h	-	-	-	-
					Day 8	Susp vancomycin administration		25.7	41.5	2.08	1.47
23	Fem	90	45	160	Day 1	-	-	-	-	1.14	1.40
					Day 4	700	12 h	-	-	1.19	1.34
					Day 7	500	12 h	21.0	30.3	1.11	1.44
					Day 10	500	12 h	-	29.5	0.97	1.64
					Day 16	Susp 2 doses > 800 mg 24/24 h		20.3	-	1.19	1.34
					Day 18	-	-	-	-	1.38	1.15
					Day 21	500	24 h	22.1	-	1.49	1.07
24	Fem	85	80	163	Day 1	500	12 h	-	-	-	-
					Day 2	-	-	-	-	1.20	2.60
					Day 3	Susp 2 doses > 650 mg 24/24 h		25.4	-	0.83	3.76
					Day 4	650	24 h	16.8	25.8	-	-
25	Fem	63	70	165	Day 1	-	-	-	-	0.54	7.07
					Day 2	1000	12 h	-	-	-	-
					Day 3	-	-	-	-	0.93	4.11
					Day 4	Susp 1 dose > 650 mg 8/8 h		12.3	16.3	0.86	4.44
26	Male	71	60	165	Day 1	-	-	-	-	1.36	2.54
					Day 3	1000	12 h	-	-	1.04	3.32
					Day 5	Susp 1 dose > 600 mg 12/12 h		23.3	36.0	0.89	3.88
27	Male	59	70	180	Day 1	1000	12 h	-	-	-	-
					Day 4	Susp 1 dose > 500 mg 12/12 h		32.2	44.5	-	-
					Day 5	-	-	-	-	1.22	3.87
					Day 8	-	-	17.9	22.4	1.17	4.04

(Table 1) contd....

#ID	Sex	Age (Years)	Weight (kg)	Height (cm)	Date	Recommended Posology		C_{min} (mg/L)	C_{max} (mg/L)	[creatinine] (mg/dL)	Clearance (L/h)
						Dose (mg)	Interval				
-	-	-	-	-	Day 9	850	6 h	-	-	-	-
					Day 15	1000	12 h	-	-	-	-
					Day 18	-	-	-	-	1.11	4.26
					Day 20	-	-	-	-	1.06	4.46
					Day 22	Susp vancomycin administration		45.6	57.1	1.25	3.78
					Day 25	-		(Occasional monitoring) 27.2		-	-
28	Male	23	60	163	Day 1	1000	12 h	-	-	-	-
					Day 3	850	6 h	5.1	-	0.88	6.65
					Day 6	850	6 h	12.0	-	1.02	5.74
					Day 10	-	-	-	-	1.00	5.85
					Day 13	900	6 h	10.2	-	0.96	6.09
					Day 17	900	6 h	17.0	-	0.98	5.97
					Day 20	900	6 h	9.6[a]	-	0.94	6.22
29	Male	78	70	172	Day 1	1000	12 h	-	-	-	-
					Day 7	-	-	21.0	28.0	0.83	4.36
					Day 8	750	12 h	-	-	0.94	3.85
					Day 9	-	-	22.1	-	0.82	4.41
					Day 10	-	-	-	-	0.86	4.21
					Day 11	-	-	-	-	0.82	4.41
					Day 12	-	-	16.9	-	0.93	3.89
					Day 15	-	-	16.9	25.9	-	-
					Day 27	1000	12 h	-	-	-	-
					Day 34	-	-	25.0	34.7	-	-
					Day 35	-	-	18.5	29.4	-	-
					Day 40	Susp vancomycin administration		26.2	-	-	-
					Day 42	-	-	(Occasional monitoring) 11.4		-	4.21
30	Male	53	70	180	Day 1	-	-	-	-	-	14.50
					Day 5	1000	12 h	-	-	0.27	18.80
					Day 11	-	-	5.3	12.8	0.38	13.36
					Day 14	850	8 h	6.7	15.0	0.30	16.92
					Day 18	950	8 h	14.8	15.4	-	-
					Day 20	800	6 h	12.4	19.8	0.32	15.86
31	Male	41	75	175	Day 1	1000	12 h	-	-	-	-
					Day 3	900	12 h	16.7	25.2	1.55	3.99
					Day 8	Susp 2 doses > 600 mg 12/12 h		24.9	33.8	1.44	4.30
					Day 11	550	12 h	17.8	23.1	1.68	3.68
					Day 14	600	12 h	16.1	21.9	1.20	5.16
					Day 18	650	12 h	14.4	28.6	1.01	6.13
					Day 22	650	12 h	16.7	26.4	1.02	6.07
					Day 25	650	12 h	16.0	44.3[a]	1.02	6.07
32	Male	81	95	170	Day 1	1000	12 h	-	-	-	-
					Day 2	800	12 h	8.4	-	1.34	3.49
					Day 4	600	12 h	25.7	34.0	-	-
					Day 5	Susp 3 doses > 1000 mg 24/24 h		27.1	31.7	1.39	3.36
					Day 6	-	-	-	-	1.25	3.74
					Day 8	1000	24 h	16.3	-	1.19	3.93
					Day 11	-	-	19.0	-	-	-
					Day 12	-	-	-	-	1.11	4.21
					Day 15	-	-	23.3	42.6	1.17	3.99
					Day 16	Susp vancomycin administration		25.8	-	1.28	3.65
33	Fem	52	68	164	Day 1	1000	12 h	-	-	-	-
					Day 6	700	8 h	12.7	-	0.70	6.06
34	Male	54	70	165	Day 1	1000	12 h	-	-	-	-
					Day 6	-	-	17.6	-	-	-

(Table 1) contd....

#ID	Sex	Age (Years)	Weight (kg)	Height (cm)	Date	Recommended Posology		C_{min} (mg/L)	C_{max} (mg/L)	[creatinine] (mg/dL)	Clearance (L/h)
						Dose (mg)	Interval				
-	-	-	-	-	Day 7	-	-	-	-	0.96	5.23
					Day 8	-	-	-	-	1.08	4.65
					Day 9	-	-	23.2	-	0.89	5.64
					Day 10	600	12 h	18.0	-	0.82	6.12
					Day 17	Susp 1 dose > 750 mg 24/24 h		calc 24-26	32.5	-	-
					Day 18	-	-	-	-	1.25	4.01
					Day 19	-	-	-	-	0.97	5.17
					Day 20	Susp 1 dose > 1000 mg 24/24 h[b]		13.3	23.2	0.93	5.39
					Day 23	450	12 h	11.9	-	-	-
					Day 24	-	-	-	-	0.63	7.96
					Day 25	-	-	-	-	0.64	7.84
					Day 26	-	-	-	-	0.65	7.72
					Day 27	-	-	-	-	0.56	8.96
35	Male	62	121	176	Day 1	1000	12 h	-	-	-	-
					Day 4	1000	8 h	6.5	14.9	0.76	10.35
					Day 7	Susp 1 dose > 800 mg 6/6 h		12.0	20.0	0.82	9.59
					Day 11	-	-	-	-	0.87	9.04
					Day 12	1000	12 h	16.0	19.7	-	-
					Day 19	750	6 h	8.1	14.5	0.77	10.21
					Day 21	800	6 h	12.3	14.4[a]	0.79	9.96
					Day 25	900	6 h	12.2	15.1	0.73	10.77
					Day 29	-	-	14.9	20.1	0.82	9.59
					Day 31	-	-	-	-	0.87	9.04
					Day 33	900	6 h	16.9	20.5	0.77	10.21
					Day 36	Susp 2 doses > 800 mg 6/6 h		11.6	16.9	0.84	9.36
					Day 39	900	6 h	17.4	21.2	0.80	9.83
36	Male	62	65	170	Day 1	500	6 h	-	-	-	-
					Day 10	-	-	-	-	1.38	3.06
					Day 15	600	6 h	13.4	17.8	0.94	4.49
37	Fem	80	60	165	Day 1	1000	12 h	-	-	0.62	4.11
					Day 3	600	6 h	7.2	17.4	0.40	6.38
					Day 6	600	6 h	13.2	16.7	0.34	7.50
					Day 8	500	6 h	16.8	20.8	0.32	7.97
38	Fem	86	50	155	Day 1	1000	12 h	19.2	35.5	0.65	2.94
39	Fem	20	50	157	Day 1	1000	12 h	4.5	14.9	0.43	9.88
40	Male	54	58	160	Day 1	1000	12 h	15.0	34.6	0.63	6.60
41	Fem	46	70	156	Day 1	1000	12 h	6.6	19.2	0.38	12.27
42	Fem	78	47	160	Day 1	650	12 h	14.9	29.0	0.74	2.79
42	Fem	63	70	170	Day 1	1000	12 h	9.0	19.2	0.55	6.94
44	Male	83	70	170	Day 1	1000	12 h	15.1	26.9	0.97	3.43
45	Male	75	57	170	Day 1	1000	12 h	24.9	41.0	1.03	3.00
46	Male	83	65	170	Day 1	1000	12 h	22.3	36.8	1.28	2.41
47	Fem	19	60	170	Day 1	1000	8 h	18.0	43.1	1.87	2.75

[a] probable irregularity in the analytical determination of vancomycin concentration. [b] previous posology was followed.
Susp X dose: X number of scheduled doses were suspended and recommended posology for when vancomycin administrations are resumed is presented.

Regarding the dosing interval, C_{max} is higher and AUC increases by 2-fold when vancomycin is administered twice daily when compared to once-daily administrations of the same dose.

3.2. Vancomycin Accumulates in Plasma Over Time

As described in the literature [11], vancomycin can accumulate in plasma, especially over prolonged treatment, and in patients with impaired renal function. This effect was observed in the study population and was also predicted even when considering an administration of 1000 mg twice daily (standard initial posology) for the average clearance of the study population (Fig. **2**). C_{min} after the first administration is about 4.9 mg/L, but 12 h after the sixth dose (at the end of this 72-h simulation), $C_{vancomycin}$ is 8.8 mg/L. This shows that vancomycin is not completely cleared from the organism before the next dose is administered, leading to increased plasmatic levels over time.

3.3. Dependence on Age, Weight and Renal Function

According to the results of this assessment Table **5**, age itself has no influence on the PK of vancomycin (Fig. **3**). However, it

should be mentioned that renal function worsens with age and usually aggravates more easily and rapidly in case of disease. On the other hand, both weight and renal function have a significant influence on the PK of this antibiotic. With increased body weight, the main difference is in C_{max} (from 48.4 mg/L considering the lowest weight, to 22.5 mg/L considering the highest weight), and although after the first dose vancomycin seems to be cleared to the same trough levels, there is a difference in the predicted C_{min} after 72 h indicating accumulation in heavier patients (Fig. **4**).

Table 2. Summary of collected clinical data, with the indication of lower and upper limits and calculation of average value for each parameter.

Characteristics	-	-	-	-
Gender n (%)	Female: 21 (44.7%); Male: 26 (55.3%)			
Age lower limit (years)	19	Average	63.3	(ID #47; female, 60 kg, 170 cm)
Age upper limit (years)	93			(ID #17; male, 50 kg, 170 cm)
Weight lower limit (kg)	29	Average	69.0	(ID #13; female, 20 yo, 155 cm)
Weight upper limit (kg)	140			(ID #8; female, 66 yo, 163 cm)
Height lower limit (cm)	147	Average	163.3	(ID #10; female, 47 yo, 65 kg)
Height upper limit (cm)	185			(ID #5; male, 58 yo, 87 kg)
C_{min} lower limit (mg/L)	4.5	Average	16.34	(ID #39; female, 20 yo, 50 kg, 157 cm)
C_{min} upper limit (mg/L)	45.6			(ID #27; male, 59 yo, 70 kg, 180 cm)
C_{max} lower limit (mg/L)	11.2	Average	25.99	(ID #16; male, 53 yo, 70 kg, 170 cm)
C_{max} upper limit (mg/L)	60.1			(ID #17; male, 93 yo, 50 kg, 170 cm)
[Creatinine] lower limit (mg/dL)	0.27	Average	1.00	(ID #30; male, 53 yo, 70 kg, 180 cm)
[Creatinine] upper limit (mg/dL)	4.78			(ID #14; male, 80 yo, 60 kg, 160 cm)
Clearance lower limit (L/h)	0.59	Average	5.79	(ID #17; male, 93 yo, 50 kg, 170 cm)
Clearance upper limit (L/h)	18.80			(ID #30; male, 53 yo, 70 kg, 180 cm)

yo: Years old.

Table 3. Physicochemical properties of vancomycin and input parameters in GastroPlus™.

Parameter	Value
Molecular weight	1449.28
logP (neutral)	2.48 [1]
Solubility	4.00 mg/mL (@pH 8.17) [2]
Dose-volume	250 mL
Human jejunal permeability	0.51 x 10^{-4} cm/s
Drug particle density	1.2 g/mL

[1] predicted by GastroPlus™ ADMET Predictor™.
[2] optimized values considering the Biopharmaceutics Classification System (BCS).

Table 4. Pharmacokinetic properties of vancomycin; influence of dose regimen.

Posology		T_{simul} [1]	Fa (%)[2]	FDp (%)[3]	F (%)[4]	C_{max} (mg/L)[5]	T_{max} (h)[6]	AUC 0-inf (µg.h/mL)[7]	AUC 0-t (µg.h/mL)[8]	$C_{maxliver}$ (mg/L)[9]
Dose (mg)	Interval									
1000	24 h (1x day)	24 h	99.873	99.861	99.861	23.067	1	172.420	140.050	44.990
		72 h	99.890	99.885	99.885	25.520	49	512.270	477.270	49.992
	12 h (2x day)	24 h	99.860	99.840	99.840	27.687	13	344.790	239.500	54.411
		72 h	99.884	99.876	99.876	31.227	61	1034.500	904.380	61.632
850	24 h (1x day)	24 h	99.873	99.861	99.861	19.607	1	146.560	119.040	38.242
		72 h	99.890	99.885	99.885	21.692	49	439.680	405.680	42.493
	12 h (2x day)	24 h	99.860	99.840	99.840	23.534	13	293.070	203.580	46.250
		72 h	99.884	99.876	99.876	26.543	61	879.310	768.730	52.387
500	24 h (1x day)	24 h	99.873	99.861	99.861	11.534	1	86.211	70.026	22.495
		72 h	99.890	99.885	99.885	12.760	49	258.630	238.640	24.996
	12 h (2x day)	24 h	99.860	99.840	99.840	13.843	13	172.390	119.750	27.206
		72 h	99.884	99.876	99.876	15.613	61	517.240	452.190	30.816

[1] Duration of simulation; [2] fraction absorbed as a percent of the dose (crossing the lumen and entering enterocytes); [3] percent of the dose that has reached the portal vein; [4] bioavailability; [5] maximum plasma concentration reached in the central compartment, in mg/L; [6] time to reach maximum plasma concentration, in hours; [7] area under the plasma concentration-time curve, in µg.h/mL, extrapolated to infinity; [8] area under the plasma concentration-time curve, in µg.h/mL, for the time of the simulation; [9] maximum concentration reached in the liver, in mg/L.

Table 5. Influence of age, total body weight, and renal clearance of patients on the pharmacokinetic properties of vancomycin (for a 1000 mg dose twice daily).

-	T_{simul} [1]	Fa (%)[2]	FDp (%)[3]	F (%)[4]	C_{max} (mg/L)[5]	T_{max} (h)[6]	AUC_{0-inf} (µg.h/mL)[7]	AUC_{0-t} (µg.h/mL)[8]	$C_{maxliver}$ (mg/L)[9]
Youngest age (19 yo)	24 h	99.860	99.840	99.840	26.811	13	344.790	239.090	52.864
	72 h	99.884	99.876	99.876	30.363	61	1034.500	904.070	60.105
Oldest age (85 yo; max allowed)	24 h	99.860	99.841	99.841	29.025	13	344.770	240.940	56.448
	72 h	99.884	99.876	99.876	32.517	61	1034.500	906.160	63.582
Lowest weight (29 kg)	24 h	99.917	99.911	99.911	47.740	13	344.950	314.490	94.211
	72 h	99.928	99.926	99.926	48.405	61	1034.900	1003.600	95.574
Highest weight (140 kg)	24 h	99.886	99.867	99.867	16.698	13	344.670	161.130	32.694
	72 h	99.889	99.879	99.879	22.513	61	1034.300	735.410	44.527
Lowest CL (0.59 L/h)	24 h	99.710	99.652	99.652	36.736	13	3351.800	431.910	72.363
	72 h	99.605	99.555	99.555	73.070	61	10070.000	2654.500	146.100
Highest CL (18.80 L/h)	24 h	99.952	99.949	99.949	19.254	13	106.350	101.040	37.897
	72 h	99.964	99.963	99.963	19.343	61	319.050	313.680	38.080

[1] Duration of simulation; [2] fraction absorbed as a percent of the dose (crossing the lumen and entering enterocytes); [3] percent of the dose that has reached the portal vein; [4] bioavailability; [5] maximum plasma concentration reached in the central compartment, in mg/L; [6] time to reach maximum plasma concentration, in hours; [7] area under the plasma concentration-time curve, in µg.h/mL, extrapolated to infinity; [8] area under the plasma concentration-time curve, in µg.h/mL, for the time of the simulation; [9] maximum concentration reached in the liver, in mg/L.

Table 6. Population simulation results (mean and 90% CI ln-transformed values); 2500 virtual subjects, 55.3% male subjects, between 19 and 93 years old, average clearance of 5.79 L/h.

-	Fa (%)[1]	FDp (%)[2]	F (%)[3]	C_{max} (mg/L)[4]	T_{max} (h)[5]	AUC_{0-inf} (µg.h/mL)[6]	AUC_{0-t} (µg.h/mL)[7]
Mean	99.703	99.664	99.664	53.257	61	5299.4	1925.8
(90% CI-LnTrans)	(99.70-99.71)	(99.66-99.67)	(99.66-99.67)	(52.05-52.69)	(61.00-61.00)	(4789.6-4922.9)	(1875.2-1900.3)

[1] fraction absorbed as a percent of the dose (crossing the lumen and entering enterocytes); [2] percent of the dose that has reached the portal vein; [3] bioavailability; [4] maximum plasma concentration reached in the central compartment, in mg/L; [5] time to reach maximum plasma concentration, in hours; [6] area under the plasma concentration-time curve, in µg.h/mL, extrapolated to infinity; [7] area under the plasma concentration-time curve, in µg.h/mL, for the time of the simulation.

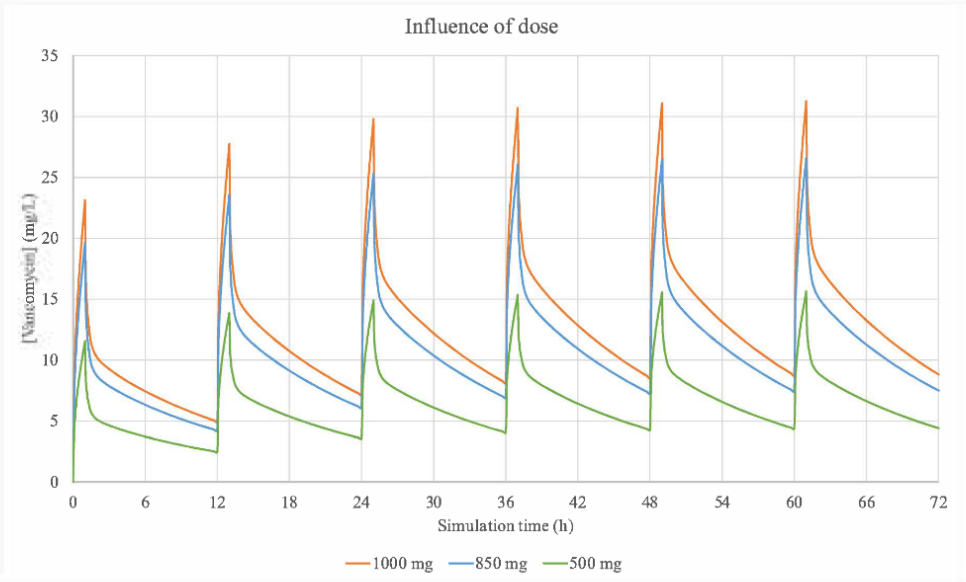

Fig. (1). Vancomycin plasma concentration-time profiles showing the influence of dose (considering the average of the study population: 63 years old, 69 kg, 163 cm, CL = 5.7936 L/h). (*A higher resolution / colour version of this figure is available in the electronic copy of the article*).

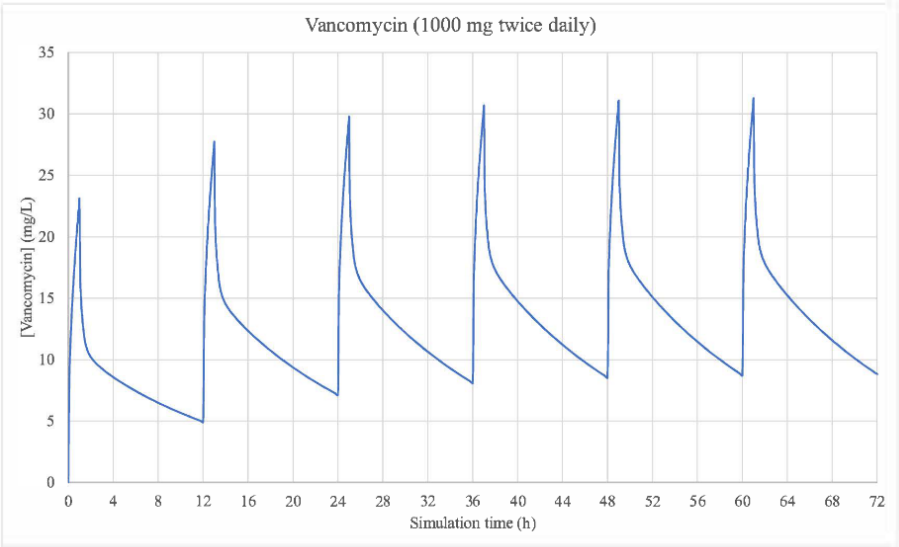

Fig. (2). Vancomycin plasma concentration-time profile for a 1000 mg dose twice daily (considering the average of the study population: 63 years old, 69 kg, 163 cm, CL = 5.7936 L/h). (*A higher resolution / colour version of this figure is available in the electronic copy of the article*).

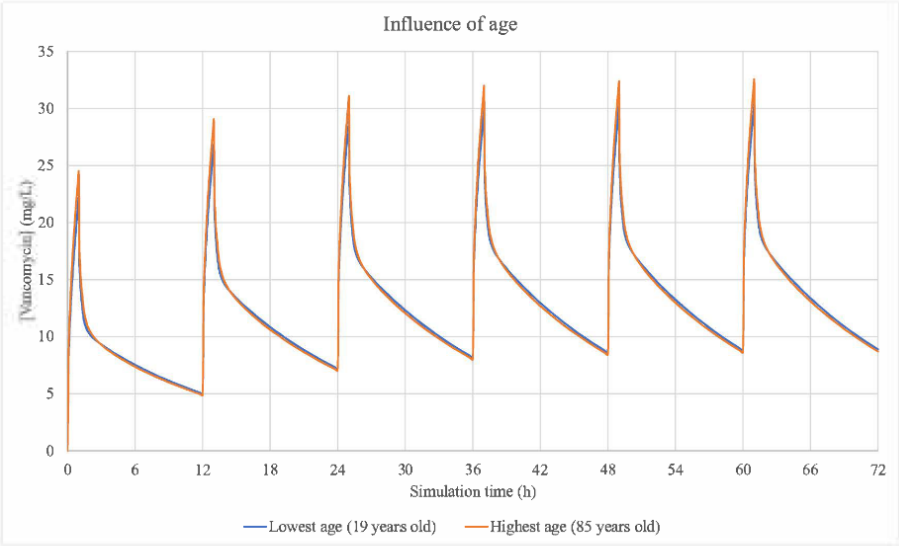

Fig. (3). Vancomycin plasma concentration-time profiles showing the influence of patients' age (for a 1000 mg dose twice daily; weight and renal function defined as the average of the study population). (*A higher resolution / colour version of this figure is available in the electronic copy of the article*).

Fig. (4). Vancomycin plasma concentration-time profiles showing the influence of patients' total body weight (for a 1000 mg dose twice daily; age and renal function defined as the average of the study population). (*A higher resolution / colour version of this figure is available in the electronic copy of the article*).

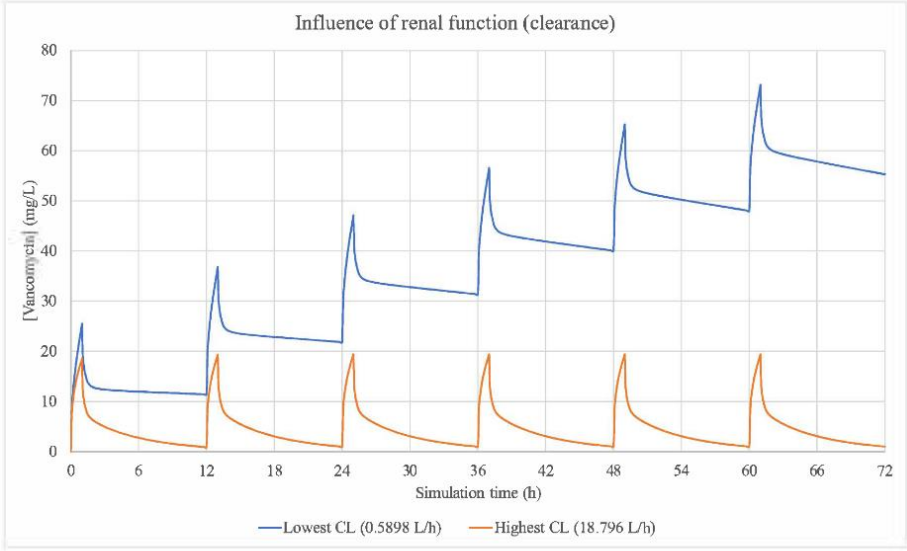

Fig. (5). Vancomycin plasma concentration-time profiles showing the influence of patients' renal function (for a 1000 mg dose twice daily; age and weight defined as the average of the study population). (*A higher resolution / colour version of this figure is available in the electronic copy of the article*).

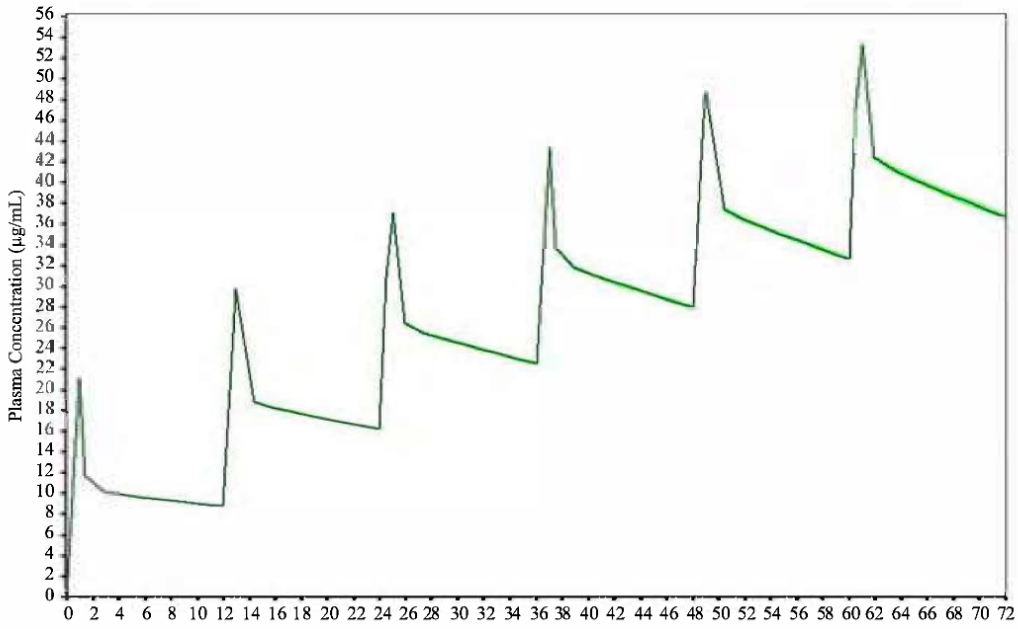

Fig. (6). Population simulation results - plasma concentration-time profile (mean and confidence range); population setup: 55.3% of male subjects, between 19 and 93 years old, and an average clearance of 5.79 L/h; 1000 mg dose twice daily. (*A higher resolution / colour version of this figure is available in the electronic copy of the article*).

Renal function has a more accentuated influence in the PK of vancomycin (Fig. **5**). While if a high clearance is considered, vancomycin is systematically cleared from the plasma, with no indications of accumulation over time, patients with the impaired renal function must be closely monitored, as only approximately 50% of the vancomycin dose was predicted to be cleared before the next dose for the lowest clearance observed and simulated. In this case, the predicted C_{min} increased from 11.1 mg/L after the first dose to 55.3 mg/L after 6 doses.

3.4. Population Simulation

The results from the population simulation developed in this project are presented in Fig. (**6**) and in Table **6** as the mean and 90% confidence interval (CI) using ln-transformed data of each pharmacokinetic parameter. This simulation represents an average of the study population, and results show an accumulation of vancomycin in plasma, given the drug is not completely cleared from the systemic circulation after a short period of time and before the next dose. As previously mentioned, this accumulation is more accentuated in patients who present or develop renal function impairment during the treatment.

CONCLUSION

This work highlights the importance of therapeutic monitoring of vancomycin. The clinical data observed in our study population and the results of the *in silico* study on the pharmacokinetics of this antibiotic presented here substantiate the evidence of accumulation of vancomycin plasmatic levels, reinforcing the need to monitor patients receiving this antibiotic and adjust their posology. A direct effect of vancomycin dose in plasma levels, but more importantly, the influence of certain patients' characteristics, particularly total body weight and renal function, was predicted in the PBPK simulations. Renal function can deteriorate during treatment (even if not very significantly), so particular populations such as the elderly and overweight patients, need to be closely monitored to avoid high levels and accumulation of this drug that can lead to toxic effects. PBPK modeling has shown potential to assist this dosage adjustment process.

ETHICS APPROVAL AND CONSENT TO PARTICIPATE

Not applicable.

HUMAN AND ANIMAL RIGHTS

No animals/humans were used for studies that are the basis of this research.

CONSENT FOR PUBLICATION

Not applicable.

FUNDING

This work was financed by FEDER - Fundo Europeu de Desenvolvimento Regional funds through the COMPETE 2020 - Operational Programme for Competitiveness and Internationalisation

(POCI), Portugal 2020, and by Portuguese funds through FCT - Fundação para a Ciência e a Tecnologia, within CINTESIS, R&D Unit (reference UIDB/4255/2020). Nuno Vale thanks FCT and FEDER (European Union) also supported these studies through project number IF/00092/2014/CP1255/CT0004. Rui Lapa thanks FCT through grant UID/QUI/50006/2019 (LAQV-REQUIMTE). Abigail Ferreira thanks also FCT for a doctoral fellowship (PD/BD/135120/2017). The contents of this article are solely the responsibility of the authors and do not necessarily represent the official view of the FCT.

CONFLICT OF INTEREST

The authors have no conflicts of interest, financial or otherwise.

ACKNOWLEDGEMENTS

Declared none.

REFERENCES

[1] Levine, D.P. Vancomycin: a history. *Clin. Infect. Dis.,* **2006**, *42*(Supplement_1), S5-S12.
http://dx.doi.org/10.1086/491709

[2] Cataldo, M.A.; Tacconelli, E.; Grilli, E.; Pea, F.; Petrosillo, N. Continuous *versus* intermittent infusion of vancomycin for the treatment of Gram-positive infections: systematic review and meta-analysis. *J. Antimicrob. Chemother.,* **2012**, *67*(1), 17-24.
http://dx.doi.org/10.1093/jac/dkr442 PMID: 22028203

[3] Levine, J.F. Vancomycin: a review. *Med. Clin. North Am.,* **1987**, *71*(6), 1135-1145.
http://dx.doi.org/10.1016/S0025-7125(16)30801-X PMID: 3320615

[4] Rybak, M.; Lomaestro, B.; Rotschafer, J.C.; Moellering, R., Jr; Craig, W.; Billeter, M.; Dalovisio, J.R.; Levine, D.P. Therapeutic monitoring of vancomycin in adult patients: a consensus review of the American Society of Health-System Pharmacists, the Infectious Diseases Society of America, and the Society of Infectious Diseases Pharmacists. *Am. J. Health Syst. Pharm.,* **2009**, *66*(1), 82-98.
http://dx.doi.org/10.2146/ajhp080434 PMID: 19106348

[5] Liu, C.; Bayer, A.; Cosgrove, S.E.; Daum, R.S.; Fridkin, S.K.; Gorwitz, R.J.; Kaplan, S.L.; Karchmer, A.W.; Levine, D.P.; Murray, B.E.; J Rybak, M.; Talan, D.A.; Chambers, H.F. Infectious Diseases Society of America. Clinical practice guidelines by the infectious diseases society of america for the treatment of methicillin-resistant *Staphylococcus aureus* infections in adults and children. *Clin. Infect. Dis.,* **2011**, *52*(3), e18-e55.
http://dx.doi.org/10.1093/cid/ciq146 PMID: 21208910

[6] Marsot, A.; Boulamery, A.; Bruguerolle, B.; Simon, N. Vancomycin: a review of population pharmacokinetic analyses. *Clin. Pharmacokinet.,* **2012**, *51*(1), 1-13.
http://dx.doi.org/10.2165/11596390-000000000-00000 PMID: 22149255

[7] Álvarez, R.; López Cortés, L.E.; Molina, J.; Cisneros, J.M.; Pachón, J. Optimizing the clinical use of vancomycin. *Antimicrob. Agents Chemother.,* **2016**, *60*(5), 2601-2609.
http://dx.doi.org/10.1128/AAC.03147-14 PMID: 26856841

[8] Bruniera, F.R.; Ferreira, F.M.; Saviolli, L.R.; Bacci, M.R.; Feder, D.; da Luz Gonçalves Pedreira, M.; Sorgini Peterlini, M.A.; Azzalis, L.A.; Campos Junqueira, V.B.; Fonseca, F.L. The use of vancomycin with its therapeutic and adverse effects: a review. *Eur. Rev. Med. Pharmacol. Sci.,* **2015**, *19*(4), 694-700.
PMID: 25753888

[9] Bamgbola, O. Review of vancomycin-induced renal toxicity: an update. *Ther. Adv. Endocrinol. Metab.,* **2016**, *7*(3), 136-147.
http://dx.doi.org/10.1177/2042018816638223 PMID: 27293542

[10] Rybak, M.J. Pharmacodynamics: relation to antimicrobial resistance. *Am. J. Infect. Control,* **2006**, *34*(5)(Suppl. 1), S38-S45.
http://dx.doi.org/10.1016/j.ajic.2006.05.227 PMID: 16813981

[11] Ye, Z.K.; Tang, H.L.; Zhai, S.D. Benefits of therapeutic drug monitoring of vancomycin: a systematic review and meta-analysis. *PLoS One,* **2013**, *8*(10), e77169.
http://dx.doi.org/10.1371/journal.pone.0077169 PMID: 24204764

[12] Avent, M.L.; Vaska, V.L.; Rogers, B.A.; Cheng, A.C.; van Hal, S.J.; Holmes, N.E.; Howden, B.P.; Paterson, D.L. Vancomycin therapeutics and monitoring: a contemporary approach. *Intern. Med. J.,* **2013**, *43*(2), 110-119.
http://dx.doi.org/10.1111/imj.12036 PMID: 23185970

[13] Lodise, T.P.; Drusano, G.L.; Zasowski, E.; Dihmess, A.; Lazariu, V.; Cosler, L.; McNutt, L.A. Vancomycin exposure in patients with methicillin-resistant *Staphylococcus aureus* bloodstream infections: how much is enough? *Clin. Infect. Dis.,* **2014**, *59*(5), 666-675.
http://dx.doi.org/10.1093/cid/ciu398 PMID: 24867791

[14] Miller, N.A.; Reddy, M.B.; Heikkinen, A.T.; Lukacova, V.; Parrott, N. Physiologically based pharmacokinetic modelling for first-in-human predictions: an updated model building strategy illustrated with challenging industry case studies. *Clin. Pharmacokinet.,* **2019**, *58*(6), 727-746.
http://dx.doi.org/10.1007/s40262-019-00741-9 PMID: 30729397

[15] Wagner, C.; Zhao, P.; Pan, Y.; Hsu, V.; Grillo, J.; Huang, S.M.; Sinha, V. Application of physiologically based pharmacokinetic (PBPK) modeling to support dose selection: report of an FDA public workshop on PBPK. *CPT Pharmacometrics Syst. Pharmacol.,* **2015**, *4*(4), 226-230.
http://dx.doi.org/10.1002/psp4.33 PMID: 26225246

[16] Ferreira, A.; Lapa, R.; Vale, N. Combination of gemcitabine with cell-penetrating peptides: a pharmacokinetic approach using *in silico* tools. *Biomolecules,* **2019**, *9*(11), E693.
http://dx.doi.org/10.3390/biom9110693 PMID: 31690028

[17] Cockcroft, D.W.; Gault, M.H. Prediction of creatinine clearance from serum creatinine. *Nephron,* **1976**, *16*(1), 31-41.
http://dx.doi.org/10.1159/000180580 PMID: 1244564

CHAPTER 6

PBPK modeling and simulation of antibiotics amikacin, gentamicin, tobramycin, and vancomycin used in hospital practice

Abigail Ferreira, Helena Martins, José Carlos Oliveira, Rui Lapa, Nuno Vale

Life, **2021**, 11(11), pp. 1130. DOI: 10.3390/life11111130

Following the previous work, a broader study was carried out, including clinically used antibiotics amikacin, gentamicin, tobramycin, and vancomycin. The clinical and demographic data was collected and analyzed, and the PK profile of these antibiotics was evaluated using PBPK modeling and simulation in GastroPlus™. Similarly to what had been observed for vancomycin, renal function and weight were the predominant parameters impacting the biodistribution of these drugs. Importantly, of the four studied antibiotics, vancomycin had the most substantial accumulation in plasma over time.

Once again, the importance of monitoring patients, specifically those with impaired renal function, the elderly and obese patients, and conducting therapeutic drug monitoring (TDM) was demonstrated to be essential, as dose adjustment can be crucial not only to ensure a favorable clinical outcome, but also to prevent adverse toxic effects. Furthermore, the value of *in silico* tools and PBPK modeling and simulation was verified as very useful and helpful in providing assorted knowledge.

life

MDPI

Article

PBPK Modeling and Simulation of Antibiotics Amikacin, Gentamicin, Tobramycin, and Vancomycin Used in Hospital Practice

Abigail Ferreira [1,2], Helena Martins [3], José Carlos Oliveira [3], Rui Lapa [2] and Nuno Vale [1,4,*]

1 OncoPharma Research Group, Center for Health Technology and Services Research (CINTESIS), Rua Doutor Plácido da Costa, 4200-450 Porto, Portugal; abigail.ferreira@fc.up.pt
2 LAQV/REQUIMTE, Laboratory of Applied Chemistry, Department of Chemical Sciences, Faculty of Pharmacy, University of Porto, Rua de Jorge Viterbo Ferreira, 228, 4050-313 Porto, Portugal; laparuas@ff.up.pt
3 Departament of Pathology, Clinical Chemistry Service, Centro Hospitalar Universitário do Porto (CHUP), 4099-001 Porto, Portugal; helena.martins.sqc@chporto.min-saude.pt (H.M.); director.sqc@chporto.min-saude.pt (J.C.O.)
4 Department of Community Medicine, Health Information and Decision (MEDCIDS), Faculty of Medicine, University of Porto, 4200-319 Porto, Portugal
* Correspondence: nunovale@med.up.pt; Tel.: +351-220426537

Abstract: The importance of closely observing patients receiving antibiotic therapy, performing therapeutic drug monitoring (TDM), and regularly adjusting dosing regimens has been extensively demonstrated. Additionally, antibiotic resistance is a contemporary concerningly dangerous issue. Optimizing the use of antibiotics is crucial to ensure treatment efficacy and prevent toxicity caused by overdosing, as well as to combat the prevalence and wide spread of resistant strains. Some antibiotics have been selected and reserved for the treatment of severe infections, including amikacin, gentamicin, tobramycin, and vancomycin. Critically ill patients often require long treatments, hospitalization, and require particular attention regarding TDM and dosing adjustments. As these antibiotics are eliminated by the kidneys, critical deterioration of renal function and toxic effects must be prevented. In this work, clinical data from a Portuguese cohort of 82 inpatients was analyzed and physiologically based pharmacokinetic (PBPK) modeling and simulation was used to study the influence of different therapeutic regimens and parameters as biological sex, body weight, and renal function on the biodistribution and pharmacokinetic (PK) profile of these four antibiotics. Renal function demonstrated the greatest impact on plasma concentration of these antibiotics, and vancomycin had the most considerable accumulation in plasma over time, particularly in patients with impaired renal function. Thus, through a PBPK study, it is possible to understand which pharmacokinetic parameters will have the greatest variation in a given population receiving antibiotic administrations in hospital context.

Keywords: PBPK modeling; therapeutic drug monitoring; antibiotics use; amikacin; gentamicin; tobramycin; vancomycin; GastroPlus™

Citation: Ferreira, A.; Martins, H.; Oliveira, J.C.; Lapa, R.; Vale, N. PBPK Modeling and Simulation of Antibiotics Amikacin, Gentamicin, Tobramycin, and Vancomycin Used in Hospital Practice. *Life* **2021**, *11*, 1130. https://doi.org/10.3390/life11111130

Academic Editor: Milan Kolář

Received: 3 September 2021
Accepted: 22 October 2021
Published: 23 October 2021

1. Introduction

Therapeutic drug monitoring (TDM) was implemented in the 1960s to improve patient care and clinical outcome, and specializes in the measurement of circulating drug concentrations to adjust dosing regimens, so as to reach a defined target exposure associated with optimal efficacy and minimal toxicity [1,2]. Since then, some pharmacological properties have been identified (particularly narrow therapeutic window and significant interpatient variability) and the cases that required such dosage individualization have been comprehensively reviewed. TDM is now indicated and recommended for critically ill patients undergoing sufficiently long treatment to justify dosage adjustment [3], whether with

anticancer drugs [4], anti-infectives [5], antiretrovirals [6], biologic therapeutic agents [7] or psychotropic agents [8], etc.

Importantly for this work, therapeutic drug monitoring and dosage adjustments are crucial for antibiotics, and have confirmed beneficial results [9–15]. The four antibiotics studied here, amikacin, gentamicin, tobramycin, and vancomycin, are the most frequently monitored in inpatients, which can be explained by their narrow therapeutic indexes and potential to cause adverse effects, namely nephrotoxicity, particularly in prolonged treatments [15–17]. The value of TDM of these antibiotics has been extensively demonstrated [13,14,18–27].

Furthermore, the increasing resistance rates to antimicrobial agents are a pressing problem that has been indefectibly associated with the inappropriate administration and overuse of these drugs, which has accelerated this process over the past 80 years. About half of the antimicrobial agents prescribed to hospital inpatients are considered inappropriate [28]. Different approaches have been promoted, and antimicrobial stewardship is currently considered the most promising and has been promoted for all hospitals and health care facilities [29–32]. In 2014, the U.S. Centers for Disease Control and Prevention (CDC) identified seven core elements of antibiotic stewardship and recommend that all hospitals have an antibiotic stewardship program (ASP). Tracking (monitoring process measures), reporting information on antibiotic use and resistance, and education of clinicians and health care providers are three of these core elements [33].

These four antimicrobial agents are an example of antibiotics that have been reserved for the treatment of severe infections, in an attempt to save these valuable drugs from the threat of selection of resistant bacteria. Healing these infections often requires long periods of time of antibiotic therapy and hospitalization. This poses serious concerns, namely regarding plasma accumulation of these drugs, toxicity, and impairment of renal function. Kidneys' deterioration can be an effect of the disease or a consequence of long-term treatment. Since these antibiotics are mainly renally eliminated and their clearance is an important factor to consider when determining treatment regimens, therapeutic drug monitoring and dose adjustment are imperative to ensure a good clinical outcome of these patients.

In this work, clinical data from a cohort of Portuguese inpatients with severe infections were collected and analyzed, and the influence of therapeutic regimens, biological sex, total body weight, and renal function on the pharmacokinetic (PK) profile was studied for four antibiotics: aminoglycosides amikacin, gentamicin, and tobramycin, and glycopeptide vancomycin. PK studies including physiologically based pharmacokinetic (PBPK) modeling and simulations were performed using GastroPlus™, based on our experience and previous works that have highlighted the value of in silico tools [34–36].

2. Materials and Methods

2.1. Study Population

Demographic data (biological sex, age, weight, and height) and clinical information were collected from 82 inpatients hospitalized in *Centro Hospitalar Universitário do Porto* (CHUP, Portugal) with severe systemic infections of different etiologies. These patients received intravenous (IV) treatment with one of four antibiotics: aminoglycoside amikacin, gentamicin, or tobramycin, or glycopeptide vancomycin. Drugs were administered via 30-min infusions in the case of aminoglycosides and 1-h infusions for vancomycin. Throughout the hospitalization and treatment period, trough and peak antibiotic concentrations as well as serum creatinine levels were determined to adjust posology and evaluate renal function (estimating creatinine clearance using the Cockcroft–Gault formula [37]). Recommended and followed treatment regimens were also recorded. The gathered information is presented in Supplementary Table S1 and summarized in Table 1.

Table 1. Summary of collected clinical data, with the indication of the average value, lower and upper limits for each parameter. Normal range values (CHUP reference) are also presented.

	Amikacin	Gentamicin	Tobramycin	Vancomycin
n_t (n_{sex})	8 (F: 1; M: 7)	22 (F: 8; M: 14)	5 (F: 4; M: 1)	47 (F: 21; M: 26)
Age (years)	14–87 (avg 57)	7–88 (avg 58)	13–19 (avg 15)	19–93 (avg 63)
Weight (kg)	50.0–92.5 (avg 66.0)	15.5–85.0 (avg 66.0)	25.8–44.5 (avg 33.0)	29.0–140. (avg 69.0)
Height (cm)	163–180 (avg 169)	108–185 (avg 165)	130–158 (avg 146)	147–185 (avg 163)
C_{min} (mg/L)	0.30–16.40 (avg 3.70) (ref 1–8)	0.20–4.80 (avg 1.05) (ref 0.5–2)	0.06–0.23 (avg 0.17) (ref 0.5–2; <1 CF)	4.50–45.60 (avg 16.34) (ref 15–20)
C_{max} (mg/L)	19.70–87.80 (avg 38.97) (ref 20–30)	2.90–19.50 (avg 9.22) (ref 5–10)	16.32–36.12 (avg 27.05) (ref 5–10; 20–30 CF)	11.20–60.10 (avg 25.99) (ref < 40)
[Cr] (mg/dL)	0.47–1.58 (avg 0.93)	0.29–1.89 (avg 0.83)	0.35–0.64 (avg 0.49)	0.27–4.78 (avg 1.00)
CL (L/h) *	1.40–11.30 (avg 6.07)	1.67–15.89 (avg 5.94)	3.87–8.77 (avg 6.01)	0.59–18.80 (avg 5.79)

* Estimation using the Cockcroft–Gault equation. Ref: normal range (CHUP). CF: Cystic fibrosis.

2.2. Pharmacokinetic Analysis Software

PBPK modeling and simulation software GastroPlus™ version 9.5 (Simulations Plus Inc., Lancaster, CA, USA) was used for the prediction of PK parameters and generation of simulated human plasma concentration profiles. Some physicochemical properties of the four antibiotics and input parameters used in the simulations are presented in Table 2.

Table 2. Physicochemical properties of antibiotics and input parameters in GastroPlus™.

	Amikacin	Gentamicin	Tobramycin	Vancomycin
Molecular weight	585.61	477.61	467.52	1449.28
logP	−5 [1]	−1.79 [1]; −3.1 [2]	−4.8 [1]; −5.8 [2]	2.48 [1]; −3.1 [2]
pKa	8.1 [2]	12.55; 10.18 [2]	12.54; 9.83 [2]	2.99; 9.93 [2]
Solubility	166.49 g/L, pH = 11.73 [1]; 50 g/L [2]	56.54 g/L, pH = 11.51 [1]; 12.6 g/L [2]	59.47 g/L, pH = 11.34 [1]; freely soluble [2]	0.26 g/L, pH = 8.17 [1]; 0.225 g/L [2]
Diffusion Coefficient	0.53 $cm^2/s \times 10^5$ [1]	0.56 $cm^2/s \times 10^5$ [1]	0.6 $cm^2/s \times 10^5$ [1]	0.32 $cm^2/s \times 10^5$ [1]
Drug particle density	1.2 g/mL	1.2 g/mL	1.2 g/mL	1.2 g/mL
Mean particle radius	25	25	25	25
P_{eff}	0.0202 cm/s $\times 10^{-4}$ [1]	0.0891 cm/s $\times 10^{-4}$ [1]	0.0368 cm/s $\times 10^{-4}$ [1]	0.0747 cm/s $\times 10^{-4}$ [1]
F_{up}	98.75% [1]; >90% [2]	85.4% [1]; >70% [2]	100% [1]; >70% [2]	21.36% [1]; ~50% [2]
Blood/plasma ratio	1.23 [1]	1.11 [1]	1.31 [1]	0.68 [1]
$T_{1/2}$	2–3 h	2–3 h	2–3 h	~6 h (4–11 h)
V_c	0.24 [1]; ~0.34 L/kg [2]	0.38 [1]; 0.2–0.3 L/kg	0.3 [1]; 0.2–0.3 L/kg	0.4–1 L/kg
Clearance	6.00 L/h	3.42 L/h	8.48 L/h	4.03 L/h
Typical dosing for susceptible infections	7.5 mg/kg q12h 15 mg/kg q24h	1 mg/kg q8h	1 mg/kg q8h	1000 mg q12h
Common dosing in CHUP	Variable: 400–800 mg q24h or q48h	120 mg q8h 200 mg q24h 70 mg q12h	70 mg q8h 420 mg q24h	1 g q12h 1 g q24h

[1] predicted by GastroPlus™; [2] from DrugBank and references [38–44].

GastroPlus™, a powerful mechanistically based simulation and modeling software, has been specifically developed for pharmaceutical research. Physiological parameters of several species, including human, are preinstalled, allowing for the amount of drug that is released, dissolved, and absorbed to be modeled for nine compartments, corresponding to different segments of the digestive tract, based on a set of differential equations. The

Advanced Compartmental Absorption and Transit (ACAT) and Physiologically Based Pharmacokinetic (PBPK) models support model-based drug development throughout multiple stages of drug discovery, translational research, and clinical development, making it a powerful tool. As such, this software has been used in numerous research studies, but also by distinguished pharmaceutical companies and by the U.S. Food and Drug Administration, the U.S. Centers for Disease Control and Prevention, the U.S. National Institutes of Health, the U.S. National Cancer Institute, and the China Food and Drug Administration [45,46]. A PBPK analysis uses models and simulations that combine physiology, population, and drug characteristics to mechanistically describe the PK behavior of a drug. Throughout a drug's life cycle, PBPK model predictions can be used to support decisions on whether, when, and how to conduct certain clinical pharmacology studies and to support dosing recommendations in product labeling. The predictive performance of PBPK models in specific clinical settings with heterogeneous and chronically ill patients characterized by numerous unknown individual and clinical factors can be developed [47–51].

2.3. PBPK Modeling and Simulation

Every simulation was performed to study the PK for 72 h after IV administrations of each antibiotic, over 30-min infusions for aminoglycosides amikacin, gentamicin and tobramycin, and 1-h infusions for vancomycin.

For each antibiotic, a customized PBPK model was built to represent the average of that subpopulation (receiving treatment with a particular antibiotic). The input parameters were age, total body weight, and renal clearance (Table 1). Different therapeutic regimens (doses and dosing intervals) were studied for each antibiotic, based on the most common schemes administered to the patients in CHUP. Then, the most recurrent therapeutic regimen was chosen for each antibiotic and the influence of biological sex, body weight and renal function was assessed. Customized PBPK models were set up for male and female individuals with the average characteristics of the subpopulation. The effect of body weight and renal function was studied, defining these parameters as the lower and upper limit of the observed range (Table 1), creating 4 additional tailored PBPK models to represent these different conditions: lowest and highest body weight, and lowest and highest renal function, estimated by creatinine clearance.

The available data only included measured concentrations from 2 time points: right before a dose and 1 h (aminoglycosides) or 3 h (vancomycin) after the beginning of an infusion. Since in GastroPlus™ the observed data can only be used as input referring to a single administration, this prevented a further refined parameterization and validation of the developed models. Nevertheless, the predicted pharmacokinetic parameters were reasonably consistent with the observed values after administration of all analyzed doses for these 4 antibiotics.

3. Results

3.1. Influence of Dose Regimens and Biological Sex

Different therapeutic regimens (doses and dosing intervals) were studied for each antibiotic, based on the most common schemes administered to the patients in the study population. The influence of biological sex was also assessed. The simulation-calculated PK parameters are presented in Table 3 and the plasma concentration–time profiles showing the influence of these two factors are presented for each antibiotic in Figures 1–4. As expected for IV infusions, the predicted fraction absorbed (Fa) and bioavailability (F) of all antibiotics were >99%, and a peak in antibiotic concentration was always predicted to be reached at the end of infusions. GastroPlus™ also calculated a direct proportionality of dose with C_{max} and AUC: doubling the dose increased these PK parameters by 2-fold. Additionally, with shorter time intervals between doses, antibiotic accumulation in plasma was more evident. Regarding biological sex, slight differences were observed between the profiles simulated for male and female subjects; a higher C_{max}, but lower concentrations

until following administration is predicted for male individuals, except for vancomycin, where only differences in C_{max} were noted.

Table 3. Influence of therapeutic regimens and biological sex on the pharmacokinetic parameters of the four studied antibiotics.

Drug & Posology	Fa (%) [1]	FDp (%) [2]	F (%) [3]	C_{max} (mg/L) [4]	T_{max} (h) [5]	$AUC_{0\text{-}inf}$ (µg·h/mL) [6]	$AUC_{0\text{-}t}$ (µg·h/mL) [7]	$C_{max\ liver}$ (mg/L) [8]
Amikacin								
400 mg q24h	99.980	99.964	99.964	5.981	48.5	197.570	94.836	64.761
800 mg q24h	99.980	99.964	99.964	11.962	48.5	395.150	189.670	129.520
800 mg q24h female	99.978	99.960	99.960	11.790	48.5	395.060	209.520	128.610
Gentamicin								
70 mg q12h	99.859	99.834	99.834	1.446	60.5	68.971	32.731	14.831
120 mg q8h	99.864	99.838	99.838	2.981	64.5	163.850	81.287	31.975
200 mg q24h	99.845	99.822	99.822	3.304	48.5	100.650	51.345	31.876
200 mg q24h female	99.829	99.806	99.806	3.246	48.5	100.630	56.321	31.524
Tobramycin								
250 mg q24h	99.971	99.971	99.971	5.702	48.5	124.780	78.230	62.346
500 mg q24h	99.971	99.971	99.971	11.403	48.5	249.570	156.460	124.690
420 mg q24h	99.971	99.971	99.971	9.579	48.5	209.640	131.430	104.740
420 mg q24h female	99.969	99.969	99.969	9.460	48.5	209.640	139.840	104.770
Vancomycin								
500 mg q12h	99.929	99.921	99.921	15.632	61.0	517.990	452.870	30.871
1000 mg q24h	99.926	99.921	99.921	25.547	49.0	518.000	477.990	50.086
1000 mg q12h	99.929	99.921	99.921	31.263	61.0	1036.000	905.740	61.742
1000 mg q12h female	99.930	99.921	99.921	29.202	61.0	1036.000	901.460	57.773

[1] fraction absorbed as a percent of the dose (crossing the lumen and entering enterocytes); [2] percent of the dose that has reached the portal vein; [3] bioavailability; [4] maximum plasma concentration reached in the central compartment, in mg/L; [5] time to reach maximum plasma concentration, in hours; [6] area under the plasma concentration–time curve, in µg·h/mL, extrapolated to infinity; [7] area under the plasma concentration–time curve, in µg·h/mL, for the time of the simulation; [8] maximum concentration reached in the liver, in mg/L.

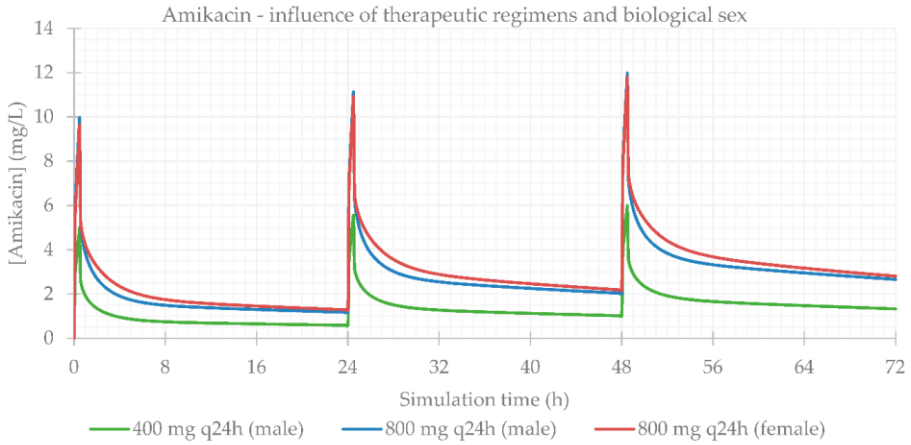

Figure 1. Amikacin plasma concentration–time profile showing the influence of therapeutic regimens and biological sex (considering the average of the study population: 57 years old, 66.0 kg, 169 cm, CL = 6.07 L/h).

3.2. Influence of Total Body Weight

Concerning body composition, the influence of total body weight was assessed, and the resulting PK parameters are presented in Table 4. As expected, simulations for patients with a lower weight result in a higher C_{max} and higher drug concentrations maintained throughout time. The plasma concentration–time profiles showing the influence of this parameter are shown for each antibiotic in Figures 5–8.

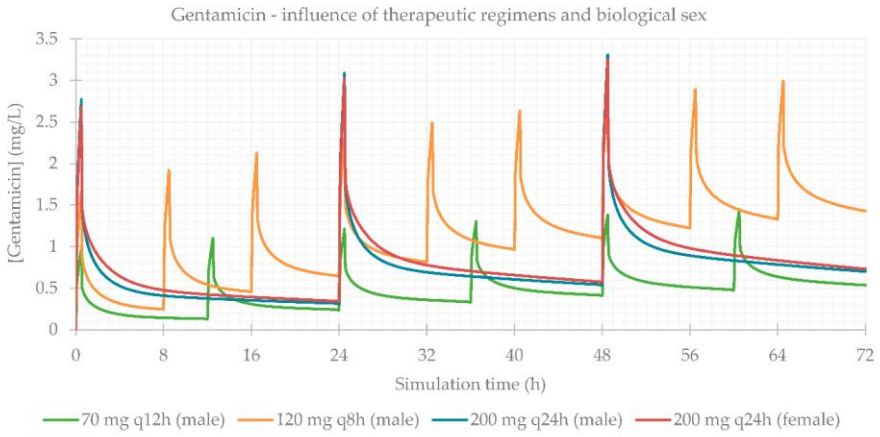

Figure 2. Gentamicin plasma concentration–time profile showing the influence of therapeutic regimens and biological sex (considering the average of the study population: 58 years old, 66.0 kg, 165 cm, CL = 5.94 L/h).

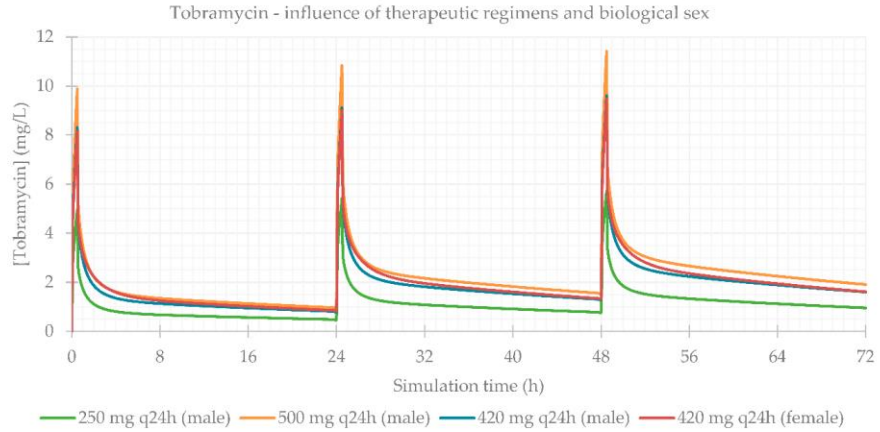

Figure 3. Tobramycin plasma concentration–time profile showing the influence of therapeutic regimens and biological sex (considering the average of the study population: 15 years old, 33.0 kg, 146 cm, CL = 6.01 L/h).

Table 4. Influence of total body weight on the pharmacokinetic parameters of the four studied antibiotics.

Drug & Posology	Fa (%) [1]	FDp (%) [2]	F (%) [3]	C_{max} (mg/L) [4]	T_{max} (h) [5]	$AUC_{0\text{-}inf}$ (µg·h/mL) [6]	$AUC_{0\text{-}t}$ (µg·h/mL) [7]	$C_{max\ liver}$ (mg/L) [8]
Amikacin								
800 mg q24h BW avg (66.0 kg)	99.980	99.964	99.964	11.962	48.5	395.150	189.670	129.520
800 mg q24h BW min (50.0 kg)	99.981	99.965	99.965	14.813	48.5	395.250	223.520	161.780
800 mg q24h BW max (92.5 kg)	99.982	99.966	99.966	9.161	48.5	394.940	151.390	97.834
Gentamicin								
200 mg q24h BW avg (66.0 kg)	99.845	99.822	99.822	3.304	48.5	100.650	51.345	31.876
200 mg q24h BW min (15.5 kg)	99.910	99.905	99.905	9.555	48.5	100.890	90.418	97.446
200 mg q24h BW max (85.0 kg)	99.680	99.656	99.656	9.546	48.5	100.630	90.200	97.126

Table 4. *Cont.*

Drug & Posology	Fa (%) [1]	FDp (%) [2]	F (%) [3]	C_{max} (mg/L) [4]	T_{max} (h) [5]	$AUC_{0\text{-}inf}$ (µg·h/mL) [6]	$AUC_{0\text{-}t}$ (µg·h/mL) [7]	$C_{max\ liver}$ (mg/L) [8]
Tobramycin								
420 mg q24h BW avg (33.0 kg)	99.971	99.971	99.971	9.579	48.5	209.640	131.430	104.740
420 mg q24h BW min (25.8 kg)	99.973	99.973	99.973	11.479	48.5	209.660	147.220	127.010
420 mg q24h BW max (44.5 kg)	99.970	99.970	99.970	7.646	48.5	209.600	111.740	82.333
Vancomycin								
1000 mg q12h BW avg (69.0 kg)	99.929	99.921	99.921	31.263	61.0	1036.000	905.740	61.742
1000 mg q12h BW min (29.0 kg)	99.956	99.954	99.954	48.459	61.0	1036.300	1005.000	95.749
1000 mg q12h BW max (140.0 kg)	99.936	99.926	99.926	22.535	61.0	1035.800	736.330	44.587

[1] fraction absorbed as a percent of the dose (crossing the lumen and entering enterocytes); [2] percent of the dose that has reached the portal vein; [3] bioavailability; [4] maximum plasma concentration reached in the central compartment, in mg/L; [5] time to reach maximum plasma concentration, in hours; [6] area under the plasma concentration–time curve, in µg·h/mL, extrapolated to infinity; [7] area under the plasma concentration–time curve, in µg·h/mL, for the time of the simulation; [8] maximum concentration reached in the liver, in mg/L.

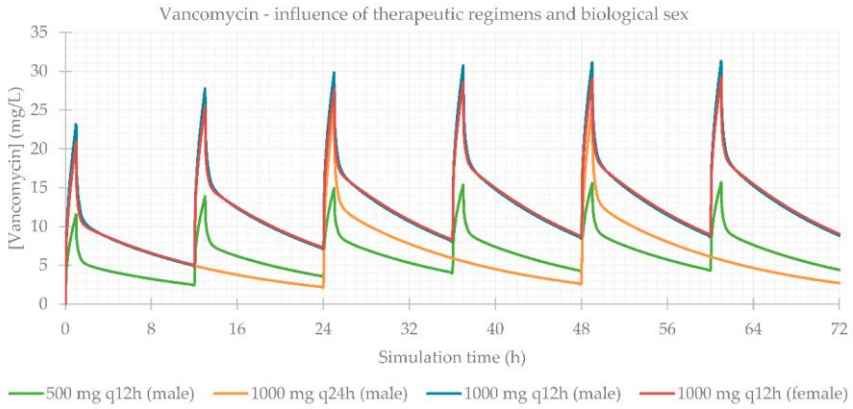

Figure 4. Vancomycin plasma concentration–time profile showing the influence of therapeutic regimens and biological sex (considering the average of the study population: 63 years old, 69.0 kg, 163 cm, CL = 5.79 L/h).

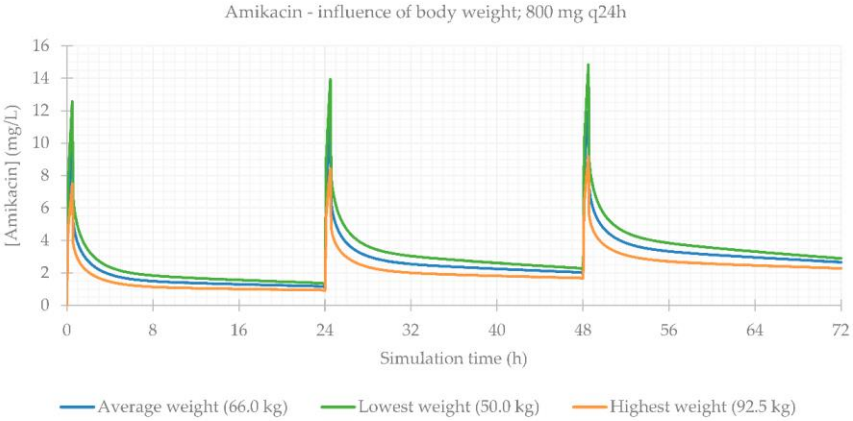

Figure 5. Amikacin plasma concentration–time profile showing the influence of body weight (for an 800 mg q24h dose, considering a male individual with the average characteristics of the study population: 57 years old, 169 cm, CL = 6.07 L/h).

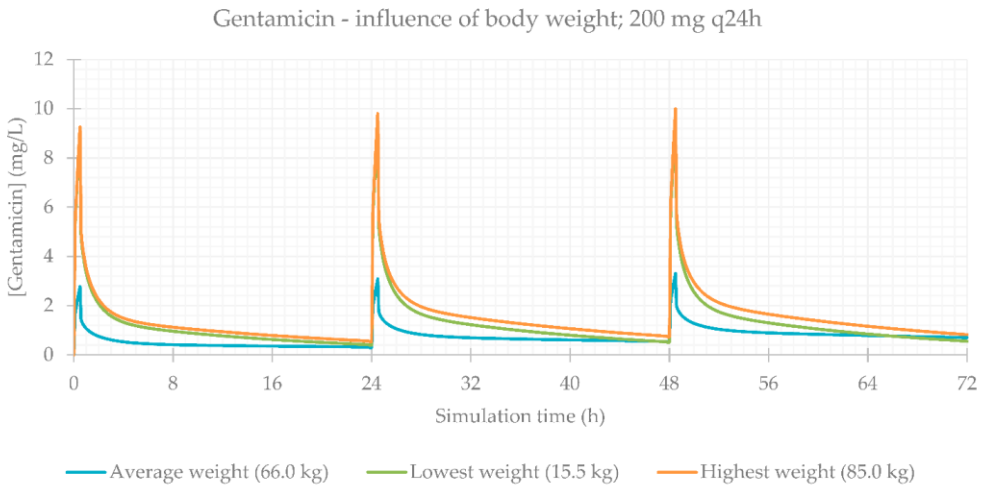

Figure 6. Gentamicin plasma concentration–time profile showing the influence of body weight (for a 200 mg q24h dose, considering a male individual with the average characteristics of the study population: 58 years old, 165 cm, CL = 5.94 L/h).

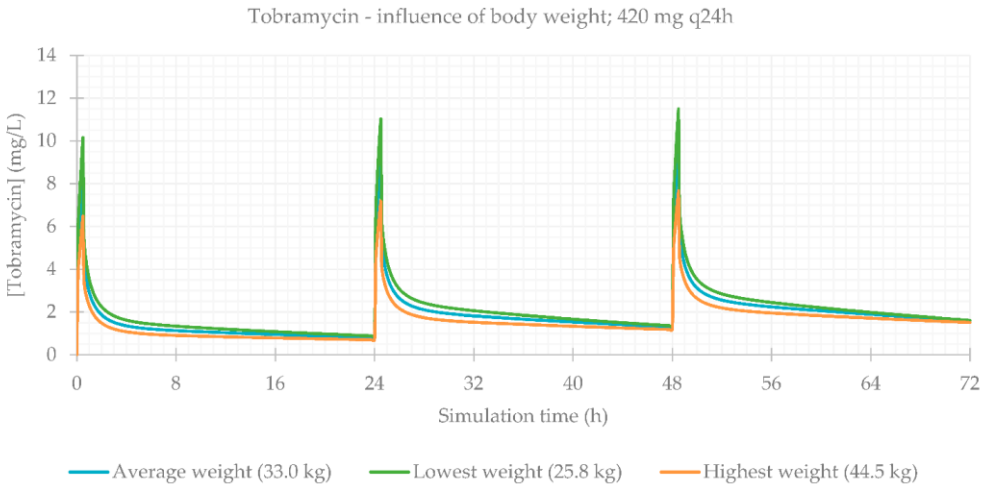

Figure 7. Tobramycin plasma concentration–time profile showing the influence of body weight (for a 420 mg q24h dose, considering a male individual with the average characteristics of the study population: 15 years old, 146 cm, CL = 6.01 L/h).

3.3. *Influence of Renal Function*

Finally, the influence of renal function was evaluated. This is a particularly relevant consideration, since during treatment (especially for long periods of time), kidneys can be affected as a side effect of medication, and renal function is often impaired. The PBPK simulations confirmed this, and CL_{Cr} was the most significantly impacting factor on antibiotics plasma concentrations. PK parameters are presented in Table 5 and plasma concentration–time profiles are illustrated for each antibiotic in Figures 9–12.

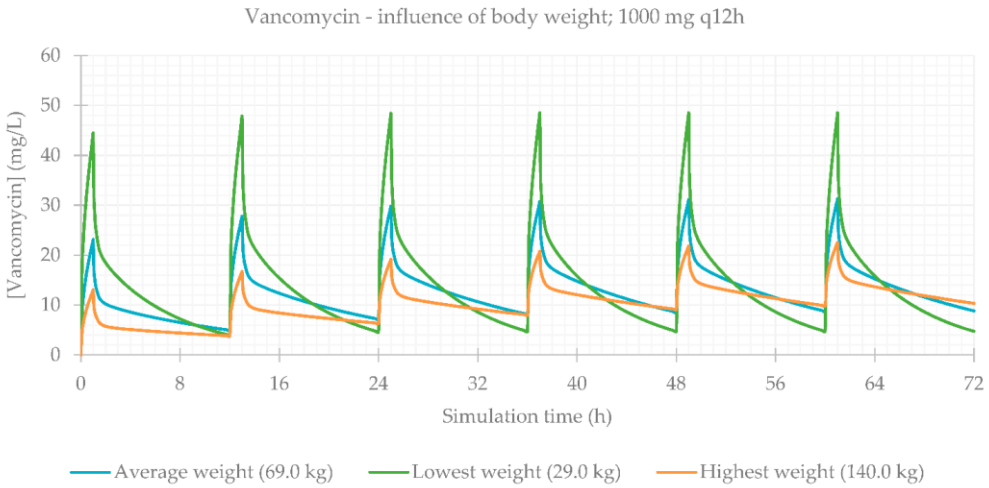

Figure 8. Vancomycin plasma concentration–time profile showing the influence of body weight (for a 1000 mg q12h dose, considering a male individual with the average characteristics of the study population: 63 years old, 163 cm, CL = 5.79 L/h).

Table 5. Influence of renal function (creatinine clearance) on the pharmacokinetic parameters of the four studied antibiotics.

Drug & Posology	Fa (%) [1]	FDp (%) [2]	F (%) [3]	C_{max} (mg/L) [4]	T_{max} (h) [5]	$AUC_{0\text{-}inf}$ (µg·h/mL) [6]	$AUC_{0\text{-}t}$ (µg·h/mL) [7]	$C_{max\ liver}$ (mg/L) [8]
Amikacin								
800 mg q24h CL avg (6.068 L/h)	99.980	99.964	99.964	11.962	48.5	395.150	189.670	129.520
800 mg q24h CL min (1.401 L/h)	99.974	99.950	99.950	13.293	48.5	1705.900	258.260	147.360
800 mg q24h CL max (11.298 L/h)	99.985	99.973	99.973	11.015	48.5	212.320	142.930	117.190
Gentamicin								
200 mg q24h CL avg (5.941 L/h)	99.845	99.822	99.822	3.304	48.5	100.650	51.345	31.876
200 mg q24h CL min (1.667 L/h)	99.789	99.751	99.751	3.667	48.5	355.600	69.999	36.212
200 mg q24h CL max (15.887 L/h)	99.908	99.899	99.899	2.860	48.5	37.744	30.152	26.809
Tobramycin								
420 mg q24h CL avg (6.007 L/h)	99.971	99.971	99.971	9.579	48.5	209.640	131.430	104.740
420 mg q24h CL min (3.868 L/h)	99.965	99.965	99.965	10.149	48.5	325.460	158.850	111.740
420 mg q24h CL max (8.771 L/h)	99.977	99.977	99.977	9.032	48.5	143.600	106.330	98.209
Vancomycin								
1000 mg q12h CL avg (5.787 L/h)	99.929	99.921	99.921	31.263	61.0	1036.000	905.740	61.742
1000 mg q12h CL min (0.590 L/h)	99.789	99.743	99.743	73.192	61.0	10090.000	2659.400	146.400
1000 mg q12h CL max (18.796 L/h)	99.976	99.974	99.974	19.356	61.0	319.140	313.790	38.136

[1] fraction absorbed as a percent of the dose (crossing the lumen and entering enterocytes); [2] percent of the dose that has reached the portal vein; [3] bioavailability; [4] maximum plasma concentration reached in the central compartment, in mg/L; [5] time to reach maximum plasma concentration, in hours; [6] area under the plasma concentration–time curve, in µg·h/mL, extrapolated to infinity; [7] area under the plasma concentration–time curve, in µg·h/mL, for the time of the simulation; [8] maximum concentration reached in the liver, in mg/L.

When considering the lowest CL_{Cr}, antibiotic concentrations are much higher in comparison to individuals with normal functioning kidneys. This is exceptionally important in the case of vancomycin, where the differences between the lower and upper limits of observed CL_{Cr} were exceedingly significant.

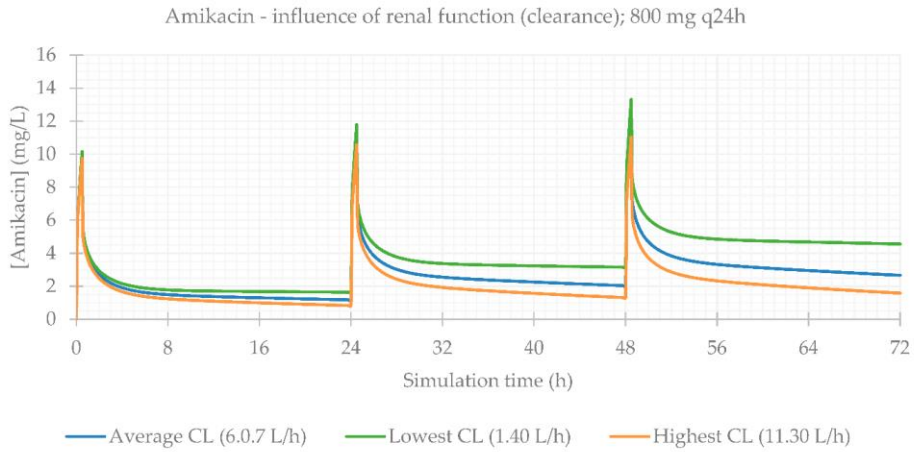

Figure 9. Amikacin plasma concentration–time profile showing the influence of renal function (for an 800 mg q24h dose, considering a male individual with the average characteristics of the study population: 57 years old, 66.0 kg, 169 cm).

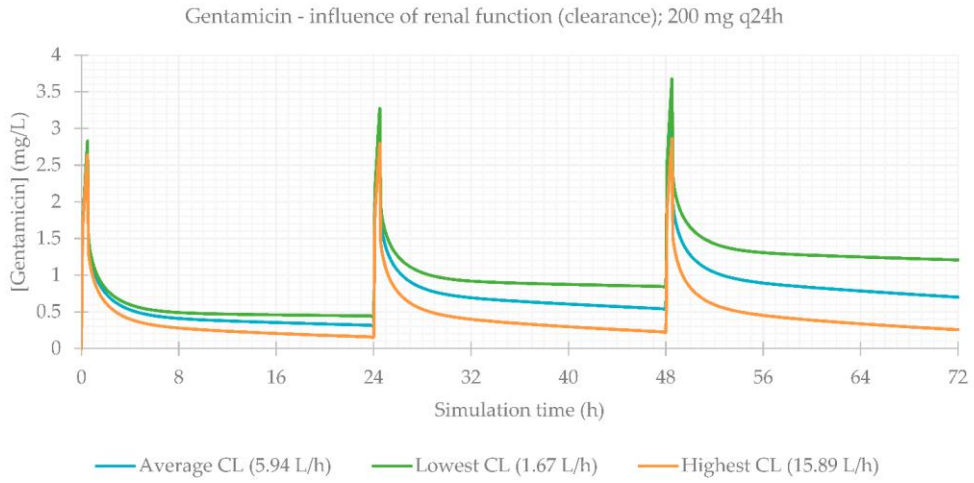

Figure 10. Gentamicin plasma concentration–time profile showing the influence of renal function (for a 200 mg q24h dose, considering a male individual with the average characteristics of the study population: 58 years old, 66.0 kg, 165 cm).

3.4. Effect of Renal Function on the Accumulation of Drugs in Plasma over Time

Since the influence of renal function on the PK profile of the antibiotics was so significant, the observed differences were further analyzed.

The differences in the predicted antibiotics concentrations at 72 h between the simulation for the lowest and average CL, and lowest and highest CL were calculated (Figure 13). For the simulations customized to represent the patients with the lowest CL, the differences between the C_{peak} of the last and C_{peak} of the first administrations were also determined (Figure 14). As aforementioned, renal function has a major impact on the plasma concentration profile of antibiotic vancomycin. As such, it is particularly important to closely observe patients receiving this antibiotic, monitoring their drug's plasma concentration and changes in their renal function. Vancomycin can easily accumulate and rapidly reach toxic levels in plasma, which can lead to severe adverse effects and cause permanent damage to the kidneys.

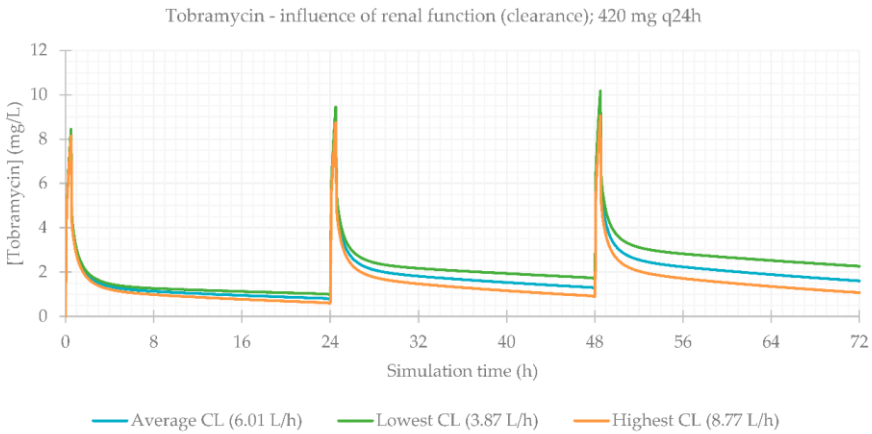

Figure 11. Tobramycin plasma concentration–time profile showing the influence of renal function (for a 420 mg q24h dose, considering a male individual with the average characteristics of the study population: 15 years old, 33.0 kg, 146 cm).

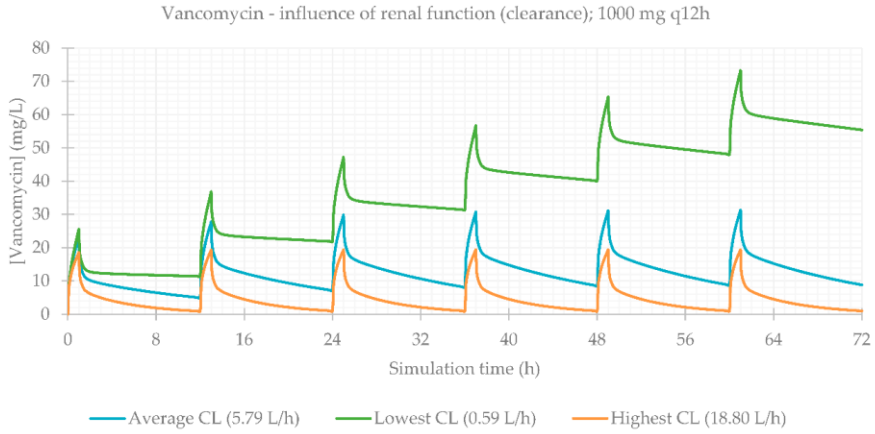

Figure 12. Vancomycin plasma concentration–time profile showing the influence of renal function (for a 1000 mg q12h dose, considering a male individual with the average characteristics of the study population: 63 years old, 69.0 kg, 163 cm).

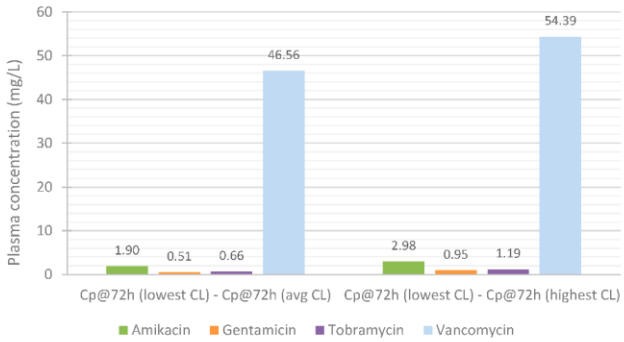

Figure 13. Influence of renal function on the accumulation of the antibiotics in plasma throughout treatment: difference in the plasma concentration at 72 h.

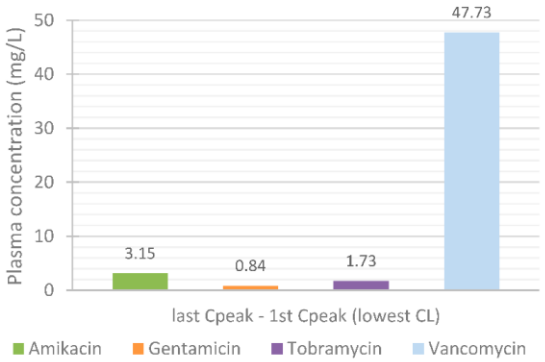

Figure 14. Influence of renal function on the accumulation of the antibiotics in plasma throughout treatment: difference between the C_{peak} of the last and C_{peak} of the first simulated administration.

4. Conclusions

In this work, clinical data from inpatients with severe systemic infections were analyzed and PBPK simulations were performed to study the pharmacokinetic profile of four clinically used antibiotics: amikacin, gentamicin, tobramycin, and vancomycin. The importance of therapeutic drug monitoring and regimen adjustment was further demonstrated, by highlighting the influence of parameters such as a patient's total body weight and the significant impact of renal function on antibiotic plasma concentrations. It was made evident that patients with low body weight and especially those with impaired renal function, whether preexisting or due to kidney deterioration throughout treatment, must be closely monitored and their therapeutic regimens frequently revised to adjust to their plasma antibiotic concentrations and PK profile. We also found that renal function is the parameter that has the greatest impact on the Cp-time profile of these antibiotics, especially vancomycin, but that there are certainly other factors affecting PK and more optimizations to be made to these PBPK models, since the values obtained in the simulations may come even closer to those observed clinically. In particular, it is known that hospitalized and critically ill patients have altered PK and the fact that in this project it was not possible, due to software limitation, to insert the observed concentrations into the models, refining, optimizing, and then validating them, also contributed to the slight differences between the simulated and clinical results.

The results presented here deepen the knowledge on the impact and influence of these parameters on the biodistribution of these antibiotics. This is crucial not only to ensure a successful clinical outcome, but also to prevent serious side effects, and, as such, can assist clinicians in the process of adjusting therapeutic regimens. In this context, the helpfulness of in silico tools, such as PBPK modeling and software such as GastroPlus™, was also verified.

Supplementary Materials: The following are available online at https://www.mdpi.com/article/10.3390/life11111130/s1, Table S1: Demographic information and clinical data of the study population.

Author Contributions: Conceptualization, N.V.; methodology, A.F., H.M. and N.V.; software, A.F.; validation, N.V., A.F., H.M., J.C.O. and R.L.; investigation, A.F. and N.V.; resources, N.V. and R.L.; writing—original draft preparation, A.F.; writing—review and editing, H.M.; J.C.O., R.L. and N.V.; supervision, N.V.; project administration, N.V.; funding acquisition, R.L. and N.V. All authors have read and agreed to the published version of the manuscript.

Funding: This work was financed by FEDER—Fundo Europeu de Desenvolvimento Regional through the COMPETE 2020—Operational Programme for Competitiveness and Internationalization (POCI), Portugal 2020, and by Portuguese funds through FCT—Fundação para a Ciência e a Tecnologia, in a framework of CINTESIS, R&D Unit (reference UIDB/4255/2020). N.V. also thanks support

FCT and FEDER (European Union), award number IF/00092/2014/CP1255/CT0004. RL thanks FCT through grant UID/QUI/50006/2019 (LAQV-REQUIMTE).

Institutional Review Board Statement: Not applicable.

Informed Consent Statement: Not applicable.

Data Availability Statement: Not applicable.

Acknowledgments: AF thanks FCT for a doctoral fellowship (PD/BD/135120/2017). The contents of this article are solely the responsibility of the authors and do not necessarily represent the official view of the FCT.

Conflicts of Interest: The authors declare no conflict of interest.

References

1. Clarke, W.; Dasgupta, A. *Clinical Challenges in Therapeutic Drug Monitoring: Special Populations, Physiological Conditions and Pharmacogenomics*; Elsevier Science: Amsterdam, The Netherlands, 2016; ISBN 9780128020524.
2. Kang, J.S.; Lee, M.H. Overview of therapeutic drug monitoring. *Korean J. Intern. Med.* **2009**, *24*, 1–10. [CrossRef]
3. Buclin, T.; Thoma, Y.; Widmer, N.; André, P.; Guidi, M.; Csajka, C.; Decosterd, L.A. The Steps to Therapeutic Drug Monitoring: A Structured Approach Illustrated With Imatinib. *Front. Pharmacol.* **2020**, *11*, 177. [CrossRef]
4. Widmer, N.; Bardin, C.; Chatelut, E.; Paci, A.; Beijnen, J.; Levêque, D.; Veal, G.; Astier, A. Review of therapeutic drug monitoring of anticancer drugs part two-Targeted therapies. *Eur. J. Cancer* **2014**, *50*, 2020–2036. [CrossRef]
5. Muller, A.E.; Huttner, B.; Huttner, A. Therapeutic Drug Monitoring of Beta-Lactams and Other Antibiotics in the Intensive Care Unit: Which Agents, Which Patients and Which Infections? *Drugs* **2018**, *78*, 439–451. [CrossRef] [PubMed]
6. Maitre, T.; Muret, P.; Blot, M.; Waldner, A.; Duong, M.; Si-Mohammed, A.; Chavanet, P.; Aho, S.; Piroth, L. Benefits and Limits of Antiretroviral Drug Monitoring in Routine Practice. *Curr. HIV Res.* **2019**, *17*, 190–197. [CrossRef]
7. Papamichael, K.; Cheifetz, A.S. Therapeutic drug monitoring in patients on biologics: Lessons from gastroenterology. *Curr. Opin. Rheumatol.* **2020**, *32*, 371–379. [CrossRef] [PubMed]
8. Schoretsanitis, G.; Paulzen, M.; Unterecker, S.; Schwarz, M.; Conca, A.; Zernig, G.; Gründer, G.; Haen, E.; Baumann, P.; Bergemann, N.; et al. TDM in psychiatry and neurology: A comprehensive summary of the consensus guidelines for therapeutic drug monitoring in neuropsychopharmacology, update 2017; a tool for clinicians. *World J. Biol. Psychiatry* **2018**, *19*, 162–174. [CrossRef] [PubMed]
9. Leekha, S.; Terrell, C.L.; Edson, R.S. General Principles of Antimicrobial Therapy. *Mayo Clin. Proc.* **2011**, *86*, 156–167. [CrossRef] [PubMed]
10. Abdul-Aziz, M.H.; Alffenaar, J.C.; Bassetti, M.; Bracht, H.; Dimopoulos, G.; Marriott, D.; Neely, M.N.; Paiva, J.A.; Pea, F.; Sjovall, F.; et al. Antimicrobial therapeutic drug monitoring in critically ill adult patients: A Position Paper. *Intensive Care Med.* **2020**, *46*, 1127–1153. [CrossRef]
11. Mabilat, C.; Gros, M.F.; Nicolau, D.; Mouton, J.W.; Textoris, J.; Roberts, J.A.; Cotta, M.O.; van Belkum, A.; Caniaux, I. Diagnostic and medical needs for therapeutic drug monitoring of antibiotics. *Eur. J. Clin. Microbiol. Infect. Dis.* **2020**, *39*, 791–797. [CrossRef] [PubMed]
12. Wicha, S.G.; Märtson, A.G.; Nielsen, E.I.; Koch, B.C.P.; Friberg, L.E.; Alffenaar, J.W.; Minichmayr, I.K. From Therapeutic Drug Monitoring to Model-Informed Precision Dosing for Antibiotics. *Clin. Pharmacol. Ther.* **2021**, *109*, 928–941. [CrossRef] [PubMed]
13. Choi, R.; Woo, H.I.; Park, H.D.; Lee, S.Y. A nationwide utilization survey of therapeutic drug monitoring for five antibiotics in South Korea. *Infect. Drug Resist.* **2019**, *12*, 2163–2173. [CrossRef]
14. Begg, E.J.; Barclay, M.L.; Kirkpatrick, C.M. The therapeutic monitoring of antimicrobial agents. *Br. J. Clin. Pharmacol.* **2001**, *52* (Suppl. 1), S35–S43. [CrossRef]
15. Reeves, D.; Lovering, A.; Thomson, A. Therapeutic drug monitoring in the past 40 years of the Journal of Antimicrobial Chemotherapy. *J. Antimicrob. Chemother.* **2016**, *71*, 3330–3332. [CrossRef]
16. Cunha, B.A. Antibiotic side effects. *Med. Clin. N. Am.* **2001**, *85*, 149–185. [CrossRef]
17. Yılmaz, Ç.; Özcengiz, G. Antibiotics: Pharmacokinetics, toxicity, resistance and multidrug efflux pumps. *Biochem. Pharmacol.* **2017**, *133*, 43–62. [CrossRef]
18. Möhlmann, J.E.; van Luin, M.; Mascini, E.M.; van Leeuwen, H.J.; de Maat, M.R. Monitoring of tobramycin serum concentrations in selected critically ill patients receiving selective decontamination of the digestive tract: A retrospective evaluation. *Eur. J. Clin. Pharmacol.* **2019**, *75*, 831–836. [CrossRef]
19. Coulthard, K.P.; Peckham, D.G.; Conway, S.P.; Smith, C.A.; Bell, J.; Turnidge, J. Therapeutic drug monitoring of once daily tobramycin in cystic fibrosis–caution with trough concentrations. *J. Cyst. Fibros.* **2007**, *6*, 125–130. [CrossRef]
20. Ye, Z.K.; Tang, H.L.; Zhai, S.D. Benefits of therapeutic drug monitoring of vancomycin: A systematic review and meta-analysis. *PLoS ONE* **2013**, *8*, e77169. [CrossRef] [PubMed]
21. Rybak, M.J. The pharmacokinetic and pharmacodynamic properties of vancomycin. *Clin. Infect. Dis. Off. Publ. Infect. Dis. Soc. Am.* **2006**, *42* (Suppl. 1), S35–S39. [CrossRef] [PubMed]

22. Rybak, M.; Lomaestro, B.; Rotschafer, J.C.; Moellering, R., Jr.; Craig, W.; Billeter, M.; Dalovisio, J.R.; Levine, D.P. Therapeutic monitoring of vancomycin in adult patients: A consensus review of the American Society of Health-System Pharmacists, the Infectious Diseases Society of America, and the Society of Infectious Diseases Pharmacists. *Am. J. Health Pharm.* **2009**, *66*, 82–98. [CrossRef] [PubMed]
23. Jenkins, A.; Thomson, A.H.; Brown, N.M.; Semple, Y.; Sluman, C.; MacGowan, A.; Lovering, A.M.; Wiffen, P.J. Amikacin use and therapeutic drug monitoring in adults: Do dose regimens and drug exposures affect either outcome or adverse events? A systematic review. *J. Antimicrob. Chemother.* **2016**, *71*, 2754–2759. [CrossRef]
24. Kovačević, T.; Avram, S.; Milaković, D.; Špirić, N.; Kovačević, P. Therapeutic monitoring of amikacin and gentamicin in critically and noncritically ill patients. *J. Basic Clin. Pharm.* **2016**, *7*, 65–69. [CrossRef]
25. de Velde, F.; Mouton, J.W.; de Winter, B.C.M.; van Gelder, T.; Koch, B.C.P. Clinical applications of population pharmacokinetic models of antibiotics: Challenges and perspectives. *Pharmacol. Res.* **2018**, *134*, 280–288. [CrossRef]
26. Hodiamont, C.J.; Janssen, J.M.; de Jong, M.D.; Mathôt, R.A.; Juffermans, N.P.; van Hest, R.M. Therapeutic Drug Monitoring of Gentamicin Peak Concentrations in Critically Ill Patients. *Ther. Drug Monit.* **2017**, *39*, 522–530. [CrossRef]
27. Drennan, P.G.; Thoma, Y.; Barry, L.; Matthey, J.; Sivam, S.; van Hal, S.J. Bayesian Forecasting for Intravenous Tobramycin Dosing in Adults With Cystic Fibrosis Using One Versus Two Serum Concentrations in a Dosing Interval. *Ther. Drug Monit.* **2021**, *43*, 505–511. [CrossRef]
28. Gottlieb, T.; Nimmo, G.R. Antibiotic resistance is an emerging threat to public health: An urgent call to action at the Antimicrobial Resistance Summit 2011. *Med. J. Aust.* **2011**, *194*, 281–283. [CrossRef]
29. Dellit, T.H.; Owens, R.C.; McGowan, J.E.; Gerding, D.N.; Weinstein, R.A.; Burke, J.P.; Huskins, W.C.; Paterson, D.L.; Fishman, N.O.; Carpenter, C.F.; et al. Infectious Diseases Society of America and the Society for Healthcare Epidemiology of America Guidelines for Developing an Institutional Program to Enhance Antimicrobial Stewardship. *Clin. Infect. Dis.* **2007**, *44*, 159–177. [CrossRef] [PubMed]
30. Lee, C.R.; Cho, I.H.; Jeong, B.C.; Lee, S.H. Strategies to minimize antibiotic resistance. *Int. J. Environ. Res. Public Health* **2013**, *10*, 4274–4305. [CrossRef] [PubMed]
31. MacDougall, C.; Polk, R.E. Antimicrobial stewardship programs in health care systems. *Clin. Microbiol. Rev.* **2005**, *18*, 638–656. [CrossRef]
32. Michaels, K.; Mahdavi, M.; Krug, A.; Kuper, K. Implementation of an antimicrobial stewardship program in a community hospital: Results of a three-year analysis. *Hosp. Pharm.* **2012**, *47*, 608–616. [CrossRef]
33. Pollack, L.A.; Srinivasan, A. Core elements of hospital antibiotic stewardship programs from the Centers for Disease Control and Prevention. *Clin. Infect. Dis.* **2014**, *59* (Suppl. 3), S97–S100. [CrossRef] [PubMed]
34. Ferreira, A.; Martins, H.; Oliveira, J.C.; Lapa, R.; Vale, N. In silico pharmacokinetic study of vancomycin using PBPK modeling and therapeutic drug monitoring. *Curr. Drug Metab.* **2021**, *22*, 150–162. [CrossRef]
35. Ferreira, A.; Lapa, R.; Vale, N. Combination of Gemcitabine with Cell-Penetrating Peptides: A Pharmacokinetic Approach Using In Silico Tools. *Biomolecules* **2019**, *9*, 693. [CrossRef] [PubMed]
36. Santos, J.; Lobato, L.; Vale, N. Clinical pharmacokinetic study of latrepirdine via in silico sublingual administration. *In Silico Pharmacol.* **2021**, *9*, 29. [CrossRef] [PubMed]
37. Cockcroft, D.W.; Gault, M.H. Prediction of creatinine clearance from serum creatinine. *Nephron* **1976**, *16*, 31–41. [CrossRef]
38. Amikacin. Available online: https://go.drugbank.com/drugs/DB00479 (accessed on 1 February 2021).
39. Gentamicin. Available online: https://go.drugbank.com/drugs/DB00798 (accessed on 1 February 2021).
40. Gonçalves-Pereira, J.; Martins, A.; Póvoa, P. Pharmacokinetics of gentamicin in critically ill patients: Pilot study evaluating the first dose. *Clin. Microbiol. Infect.* **2010**, *16*, 1258–1263. [CrossRef]
41. Tobramycin. Available online: https://go.drugbank.com/drugs/DB00684 (accessed on 1 February 2021).
42. Aminimanizani, A.; Beringer, P.M.; Kang, J.; Tsang, L.; Jelliffe, R.W.; Shapiro, B.J. Distribution and elimination of tobramycin administered in single or multiple daily doses in adult patients with cystic fibrosis. *J. Antimicrob. Chemother.* **2002**, *50*, 553–559. [CrossRef] [PubMed]
43. Tobramycin for Injection. Available online: https://reference.medscape.com/drug/nebcin-injection-tobramycin-342521#10 (accessed on 1 February 2021).
44. Vancomycin. Available online: https://go.drugbank.com/drugs/DB00512 (accessed on 1 February 2021).
45. Miller, N.A.; Reddy, M.B.; Heikkinen, A.T.; Lukacova, V.; Parrott, N. Physiologically Based Pharmacokinetic Modelling for First-In-Human Predictions: An Updated Model Building Strategy Illustrated with Challenging Industry Case Studies. *Clin. Pharmacokinet.* **2019**, *58*, 727–746. [CrossRef] [PubMed]
46. Wagner, C.; Zhao, P.; Pan, Y.; Hsu, V.; Grillo, J.; Huang, S.M.; Sinha, V. Application of Physiologically Based Pharmacokinetic (PBPK) Modeling to Support Dose Selection: Report of an FDA Public Workshop on PBPK. *CPT Pharmacomet. Syst. Pharmacol.* **2015**, *4*, 226–230. [CrossRef]
47. Kovar, L.; Schräpel, C.; Selzer, D.; Kohl, Y.; Bals, R.; Schwab, M.; Lehr, T. Physiologically-Based Pharmacokinetic (PBPK) Modeling of Buprenorphine in Adults, Children and Preterm Neonates. *Pharmaceutics* **2020**, *12*, 578. [CrossRef] [PubMed]
48. Fuhr, L.M.; Marok, F.Z.; Hanke, N.; Selzer, D.; Lehr, T. Pharmacokinetics of the CYP3A4 and CYP2B6 Inducer Carbamazepine and Its Drug–Drug Interaction Potential: A Physiologically Based Pharmacokinetic Modeling Approach. *Pharmaceutics* **2021**, *13*, 270. [CrossRef]

49. Zapke, S.E.; Willmann, S.; Grebe, S.-O.; Menke, K.; Thürmann, P.A.; Schmiedl, S. Comparing Predictions of a PBPK Model for Cyclosporine With Drug Levels From Therapeutic Drug Monitoring. *Front. Pharmacol.* **2021**, *12*, 1134. [CrossRef] [PubMed]
50. Li, J.; Jiang, J.; Wu, J.; Bao, X.; Sanai, N. Physiologically based pharmacokinetic modeling of central nervous system pharmacokinetics of CDK4/6 inhibitors to guide selection of drug and dosing regimen for brain cancer treatment. *Clin. Pharmacol. Ther.* **2021**, *109*, 494–506. [CrossRef] [PubMed]
51. Wang, K.; Yao, X.; Zhang, M.; Liu, D.; Gao, Y.; Sahasranaman, S.; Ou, Y.C. Comprehensive PBPK model to predict drug interaction potential of Zanubrutinib as a victim or perpetrator. *CPT Pharmacomet. Syst. Pharmacol.* **2021**, *10*, 441–454. [CrossRef] [PubMed]

life

MDPI

SUPPLEMENTARY MATERIALS

PBPK modeling and simulation of antibiotics amikacin, gentamicin, tobramycin, and vancomycin used in hospital practice

Abigail Ferreira [1,3], Helena Martins [2], José Carlos Oliveira [2], Rui Lapa [3] and Nuno Vale [1,4,*]

1 OncoPharma Research Group, Center for Health Technology and Services Research (CINTESIS), Rua Doutor Plácido da Costa, 4200-450 Porto, Portugal; abigail.ferreira@fc.up.pt
2 LAQV/REQUIMTE, Laboratory of Applied Chemistry, Department of Chemical Sciences, Faculty of Pharmacy, University of Porto, Rua de Jorge Viterbo Ferreira, 228, 4050-313 Porto, Portugal; laparuas@ff.up.pt
3 Departament of Pathology, Clinical Chemistry Service, Centro Hospitalar Universitário do Porto (CHUP), Largo Professor Abel Salazar, 4099-001 Porto, Portugal; helena.martins.sqc@chporto.min-saude.pt (H.M.); director.sqc@chporto.min-saude.pt (J.C.O.)
4 Department of Community Medicine, Health Information and Decision (MEDCIDS), Faculty of Medicine, University of Porto, Alameda Professor Hernâni Monteiro, 4200-319 Porto, Portugal
* Correspondence: nunovale@med.up.pt; Tel.: +351-220426537

Life **2021**, *11*, 1130. https://doi.org/10.3390/life11111130 www.mdpi.com/journal/life

Table S1. Demographic information and clinical data of the study population.
Blood samples were typically collected prior to the following antibiotic administration to determine C_{min} (at most 30 minutes before infusion) and 1 h (aminoglycosides) or 3 h (vancomycin) after the beginning of an infusion to determine C_{max}. When an occasional sample was collected, the measured concentration is presented with the indication of the time of blood sample collection. In some cases, it was not possible to determine the antibiotic concentration and a calculated range is presented (estimation of the software used in the clinical setting, PKS, ABBOTTBASE® Pharmacokinetic Systems, version 1.10, Abbott Laboratories, Texas, USA). The considered normal range of creatinine concentration in plasma is 0.7 - 1.2 mg/dL for male patients and 0.5 - 0.9 mg/dL for female patients. Clearance was calculated from creatinine concentration using the Cockcroft-Gault formula [1]: CL = ((140-age) x weight)/(72 x [creatinine]); multiply by 0.85 for female individuals; CL in mL/min, weight in kg, [creatinine] in mg/dL.

Recommended posology											
#ID	**Sex**	**Age (years)**	**Weight (kg)**	**Height (cm)**	**Date**	**Dose (mg)**	**Interval**	**C_{min} (mg/L)**	**C_{max} (mg/L)**	**[Cr] (mg/dL)**	**CL (L/h)**
AMIKACIN											
25	Male	67	72.5	163	Day 1	900	24 h				
					Day 3	750	24 h	2.1	60.2	0.66	6.91
					Day 6	750	24 h			0.63	7.24
					Day 7	800	24 h	2.7	33.3	0.72	6.34
26	Male	79	60	168	Day 1	450	12 h			1.10	2.77
					Day 4	450	12 h			1.00	3.05
					Day 5	Susp 1 dose > 450 mg q24h		16.4	44.0	1.11	2.75
					Day 6	450	24 h	5.7	34.3	0.99	3.08
					Day 11	450	24 h	4.0	36.2	1.09	2.80
28	Fem	87	50	167	Day 1					1.34	1.40
					Day 7	750	24 h			0.91	2.06
					Day 9	500	24 h	4.3	56.0	0.79	2.38
					Day 14	500	24 h	3.5	41.3	0.67	2.80
					Day 19	500	24 h	3.3	40.6	0.71	2.64
29	Male	14	53.8	168	Day 1	1500	24 h				
					Day 4	1100	24 h	0.5	87.8	0.50	11.30
					Day 8	1100	24 h	0.3	51.7	0.53	10.66
32	Male	77	70	170	Day 1	500	24 h			1.26	2.92
					Day 2	500	24 h			1.19	3.09
					Day 3	500	24 h			1.28	2.87
					Day 4	800	24 h	2.4	19.7	1.09	3.37
					Day 5	800	24 h			1.03	3.57
					Day 6	700	24 h	4.6	41.3	1.01	3.64
					Day 9	700	24 h			1.14	3.22
					Day 10	700	24 h			1.21	3.04
					Day 11	Susp 1 dose > 800 mg q48h		7.6	49.3	1.25	2.94
36	Male	18	53.6	168	Day 1	500	8 h				
					Day 5	Susp 3 doses > 850 mg q24h		2.5	calc 27-28	0.62	8.79
					Day 9	850	24 h	0.5	calc 43-45	0.62	8.79
					Day 13	850	24 h	0.6	47.2	0.58	9.40
37	Male	58	92.5	180	Day 1					1.54	4.44
					Day 3	500	24 h				
					Day 5	650	24 h		(occas 3.5 h) 13.4	1.22	5.60
					Day 8	650	24 h			1.06	6.45
					Day 9	800	24 h	2.7	24.5	0.95	7.19
					Day 10	800	24 h			1.02	6.70
					Day 12	800	24 h	3.1	(occas 2 h) 23.4	1.22	5.60
					Day 15	800	24 h	3.4	(occas 1.5 h) 39.1	1.11	6.16
					Day 17	800	24 h			1.22	5.60

					Recommended posology					
#ID	Sex	Age (years)	Weight (kg)	Height (cm)	Date	Dose (mg)	Interval	C_{min} (mg/L)	C_{max} (mg/L)	[Cr] (mg/dL)	CL (L/h)
					Day 18	800	24 h	4.2	39.2		
					Day 19	800	24 h			1.38	4.95
					Day 20	800	24 h			1.03	6.63
					Day 22	800	24 h			1.23	5.56
					Day 23	800	24 h	5.5	35.4	1.09	6.27
					Day 25	800	24 h			1.27	5.38
					Day 26	650	24 h	5.8	38.5	1.23	5.56
					Day 29	650	24 h			1.30	5.26
					Day 30	Susp 1 dose > 800 mg q48h		5.7	25.3	1.48	4.62
					Day 31					1.45	4.71
					Day 33	800	48 h			1.47	4.65
					Day 36	750	48 h	1.8	33.3	1.36	5.02
					Day 37	750	48 h			1.52	4.50
					Day 38	750	48 h			1.58	4.32
					Day 40	750	48 h	2.0	24.7	1.43	4.78
					Day 43	750	48 h			1.37	4.99
					Day 45	750	48 h			1.36	5.02
					Day 46	750	48 h	1.9	28.8		
					Day 1	800	24 h			0.74	7.09
					Day 2	800	24 h			0.82	6.40
					Day 3	800	24 h			0.75	7.00
					Day 4	800	24 h			0.58	9.05
					Day 5	800	24 h			0.55	9.55
					Day 6	800	24 h			0.54	9.72
					Day 7	800	24 h	4.7	34.4	0.61	8.61
					Day 8	800	24 h			0.51	10.29
					Day 9	800	24 h			0.63	8.33
					Day 10	800	24 h	calc 3-4	calc 31-33	0.60	8.75
					Day 13	400	12 h			0.50	10.50
					Day 18	650	24 h	4	23	0.50	10.50
					Day 19	650	24 h			0.47	11.17
					Day 20	550	24 h	5.6	(occas 1.5 h) 39.7	0.53	9.91
					Day 21	550	24 h			0.54	9.72
38	Male	56	75	170	Day 22	550	24 h			0.64	8.20
					Day 23	550	24 h			0.83	6.33
					Day 24	550	24 h			0.77	6.82
					Day 25	550	24 h			0.59	8.90
					Day 26	Susp 1 dose > 700 mg q48h		5.2	28.7	0.69	7.61
					Day 27	700	48 h			0.88	5.97
					Day 28	700	48 h			0.66	7.95
					Day 29	700	48 h			0.70	7.50
					Day 30	700	48 h			0.75	7.00
					Day 31	700	48 h			0.90	5.83
					Day 32	700	48 h	2.2	calc 31-33	0.86	6.10
					Day 33	700	48 h			0.92	5.71
					Day 34	700	48 h	2.0	34.5	0.76	6.91
					Day 35	700	48 h			0.70	7.50
					Day 36	700	48 h			0.71	7.39

Recommended posology											
#ID	**Sex**	**Age (years)**	**Weight (kg)**	**Height (cm)**	**Date**	**Dose (mg)**	**Interval**	**C_{min} (mg/L)**	**C_{max} (mg/L)**	**[Cr] (mg/dL)**	**CL (L/h)**
					Day 37	700	48 h			0.59	8.90
					Day 38	700	48 h			0.74	7.09
					Day 39	700	48 h	1.3	(occas 1.3 h) 37.2	0.65	8.08
GENTAMICIN											
7	Male	49	67	175	Day 1					0.67	7.58
					Day 3	180	12 h			0.63	8.06
					Day 4	180	12 h	0.3	calc 9.5 - 10.5	0.63	8.06
					Day 6	220	12 h	0.3	6.7	0.52	9.77
					Day 10	220	12 h	0.6	(occas 1.5 h) 9.1	0.70	7.26
					Day 12	220	12 h	0.5	8.9	0.69	7.36
18	Fem	72	70	160	Day 1	210	24 h				
					Day 2	210	24 h			1.09	3.09
					Day 4	120	24 h	0.5	13.7		
					Day 5	120	24 h			1.08	3.12
					Day 7	120	24 h			1.16	2.91
					Day 8	100	24 h	0.4	7.1	1.30	2.59
19	Male	78	47	170	Day 1					0.61	3.98
					Day 2	240	24 h				
					Day 3	240	24 h			0.68	3.57
					Day 4	240	24 h				
					Day 5	240	24 h			0.65	3.74
					Day 6	350	24 h	0.8	(occas 1.5 h) 8.6	0.62	3.92
					Day 7	350	24 h	1.1	16.9	0.81	3.00
					Day 9	380	24 h	1.8	18.3	0.84	2.89
22	Fem	88	75	155	Day 1	300	24 h			0.68	4.06
					Day 5	Susp 2 doses > 160 mg q48h		4.2	19.17	0.81	3.41
					Day 8	160	48 h			0.90	3.07
					Day 12	Susp 3 doses > 170 mg q72h		1.7	9.9	1.42	1.95
23	Fem	60	65.3	165	Day 1	62	8 h		(occas 5 h) 1.7	0.48	7.59
					Day 2	150	12 h			0.64	5.69
					Day 3	150	12 h		(occas 5 h) 2.1	0.51	7.14
					Day 6	150	12 h			0.77	4.73
					Day 7	170	12 h	0.8	5.8	0.58	6.28
					Day 8	170	12 h			0.66	5.52
					Day 9	170	12 h			0.60	6.07
					Day 10	Susp 2 doses > 200 mg q24h		1.3	6.8[a]	0.58	6.28
					Day 11	200	24 h				
					Day 13	200	24 h			0.71	5.13
					Day 14	150	24 h	0.8	10.6	0.70	5.21
					Day 16	150	24 h			0.82	4.44
					Day 20	Susp 1 dose > 120 mg q48h		1.3	9.9	1.23	2.96
					Day 22	120	48 h			0.90	4.05
					Day 24	150	48 h	0.2	5.1	0.73	4.99
					Day 26	100	24 h	0.1	5.1		
24	Fem	50	65	157	Day 1					0.96	4.32
					Day 4	100	8 h			0.84	4.93
					Day 8	Susp 1 dose > 130 mg q24h		3.8	10.0	0.91	4.55

Recommended posology											
#ID	Sex	Age (years)	Weight (kg)	Height (cm)	Date	Dose (mg)	Interval	C_{min} (mg/L)	C_{max} (mg/L)	[Cr] (mg/dL)	CL (L/h)
					Day 9	130	24 h				
					Day 11	140	24 h	0.8	7.5	0.95	4.36
					Day 15	120	24 h	0.6	12.2	1.12	3.70
27	Male	20	70	175	Day 1	70	8 h			0.87	8.05
					Day 2	70	8 h			0.71	9.86
					Day 3	70	8 h			0.75	9.33
					Day 4	70	8 h			0.76	9.21
					Day 5	160	12 h	0.3	3.4	0.86	8.14
					Day 8	160	12 h	0.4	7.6	0.75	9.33
					Day 10	160	12 h	0.4	8.2	0.88	7.95
					Day 12	160	12 h	0.3	7.8	0.78	8.97
					Day 13	160	12 h			0.70	10.00
					Day 16	140	12 h	0.6	7.6	0.86	8.14
33	Male	75	53	170	Day 1					1.49	1.93
					Day 3	60	8 h			0.90	3.19
					Day 6	Susp 1 dose > 150 mg q24h		2.5	5.3	0.89	3.23
					Day 11	100	24 h	1.0	13.2		
					Day 13	100	24 h	0.6	8.2		
34	Male	69	83	180	Day 1					1.04	4.72
					Day 4	240	24 h			0.85	5.78
					Day 7	150	24 h	0.2	(occas 1.5 h) 9.1	0.97	5.06
					Day 11	150	24 h	0.2	4.6	1.04	4.72
					Day 12	170	24 h			1.10	4.46
					Day 14	160	24 h	0.2	(occas 1.5 h) 5.6	1.04	4.72
35	Male	50	80	185	Day 1	160	24 h				
					Day 6	190	12 h	0.2	6.6	0.49	12.24
					Day 8	Susp 1 dose > 200 mg q24h		1.1	10.4	0.51	11.76
					Day 15	200	24 h	0.4	9.4	0.52	11.54
					Day 21	Susp 1 dose > 190 mg q24h		1.9	12.8	0.65	9.23
					Day 23	190	24 h	0.5	10.8	0.82	7.32
					Day 27	190	24 h			1.14	5.26
					Day 28	Susp 2 doses > 180 mg q48h		2.2	13.4	1.47	4.08
50	Male	73	80	170	Day 1	200	24 h				
					Day 7	150	24 h	1.2	calc 10-12	1.14	3.92
62	Fem	7	15.5	108	Day 1	80	24 h			0.68	2.15
					Day 3	80	24 h	(occas) 0.4	calc 10-11	0.37	3.95
63	Male	62	85	180	Day 1	433.5	24 h				
					Day 8	433.5	24 h			0.76	7.27
					Day 9	433.5	24 h			0.72	7.67
					Day 10	500	24 h	0.3	19.5	0.73	7.57
-1	Male	86	70	165	Day 1	70	12 h	1.2	4.1	1.89	1.67
-2	Male	33	70	170	Day 1	80	8 h	0.3	3.1	0.59	10.58
-3	Male	60	85	161	Day 1	140	8 h	2.9	9.0	0.85	6.67
-4	Fem	78	44	160	Day 1	130	24 h	0.6	5.2	0.74	2.61
-5	Male	55	65	165	Day 1	120	8 h	0.2	2.9	0.29	15.88
-6	Male	34	71.4	165	Day 1	240	24 h	0.5	5.9	0.61	10.34
-7	Fem	73	62	165	Day 1	180	24 h	1.3	11.1	1.00	2.94

Recommended posology											
#ID	Sex	Age (years)	Weight (kg)	Height (cm)	Date	Dose (mg)	Interval	C_{min} (mg/L)	C_{max} (mg/L)	[Cr] (mg/dL)	CL (L/h)
-8	Male	56	72	170	Day 1	210	24 h	4.8	14.4	1.00	5.04
-9	Fem	51	63	160	Day 1	180	24 h	0.2	6.6	0.64	6.21
TOBRAMYCIN											
30	Fem	13	40.8	146	Day 1	400	24 h				
					Day 3	400	24 h	0.2	18.8	0.51	7.20
					Day 5	500	24 h				
					Day 7	450	24 h	---	33.7	0.49	7.49
					Day 12	450	24 h	0.23	calc 24-26	0.46	7.98
31	Fem	13	27	140	Day 1	270	24 h				
					Day 3	270	24 h	0.2	25.9	0.49	4.96
					Day 7	270	24 h	---	26.4	0.41	5.92
39	Fem	13	25.8	130	Day 1	250	24 h				
					Day 6	250	24 h	0.2	29.4	0.48	4.84
					Day 9	250	24 h	0.1	24.1	0.60	3.87
					Day 13	250	24 h	0.1	---	0.55	4.22
40	Fem	19	29	155	Day 1	300	24 h			0.40	6.21
					Day 2	300	24 h			0.43	5.78
					Day 3	300	24 h	(occas) 0.2	calc 29-30	0.43	5.78
					Day 6	300	24 h	(occas) 0.1	calc 28-30		
					Day 8	300	24 h	(occas) 0.1	calc 28-30	0.35	7.10
					Day 12	350	24 h	---	17.0	0.64	3.88
					Day 16	350	24 h	---	16.3	0.47	5.29
					Day 19	300	24 h	---	34.8	0.39	6.37
					Day 23	300	24 h	---	36.1	0.54	4.60
41	Male	17	44.5	158	Day 1	430	24 h				
					Day 7	400	24 h	0.2	35	0.52	8.77
					Day 10	400	24 h	0.2	calc 29-30	0.58	7.86
VANCOMYCIN											
1	Fem	88	66	155	Day 1					0.95	2.56
					Day 4	1000	12 h			0.90	2.70
					Day 6	750	12 h	17.7	31.0	0.80	3.04
					Day 8	Susp 1 dose > 500 mg q12h		23.4	34.1	0.81	3.00
					Day 12	Susp 1 dose > 750 mg q24h		22.1	27.3	1.04	2.34
					Day 20	500	24 h	21.2	34.7	1.18	2.06
2	Fem	51	90	165	Day 1	1000	12 h				
					Day 3	800	8 h	9.3	19.8	0.86	6.60
					Day 4					0.72	7.88
					Day 6	800	8 h	10.2	19.1	0.55	10.32
					Day 9					0.74	7.67
					Day 10					0.79	7.18
					Day 11	950	8 h	12.2	21.2	0.60	9.46
3	Fem	50	80	165	Day 1	1000	12 h				
					Day 8	Susp 1 dose > 600 mg q12h		26.0	36.1	1.05	5.46
					Day 11	600	12 h	15.6	24.3	1.12	5.12
					Day 16	700	12 h	12.5	23.9	0.90	6.38
					Day 19	600	12 h	18.6	(occas 4 h) 29.7	1.02	5.63
4	Fem	61	71.5	160	Day 1					0.72	5.28

					Recommended posology					
#ID	**Sex**	**Age (years)**	**Weight (kg)**	**Height (cm)**	**Date**	**Dose (mg)**	**Interval**	**C_{min} (mg/L)**	**C_{max} (mg/L)**	**[Cr] (mg/dL)**	**CL (L/h)**
					Day 2	1000	12 h			0.63	6.04
					Day 3	1000	8 h	6.6	16.1	0.52	7.32
					Day 4					0.58	6.56
					Day 5					0.49	7.77
					Day 6	Susp 1 dose > 700 mg q8h		23.8	36.2	0.45	8.46
					Day 9	700	8 h	7.8	18.9	0.56	6.79
5	Male	58	87	185	Day 1	1000	12 h				
					Day 3					0.71	8.37
					Day 4	1000	8 h	7.3	16.8	0.72	8.26
					Day 6	Suspend administration		16.7	23.7	1.32	4.50
6	Male	62	71.9	172	Day 1	1000	12 h				
					Day 2					0.57	7.98
					Day 3	650	6 h	8.5	17.1	0.52	8.75
					Day 5	700	6 h	10.8	15.2	0.53	8.58
8	Male	53	65	165	Day 1					0.97	4.86
					Day 2	1000	12 h			1.16	4.06
					Day 5	850	12 h	calc 19-21	(occas 4 h) 30.2	0.88	5.36
					Day 6	850	12 h	15.4	27.3	1.10	4.28
					Day 7	850	12 h	14.9	28.4	1.01	4.67
					Day 9					1.23	3.83
					Day 13	600	12 h	22.3	34.0	1.13	4.17
9	Fem	66	140	163	Day 1	1000	12 h				
					Day 3	Susp 1 dose > 500 mg q12h		19.6	28.3		
					Day 7	Susp 1 dose > 950 mg q24h		17.4	22.9	0.84	8.74
					Day 13	800	24 h	14.1	(occas 4 h) 23.7		
10	Male	64	70	168	Day 1	1000	12 h				
					Day 5	1000	12 h	14.7	28.0		
					Day 7	850	12 h	19.3	21.1	1.17	3.79
					Day 12	Susp 1 dose > 1000 mg q24h		28.0	33.4	1.29	3.44
					Day 15	500	12 h	10.7	calc 27-29	1.35	3.28
11	Fem	47	65	147	Day 1	1000	12 h				
					Day 3	Susp 1 dose > 750 mg q12h		17.3	42.5	1.10	3.89
					Day 7	500	8 h	10.5	23.0		
					Day 10	500	8 h	13.1	22.4	0.70	6.12
12	Fem	73	80	160	Day 1	1000	12 h				
					Day 6	Susp 1 dose > 650 mg q12h		26.4	32.6	0.53	7.16
					Day 14	600	12 h	19.1	25.3		
					Day 19	600	12 h	15.5	23.7		
					Day 23	650	12 h	16.5	---		
					Day 25					0.47	8.08
					Day 27	600	12 h	20.9	26.6	0.45	8.44
					Day 30	500	12 h	22.4	31.0	0.41	9.26
14	Male	59	85	174	Day 1	500	6 h				
					Day 3	700	6 h	10.7	11.8		
					Day 4					0.48	11.95
					Day 5	800	6 h	11.4	14.8		
15	Fem	20	29	155	Day 1	1000	12 h				

Recommended posology											
#ID	Sex	Age (years)	Weight (kg)	Height (cm)	Date	Dose (mg)	Interval	C_{min} (mg/L)	C_{max} (mg/L)	[Cr] (mg/dL)	CL (L/h)
					Day 3	500	6 h	5.8	---	0.35	7.04
					Day 5	300	4 h	8.1	15.0	0.35	7.04
					Day 8	300	4 h	13.2	---	0.41	6.01
					Day 11	300	4 h	1.6[a]; calc 12-14		0.40	6.16
					Day 1					4.78	0.63
					Day 2	900	12 h				
					Day 3					4.46	0.67
					Day 4					4.43	0.68
					Day 5	Suspend administration		22.3	(occas 4 h) 39.6	3.99	0.75
16	Male	80	60	160	Day 6					2.98	1.01
					Day 7			24.3	---	3.32	0.90
					Day 8	500	24 h			2.83	1.06
					Day 9					2.24	1.34
					Day 11					1.78	1.69
					Day 12	400	24 h	21.4	27.5	1.95	1.54
					Day 1					0.93	3.09
					Day 2					0.80	3.59
					Day 3					0.89	3.23
					Day 4					0.78	3.69
17	Fem	82	70	165	Day 5	1000	12 h				
					Day 6	1000	12 h	10.6	23.0	0.80	3.59
					Day 9					1.01	2.85
					Day 11	900	12 h	17.2	32.5	0.96	3.00
					Day 13	Susp 1 dose > 500 mg q12h		27.2	36.5	0.92	3.13
					Day 1	1000	12 h			0.50	10.15
					Day 3					0.40	12.69
					Day 4	850	6 h	4.8	11.2	0.40	12.69
					Day 6	850	6 h	9.6	14.2	0.54	9.40
21	Male	53	70	170	Day 7	900	6 h	9.5	13.0	0.40	12.69
					Day 9					0.68	7.46
					Day 10					0.78	6.51
					Day 11	850	6 h	18.5	28.1	0.68	7.46
					Day 1					3.32	0.59
					Day 2					2.85	0.69
					Day 4	1000	12 h				
42	Male	93	50	170	Day 8	Susp 3 days > 900 mg q24h		44.5	60.1	2.04	0.96
					Day 13	Suspend administration		31.4	45.3	2.06	0.95
					Day 1	1000	12 h				
					Day 6	750	6 h	7.9	15.6	0.61	6.66
					Day 9	850	6 h	12.9	17.7	0.69	5.89
43	Male	65	65	170	Day 13	Susp 2 doses > 650 mg q6h		21.1	27.9	0.74	5.49
					Day 22	1000	12 h				
					Day 26	600	6 h	11.0	21.3		
					Day 1	1000	8 h				
44	Male	54	70	172	Day 2	850	6 h	10.7	19.8		
					Day 4	800	6 h	13.7	21.9		

					Recommended posology					
#ID	Sex	Age (years)	Weight (kg)	Height (cm)	Date	Dose (mg)	Interval	C_{min} (mg/L)	C_{max} (mg/L)	[Cr] (mg/dL)	CL (L/h)
					Day 6					0.47	10.67
					Day 7					0.41	12.24
					Day 8	800	8 h	5.4	---	0.49	10.24
					Day 9					0.61	8.22
					Day 10	700	8 h	21.5[a]	---	0.53	9.47
					Day 11			9.5	14.2		
					Day 12					0.47	10.67
					Day 14					0.37	13.56
					Day 15			14.7		0.45	11.15
					Day 1	1000	12 h				
45	Male	61	90	175	Day 3					1.01	5.87
					Day 4					0.93	6.37
					Day 7	Suspend administration		14.9	30.2	0.81	7.31
					Day 1	1000	12 h			0.77	3.93
46	Fem	70	61	158	Day 3					0.74	4.09
					Day 6	700	12 h	20.5	35.6	0.76	3.98
					Day 1					1.98	1.54
47	Male	79	60	150	Day 3					1.98	1.54
					Day 4	1000	24 h				
					Day 8	Suspend administration		25.7	41.5	2.08	1.47
					Day 1					1.14	1.40
					Day 4	700	12 h			1.19	1.34
					Day 7	500	12 h	21.0	30.3	1.11	1.44
48	Fem	90	45	160	Day 10	500	12 h	---	29.5	0.97	1.64
					Day 16	Susp 2 doses > 800 mg q24h		20.3	---	1.19	1.34
					Day 18					1.38	1.15
					Day 21	500	24 h	22.1	---	1.49	1.07
					Day 1	500	12 h				
49	Fem	85	80	163	Day 2					1.20	2.60
					Day 3	Susp 2 doses > 650 mg q24h		25.4	---	0.83	3.76
					Day 4	650	24 h	16.8	25.8		
					Day 1					0.54	7.07
51	Fem	63	70	165	Day 2	1000	12 h				
					Day 3					0.93	4.11
					Day 4	Susp 1 dose > 650 mg q8h		12.3	16.3	0.86	4.44
					Day 1					1.36	2.54
52	Male	71	60	165	Day 3	1000	12 h			1.04	3.32
					Day 5	Susp 1 dose > 600 mg q12h		23.3	36.0	0.89	3.88
					Day 1	1000	12 h				
					Day 4	Susp 1 dose > 500 mg q12h		32.2	44.5		
					Day 5					1.22	3.87
					Day 8			17.9	22.4	1.17	4.04
53	Male	59	70	180	Day 9	850	6 h				
					Day 15	1000	12 h				
					Day 18					1.11	4.26
					Day 20					1.06	4.46
					Day 22	Suspend administration		45.6	57.1	1.25	3.78

					Recommended posology					
#ID	Sex	Age (years)	Weight (kg)	Height (cm)	Date	Dose (mg)	Interval	C_{min} (mg/L)	C_{max} (mg/L)	[Cr] (mg/dL)	CL (L/h)
					Day 25			27.2	---		
					Day 1	1000	12 h				
					Day 3	850	6 h	5.1	---	0.88	6.65
					Day 6	850	6 h	12.0	---	1.02	5.74
54	Male	23	60	163	Day 10					1.00	5.85
					Day 13	900	6 h	10.2	---	0.96	6.09
					Day 17	900	6 h	17.0	---	0.98	5.97
					Day 20	900	6 h	9.6[a]	---	0.94	6.22
					Day 1	1000	12 h				
					Day 7			21.0	28.0	0.83	4.36
					Day 8	750	12 h			0.94	3.85
					Day 9			22.1	---	0.82	4.41
					Day 10					0.86	4.21
					Day 11					0.82	4.41
55	Male	78	70	172	Day 12			16.9	---	0.93	3.89
					Day 15			16.9	25.9		
					Day 27	1000	12 h				
					Day 34			25.0	34.7		
					Day 35			18.5	29.4		
					Day 40	Suspend administration		26.2	37.6		
					Day 42				(occas) 11.4	0.86	4.21
					Day 1					0.35	14.50
					Day 5	1000	12 h			0.27	18.80
					Day 11			5.3	12.8	0.38	13.36
56	Male	53	70	180	Day 14	850	8 h	6.7	15.0	0.30	16.92
					Day 18	950	8 h	14.8	15.4		
					Day 20	800	6 h	12.4	19.8	0.32	15.86
					Day 1	1000	12 h				
					Day 3	900	12 h	16.7	25.2	1.55	3.99
					Day 8	Susp 2 doses > 600 mg q12h		24.9	33.8	1.44	4.30
					Day 11	550	12 h	17.8	23.1	1.68	3.68
57	Male	41	75	175	Day 14	600	12 h	16.1	21.9	1.20	5.16
					Day 18	650	12 h	14.4	28.6	1.01	6.13
					Day 22	650	12 h	16.7	26.4	1.02	6.07
					Day 25	650	12 h	16.0	44.3[a]	1.02	6.07
					Day 1	1000	12 h				
					Day 2	800	12 h	8.4	---	1.34	3.49
					Day 4	600	12 h	25.7	34.0		
					Day 5	Susp 3 doses > 1000 mg q24h		27.1	31.7	1.39	3.36
					Day 6					1.25	3.74
58	Male	81	95	170	Day 8	1000	24 h	16.3	---	1.19	3.93
					Day 11			19.0	---		
					Day 12					1.11	4.21
					Day 15			23.3	42.6	1.17	3.99
					Day 16	Suspend administration		25.8		1.28	3.65
					Day 1	1000	12 h				
59	Fem	52	68	164	Day 6	700	8 h	12.7	---	0.70	6.06

Recommended posology											
#ID	**Sex**	**Age (years)**	**Weight (kg)**	**Height (cm)**	**Date**	**Dose (mg)**	**Interval**	**C_{min} (mg/L)**	**C_{max} (mg/L)**	**[Cr] (mg/dL)**	**CL (L/h)**
					Day 1	1000	12 h				
					Day 6			17.6	---		
					Day 7					0.96	5.23
					Day 8					1.08	4.65
					Day 9			23.2	---	0.89	5.64
					Day 10	600	12 h	18.0	---	0.82	6.12
					Day 17	Susp 1 dose > 750 mg q24h		calc 24-26	32.5		
60	Male	54	70	165	Day 18					1.25	4.01
					Day 19					0.97	5.17
					Day 20	Susp 1 dose > 1000 mg q24h[b]		13.3	23.2	0.93	5.39
					Day 23	450	12 h	11.9	---		
					Day 24					0.63	7.96
					Day 25					0.64	7.84
					Day 26					0.65	7.72
					Day 27					0.56	8.96
					Day 1	1000	12 h				
					Day 4	1000	8 h	6.5	14.9	0.76	10.35
					Day 7	Susp 1 dose > 800 mg q6h		12.0	20.0	0.82	9.59
					Day 11					0.87	9.04
					Day 12	1000	12 h	16.0	19.7		
					Day 19	750	6 h	8.1	14.5	0.77	10.21
61	Male	62	121	176	Day 21	800	6 h	12.3	14.4[a]	0.79	9.96
					Day 25	900	6 h	12.2	15.1	0.73	10.77
					Day 29			14.9	20.1	0.82	9.59
					Day 31					0.87	9.04
					Day 33	900	6 h	16.9	20.5	0.77	10.21
					Day 36	Susp 2 doses > 800 mg q6h		11.6	16.9	0.84	9.36
					Day 39	900	6 h	17.4	21.2	0.80	9.83
					Day 1	500	6 h				
64	Male	62	65	170	Day 10					1.38	3.06
					Day 15	600	6 h	13.4	17.8	0.94	4.49
					Day 1	1000	12 h			0.62	4.11
65	Fem	80	60	165	Day 3	600	6 h	7.2	17.4	0.40	6.38
					Day 6	600	6 h	13.2	16.7	0.34	7.50
					Day 8	500	6 h	16.8	20.8	0.32	7.97
66	Fem	86	50	155	Day 1	1000	12 h	19.2	35.5	0.65	2.94
67	Fem	20	50	157	Day 1	1000	12 h	4.5	14.9	0.43	9.88
68	Male	54	58	160	Day 1	1000	12 h	15.0	34.6	0.63	6.60
69	Fem	46	70	156	Day 1	1000	12 h	6.6	19.2	0.38	12.27
70	Fem	78	47	160	Day 1	650	12 h	14.9	29.0	0.74	2.79
71	Fem	63	70	170	Day 1	1000	12 h	9.0	19.2	0.55	6.94
72	Male	83	70	170	Day 1	1000	12 h	15.1	26.9	0.97	3.43
73	Male	75	57	170	Day 1	1000	12 h	24.9	41.0	1.03	3.00
74	Male	83	65	170	Day 1	1000	12 h	22.3	36.8	1.28	2.41
75	Fem	19	60	170	Day 1	1000	8 h	18.0	43.1	1.87	2.75

[a] probable irregularity in the analytical determination of antibiotic concentration.
[b] previous posology was followed.

Susp X dose: X number of scheduled doses were suspended and recommended posology for when antibiotic administrations were resumed is presented.

Reference
Cockcroft, D.W.; Gault, M.H. Prediction of creatinine clearance from serum creatinine. *Nephron* **1976**, *16*, 31–41.

CHAPTER 7

A retrospective study comparing creatinine clearance estimation using different equations on a population-based cohort

Abigail Ferreira, Rui Lapa and Nuno Vale

Mathematical Biosciences and Engineering, **2021**, 18(5), pp. 5680-5691.

DOI: 10.3934/mbe.2021287

Given the critical impact of renal function on the dose adjustment process and on the pharmacokinetic profile of the antibiotics studied in this thesis, this parameter was considered and examined further. As the actual most accurate indicator glomerular filtration rate (GFR) is not easily measured in clinical settings, numerous equations were developed over the decades to estimate renal function. Twelve of these equations were selected and analyzed to better understand the differences between them in the resulting estimated renal clearance, as well as the influence of the input parameters sex, age, and body composition. Demographic data and serum creatinine concentrations from the population previously studied were analyzed and renal clearance was estimated according to each equation. The highlighted differences complement the knowledge about the available methods to estimate renal function and can help clinicians make a customized and best fitted decision when choosing how to evaluate a patient's renal function.

Mathematical Biosciences and Engineering

http://www.aimspress.com/journal/MBE

MBE, 18(5): 5680–5691.
DOI: 10.3934/mbe.2021287
Received: 21 April 2021
Accepted: 17 June 2021
Published: 23 June 2021

Research article

A retrospective study comparing creatinine clearance estimation using different equations on a population-based cohort

Abigail Ferreira[1,2], Rui Lapa[2] and Nuno Vale[1,2,*]

[1] OncoPharma Research Group, Center for Health Technology and Services Research (CINTESIS), Rua Dr. Plácido da Costa, Porto 4200-450, Portugal
[2] LAQV/REQUIMTE, Laboratory of Applied Chemistry, Department of Chemical Sciences, Faculty of Pharmacy, University of Porto, Rua de Jorge Viterbo Ferreira, 228, Porto 4050-313, Portugal
[3] Department of Community Medicine, Health Information and Decision (MEDCIDS), Faculty of Medicine, University of Porto, Al. Prof. Hernâni Monteiro, Porto 4200-319, Portugal

* **Correspondence:** Email: nunovale@med.up.pt; Tel: +351225513622; Fax: +351225513668.

Abstract: Renal elimination is an important part of drugs' excretion. At the same time, renal function can be impaired as a side effect of medication, particularly during prolonged treatments. Thus, the assessment of patients' renal function is of major consequence, especially in cases where the therapeutic regimen is adjusted taking into consideration renal clearance. Serum creatinine concentration is the most common indicator of renal clearance, since the most accurate indicator, glomerular filtration rate (GFR), is not easily measured. Using equations developed over the last decades, creatinine clearance (CL_{Cr}) is readily estimated taking into account patients' biological sex, age, body composition, and sometimes race. In this work, differences in estimated CL_{Cr} between different equations were studied and the influence of some patients' characteristics evaluated. Data collected from 82 inpatients receiving antibiotic therapy was analyzed and CL_{Cr} was estimated using a total of 12 equations. Patients were stratified according to their sex, age, and body composition to shed some light on the impact of these parameters in the estimations of renal function. More variability between estimation methods was highlighted (a) in patients between 51 and 60 years old, (b) within the normal body mass index group, and (c) in patients with serum creatinine levels below normal criteria. Furthermore, the Cockcroft-Gault equation considering lean body weight produced lower estimated CL_{Cr} in almost all groups.

Keywords: creatinine clearance estimation; renal function; therapeutic drug monitoring (TDM); antibiotics; Cockcroft-Gault formula; Jelliffe formula; Wright formula; Corcoran-Salazar formula

1. Introduction

Kidneys play an important role in the elimination of many drugs, including antibiotics. Renal function varies according to age, sex, body size, and race, is influenced by strenuous physical activity, diet, and consumption of red meat, certain herbs, and supplements, and is altered during pregnancy. Most importantly, it can be impaired as a collateral effect of medication, which is particularly significant during prolonged treatments. As such, evaluating patients' renal function is a key component of therapeutic drug monitoring (TDM), along with examining peak and trough plasma levels of the drug. Glomerular filtration rate (GFR) is regarded as a crucial indicator of kidney function. Generally, a GFR above 90 mL/min indicates a normal kidney function [1]. Unfortunately, GFR is not easily determined in a clinical setting; instead, renal function is often estimated from serum creatinine concentration (SCr), using numerous equations developed over the last decades and demographic parameters as sex, body size, age, and race [2,3]. SCr is rapidly determined, and these estimations can be readily calculated. However, these equations were derived from data collected from very diverse study populations, and there is neither a universal nor subpopulation-specific standard equation. As such, clinicians must decide how to calculate this estimation (what equation to use) or most frequently, follow what the institution has established. Since each equation results in dissimilar estimated clearance for the same individual, therapeutic adjustment can be significantly different according to the chosen method.

Antibiotics are one of the most prescribed drugs. Monitoring patients and appropriately adjusting the dose of the antibiotic or the treatment regimen is important to optimize the clinical outcome, reduce the risk of toxic side effects and avoid serious deterioration of renal function associated with increased plasmatic levels and drug accumulation while aiming at improving efficacy, and also due to great inter-individual variability. This can also help limit antibiotic resistance.

Table 1. Pharmacokinetic (PK) properties of antibiotics amikacin, gentamicin, tobramycin, and vancomycin [4–10].

PK	Amikacin	Gentamicin	Tobramycin	Vancomycin
Hydrophilicity	Hydrophilic			
Metabolism	Eliminated unchanged in urine			
F_{up}	> 90%	> 70%	> 70%	50–90%
$T_{1/2}$	2–3 h	2–3 h	2–3 h	~6 h (4–11 h)
V_c	~0.34 L/kg	0.2–0.3 L/kg	0.2–0.3 L/kg	0.4–1 L/kg
Clearance	100 mL/min	57 mL/min	141 mL/min	67.7 mL/min
Typical dosing for susceptible infections	7.5 mg/kg 12/12 h	1 mg/kg 8/8 h	1 mg/kg 8/8 h	1000 mg 12/12 h

F_{up}: fraction unbound in plasma; $T_{1/2}$: half-life; V_c: central volume of distribution.

In this work, data was collected from inpatients receiving intravenous antibiotic therapy with amikacin, gentamicin, tobramycin, or vancomycin (chemical structures are presented in Figure 1 and some properties are summarized in Table 1), and their creatine clearance was estimated using five

equations plus seven variations of the Cockcroft-Gault formula (total of 12 different estimations). A direct measurement of GFR was not available, a limitation that prevented the comparison between observed and estimated clearance. The aim of this study was to evaluate the differences in estimated creatinine clearance produced by different equations and the influence of some patients' characteristics in these estimations, to better understand the impact of the choice of estimation method.

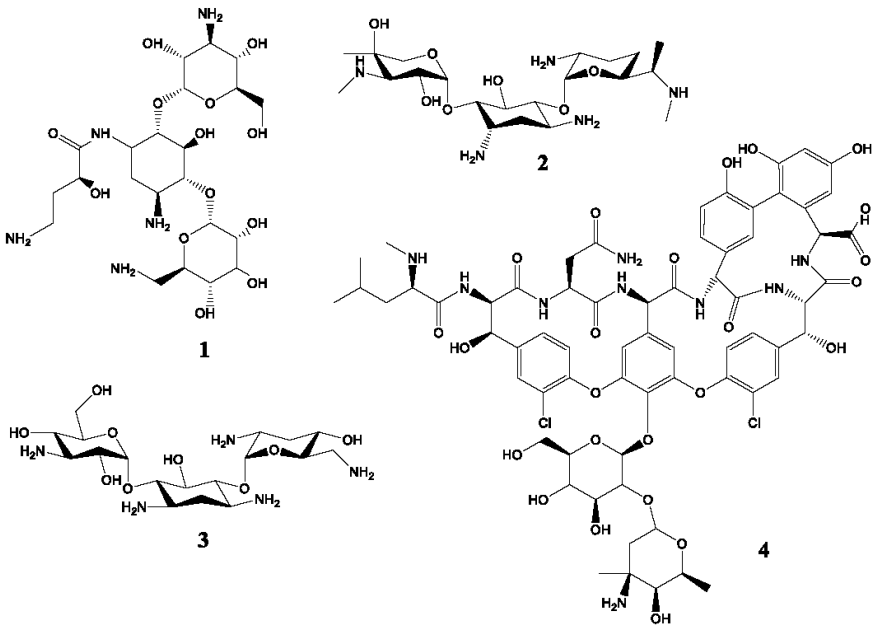

Figure 1. Chemical structure of amikacin (1), gentamicin (2), tobramycin (3) and vancomycin (4).

2. Materials and methods

2.1. Patients and methods

Data was gathered from 82 inpatients receiving antibiotic therapy for the treatment of serious infections of different etiologies with intravenous amikacin, gentamicin, tobramycin, or vancomycin in CHUP (*Centro Hospitalar Universitário do Porto*). This information included demographics, such as biological sex, age, total body weight, and height, as well as creatinine (enzymatic method) and drug plasma concentrations determined in multiple days throughout the treatment. All the collected creatinine concentrations were included in this study, in a total of 374 measurements. A summary of all collected data is presented in Table 2.

Creatinine clearance (CL_{Cr}) was estimated, in mL/min, according to Eqs (2) through (7). Seven adaptations of the Cockcroft-Gault (CG) equation were included, incorporating body weight as actual (TBW), ideal (IBW), adjusted (AdjBW), modified-adjusted (mAdjBW), and lean body weight (LBW), as described in Eqs (8) through (12). Additionally, variations of ideal plus a fixed percentage of 30, 40, or 50% were calculated. In these equations, body weight is in kg, H is height in m, age is in years, and SCr is the measured serum creatinine in mg/dL. BSA is the body surface area in m^2, calculated

according to the DuBois formula (1) [11] (height in cm).

$$\mathrm{BSA} = 0.007184 \times TBW^{0.425} \times H^{0.725} \tag{1}$$

Cockcroft-Gault (CG) Eq (2) must be multiplied by 0.85 for female individuals [12].

$$\mathrm{CL_{Cr}} = \frac{(140 - \mathrm{Age}) \times \mathrm{BW}}{\mathrm{SCr} \times 72} \tag{2}$$

Jelliffe [13] developed Eq (3), that can be normalized considering BSA Eq (4). Both equations should be multiplied by 0.9 for female individuals.

$$\mathrm{CL_{Cr}} = \frac{98 - [0.8 \times (\mathrm{Age} - 20)]}{\mathrm{SCr}} \tag{3}$$

$$\mathrm{CL_{Cr}} = \frac{(98 - [0.8 \times (\mathrm{Age} - 20)]) \times \left(\frac{\mathrm{BSA}}{1.73}\right)}{\mathrm{SCr}} \tag{4}$$

Wright equation (5) [14] is likewise multiplied by 0.77 for female individuals:

$$\mathrm{CL_{Cr}} = \frac{(6230 - 32.8 \times \mathrm{Age}) \times \mathrm{BSA}}{\mathrm{SCr} \times 88.42} \tag{5}$$

Corcoran–Salazar (CS) [15] also developed equations to estimate clearance. For male individuals, Eq (6) should be used, while for female individuals, Eq (7) is applied:

$$\mathrm{CL_{Cr}} = \frac{(137 - \mathrm{Age}) \times (0.285 \times \mathrm{TBW} + 12.1 \times \mathrm{H^2})}{\mathrm{SCr} \times 51} \tag{6}$$

$$\mathrm{CL_{Cr}} = \frac{(146 - \mathrm{Age}) \times (0.287 \times \mathrm{TBW} + 9.74 \times \mathrm{H^2})}{\mathrm{SCr} \times 60} \tag{7}$$

Ideal body weight was calculated using the Devine equation (8) [16]:

$$\mathrm{IBW} = 50 + 2.3 \times \left(\frac{\mathrm{H}}{2.54} - 60\right) \tag{8}$$

where height (H) is in centimeters and the factor 50 is replaced by 45.5 in female individuals. The adjusted body weight was calculated as Eq (9) [18] and modified adjusted body weight as Eq (10) [17]:

$$\mathrm{AdjBW} = \mathrm{IDW} + 0.4 \times (\mathrm{TBW} - \mathrm{IBW}) \tag{9}$$

$$\mathrm{mAdjBW} = \mathrm{mIBW} + 0.4 \times (\mathrm{TBW} - \mathrm{mIBW}) \tag{10}$$

Lean body weight for male individuals was calculated as Eq (11) for males and as Eq (12) for females [19]:

$$\mathrm{LBW} = \frac{9270 \times \mathrm{TBW}}{6680 + 216 \times \mathrm{BMI}} \tag{11}$$

$$\mathrm{LBW} = \frac{9270 \times \mathrm{TBW}}{8780 + 244 \times \mathrm{BMI}} \tag{12}$$

Table 2. Summary of collected clinical data, with the indication of lower and upper limits and calculation of average value for each parameter.

	Full database	Amikacin	Gentamicin	Tobramycin	Vancomycin
Biological sex	F: 34 (41.5%) M: 48 (58.5%)	F: 1; M: 7	F: 8; M: 14	F: 4; M: 1	F: 21; M: 26
Age (years)	7–93 (avg 58)	14–87 (avg 57)	7–88 (avg 58)	13–19 (avg 15)	19–93 (avg 63)
Weight (kg)	15.5–140 (avg 66.2)	50.0–92.5 (avg 66.0)	15.5–85.0 (avg 66.0)	25.8–44.5 (avg 33.0)	44.5–121.0 (avg 70)
Height (cm)	108–185 (avg 164.7)	163–180 (avg 169)	108–185 (avg 165)	130–158 (avg 146)	147–180 (avg 166)
[Cr] (mg/dL)	0.63–4.78 (avg 0.93)	0.47–1.58 (avg 0.93)	0.29–1.89 (avg 0.83)	0.35–0.64 (avg 0.49)	0.27–4.78 (avg 1.02)
C_{min} (mg/L)	---	0.30–16.40 (avg 3.70)	0.20–4.80 (avg 1.05)	0.06–0.23 (avg 0.17)	4.50–45.60 (avg 16.45)
C_{max} (mg/L)	---	19.70–87.80 (avg 38.97)	2.90–19.50 (avg 9.22)	16.32–36.12 (avg 27.05)	11.20–60.10 (avg 25.99)

F: females; M: males; avg: average value; [Cr]: serum creatinine concentration; C_{min}: antibiotic concentration measured right before a dose; C_{max}: antibiotic concentration measured 1 h (aminoglycosides amikacin, gentamicin and tobramycin) or 3 h (vancomycin) after the beginning of an infusion.

2.2. Data analysis

Patients were stratified into four groups according to body composition, using body mass index (BMI) as an indicator: underweight (BMI < 17.9 kg/m^2), normal weight (BMI = 18–24.9 kg/m^2), overweight (BMI = 25–29.9 kg/m^2), and obese (BMI ≥ 30 kg/m^2). Data was also analyzed according to the sex and age of the patients, as well as to their measured serum creatinine concentration.

BMI was calculated as Eq (13), where TBW is total body weight in kg and H is height in m:

$$\mathrm{BMI} = \frac{\mathrm{TBW}}{\mathrm{H}^2} \tag{13}$$

Calculations of estimated CL_{Cr} values were performed in Microsoft Excel 365. Plots were also generated in Excel. The number of records of creatinine concentration of each group is indicated in every plot (as *n*).

3. Results and discussion

All the serum creatinine concentrations collected from the patients in the study population were included in this study. The distribution of this data is presented in Figure 2.

Analyzing the distribution of creatinine serum concentrations (SCr), it is noticeable that men of the population studied in this work had higher SCr, as expected. Patients with normal BMI reached more extreme values (mainly elevated) of SCr comparing to the other body composition groups. With increasing age, SCr was also increased, predominantly in patients older than 70 years old.

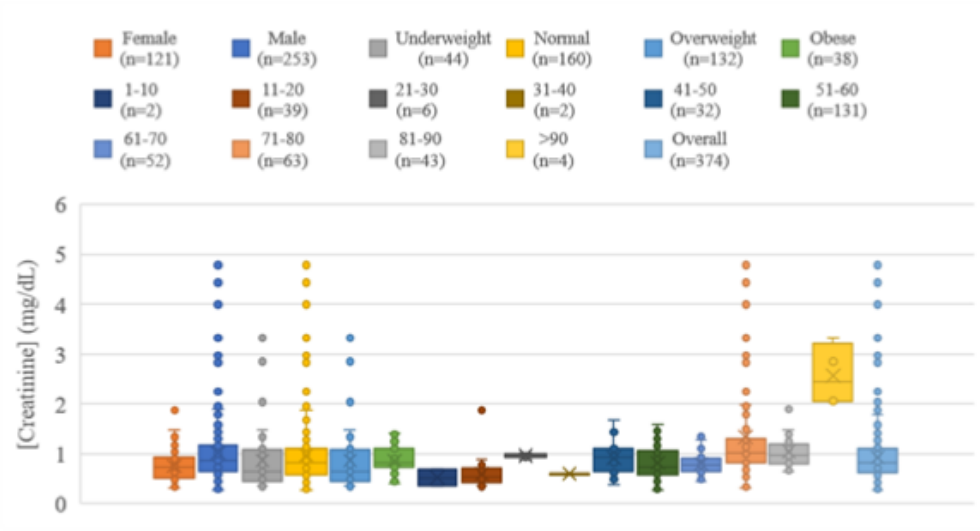

Figure 2. Distribution of measured creatinine serum concentrations in different groups (biological sex, body composition and age) and of all measures included in this study (overall).

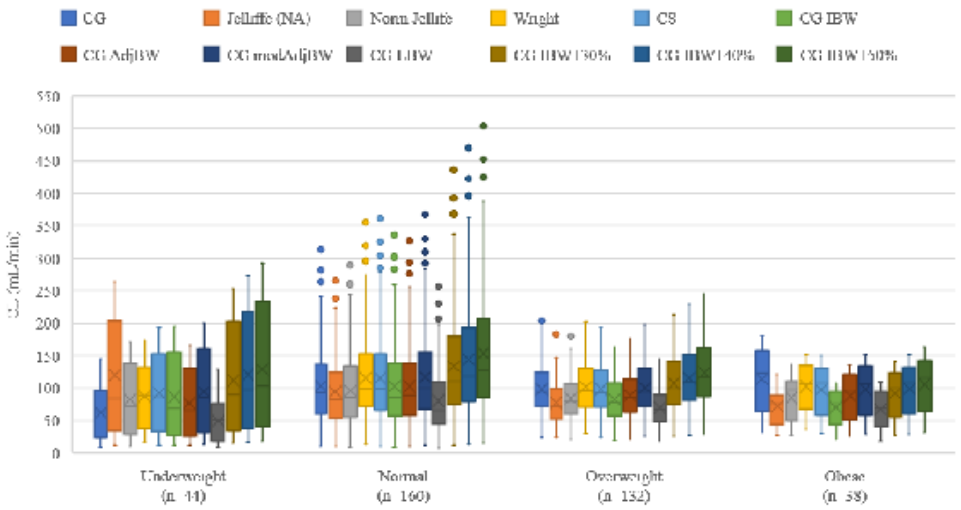

Figure 3. Distribution of clearance estimations according to body type (based on BMI).

Patients were then grouped according to their body composition based on BMI. The estimations of CL_{Cr} based on this stratification are presented in Figure 3. In the studied population, there was more variability in the estimated CL_{Cr} within the normal weight group. Furthermore, data from this group, followed by the underweight group, resulted in higher estimated CL_{Cr}. However, it is important to note that only patients under 20 years old and older than 71 years old were part of the underweight group.

Overweight and obese patients had lower and less varying estimated CLCr.

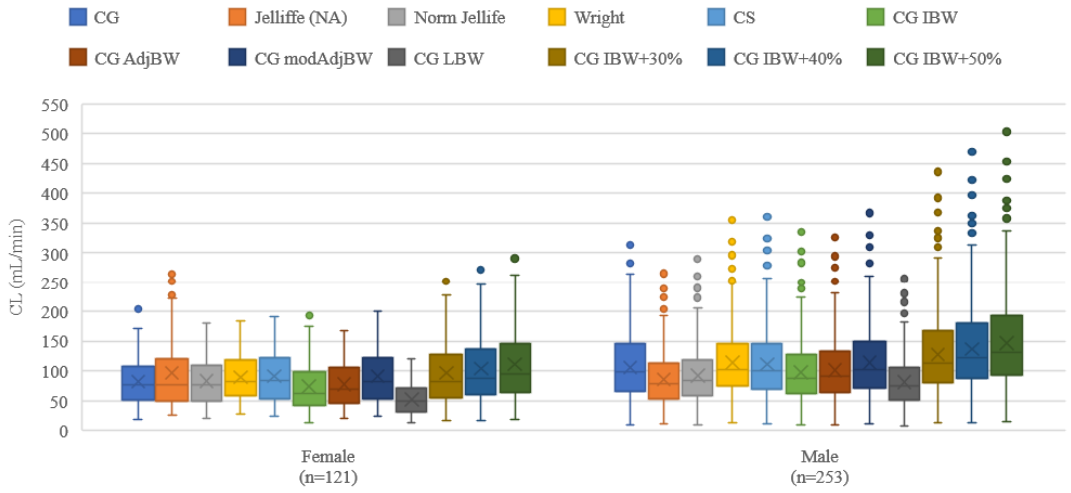

Figure 4. Distribution of clearance estimations according to biological sex.

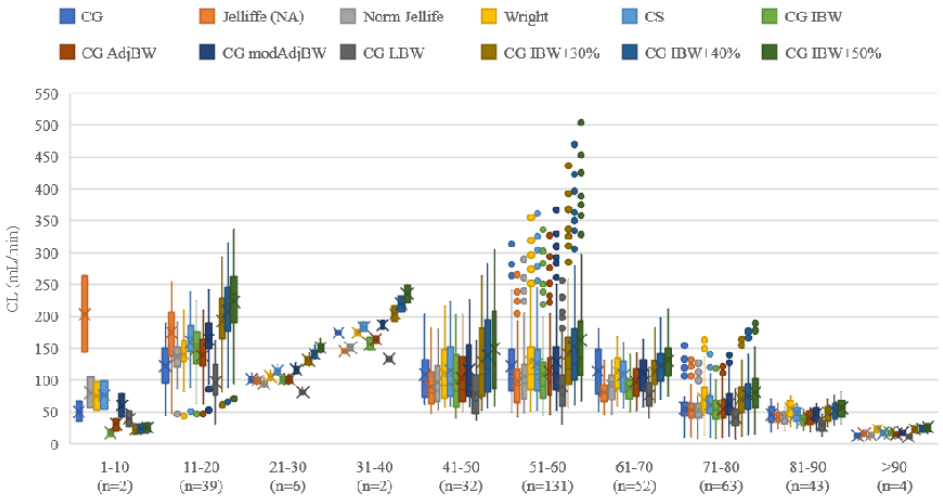

Figure 5. Distribution of clearance estimations according to age.

Regarding biological sex, the data from male individuals on populations analyzed in this study resulted in higher estimated CL_{Cr} (Figure 4), in agreement with expected.

Figure 5 presents the distribution of results considering the age group of the patients. In the age group 1–10, there are only 2 data entries, corresponding to the same patient, an underweight 7-year-old female (TBW = 15.5 kg, H = 108 cm). Since the nonadjusted Jelliffe equation only takes into consideration age and does not include any body composition parameters, this data significantly

deviates from the remaining estimations. The estimated CL_{Cr} decreased with age. The most considerable variations were observed in patients between 51 and 60 years old and were less perceptible above 80 years old.

Next, each body composition group was stratified for age groups. Results are presented in Figures 6–9. Consistently throughout every BMI group, there was less variability in patients older than 61 years. The estimation using the Cockcroft-Gault equation considering lean body weight (CG LBW) results in lower estimated CL_{Cr}.

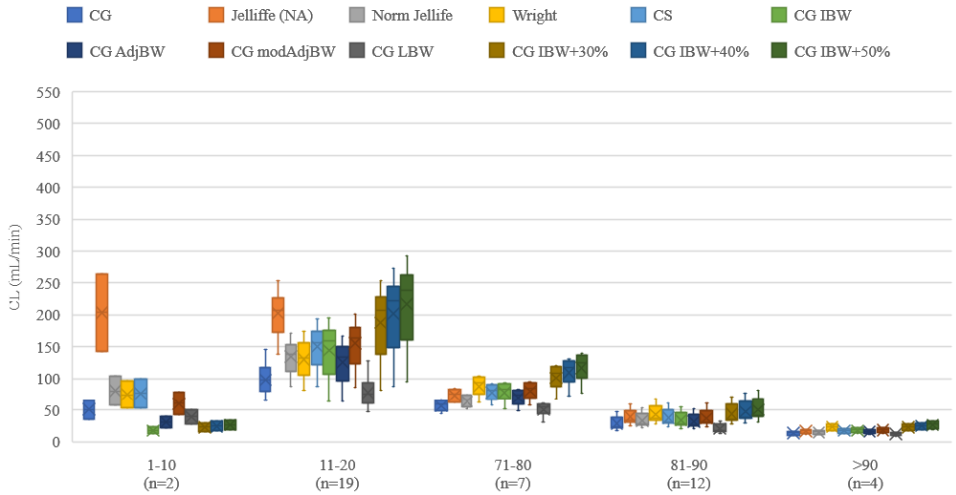

Figure 6. Distribution of clearance estimations according to age for underweight patients.

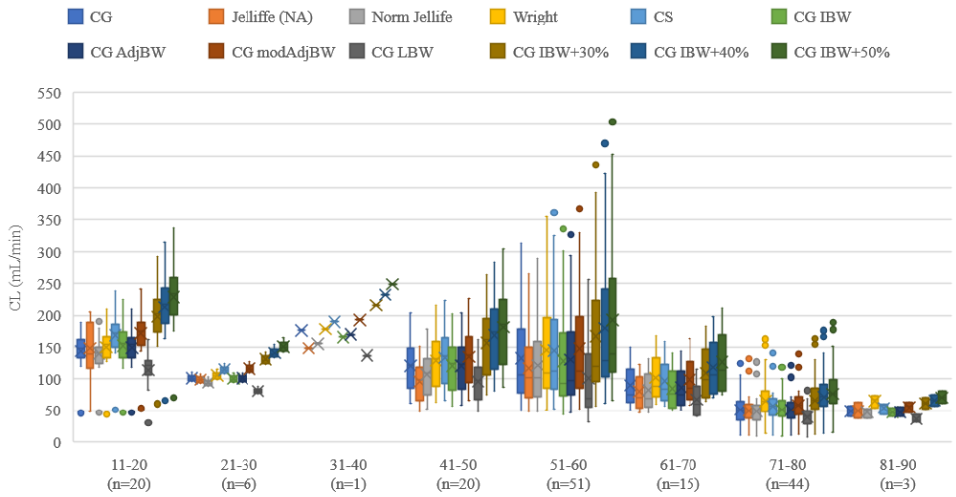

Figure 7. Distribution of clearance estimations according to age for patients with normal BMI.

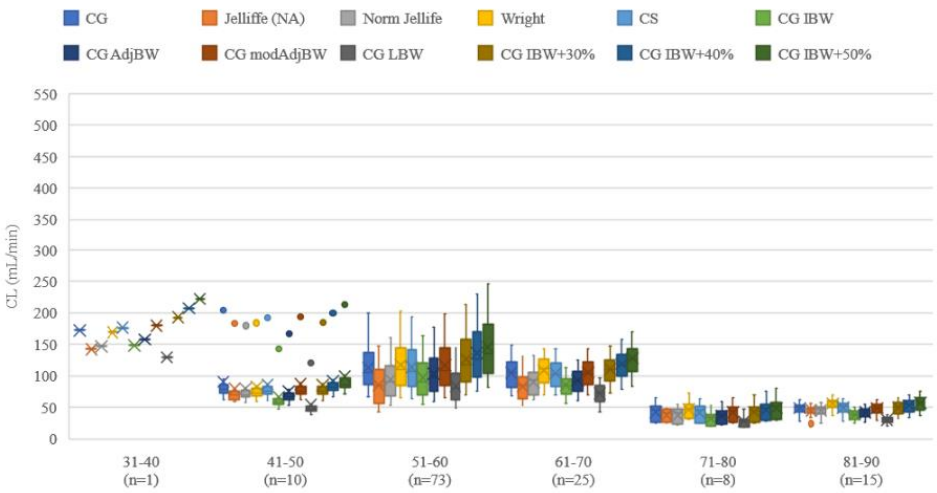

Figure 8. Distribution of clearance estimations according to age for overweight patients.

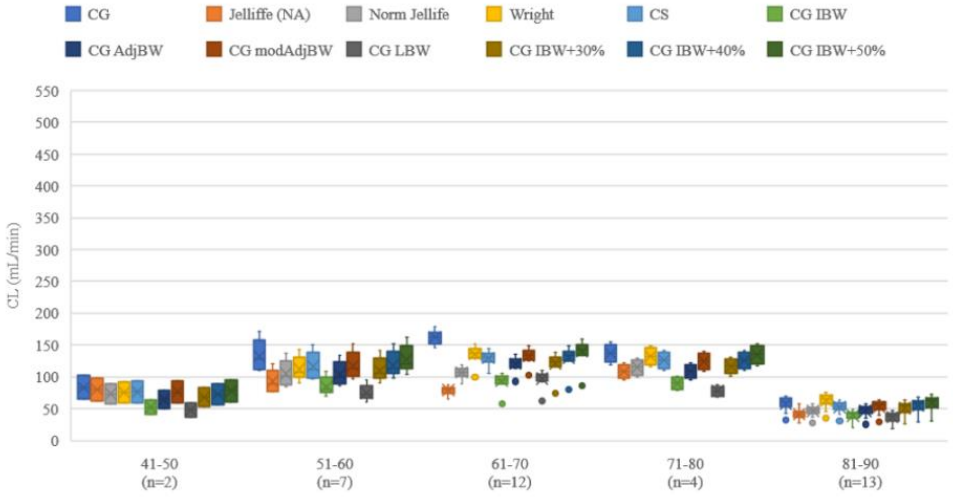

Figure 9. Distribution of clearance estimations according to age for obese patients.

The measured serum creatinine concentration was also analyzed, and this data is presented in Figure 10. Patients with serum creatinine concentration below reference criteria had an ampler range of estimated CLCr.

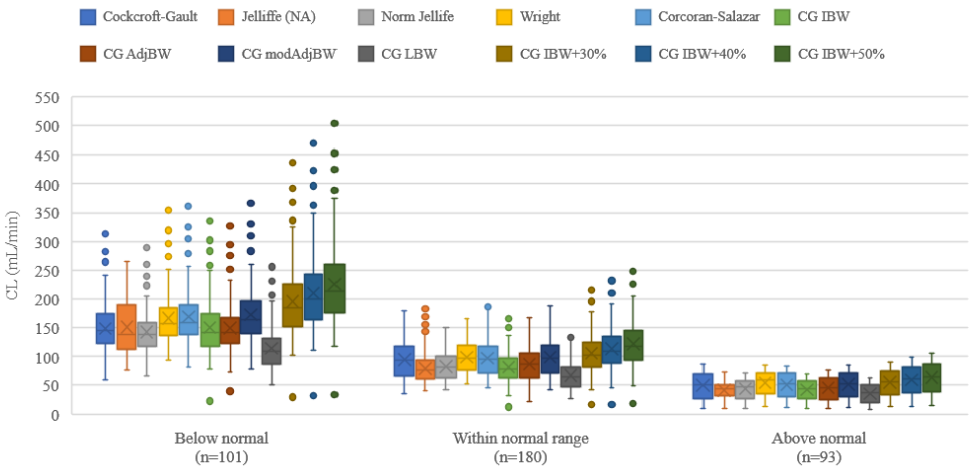

Figure 10. Distribution of clearance estimations according to measured serum creatinine concentration (CHUP reference: normal range of [Cr] is 0.7–1.2 mg/dL for male patients and 0.5–0.9 mg/dL for female patients).

4. Conclusions

Renal function can be a crucial factor to consider when adjusting therapeutic regimens of inpatients (whose kidneys can suffer significant deterioration throughout treatment duration). Since the most accurate indicator GFR is not as easily determined, creatinine serum concentration is more often used to estimate renal clearance, using various equations. As there is no standard estimation method, estimated creatinine clearance can be significantly disparate, which will influence therapeutic regimens adjustment.

Analyzing the influence of the different clearance estimation equations, the estimation using the Cockcroft-Gault equation considering lean body weight (CG LBW) produced lower estimated CL_{Cr} in almost all groups. Since creatinine is a product of natural muscle breakdown, this observation can indicate an overestimation of CL_{Cr} when using other components of body composition.

With this retrospective study, the differences between creatinine clearance estimation equations and the impact of the variables entered in these calculations were highlighted. These results supplement the knowledge about creatinine clearance estimation and provide insight on the disparities of the available estimation methods, that can help clinicians make a better informed and tailored decision when choosing how to evaluate a patient's renal function.

Acknowledgments

This work was financed by FEDER–Fundo Europeu de Desenvolvimento Regional through the COMPETE 2020–Operational Programme for Competitiveness and Internationalization (POCI), Portugal 2020, and by Portuguese funds through FCT–Fundação para a Ciência e a Tecnologia, in a framework of CINTESIS, R&D Unit (reference UIDB/4255/2020). N.V. also thanks support from FCT and FEDER (European Union), award number IF/00092/2014/CP1255/CT0004. RL thanks FCT for

support of UID/QUI/50006/2019 (LAQV-REQUIMTE). AF thanks FCT for a doctoral fellowship (PD/BD/135120/2017). The authors also thank *Serviço de Química Clínica* from CHUP for technical support in obtaining clinical data. The contents of this article are solely the responsibility of the authors and do not necessarily represent the official view of the FCT.

Conflict of interest

On behalf of all authors, the corresponding author states that there is no conflict of interest.

References

1. *National Kidney Foundation*, *Estimated Glomerular Filtration Rate (eGFR)*, Available from: https: //www.kidney.org/atoz/content/gfr.
2. A. S. Levey, J. Coresh, K. Bolton, B. Culleton, K. S. Harvey, T. A. Ikizler, et al., K/DOQI clinical practice guidelines for chronic kidney disease: evaluation, classification, and stratification, *Am. J. Kidney Dis.* **39** (2002), S1-266.
3. L. A. Stevens, J. Coresh, T. Greene, A. S. Levey, Assessing kidney function-measured and estimated glomerular filtration rate, *New Engl. J. Med.*, **354** (2006), 2473–2483.
4. *Amikacin*, *DrugBank*, 2021. Available from: https://go.drugbank.com/drugs/DB00479.
5. A. Aminimanizani, P. Beringer, J. Kang, L. Tsang, R. W. Jelliffe, B. J. Shapiro, Distribution and elimination of tobramycin administered in single or multiple daily doses in adult patients with cystic fibrosis, *J. Antimicrob. Chemother.*, **50** (2002), 553–559.
6. *Gentamicin*, *DrugBank*, 2021. Available from: https://go.drugbank.com/drugs/DB00798.
7. J. Gonçalves-Pereira, A. Martins, P. Póvoa, Pharmacokinetics of gentamicin in critically ill patients: pilot study evaluating the first dose, *Clin. Microbiol. Infect.*, **16** (2010), 1258–1263.
8. Tobramycin, DrugBank, 2021. Available from: https://go.drugbank.com/drugs/DB00684.
9. *Tobramycin for injection*, *Medscape*, 2021. Available from: https://reference.medscape.com/drug/nebcin-injection-tobramycin-342521#10.
10. *Vancomycin*, *DrugBank*, 2021. Available from: https: //go.drugbank.com/drugs/DB00512.
11. D. D. Bois, A formula to estimate the approximate surface area if height and weight be known, *Nutrition*, **5** (1989), 303–313.
12. D. W. Cockcroft, M. H. Gault, Prediction of creatinine clearance from serum creatinine, *Nephron*, **16** (1976), 31–41.
13. R. W. Jelliffe, Creatinine clearance: bedside estimate, *Ann. Intern. Med.*, **79** (1973), 604–605.
14. J. G. Wright, A. V. Boddy, M. Highley, J. Fenwick, A. McGill, A. H. Calvert, Estimation of glomerular filtration rate in cancer patients, *Br. J. Cancer*, **84** (2001), 452–459.
15. D. E. Salazar, G. B. Corcoran, Predicting creatinine clearance and renal drug clearance in obese patients from estimated fat-free body mass, *Am. J. Med.*, **84** (1988), 1053–1060.
16. B. Devine, Gentamicin therapy, *Drug Intell. Clin. Pharm.*, **8** (1974), 650–655.
17. J. Chambers, W. Cleveland, B. Kleiner, P. A. Tukey, *Graphical Methods for Data Analysis*, Monterey, CA: Boston, 1983.
18. M. P. Pai, F. P. Paloucek, The origin of the "ideal" body weight equations, *Ann. Pharmacother.*, **34** (2000), 1066–1069.

19. S. Janmahasatian, S. B. Duffull, S. Ash, L. C. Ward, N. M. Byrne, B. Green, Quantification of lean bodyweight, *Clin. Pharmacokinet.*, **44** (2005), 1051–1065.

AIMS Press

FINAL REMARKS AND FUTURE PERSPECTIVES

FINAL REMARKS AND FUTURE PERSPECTIVES

FINAL REMARKS AND FUTURE PERSPECTIVES

Throughout this PhD project, the importance of pharmacokinetics was highlighted and some of its applications explored. Some of these applications were addressed in this thesis, from basic research, drugs' R&D, to optimization of patients' clinical outcomes in hospital settings, and the advancements towards precision medicine.

Regarding cancer treatment, aiming at the enhancement of therapeutic agents' efficacy and reduction of side effects, a number of strategies were approached in this project. Gemcitabine was the selected drug to the studies developed, which revealed very promising results.

The first approach consisted of conjugating gemcitabine with Cell-Penetrating Peptides (CPPs). A preliminary assessment on the PK disposition of previously developed Gem-CPP conjugates was performed, and the relationship between the penetration ability of CPPs and their physicochemical properties was also analyzed.

Hexapeptides CPP6 were likewise conjugated with gemcitabine. The bioactivity of these conjugates had been determined and, since permeability is a physicochemical property strongly influencing ADMET profile, the transport of these conjugates across a monolayer of Caco-2 cells was examined, an *in vitro* standard for these determinations.

These studies demonstrated these peptides are able to effectively transport gemcitabine into cells, where this antimetabolite can act as a cytotoxic agent, substantiating their potential as drug delivery vehicles.

Given gemcitabine is administered intravenously, an invasive and unpleasant route, an alternative oral route of administration was proposed and evaluated. Some of the studied regimens of oral administration reached higher AUC compared to the IV infusion, supporting this route of administration as a viable alternative to the traditional method.

The combination of gemcitabine, as well as of 5-FU, with repurposed drugs itraconazole, tacrine and verapamil, was evaluated. The results from *in vitro* studies were modeled and analyzed using *in silico* PK models to predict the *in vivo* performance of these combinations. Itraconazole combined with either chemotherapeutic agent was considered the most favorable.

Furthermore, the work from the first part of this project provided the knowledge and experience on the development of PBPK models, later used to analyze clinical data of patients receiving antibiotic therapy and assess the influence of their individual characteristics, as biological sex, age, body weight, and renal function.

Studying different dosing regimens and parameters of interindividual variability, these models confirmed the impact of renal function on the drug disposition and PK profile of antibiotics amikacin, gentamicin, tobramycin, and vancomycin, as well as the considerable influence of body weight. This was particularly significant in the case of glycopeptide vancomycin, where impaired renal function can lead to the accumulation of this antibiotic in plasma that can quickly reach toxic levels.

Future perspectives

Continuing the work developed in this project, these studies can be transferable and applied to other patient populations benefiting from therapeutic drug monitoring and dosing adjustments. To further refine and validate these models, being able to determine plasma concentrations more frequently between drug administrations to confirm PK disposition would be immensely advantageous, along with assessing patients before, throughout and after therapy, ideally in larger study populations.

The investigations achieved in this project provided insights that can contribute to the development of novel and improved therapies for cancer treatment. Additionally, analyzing population data with PBPK models is a precious tool and certainly indispensable in the progress towards a true precision medicine (Figure 11).

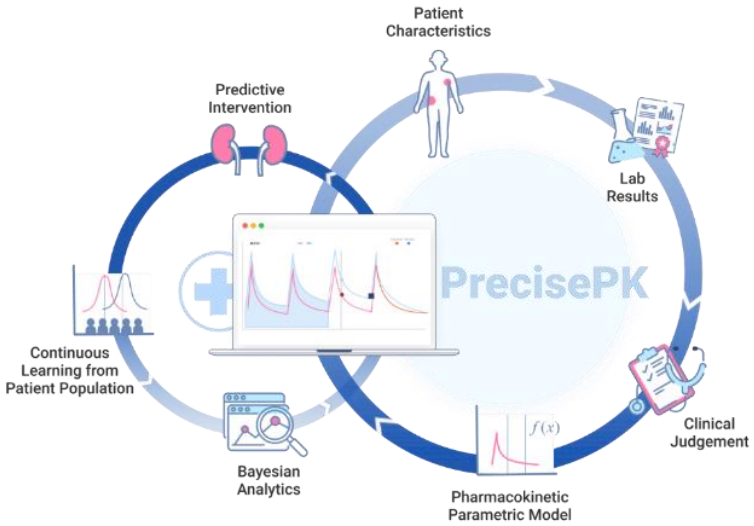

Figure 11: Model-Informed Precision Dosing workflow. Reproduced from [140].

SUPPORTING INFORMATION

SUPPORTING INFORMATION

➢ Amino Acids in the Development of Prodrugs

molecules

MDPI

Review

Amino Acids in the Development of Prodrugs

Nuno Vale [1,2,3,4,*], Abigail Ferreira [1,5], Joana Matos [6], Paula Fresco [1] and Maria João Gouveia [3,4]

1 Laboratory of Pharmacology, Department of Drug Sciences, Faculty of Pharmacy, University of Porto, Rua de Jorge Viterbo Ferreira 228, 4050-313 Porto, Portugal; abigail.ferreira@hotmail.com (A.F.); pfresco@ff.up.pt (P.F.)
2 Institute of Molecular Pathology and Immunology of the University of Porto (IPATIMUP), Rua Júlio Amaral de Carvalho, 45, 4200-135 Porto, Portugal
3 Instituto de Investigação e Inovação em Saúde (i3S), University of Porto, Rua Alfredo Allen, 208, 4200-135 Porto, Portugal; mariajoaogouveia@gmail.com
4 Department of Molecular Pathology and Immunology, Institute of Biomedical Sciences Abel Salazar (ICBAS), University of Porto, Rua de Jorge Viterbo Ferreira 228, 4050-313 Porto, Portugal
5 LAQV&REQUIMTE, Laboratory of Applied Chemistry, Department of Chemical Sciences, Faculty of Pharmacy, University of Porto, Rua de Jorge Viterbo Ferreira 228, 4050-313 Porto, Portugal
6 SpiroChem AG, Rosental Area, WRO-1074-3, Mattenstrasse 24, 4058 Basel, Switzerland; joana.c.m.matos@gmail.com
* Correspondence: nuno.vale@ff.up.pt; Tel.: +351-220428500

Received: 23 July 2018; Accepted: 6 September 2018; Published: 11 September 2018

check for updates

Abstract: Although drugs currently used for the various types of diseases (e.g., antiparasitic, antiviral, antibacterial, etc.) are effective, they present several undesirable pharmacological and pharmaceutical properties. Most of the drugs have low bioavailability, lack of sensitivity, and do not target only the damaged cells, thus also affecting normal cells. Moreover, there is the risk of developing resistance against drugs upon chronic treatment. Consequently, their potential clinical applications might be limited and therefore, it is mandatory to find strategies that improve those properties of therapeutic agents. The development of prodrugs using amino acids as moieties has resulted in improvements in several properties, namely increased bioavailability, decreased toxicity of the parent drug, accurate delivery to target tissues or organs, and prevention of fast metabolism. Herein, we provide an overview of models currently in use of prodrug design with amino acids. Furthermore, we review the challenges related to the permeability of poorly absorbed drugs and transport and deliver on target organs.

Keywords: amino acid transport; drug delivery; prodrug design; stability studies; in vitro and in vivo assays

1. The Prodrug Concept: An Overview

The term prodrug was introduced in the 1950s to describe a covalent link between a drug and a chemical moiety. The term is also used to characterize some salt forms of the active drug molecule [1]. Many drugs see medicinal use denied due to poor physical, pharmacokinetic or pharmacodynamic properties. Therefore, the use of different strategies to improve solubility, stability, permeability and targeting problems in drug discovery and development is crucial. Since prodrugs might alter the tissue distribution, efficacy and toxicity of the parent drug, the implementation of a prodrug approach in the early stages of drug development is a growing trend [2–5]. Prodrugs are bio-reversible derivatives of drug molecules that undergo enzymatic and/or chemical transformation to release the parent drug [3]. There are several pro-moieties that can be used in prodrug design, and its selection is a crucial step. The goal is achieving a chemically stable prodrug that after bioconversion does not generate toxic

metabolites [2]. Ideally, the prodrug should be converted into the parent drug as soon as the goal is achieved, followed by rapid elimination of the released derivatizing group (Figure 1).

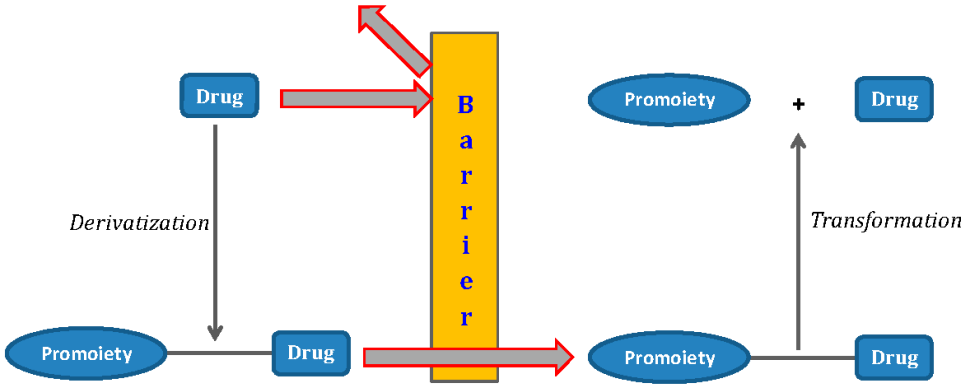

Figure 1. Illustration of prodrug concept. (Adapted from Ref. [5]).

2. Amino Acids and Routes of Transport

Drug-delivery is a cascade of molecular migration processes, in which the active principle is exposed to several biological media with various hydrophilic and lipophilic characters. Membrane penetration is controlled by several physicochemical parameters, with the most promising ones being species-specific basicity and lipophilicity. The latter property has a great importance in several scientific areas such as pharmacy, bio- and medicinal chemistry since it expresses the affinity of the molecule for a lipophilic environment [6].

One of factors that determine drug bioavailability is related to transport across biological membranes, therefore drug permeability is a crucial parameter for its effectiveness and is directly related to their physicochemical characteristics [7,8]. Water solubility and lipophilicity strongly influence drug interactions with components of the absorptive surface within the gastrointestinal tract, giving rise to differential preferences in terms of transport pathways. In many cases, drugs of poor aqueous solubility exhibit a high degree of lipophilicity, which could be demonstrated by solubilization of lipophilic compounds with monoglycerides and free fatty acids, and liposomes [9,10].

One strategy for increasing water-solubility is the use of amino acids as moieties. Amino acids are basic constituents of a cell structure but require specialized transport systems to cross the plasma membrane. Several of these transport systems have been identified and classified based on their substrate affinity, dependence on sodium ions, energy and pH [11]. Amino acids are pharmacological agents with low toxicity which makes them attractive carriers for development of prodrugs of poorly absorbed therapeutic agents. In addition, an amino acid promoiety improves the water solubility of the prodrug [12]. The importance of these transporters in pharmacokinetics has been recognized through several studies that report an improved bioavailability of amino acid linked compounds [11].

L-type amino acid transporters 1 (LAT1) and 2 (LAT2) are responsible for carrying large neutral amino acids from extracellular fluids into the cells, and hence their involvement in pharmacokinetics [13]. LAT1 is a transmembrane protein abundantly expressed at the blood-brain barrier (BBB), where it ensures the transport of hydrophobic acids from the blood to the brain. The natural substrates of LAT1 are large neutral amino acids such as *L*-leucine, *L*-tryptophan, and *L*-phenylalanine. These compounds have excellent affinity for the LAT1 transporter protein and thus rapidly pass through the BBB. Therefore, LAT1 is an interesting target for drug delivery to the central nervous system (CNS) [14]. Also, solubility and permeability interactions and their impact on intestinal drug absorption are most prominently described by the Biopharmaceutics Classification System (BCS) [15].

Previously, the transport systems for peptides, amino acids and nucleoside/nucleobase on the corneal epithelium was reported [16]. These transport mechanisms can be used for targeting drug delivery [2,17,18]. Amino acid prodrug strategies utilizing endogenous nutrient transporters that are over expressed in certain organs have become an attractive approach for improved and targeted drug delivery [4]. Among nutrient transporters, those transporting amino acids are preferred for drug delivery due to their ubiquitous nature and overlapping substrate specificity [17,18]. They are known to transport not only naturally occurring amino acids but also amino acid related compounds, making them suitable delivery targets for amino acid-based drugs and prodrugs [17]. Moreover, amino acids are building blocks for proteins and are generally regarded as safe [4,19].

The intention of this work is to review and summarize the use of amino acids in drug design in order to improve drug solubility and delivery.

3. Drugs and Diseases

3.1. Anti-Viral Drugs

3.1.1. Herpes Viruses Infections (*Herpes Simplex* or *Zoster* and *Cytomegalovirus*)

The anti-viral drug acyclovir (ACV **1**, Figure 2) has poor oral bioavailability due to the lack of a transport system on the intestinal tract capable of recognizing this drug as a substrate [20]. The attempt to improve this characteristic resulted in the preparation of several prodrugs of **1**. Different approaches have been implemented to achieve this goal [21]. Colla et al. and Maudgal et al. used amino acid moieties to prepare prodrugs of **1** which were potentially useful in the preparation of eye drop formulations [22,23]. A similar approach was used by Beauchamp et al. in order to improve oral administration. With a different purpose, Shao et al. and Yang et al. reported the synthesis, nasal and ocular absorption, and metabolism of aliphatic acid ester prodrugs of **1** [24]. Recently, Gao and Mitra have focused their work on the improvement of membrane transport of prodrugs of **1**. Their studies resulted in the preparation of a series of N-acyl-ACV, α, β and γ-amino acid esters and dicarboxylic acid esters of **1** [21,25].

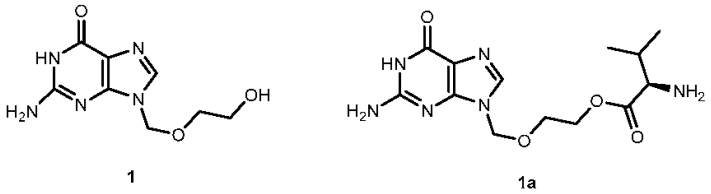

Figure 2. Chemical structures of ACV (**1**) and the amino acid prodrug valacyclovir (**1a**).

Valacyclovir (**1a**, Figure 2), an *L*-valyl ester of **1** is rapidly converted to the parent drug after oral administration, increasing the bioavailability of the parent drug by 3- to 5-fold [20,26–28]. This improvement results from the transport of **1a** by the peptide transport PEPT1, abundantly expressed in the intestine [20,29–33]. It is important to notice that a peptide bond is not required for recognition of a prodrug by the peptide transporter [31]. The study performed by Katragadda and co-workers with amino acid derivatives of **1** demonstrated an upgrade in the ocular bioavailability of **1** of approximately 2-fold after topical administration of *L*-serine and *L*-valyl esters of **1** [17]. Drug delivery to different eye structures (retina, choroid, vitreous humor and sclera) is a challenging task for the pharmaceutical industry. Another example is the drug ganciclovir (GCV; **2**, Figure 3) used in the treatment of cytomegalovirus (CMV) retinitis, that presents poor aqueous solubility [34]. Consequently, in these infections, frequent administration of the drug or surgery are necessary, which turns so crucial the development of strategies to enhance permeation of **2** into corneal or retinal tissues.

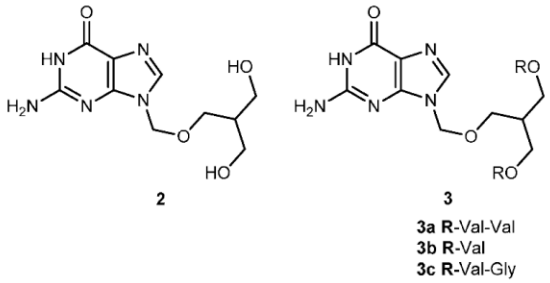

Figure 3. Ganciclovir and its diester prodrugs.

Peptide transporters (PEPT1 and PEPT2) are widely used as targets in drug design. In fact, *L*-valine ester prodrugs of **2** and **1** presented an intestinal absorbance enhancement as a result of PEPT1 mediated transport [34]. This peptide transporter is expressed in the corneal epithelium, and dipeptide derivatives of **1** have shown a better permeation in this tissue [29,34]. The physicochemical properties of di-ester prodrugs of **2** (Figure 3) were studied by Patel's research group, and most of the tested compounds showed good affinity to PEPT1. Moreover, solubility and lipophilicity properties make the derivatives **3a**, **3b** and **3c** good candidates for drug delivery [34]. The peptide approach allowed an improvement in the prodrugs lipophilicity without compromising their solubility. In fact, **3b** showed a 42 times higher solubility compared to the parent drug. It is also interesting that the di-ester prodrugs did not show a greater selectivity to the virus but were found to be more potent. This fact may be explained by the higher binding affinity of these derivatives for the peptide transporters [34].

The problems associated with antiviral drugs are of great concern. The large number of herpetic virus widespread in nature is responsible for many viral diseases affecting humans. Progress has been made on the improvement of **1**-based therapies. From a clinical point of view, this research has, so far, culminated in the *L*-valyl ester prodrug **1a**. At present, there are few studies related to dipeptide derivatives of **1**. Santos et al. evaluated the chemical stability, solubility, and antiviral activity of dipeptide derivatives of **1**. The principal use of the dipeptide-based prodrug approach occurs in drugs with an alcohol functional group [35]. However, it is important to understand how this approach works for other drugs with different functional groups. Santos et al. also studied the effect of functional groups, as the thiol and amine groups, on the chemical and enzymatic reactivity of the resulting prodrug [35]. The Phe-Gly dipeptide derivatives of **1**, **1b**, primaquine (**4**), paracetamol (**5**) and azidothymidine (**6**) and captopril methyl ester (**7**) were evaluated (Figure 4).

Kinetics studies at pH 7.4, showed that the derivative **1b** is degraded via two parallel pathways (Scheme 1). The major degradation pathway, (a), results in the formation of a diketopiperazine, which is consistent with the intramolecular cyclization expected for dipeptide alkyl and aryl esters [36].

However, high-performance liquid chromatography (HPLC) analysis showed that the dipeptide may also degrade through direct ester hydrolysis-pathway (b). Moreover, it has been established that the drug's leaving group influences the ratio between the two different pathways. In fact, degradation of derivatives **5** and **7** resulted in the quantitative formation of the diketopiperazine and parent drug. On the other hand, derivative **6** indicates that direct hydrolysis was also operating on the drug release pathway, suggesting that less bulky alcohols are more susceptible to ester hydrolysis [35,37]. When studying their degradation in human plasma, all derivatives released the correspondent parent drug and the dipeptide (Phe-Gly) moiety with the exception of derivative **4** which degradation resulted in the formation of the correspondent amino acid amide (Gly-PQ) as a reaction intermediate. Both results are consistent with the enzymatic degradation of dipeptide prodrugs via stepwise removal of amino acid residues and direct cleavage of the dipeptide carrier. Derivatives degradation has been shown to be influenced by the nature of the drug's leaving group and the rate at which the drug is released. This implies that this approach is chemical and enzymatically more adequate for drugs containing alcohol or amine functional groups [35].

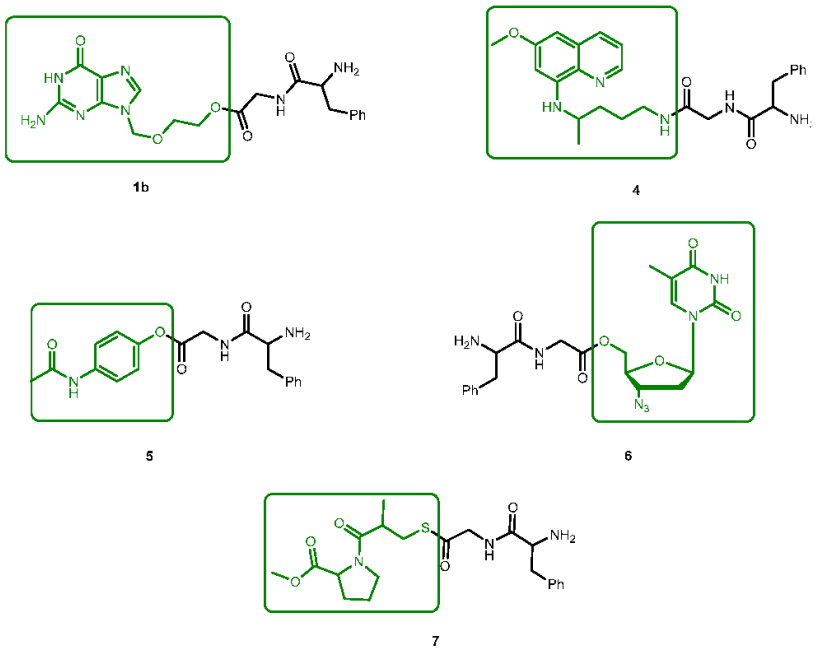

Figure 4. The Phe-Gly derivatives of **1a**, primaquine (**4**), paracetamol (**5**), azidothymidine (**6**) and captopril methyl ester (**7**). The parent drugs are highlighted in green.

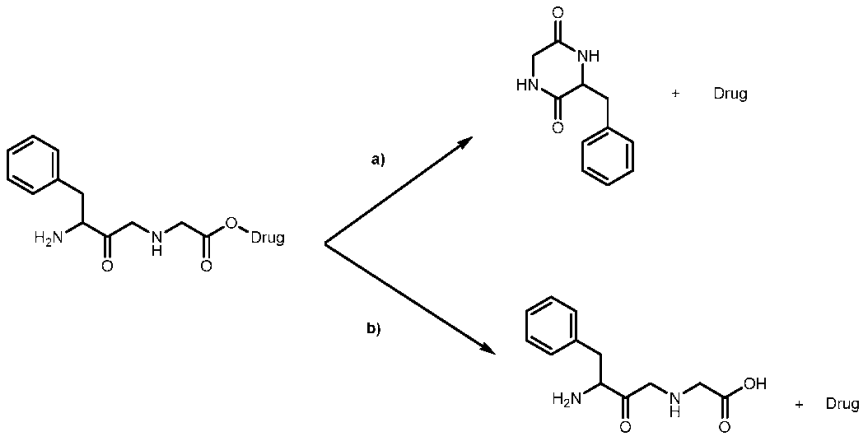

Scheme 1. General degradation pathways of dipeptide prodrugs in human plasma [35].

In general, the synthesis of prodrugs to improve bioavailability is related to the affinity for peptide transporters. Although high affinity does not necessarily imply the transport of the drug, it is essential to bioavailability improvement. Therefore, both bioavailability and pharmacokinetic studies are needed to determine a lead prodrug. Accordingly, Thomsen et al. compared the bioavailability in rats and the transport in CaCo-2 cells of prodrugs of **1** and showed that the high affinity of Glu-ACV-Sar prodrug for PEPT1 in CaCo-2 cells was not synonymous of prodrug translocation by the peptide transporter [38]. On their experiments, intracellular accumulation of Glu-ACV-Sar was studied in comparison with **1** and **1a**, as a measurement of **1** in cell extracts, and they observed that neither the prodrug nor **1** was detected when applying Glu-ACV-SAR, indicating that Gly-ACV-Sar is not translocated by PEPT1 [38]. The high affinity of the prodrug for the peptide transporter did not

result in a higher bioavailability of the parent drug. The opposite was even observed for the prodrug **1a**. These studies are very important in case of drugs used in immunocompromised cancer patients since the side effects of chemotherapy can influence drug absorption and so drugs/prodrugs with more reliable absorption are of particular value [39]. Different studies indicated that bioavailability of **1** is equal after administration of **1a** in immunocompromised cancer patients and in healthier volunteers [39,40].

Han et al. went further on the study of amino acid prodrugs. They studied the permeability and hydrolysis of amino acid ester prodrugs in CaCo-2/hPEPT1 cells, not only for derivatives of **1** but also to amino acid derivatives of azidothymidine [31,33]. Again, the *L*-valyl ester of azidothymidine and **1** were the derivatives with higher membrane permeabilities. An interesting fact is that the *L*-configuration of the amino acid is more suitable for the prodrug strategy. Comparing *L*- and *D*-valyl ester derivatives of **1**, the *L*-valyl presents the higher permeability and faster conversion relative to the parent drug [33,34].

Another issue was approached by the Hilfinger research group: they used the prodrug strategy as a protection from metabolic conversion using vidarabine (**8**, Figure 5) as a drug and different *D*- and *L*-amino acid esters were synthesized and evaluated (Figure 5) [41]. Data obtained demonstrate that substitution of 5′-OH group results in the enhanced uptake of prodrugs and parent drug, and protection of the prodrug from deamination before hydrolysis to **8**.

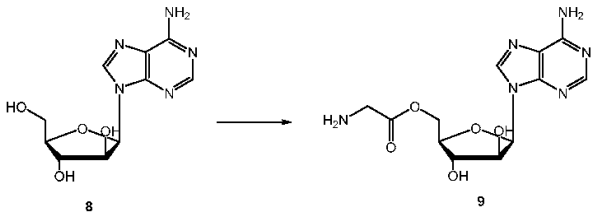

Figure 5. Chemical structures of **8** and a synthesized amino acid ester.

Penciclovir (9-(4-hydroxy-3-hydroxymethylbut-1-yl)guanine, **10**, Figure 6) is a potent and highly selective inhibitor of the replication of herpes virus, including herpes simplex virus type 1 and 2 (HSV-1 and HSV-2), varicella-zoster virus (VZV) and *Epstein-Barr* virus (EBV) both in cell cultures and in animals [42]. The main advantage of **10** over **1** is that its antiviral activity in cell culture is more persistent. However, like other acyclic nucleoside analogs (described above), **10** has poor oral bioavailability [43]. In order to overcome this, Kim et al. synthesized the *O*-acyl-*O*-amino acid esters as potential prodrugs of penciclovir. The two naturally occurring branched chain amino acyl groups, *L*-valyl and *L*-isoleucyl, were selected for the protection of one of the two hydroxyl groups. As previously shown they have an optimal combination of the side chain length and degree of branching for the oral bioavailability and chemical stability in the amino acid ester prodrug acyclovir [44,45]. All amino acid ester prodrugs **11a**–**d**, **12a**–**b** (Figure 6) were highly soluble in water, showing a remarkable increase in aqueous solubility, compared with the parent drug.

The in vitro antiviral activity of the prodrugs synthesized against HSV-1 in Vero cells were compared with thereof **10**. Compounds **11a**, **11f**, and **11d** showed no significant antiviral activity at a concentration of 100 μM. Although compounds **11c**, **11g**, **12a**, **12b** were active against HSV-1, their antiviral activity was approximately 3- to 5-fold lower than **10**. Kim et al. assessed the bioavailability of prodrugs of **10** after a single oral administration through determination of the total amount of **10** recovered in the urine over 48 h. Of the prodrugs tested, **11a** present a bioavailability approximately 4-fold higher comparatively to that of **10** [45]. The introduction of amino acid pro-moieties not only increase antiviral activity, but also improve prodrugs bioavailability, compared to the parent drug.

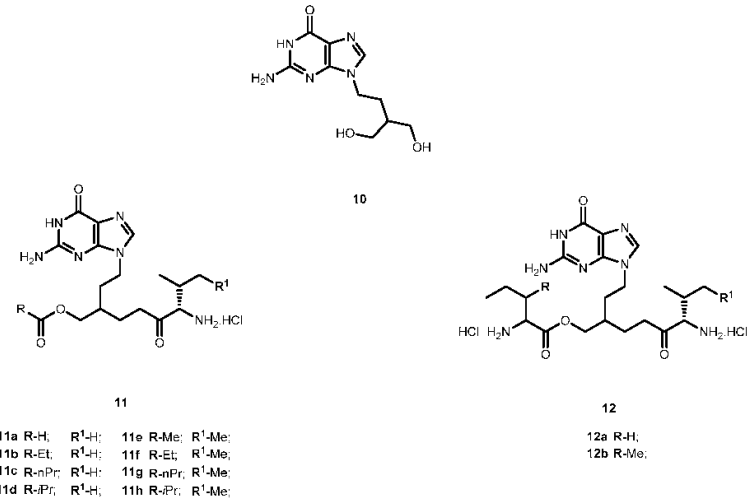

Figure 6. Structures of penciclovir (**10**) and its amino acid ester prodrugs **11** and **12**.

The antiviral agent 2-bromo-5,6-dichloro-1-(β-D-ribofuranosyl)benzimidazole (**13**, Figure 7) is a member of a novel class of benzimidazole ribonucleosides that are potent inhibitors of human cytomegalovirus (HCMV) replication, with lower cellular toxicity at concentrations inhibiting viral growth [46]. The antiviral mechanism of action of **13** is unique and involves inhibition of viral DNA processing virus assembly [47]. Like certain other nucleoside agents, **13** exhibits modest oral bioavailability due to extensive first pass effect, possibly related to its glycoside bond [48]. Song et al. synthesized amino acid ester prodrugs of **13** (**14a**–**l** and **15**) in order to (a) investigate their affinity for and transport by hPEPT1 and (b) determine if the promoiety affords stabilization of glycoside bond. For the synthesis of novel prodrugs, the amino acids were used as pro-moieties including aliphatic amino acids and its analogs, secondary amino acids and polar amino acids (Figure 7) [48].

The prodrugs of **13** were evaluated for their affinity for hPEPT1 by evaluation of their ability to inhibit [^{3}H]glycylsarcosine ([^{3}H]Gly-Sar) uptake in HeLa cells overexpressing hPEPT1 transporter. With exception for **14b**, **14k**, **14l** and **14j**, all prodrugs exhibited significantly higher affinity for hPEPT1 than the parent drug. Additionally, these authors also observed that *L*-amino acids exhibited 1.3- to 2-fold higher affinity for hPEPT1 than their counterparts [48]. It was hypothesized that amino acid ester prodrugs can enhance both in vitro potency and systemic exposure of **13** through evasion of its metabolizing enzymes. To test this hypothesis, the authors tested eight different amino acid prodrugs of **13** (**14a**, **14b**, **14c**, **14i**, **14j**, **14k**, **14l** and **14m**) for *N*-glycosidic bond stability, ester bond stability, Caco-2 cell uptake, antiviral activity in HCMV-infected cell system and cytotoxicity [49]. The prodrugs were resistant to metabolism by metabolizing enzymes, and ester bond cleavage was rate-limiting in the metabolic formation of the prodrug.

Although **13** was metabolized by the DNA repair enzymes hOOG1 and mMPG, their amino acid ester prodrugs were not a substrate of these enzymes, which suggest that prodrugs of **13** may evade metabolizing enzymes encountered in first pass organs and other tissues. Thus, metabolism of **13** could be controlled by the selection of the promoiety. The observation that high ester bond stability conferred greater *N*-glycosidic bond stability to prodrugs suggested that prodrug ester bond cleavage must take place before *N*-glycosidic bond cleavage occurs. From all prodrugs tested, **14i** was 3-fold more selective than the parent drug for inhibition of HCMV replication.

Due to its potency, selective antiviral activity, stability profile and greater half-life (5-fold than **13**), **14i** was considered an excellent candidate for in vivo assessment and pharmacokinetic comparison with the parent drug. The ability to evade of metabolizing enzymes in vitro of the amino acid ester prodrug of **13**, might provide a modular approach for translating this in vitro stability into enhanced

in vivo delivery of **13** [49]. Unfortunately, until present, there are no in vivo studies that corroborate this hypothesis. Cidofovir (**16**, Figure 8) is a broad-spectrum antiviral agent used to treat Acquired Immunodeficiency Syndrome (AIDS)-relative CMV retinitis, and a promising drug active against variola and other orthopoxviruses. However, its low oral bioavailability led to the development of novel analogs in order to improve their transport properties [50]. MacKenna et al. used a prodrug strategy targeting the peptide transporter-1 (hPEPT1) using cyclic cidofovir (**17**, Figure 8), which is a prodrug of **16**. After conversion of **17** in cells by cyclic AMP phosphodiesterase, their products were used to prepare dipeptides derivatives. The results obtained for derivatives of **17** were compared with those previously obtained for dipeptide derivatives of **16**. The in vitro transport evaluation of the **18a**–**c** showed an enhancement in permeability compared to **16** and **17**. Therefore, the derivatives of the valine amino acid were the best of the tested prodrugs [50] suggesting that this amino acid improves affinity to hPEPT1.

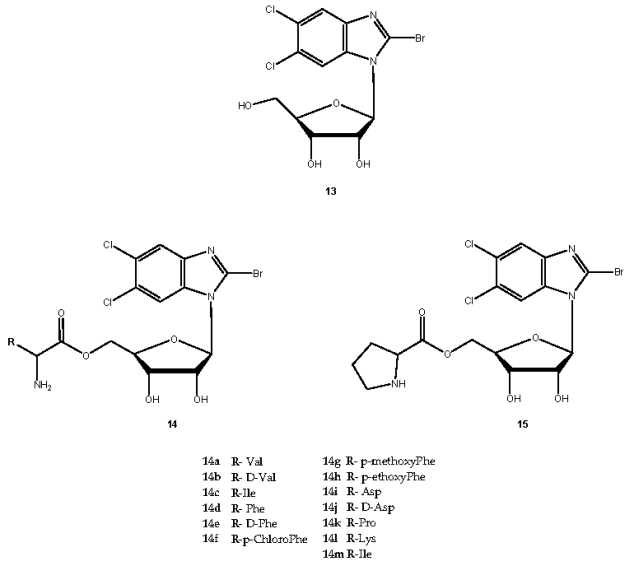

Figure 7. Structures of novel amino acid ester prodrug of **13**.

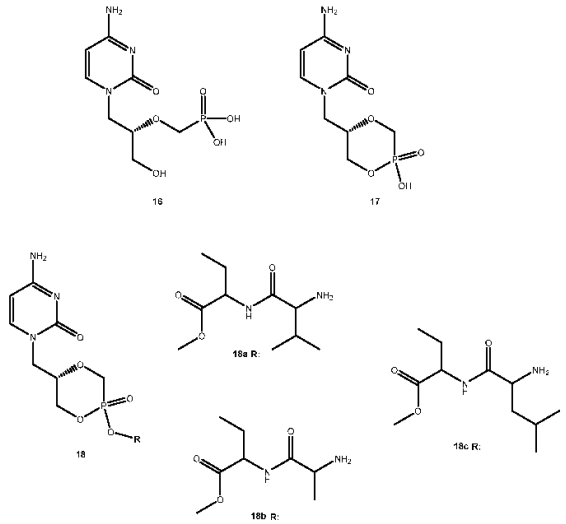

Figure 8. Structures of cidofovir (**16**), ciclocidofovir (**17**) and its dipeptide derivatives **18a**–**c**.

3.1.2. Human Immunodeficiency Virus (HIV)

Nucleoside analogs continue to play an important role as antiviral agents [51]. Nonetheless, the evaluation of several nucleoside analogues as antiretroviral chemotherapeutic agents has revealed potential drug delivery problems related to its rapid metabolism and low availability [52].

Zidovudine (AZT, 3′-azido-3′-deoxythymidide, **19**, Figure 9) was the first 2′-3′-dideoxy-nucleoside (ddN) approved by US Food and Drug Administration (FDA) for treatment of patients suffering from AIDS [53,54]. The mechanism of action of **19** involves its conversion into the corresponding 5′-*O*-triphosphate, which inhibits the replication of the virus by competitive inhibition of the viral reverse transcriptase (RT) and by incorporation and subsequent chain termination of the growing viral strand [55]. Administration of **19** is frequently associated with a significant dose-dependent toxicity, additionally to its short half-time in human plasma which requires frequent administration to maintain therapeutic drug concentrations [56,57]. Efforts have continuously been made to improve some therapeutic characteristics of **19**, most of them focused on prodrug design. Turk et al. synthesized six novel amino acid ester prodrugs of **19** (**20a**–**f** and **21**, Figure 9) using 5′-*O*-ester substitution strategies and evaluated their anti-HIV activity and cytotoxicity on different cell cultures [58].

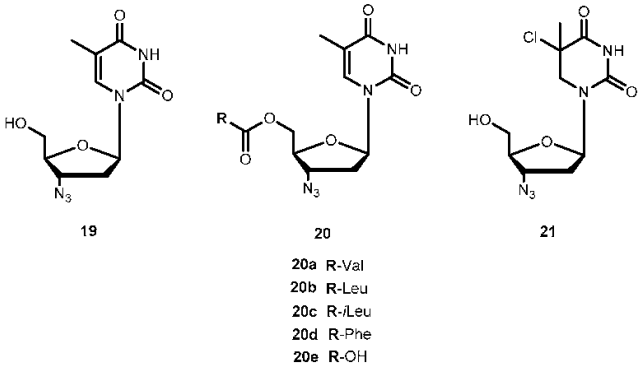

Figure 9. Chemical structures of **19** and its amino acid ester prodrug.

Cytotoxicity and inhibition assays were performed in two different cell types: peripheral blood mononuclear cells (PBMCs) and MT2. During evaluation of cell viability, the compounds also showed a dose-dependent cytotoxicity. Although parameters obtained when using different methodologies cannot be directly compared, their correlation was significant. In one or both cell cultures used, all the prodrugs synthesized have a similar or higher selectivity index than **19** itself, with the exception of **20f** which showed no anti-HIV activity and **20d** that showed a diminished capacity to inhibit HIV replication. These facts could be directly related to the high acidity of their amino acids or higher volume. However, neither acidity level nor volume explains the activity variation showed by the rest of the compounds. Authors hypothesized that it could be due to different transport mechanisms depending either on the amino acids involved (for special transport) or lipophilicity of the substituent that might be implicated in each case. **20a** and **20c** demonstrated an improved ability to inhibit HIV replication on both cell types studied. Nonetheless, using amino acids to design **19** derivatives result in increased activity of parent drug [58]. Santos et al. also designed new analogues of **19** using 5′-*O*-ester substitution, however, instead of single amino acid, they used dipeptides (**22a**–**h**, Figure 10) to target the human intestinal oligopeptide transporter hPEPT1 and evaluated their stability at pH 7.4 in buffer and human plasma, cytotoxicity and retroviral activity [59].

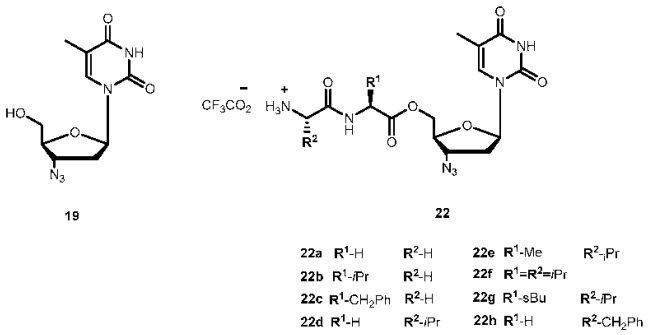

Figure 10. Structure of **19** and its dipeptide prodrugs **22a**–**h.**

The dipeptide esters of **19** undergo cyclization in buffer (pH 7.4) to release the parent drug at a rate that depends on the size of the chains of the peptide carrier. Santos et al. observed that the prodrugs were considerably more stable if the bulky α-branched amino acids (e.g., Ile and Val), were present, particularly, as C-terminal residues. In fact, substrate half-lives in plasma were remarkably higher in the presence of hydrophobic α-branched amino acids. In fact, esters were also good substrates for hPEPT1 in vitro, with Val-Gly-AZT and Val-Ala-AZT presenting the highest affinity to the transporter. They also showed that incubation in human plasma revealed that most of the dipeptide esters of **19** release the parent drug through two aminopeptidases-mediated pathways: (1) stepwise cleavage of each amino acid and (2) direct cleavage of the dipeptide drug ester bond (Scheme 2) [59].

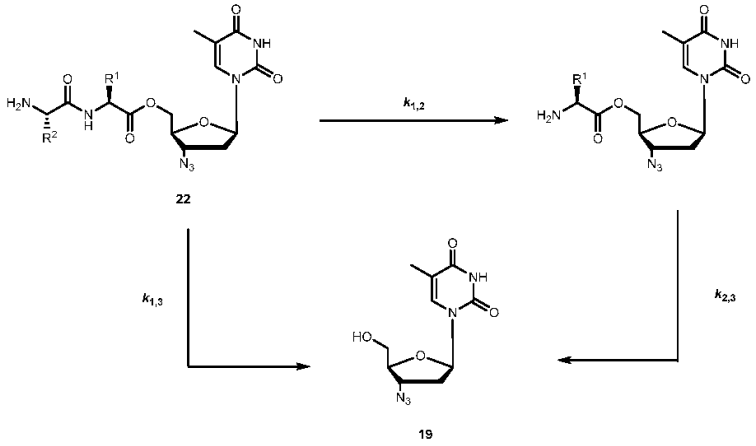

Scheme 2. Pathways observed for releasing of **19** by dipeptide esters **22** in human plasma (reproduced from [59]).

The selectivity index of the prodrugs was 2- to 3-fold higher than that of **19** for all compounds analyzed, which indicates that these are potential dipeptide-based carriers for development of effective antiviral drug-delivery system [59].

Using a similar design strategy, Zhang et al. developed a focused dipeptide conjugated of **19** libraries and screened in a PEPT1 overexpressing cell model in order to assess their abilities to compete with the known ligand cephalexin [60]. The 61 dipeptide conjugates of **19** synthesized consisted of different combination of amino acids. Their general structure is depicted in Figure 11.

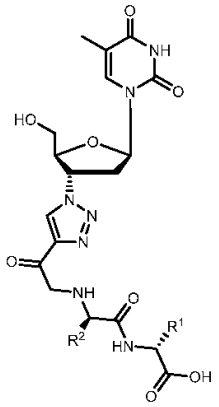

23

Figure 11. The general structure of dipeptide conjugates of **19** designed by Zhang et al. [60].

Not all the 20 natural amino acids were included. The amino acids Asn, Gln, Asp, Met, Cys, His, Trp and Tyr were excluded because they are not very stable in physiological environment. However, authors tried to include most of the amino acid that had been reported to be involved in the PEPT1 activity namely Phe, Val, Leu, Ile, Gly and Ala. To evaluate the bioactivities of the entire library as PEPT1 substrates, authors used adenovirus Ad.RSVhPepT1 transfected HeLa cells that transiently overexpressed PEPT1. After evaluating their cytotoxicity, compounds yielding a cell viability greater than 85% were included in the cephalexin competition study. Several dipeptide sequences as Ser-Glu and Pro-Ile were found to have high affinity to PEPT1 and to mediate significant active transport activity across intestinal epithelia [60].

DOT ((−)-β-d-(2R,4R)-dioxolane-thymine, **24**, Figure 12) is a pyrimidine 1,3-dioxolane nucleoside, exhibiting interesting activity against drug-resistant mutants of HIV-1. The use of amino acids for a prodrug strategy also provides advantages in the cellular transport system [61]. In view of this information, Liang et al. synthesized 5′-*O*-amino acid ester prodrugs of **24** (**25a**–**l**, Figure 12) and evaluated their anti-HIV activity in vitro. Most of the synthesized prodrugs exhibited potent anti-HIV activity against HIV-1_{LAI} in PBMC cells, without increased cytotoxicity in comparison to the parent drug.

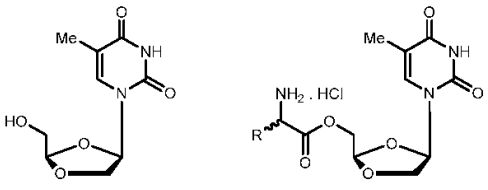

24 **25**

25a R-Gly **25g** R-2-amino-isobutyric acid
25b R-L-Ala **25h** R-L-Phe
25c R-D-Phe **25i** R-L-Val
25d R-D-Val **25j** R-L-Leu
25e R-L-Iso **25k** R-L-Glu
25f R-L-Pro **25l** R-L-Trp

Figure 12. Structures of 5′-*O*-aminoacid esters of DOT.

Despite prodrugs exhibited good chemical stability with half-lives from 3 h to 54 h at phosphate buffer (pH 2.0 and 7.4), they were labile to porcine esterases with lower half-lives (12.3 to 48 min).

The results suggest that prodrugs are effective substrate for porcine esterase. Overall, some class of prodrugs of **24** may improve the overall biological properties of the parent drug [62].

Lopinavir (**26**, Figure 13), an analog of ritonavir (**27**, Figure 13), is a protease inhibitor (PI) indicated for the treatment of HIV infection. When administrated alone, **26** exhibits low oral bioavailability in rats and humans and, usually, it is taken in combination with **27** (Kaletra®). Most likely, its low bioavailability may be related to extensive liver metabolism by CYP3A4 [63]. The compound **26** is prevented from entering the cells by membrane efflux pumps, such as P-glycoprotein (P-gp) and multidrug resistant protein (MRP2). This process diminishes its plasma concentration and thereby decreases its anti-HIV efficacy. In an attempt to prevent the first-pass metabolism and efflux of **26**, Argawal and co-workers synthesized dipeptide prodrugs of **26**, Val-Val-LVR **28a** and Gly-Val-LVR **28b** (Figure 13).

Solubility studies indicate that these prodrugs increase aqueous solubilities in comparison to parent drug that is almost insoluble in water. Moreover, prodrugs did not exhibit significant cytotoxicity to cells at concentrations ranging 5–50 μM. Although at higher concentrations (100 and 200 μM) they were significantly cytotoxic to the cells. Accumulation and transport data of **28a** and **28b** across MDCK II-MDR1 and MDCK II-MRP2 cells indicate significant evasion of prodrugs efflux by P-gp and MRP2. Also, permeability studies across Caco-2 cells indicate that the prodrugs are transported by peptide transporters and have increased permeability as compared with the parent drug. Enzymatic stability studies in Caco-2 cell homogenates indicate that the peptide prodrugs are first converted to the ester intermediate (amino acid prodrug V-LVR) and finally to the parent drug [63]. The use of peptides prodrugs of **26** resulted in targeted delivery via peptide transporters, significant evasion of efflux and prevention of CYP3A4 mediated metabolism [64].

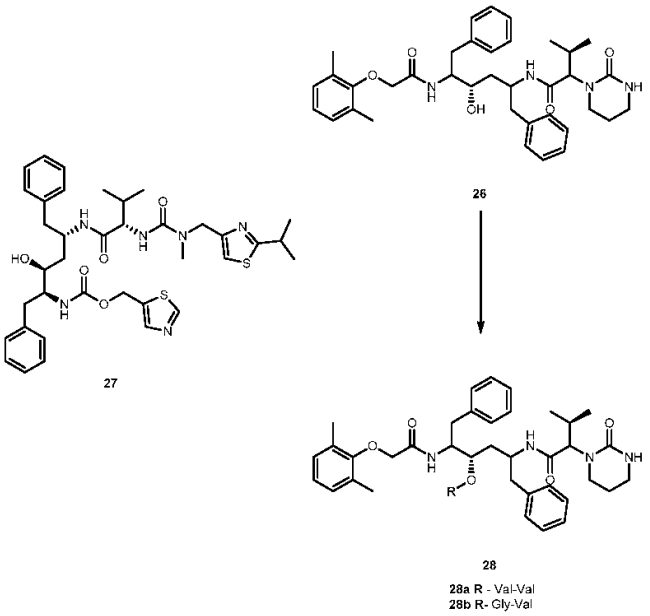

Figure 13. Structures ritonavir (**27**) lopinavir (**26**) and its dipeptides prodrugs (**28a** and **b**).

3.1.3. Hepatitis Virus (B and C)

Hepatitis B virus can cause both acute and chronic infections. Only a few drugs are currently approved by the FDA for the treatment of chronic HBV infection, namely lamivudine (**29**), adefovir (**30**), and entecavir (**31**) (Figure 14). One of major drawbacks of **29** is the low sustained response rate, and drug resistance which affects its efficacy [65,66]. **30**, an ester prodrug of

9[2-(phosphonemetoxy)ethyl]adenine (PMEA, **32**, Figure 14) has a potent in vitro and in vivo activity against HBV, in particular, the ability to suppress replication of HBV resistance to other drugs [66]. However, it presents several undesirable effects, such as dose-limiting nephrotoxicity and its potential toxic metabolites [67].

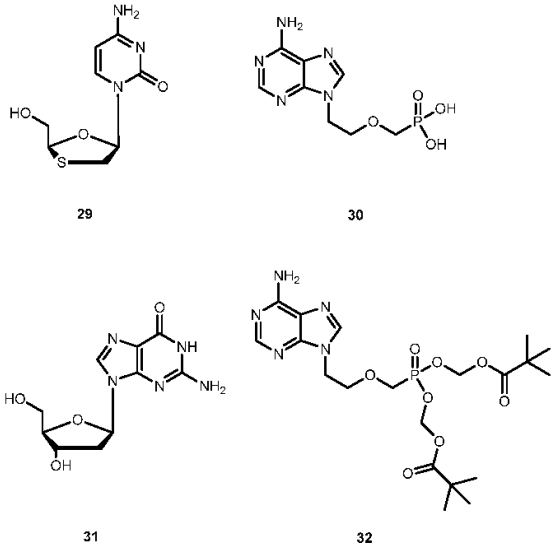

Figure 14. Chemical structures of drugs, lamivudine (**29**), adefovir (**30**), entecavir (**31**) and PMEA (**32**), used against chronic infection of hepatitis B virus.

In order to improve pharmacological properties of **32** as anti-HBV, bioavailability, and decreased cytotoxicity, Fu et al. synthesized a series of novel bis(*L*-amino acid) ester prodrugs of **32** depicted in Figure 15. The anti-HBV activity was evaluated in HepG 2.2.1.5 cells [68].

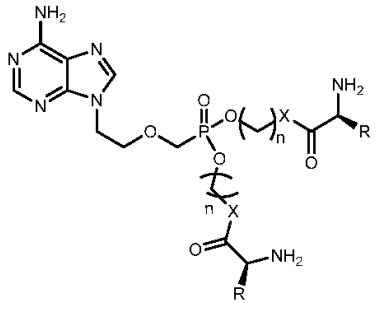

33a	**R**- Me	**X**-O	**n**-2
33b	**R**-Isopropyl	**X**-O	**n**-2
33c	**R**-2-methoxypropyl	**X**-O	**n**-2
33d	**R**-Benzyl	**X**-O	**n**-2
33e	**R**-H	**X**-S	**n**-2
33f	**R**-Me	**X**-S	**n**-2
33g	**R**- Isopropyl	**X**-S	**n**-2
33h	**R**-2-methoxypropyl	**X**-S	**n**-2
33i	**R**-Benzyl	**X**-S	**n**-2
33j	**R**-Isopropyl	**X**-O	**n**-1
33k	**R**-2-methylpropyl	**X**-O	**n**-1
33l	**R**-Benzyl	**X**-O	**n**-1

Figure 15. Structures of amino acid ester prodrugs of **32**.

The amino acid prodrugs **33c**, **33d**, **33h**, **33i**, **33j** and **33k** demonstrated to be highly active against HBV and have a higher selective index than the parent drug **32**. In comparison to **29** and **30** and all prodrugs tested (with exception of compound **33e**) had much lower activities. Compound **33c**, which was found to be the most potent, was five times more potent than **30**. In addition, selective index value was 60 and 24 times higher than **30** and **29**, respectively. Moreover, in vitro stability studies showed that compound **33c** was relatively more stable than **30** with a half-life of 270 min. Using *L*-amino acid and ester strategy it was possible to increase activity, selectivity and stability of compounds, thus, its potential should be considered in the acyclic nucleoside phosphonate prodrug design [68].

Valopicitabine (**34**) and valtorcitabine (**35**) are valine ester prodrugs of 2′-C-methylcytidine (**36**) and 2′-deoxy-β-L-cytidine (**37**) respectively (Figure 16). The **37** is a 2′-modified nucleoside analog with specific activity against Hepatitis C virus (HCV) by inhibiting HCV RNA replication. Both drugs are readily phosphorylated in cells to the corresponding active triphosphate forms. Similar to other nucleosides analogs, **36** and **37** also have low oral availability. Due to previously successful applications of valine esters, **34** and **35** were synthesized in order to improve oral bioavailability of the parent drug [69,70]. In fact, **34** has a remarkable bioavailability of 84% in monkeys in comparison to 16% demonstrated by **37** [69]. This enhancement may potentially be attributed to the involvement of PepT1 transport.

Initially, the 3′,5′-divaline ester of **37** was selected as a clinical candidate due to its ease of synthesis. However, it was replaced by the **35** during phase I/II clinical studies because **34** was more stable and had similar bioavailability compared to the 3′,5′-divaline ester in humans. Nowadays, prodrug **35** is in development for the treatment of HBV [71]. Pharmacokinetic studies of **34** showed an oral bioavailability of 34% in rats and 68% in humans [70,72] and was readily and extensively converted to the parent drug after oral doses in patients with HCV infection [73]. Due to these encouraging results, **34** is currently in clinical trials for the treatment of HCV infection [71].

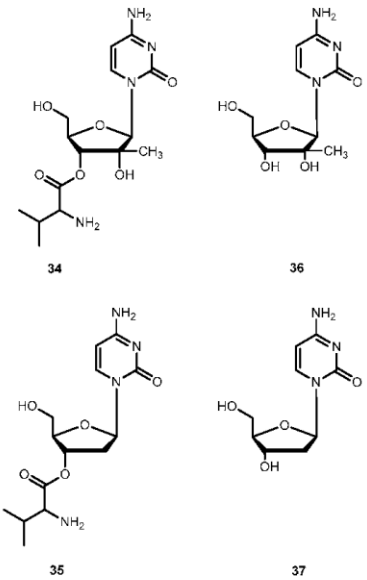

Figure 16. Ester prodrugs **34**, **35** of **36** and **37** respectively.

3.2. Anticancer

Anticancer drugs are primarily cytotoxic agents and exert their antitumor activity by interfering with some aspects of DNA replication, repair, translation or cell division. However, they do not destroy only tumor cells while sparing the normal cells, which leads to severe adverse effects [74]. Therefore, the main goal of using prodrug strategy of anticancer drugs is reduced their toxicity. As a mean to reduce the toxic effects of these agents, prodrugs designed for selective activation in target tissues are by far the most efficient and attractive option [74,75]. In order to an effective targeting, it is necessary that an enzyme or transporter that is exclusively or preferentially expressed in target tissue which constitutes a major challenge. Nonetheless, several prodrugs strategies have been also employed to improve solubility, transport and pharmacokinetic properties [75]. Since there is an excellent published review on anticancer agent prodrugs [74], here we summarize the anticancer prodrugs using amino acids or peptides as promoieties.

The successful results obtained for **1a** and valganciclovir, amino acid ester prodrugs of **1** and **2**, respectively, has prompted the potential of amino acids as promoieties for other agents. This success has been attributed to their enhanced intestinal transport via oligopeptide transporters. In fact, amino acid ester prodrugs significantly improve the cellular uptake of the parent drugs via peptide transport mechanism, though there is no peptide bond in their structures [31]. The fact that some epithelial cancer cells are rich in these transporters allows their use for the delivery of peptidomimetic anticancer agents [4,76–78].

3.2.1. Hepatocellular, Pancreatic Carcinoma and Colon-Rectal Cancer

There are in umerous studies of amino acid derivatives of floxuridine (**38**, Figure 17) [4] and gemcitabine [79], both clinically effective anticancer agents, concerning the activation of the prodrug. Unlike the desired rapid activation required for **1a**, extensive intestinal activation of **38** and gemcitabine prodrugs would lead to severe intestinal toxicity. In this regard, several studies have demonstrated that amino acid ester prodrugs (**39a**–**c**, Figure 17) provided resistance to deamination of gemcitabine [79] and to cleavage of **38** [80,81], respectively.

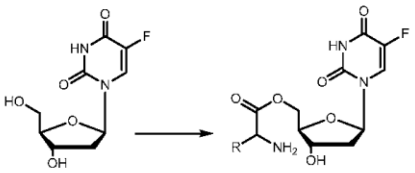

Figure 17. Structures of amino acid ester prodrugs of floxuridine (**38**).

The studies developed with the amino acid esters of **38** were consistent with previous findings. The prodrug **39a** was the most efficiently transported, exhibiting the highest PEPT1-mediated transport and permeability across Caco-2 monolayers. The length and stereochemistry of the amino acid moiety side chain influence the transport efficiency of prodrugs of **38**. The slightly more branched isoleucyl side chain reduced transport of these prodrugs to half, but the branching at γ carbon (as in leucine) side chain highly decreases this transport. The permeability of **39a**–**c** across Caco-2 monolayers was significantly higher than that of the parent drug and also reflected a profound promoiety dependency. Thus, the permeability of the **39a** was roughly 2- and 5-fold higher than the permeability of **39b** and **39c**, respectively [80,81].

The metabolic conversion of **38** to 5-fluorouracil (5-FU) following systemic delivery decreases its therapeutic efficacy. The mechanism of action of **38** and its major metabolite is well understood. The toxicity associated to 5-FU is mostly caused by its incorporation into RNA. Unlike to its metabolite, **38** is specifically incorporated into DNA leading the minimization of adverse effects. Of note that **38** has shown to inhibit cell proliferation 10- to 100-fold more than 5-FU. However, **38** is rapidly converted to 5-FU in many tissues, including the liver, by the enzyme thymidine phosphorylase [82]. Consequently, to maintain the clinical efficacy, higher doses of **38** are required which increase toxicity. In order to counteract this transformation, it is necessary development prodrugs that were protected against the action of this enzyme in order to enhance parental drugs' efficacy at low doses and reduce its toxicity. In fact, amino acid ester prodrugs were resistant to glycosidic bond cleavage by thymidine phosphorylase. This evidence reinforces the notion that the modification of one or both free hydroxyl groups on the sugar moiety provides protection from glycosidic bond cleavages. The rate of conversion of the prodrugs to the parent drug after transport would influence disposition of **38** and therapeutic action [81]. As previously reported by Vig et al., the structure, stereochemistry, and site of esterification of the amino acid promoiety affect the rates of activation of prodrugs of **38**. Therefore, relating the prodrugs structure with hydrolysis rate it is possible development a prodrug with the desired half-life [78,81].

The roughly 5- to 12-fold higher activity in Caco-2 cell homogenates compared with pH 7.4 buffer suggests the predominance of enzymatic bioconversion of the prodrugs. The results obtained for **39c** indicate that it would not be a suitable candidate. In comparison, **39b** is enzymatically more stable than **39a** and the reference drug **1a** [81]. The combined results of the in vitro studies suggest that isoleucyl monoesters of **38** may be promising candidates for improving oral bioavailability of this drug in vivo. Hypothetically, the prodrugs administered orally could improve intestinal uptake of **38** as well as shield it from unwanted degradation [81]. Tsume and co-workers described the synthesis, characterization, and stability of dipeptide monoesters prodrugs of **38**. Various dipeptides and peptidomimetics have been tested to characterize the hPEPT1 transporter and improve its affinity, and mono-amino acid ester prodrugs have been evaluated as hPEPT1 substrates [79–81]. Based on those reports, six amino acids were chosen to be *N*-terminal amino acids of the dipeptide, and other three were chosen to be paired with those six amino acids to test the hypothesis that molecular sizes may structurally affect its ester bond stability [82]. From this study, it was possible to realize that dipeptide prodrugs appeared to be less stable in pH 7.4 buffers than the corresponding mono-amino acid ester prodrugs. Since no mono-amino acid ester prodrug degradation products was detected, it is quite likely that the dipeptide monoester prodrugs degrade through parallel pathways, as previously suggested for the anti-viral dipeptide prodrugs [82].

In order to evaluate the advantages of amino acid/dipeptide monoester prodrugs for cancer treatment, Tsume and co-workers designed a series of 5′-monoester prodrugs of **38** (Figure 18) and assessed their uptake and cytotoxic effects in a secondary cancer cell monolayer following permeation across a primary cancer cell monolayer.

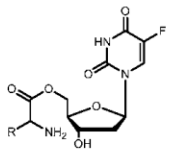

39

39d R- L-Glycine
39e R- L-Lysine
39f R- L-Valyl-L-Phenylalanine
39g R- L-Phenylalanine-L-Tyrosine
39h R- D-Valine
39i R- L-Phenylalanine-L-glycine
39j R- L-Isoleucine-L-Glycine
39k R- L-Phenylalanine
39l R- D-Phenylalanine
39m R- L-Glycine-L-Leucine
39n R- L-Leucine-L-Glycine

Figure 18. Structures of amino acid and dipeptide ester prodrugs of **38**.

Generally, all prodrugs exhibited greater permeation across the first pancreatic cancer cells monolayer, Capan-2, than the parent drug. The results of uptake and growth inhibition on the second layer indicated that amino acid/dipeptide monoester prodrugs (**39d**–**i** and **39j**–**n**), that remain as intact prodrugs following permeation across the first Capan-2 monolayer, provide an enhanced cell penetration and cytotoxic effects on a secondary layer than their metabolites or **38**. It was possible to establish a correlation between uptake and growth inhibition in the second monolayer with intact prodrug permeating the first monolayer. This suggests that permeability and enzymatic stability are essential for the sustained action of prodrugs in deeper layers of tumors. Therefore, stable prodrugs might enhance delivery of the active drug to inner layers of tumor cells compared to parent drug or metabolized prodrugs, being more efficient on cancer treatment [83].

More recently, was reported the potential activation of enzyme cathepsin D by 5′-amino acid/dipeptide monoester prodrugs of **38** in Capan-2 cells, and the feasibility of specific activation of prodrugs. Cathepsin D might be a good candidate as the target enzyme for prodrug activation due its regulation and redistribution to other cellular compartments in tumor cells and its substrate specificity. The results of stability studies with the presence of enzyme inhibition indicate there are particular enzymes activating **39g** and **39i** as cathepsin B and D that significantly activated these prodrugs to produce **38**. For tumors that express large amounts of cathepsin, it is likely that a substantial proportion of **39g** is hydrolyzed by cathepsin D and, therefore, this enzyme has the ability to activate the dipeptide monoester prodrug of **38**, and has the potential to be a target enzyme for prodrug activation in tumors [84].

Although gemcitabine (**40**, Figure 19) is clinically effective in the treatment of advanced or metastatic pancreatic cancer, it also exhibits several side effects that are attributed to its inability to distinguish between normal and target cells. It is known that **40** exerts its anti-proliferative activity via multiple mechanisms of action. It is initially phosphorylated intracellularly by deoxycytidine kinase and subsequently by nucleotide kinases to its active metabolites, diphosphate and triphosphate **40**. The influence of **40** on DNA synthesis has been strongly correlated with its triphosphate metabolite intracellular concentration. However, extensive degradation of **40** by cytidine deaminases to an inactive metabolite decreases its activity [79,85]. To overcome these disadvantages, a novel amino acid ester prodrugs of **40** was developed and their affinity to oligopeptide transporters (hPEPT1) that are overexpressed in the gastrointestinal tract and also, in tumoral cells was evaluated [78,79]. To design the amino acid ester prodrugs the aliphatic amino acids *L*-valine, *D*-valine, and *L*-isoleucine, as well as the aromatic amino acids *L*-phenylalanine and *D*-phenylalanine was used (Figure 19). Similarly to previous studies, authors preferred 5′-monoester substitutions and the *L*-configuration of amino acids. In fact, the results were consistent with previously mentioned findings of prodrugs developed using this strategy. Generally, all prodrugs of **40** have greater affinity to the oligopeptide transporter than the parent drug [79].

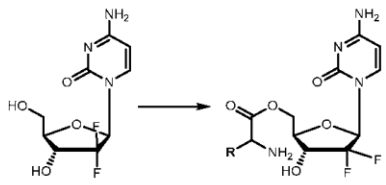

40 **41**

41a R-L-Val
41b R-L-Iso
41c R-L-Phe
41d R-D-Val
41e R-D-Phe

Figure 19. Structures of amino acid ester prodrugs of **40**.

The chemical stability and rapid enzymatic bioconversion characteristic of **41a** suggest its potential in enhancing oral absorption of the parent drug. On the other hand, **41b** showed a slow bioconversion in Caco-2 cells and in human plasma, as well as an unusual resistance to cytidine deaminase deactivation. Thus, a longer systemic circulation half-life of prodrugs may promote an accurate targeting of cells that overexpress hPEPT-1 transporter [79]. In addition to their affinity to hPEPT1, several properties of **41a**, **41b**, **41d** and **41e** were evaluated as (1) their chemical stability in different media buffers; (2) resistance to glycosidic bond metabolism; (3) enzymatic activation; (4) permeability in Caco-2 cells; (5) mouse intestinal metabolism and (6) anti-proliferation activity in cancer cells [79].

Prodrugs containing *D*-configuration amino acids (**41d** and **e**) were enzymatically more stable than *L*-configuration ones (**41a** and **b**). The activation of all prodrugs was 1.3-17.6-fold faster in cancer cell homogenates than hydrolysis in a buffer suggesting an enzymatic activation. This activation on prodrugs containing *D*-configuration of amino acid in cell homogenates was 2.2-10.9-fold slower compared with those with *L*-configuration. All prodrugs exhibited increased resistance to glycosidic bond metabolism by thymidine phosphorylase compared to parent drug and also showed superior effective permeability in mice jejunum than **40**. More importantly, the high plasma concentration of *D*-amino acid prodrugs was observed in more than one of *L*-configuration prodrugs of **40**. In general, all prodrugs exhibited higher permeability and uptake than their parent drug. Cell proliferation assay in ASPC-1 pancreatic ductal cell line indicated that prodrugs were more active than their parent drugs. In addition, the transport and enzymatic profiles of **41d** and **41e**, suggest their potential to increase oral uptake, delay enzymatic bioconversion and enhance uptake and cytotoxic activity in cancer cells [86].

More recently, novel derivatives of **40** were developed using cell-penetrating dipeptides (CPP) in order to facilitate intracellular delivery. In this case, the novel drugs were tested on three cancer cell lines as Caco-2 (Caucasian colon adenocarcinoma cell line), MKN-28 (human gastric epithelium) and HT-29 (colon adenocarcinoma). The results revealed a significant increase of antiproliferative activity of novel CPP-drug conjugates on three cell lines in vitro. In addition, their half-lives were also increased to approximately 9.6 days and 42 h. Taken together, these results demonstrated that conjugation of **40** with CPP might be a valuable strategy for the development of novel prodrugs for an accurate delivery on cancer cells, improving the efficacy of parent drug and alleviate the adverse effects induced on patients [87].

Both strategies used for development of prodrugs of **40** might have great value to develop a novel oral dosage form for anti-cancer agents, not only reducing drug toxicity but also improving targeting of cancer cells. Therefore, the quality of life for the cancer patients could be significantly improved.

Brivanib alaninate (BMS-582664, **42**, Figure 20) is an investigational amino acid ester prodrug of brivanib (BMS-540215, **43**, Figure 20), a selective dual inhibitor of vascular endothelial growth factor receptor 2 (VEGFR-2) and fibroblast growth factor receptor 1 (FGFR-1). Since 2011, **42** is in phase III clinical trials for the treatment of hepatocellular carcinoma and colon-rectal cancer [88]. It was designed in order to improve the very low aqueous solubility of **43** (<1 μg/mL, at pH 6.5), which contributes to its solubility/dissolution rate-limited oral bioavailability, particularly at high doses. **42** has very high aqueous solubility (73 mg/mL at pH 5.8), which results in a remarkably improved oral bioavailability of **43** up to 52–97% in several animal models [89,90]. In fact, **42** is rapidly and completely converted to **43**, by various esterases (Figure 20), increasing exposure to the parent drug. Therefore, **42** offers an excellent way to deliver **43**, orally [91].

Recently, novel derivatives of bromothiazole derivatives with amino acid moieties and a core of nitazoxanide (**44**, Figure 21a) were synthesized and their anticancer, antiproliferative and cytotoxicity effects evaluated [92]. Generally, **44** is used as an anthelminthic agent, mostly used against infections caused by protozoa and helminths [93]. However, the combination of **44** with irinotecan was identified as a potential candidate for the treatment of colon-rectal cancer [94]. **44** acts as a prodrug itself that is deacetylated in the gastrointestinal tract to its active metabolite tizoxanide (**45**, Figure 21). With this in mind, authors developed novel bromothiazoles using 2-amino-5-bromothiazole as starting material

and introduced α-amino acids with different nature of side-chain (from one hydrogen to a large heterocyclic group; *L*- and *D*-form) attached to their α-carbon (Figure 21b).

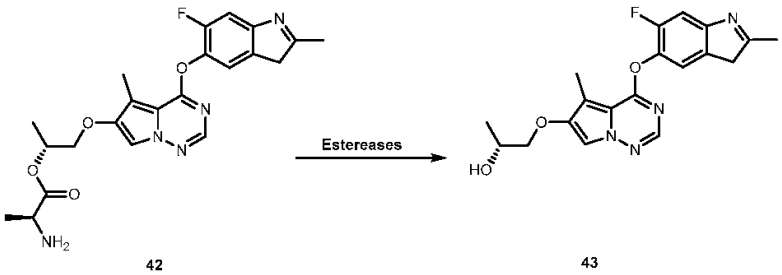

Figure 20. Bioconversion of brivanib alaninate (**42**) to brivanib (**43**) by esterases.

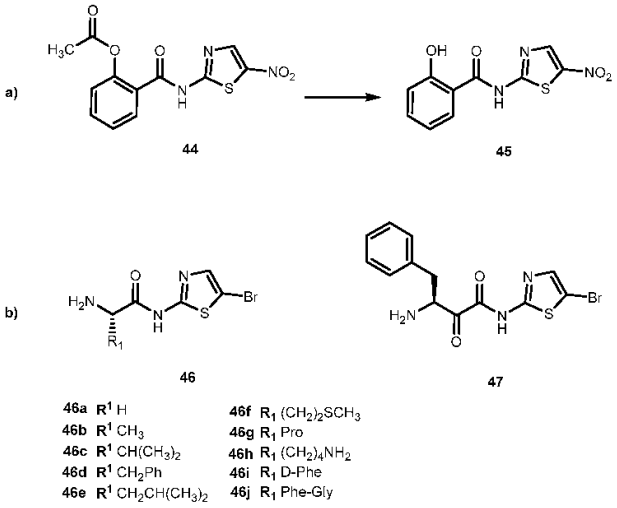

Figure 21. (**a**) Chemical structure of nitazoxanide (**44**) and its major active metabolite tizoxanide (**45**); (**b**) Bromothialozes derivatives with an amino acid moiety (**46a**–**j**) and dipeptide.

Additionally, a dipeptide was also developed. The novel derivatives presented a significant and concentration-dependent anti-proliferative effect. They were able to reduce ^{3}H-thymidine incorporation by more than 80%. When compared to drugs, butyrate, compounds **46c**, **46d**, **46g**–**i** and **47** has a similar cytotoxic effect of butyrate. In comparison to **44**, **46a**, **46c**, **46f** and **46g** have a better performance, particularly **46f** which showed an enhancement of 22% [92]. This compound has a methionine (Met) moiety which is relevant since cancer cells have a unique metabolic addition to in contrast with normal cells. Moreover, *S*-adenosylmethionine metabolism is dependent on Met availability in cancer cells [95]. This might suggest that drugs that included Met in their constitution might be suitable to target cancer cells.

3.2.2. Brain Cancer

CEP 7055 (**48**, Figure 22) is a dimethyl glycine ester of CEP 5214 (**49**, Figure 22), a pan-inhibitor of VEGFR tyrosine kinases with antitumor activity [96]. The latter has a very low aqueous solubility, which might be responsible for its poor oral bioavailability [97]. Notwithstanding, the use amino acid prodrug strategy to produce **48** increased solubility up to 4000-fold (comparatively to **49**) and improved bioavailability between 15–20%. The produg **48** is hydrolyzed to the active metabolite (**49**), during the

absorption of the enterocytes by aminopeptidases (Figure 22). Currently, **48** has advanced to clinical trials as a chemotherapeutic agent for glioblastoma and colon cancer in combined therapy [96,98].

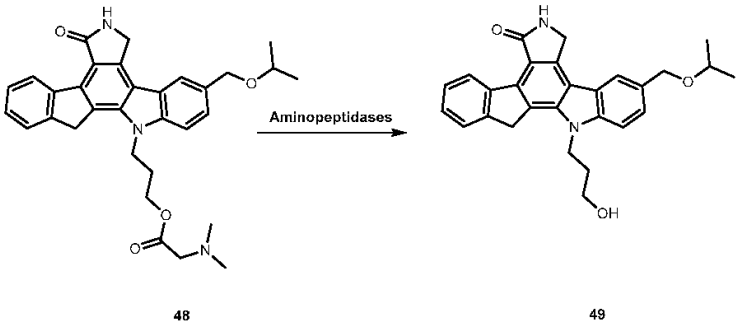

Figure 22. Bioconversion of amino acid ester prodrug **48** to its parent drug **49** by aminopeptidases (Reproduced from [4]).

3-Carbonyl thymidine analogs (3-CTAs), such as N5 (**50**, Figure 23) and N5-2-OH (**51**, Figure 23), have been developed for Boron Neutron Capture Therapy (BNCT) for high-grade brain tumors as glioblastoma multiforme (GBM) [99]. BNTC is a binary cancer treatment modality that is based on irradiation of boron-10 (^{10}B), a stable isotope, with low energy neutrons [100].

Despite the potential interest in **50** and **51** for BCNT, these compounds present a major drawback: both are very lipophilic due to the presence of the carborane cluster and the absence of any potential groups that can be ionized under physiological conditions. In order to improve this, Hasabelnaby and his co-workers synthesized amount water-soluble amino acid esters prodrugs of **50** and **51** using as promoities *L*-Val, *L*-Glu, and glycine (Figure 23). These prodrugs were prepared and stored as hydrochloride salts [101].

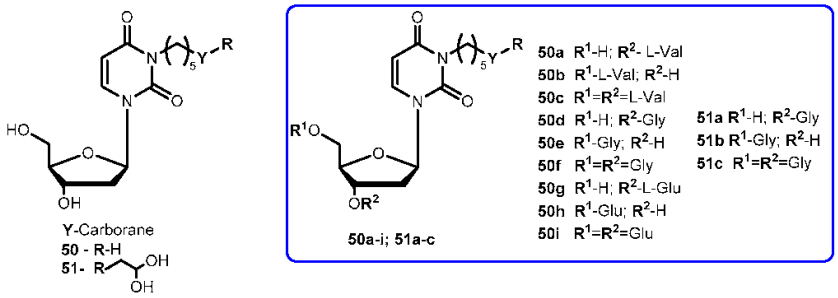

Figure 23. Chemical structures of 3-carbonyl thymidine analogs, N5 (**50**) and N5-2-OH (**51**) and its amino acids prodrugs **50a**–**i** and **51a**–**c**.

Water solubilities of synthesized prodrugs were evaluated in PBS at different pH (5.6 and 7.4) demonstrating that those improved 48–6600 times in comparison with parent drugs. Additionally, their stability was evaluated in different media: PBS at pH 7.4, bovine serum, and bovine cerebrospinal fluid (CSF). The solubilities for all prodrugs are significantly better than parent drugs and appeared to be suitable for injection formulations. The rate of the hydrolysis in all incubation media depended primarily on the amino acid promoiety and, to a lesser extent, to the site of esterification at the deoxyribose portion of 3-CTAs. Generally, glycine esters (**50d**–**f**) and **51a** were 20–25 times more sensitive to chemical hydrolysis than the correspondent glutamate **50g**–**i** and valine ester **51a**–**c**. These results may be explained by the presence of the small glycine promoiety, which sterically does not interfere with the nucleophilic hydrolytic attack at the ester bond. Comparing the hydrolysis rate of the amino acid ester prodrugs in other media: it was overall higher in bovine CSF comparatively

to PBS and somewhat lower than in bovine serum. Despite a low concentration is present in the CSF, enzymatic degradation may be possible causing an increased rate of the hydrolysis in this fluid compared with PBS. In case of **50h**, its significant rate of hydrolysis in CSF may be related to the presence of glutamate-specific enzymes, since glutamate is the most common neurotransmitters in the brain. Therefore, its presence might be crucial for developing prodrugs for brain diseases. The rapid hydrolysis in CSF with stability in PBS at pH 7.4, make compounds **50e**, **50h** and **51b** the most promising candidates for preclinical BNCT studies [101].

Rapamycin (**52**, Figure 24), an immunosuppressant and chemotherapeutical drug used to prevent rejection after organ transplantation, has low aqueous solubility and poor oral bioavailability. Rapamycin-28-*N*,*N*-dimethylglycinate methanesulfonate salt (**53**, Figure 24) was synthesized as a potential water-soluble prodrug to facilitate parenteral administration of the antineoplastic macrolide **52** [102].

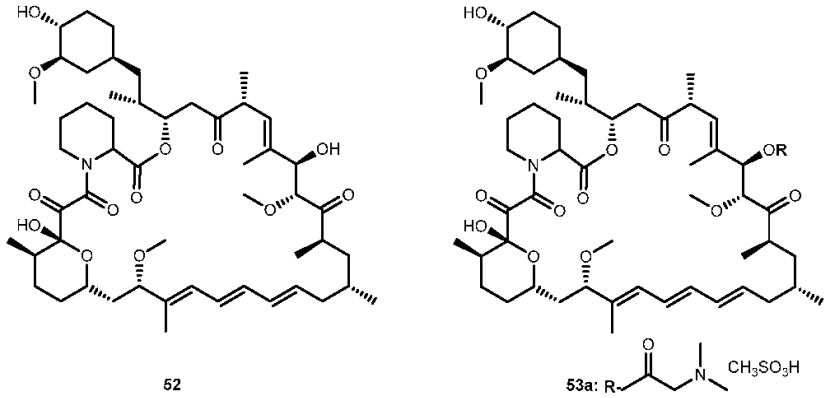

52

Figure 24. Structure of rapamycin (**52**) and its glycinate derivative (**53a**).

Effective therapeutic treatment regimens of **52** appear to be considerably less toxic to mice than other anticancer agents. The apparent penetration of **52** through the blood-barrier brain (BBB) was evident by high activity against intracranially implanted tumors, including U-251 human glioma [102].

After the introduction of dimethylglycinate methanesulfonate salt into **52**, it was noted a persistent for 5–12 h in mice treated with a dose ranging 10 to 100 mg/kg. The disposition of **53** exhibited an atypical dose-dependency that appears to originate from the saturable binding of the compound to the plasma proteins while binding to tissues remains linear. Although systematically circulating prodrug may be subject to elimination by a variety of pathways, **53** effectively served as a slow-release delivery system for the parent compound. Single doses ranging 10 to 100 mg/kg given by bolus intravenous injection provided a plasma concentration of prodrug **53a** that were sustained at a near-peak level for approximately 8 h and remained above 0.1 μm for 48 h. These observations imply the possibility of maintaining therapeutic plasma levels of the drug on a more convenient dosing regimen than a continuous infusion schedule [103]. Considering this, the demonstration of activity of **53** against in vivo brain tumors models should be pursued for the continuous development of novel and effective prodrugs for the treatment of brain neoplasms.

3.2.3. Human Lung Carcinoma

Camptothecin (**54**, Figure 25) a cytotoxic quinoline alkaloid, is a potent anticancer agent that inhibits both DNA and RNA synthesis. The lactone form of **54** (i.e., active form) is responsible for its anticancer activity [104,105].

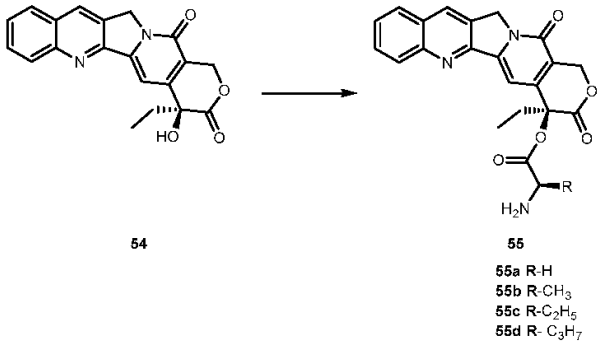

Figure 25. Structures of prodrugs of **54**.

Nonetheless, there are two major drawbacks of **54** that have made it less attractive for clinical use. First, **54** has unfavorable physical-chemical properties, and second, it has severe clinical toxicities. Moreover, it has a very poor aqueous solubility making it difficult to formulate. Moreover, under physiological conditions it is rapidly hydrolyzed to the carboxylate form. These carboxylate forms are known to induce severe cumulative hematological toxicity, diarrhea, and chemical or hemorrhagic cystitis [106]. With the intent to identify a prodrug of **54** with optimal release and cytotoxicity properties for immobilization on a passively targeted microparticle delivery system, four α-amino acid ester prodrugs of **54** were synthesized with increasing aliphatic chain length, glycine **55a**, alanine **55b**, aminobutyric acid **55c** and norvaline **55d** (Figure 24) and assessed for human lung carcinoma.

Prodrug reconversion was studied at different pH 6.6, 7.0 and 7.4, corresponding to tumor, lung and extracellular/physiological pH, respectively. **55c** and **55d** present longer release profiles of parent drug than **55a** and **55b**, at the three studied pH values. The hydrophobicity constant appears to be directly proportional to the half-life of both on the transformation into **54** as well as in **55a**–**d** hydrolysis. This evidence suggests that increasing the length of the side chain of the hydrophobic amino acid would sustain the release of **54**. The increase of prodrug reconversion might be directly related to increasing aliphatic chain lengths due to its effect of steric hindrance. Since **55d** present lower toxicity and sustain release of parent drugs, **55d** should be considered for a passively targeted sustained release lung delivery system [107]. As previously mentioned it is crucial that prodrug should be resistant to hydrolysis in order to achieve a sustained and targeted delivery. It seems that longer aliphatic chains coupled to amino acid moiety might be a very valuable strategy to achieve this goal, turning prodrug more resistant to hydrolysis performed by patient's enzymes.

3.2.4. Breast Cancer

A novel antitumor agent 2-(4-amino-3-methylphenyl)benzothiazole (**56**, Figure 26) was demonstrated to be highly selective and display potent antitumor properties both in vitro and in vivo. Apparently, the induction of CYP1A1-catalyzed biotransformation of **56** is crucial to its antitumor activity [108,109]. The formulation of an aqueous intravenous formulation constitutes a pharmacological challenge, however, it is fundamental to minimize the possibility of first pass deactivating metabolism and improve drug bioavailability [110]. Therefore, novel amino acid ester prodrugs of **56** were developed (Figure 26) and their water and chemical stability were assessed on different animal models (mice, rats, and dogs).

The introduction of alanyl- and lysyl-amide hydrochloride salts could be conjugated to the exocyclic primary amine functions of **56**, increasing water solubility, chemical stability and suitable for sustained release of the parent drug. Indeed, all prodrugs tested undergo through a rapid and quantitative release of the parent drug. In addition, after administration of **58a**–**c** in mice, plasma levels of **58** exceeding 5-fold the concentrations required to elicit 50% growth inhibition (IG_{50}), total growth

inhibition (TGI). These activities persisted for 4 h and >6 g after a single intravenous infusion of prodrug **58b** and c in MCF-7, T47D and ZR-75 breast cell lines. Of note that potent and selective antitumor activity of **58a** observed in vitro was retained in vivo. In fact, **58c** was able to suppress significantly the growth of MCF-7 breast and IGROV-1 ovarian xenografts in vivo. Intriguingly, only tumor xenografts whose growth were inhibited by **58c** demonstrated inducible CYP1A1. This suggests that CYP1A1 expression might be a biomarker in human tumors for identification of sensitive tumor phenotypes. On another hand, expression of CYP1A1 might lead to hepato or pulmonary toxicity [110]. Therefore, it is necessary to adjust dose administered in order to prevent undesirable lesions.

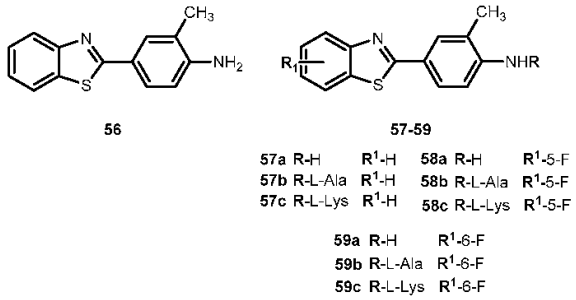

Figure 26. Structure of 2-(4-aminophenyl)benzothiazole **56** and its amino acid prodrugs **57a–c**, **58a–c**, and **59a–c**.

In view of encouraging preclinical properties achieved by *L*-Lys-amide dihydrochloride salt combined with the superior efficacy and retained selectivity of compound **58**, prodrug **58c** has been selected to undergo Phase I clinical evaluation on 2002, under auspices of the UK Cancer Researcher Campaign [110].

Enzymes are unique in a tissue, or present at a higher concentration compared to other tissues, and therefore can be exploited for site-selective prodrug conversion and hence targeting. Some tumor tissues have been shown to evoke increased prolidase activity compared to normal tissues. With this in mind, novel prodrugs that will be transformed into parent drug by the action of this enzyme could be development [4]. Melphalan (**60**, Figure 27) belongs to the class of antitumor agents with an alkylating and cross-linking action on guanine and possibly other bases of deoxyribonucleic acid (DNA) that result in arresting of all division [111].

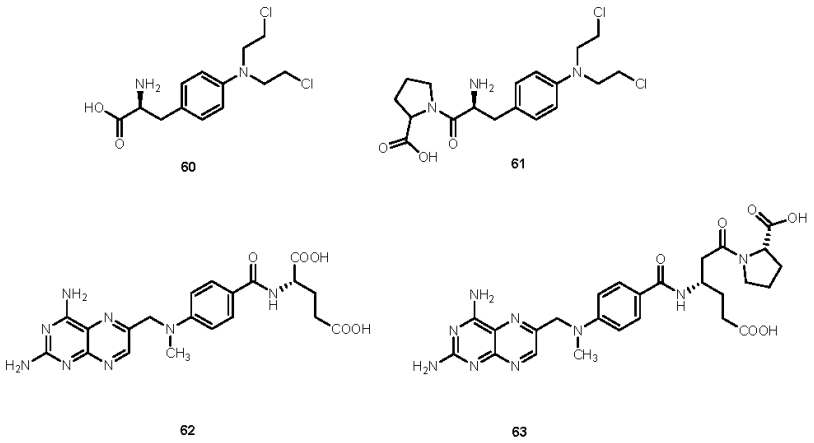

Figure 27. Chemical structures of melphalan (**60**) and methotrexate (**62**) and its proline conjugates (**61** and **63**).

Chrzanowski et al. designed conjugates of **60** with proline through imido-bond, which resulted in the formulation of a good substrate for prolidase [112]. A proline drug of methotrexate **62** was also designed as a substrate for prolidase [113]. Both prodrugs showed increased cytotoxicity for breast cancer cell line MDA-MB-213 compared with the parent drug, suggesting that the proline prodrug approach may overcome the resistance associated with parent drug, at least this specific cell line. The increased cytotoxicity was attributed to two mechanisms: (1) proline prodrugs were more effectively transported into MDA-MB-231 cells, likely by transporter-mediated mechanisms; (2) higher prolidase activity in MDA-MB-231 cells than in normal cells, contributing to the effective release of the parent drugs at the site of drug action [112,113].

3.2.5. Melanoma

Different proline prodrugs of **60** were synthesized by direct coupling of a free carboxylic group of **60** to the *N*-terminal imino acid and assessed in melanoma. Although the rationale proposed for the synthesis of proline drugs of **60** involves the targeting of prolidase, the differences in the linkage of the proline moiety to a drug may be crucial, which might affect their activation by prolidase [114].

The antiproliferative activity profiles of **60**, *D*-prophalan and *L*-prophalan in SK-MEL-5 cells (a melanoma cancer cell line with high expression of prolidase) indicate a ~7-fold high rate of activation of derivatives. The relative of GI_{50} for parent drug and proline drugs of **60**, coupled with the stability of the two prodrugs in growth medium indicate that bioconversion of the prodrug to the parent drug may determine their cytotoxic activity in cells [114]. From these reports, it is possible to conclude that prodrugs of **60** that are cleavable by prolidase offer the potential for enhanced selectivity by facilitating cytotoxic activity in cells overexpressing prolidase. Of note that the potential bioactivation of the prodrugs by prolidase expressed in normal tissues was not assessed. In addition, it is necessary to provide information regarding their chemical stability that will be necessary for targeted delivery to melanoma tumor cells [114].

Nam et al., designed a series of prodrugs of antitumor agent 3-[3-(amino-4-methoxy)phenyl-2-(3,4,5-trimethoxyphenyl)cyclopent-2-ene-1-one] (**64**, Figure 28) a novel analog of combretastin A-4, (**65**, Figure 28). The **61** has a very potent cytotoxicity against various tumor cell lines, however, this strong activity was not observed in vivo. This unexpected low tumor activity might be related to its low bioavailability, which is responsible, at least in part, to its poor aqueous solubility [115]. In order to improve this parameter, prodrugs with α-amino acid **66a**–**h**, aliphatic amino acid **67i**–**l**, and phosphoramidate and phosphate derivatives were synthesized (Figure 28) [116].

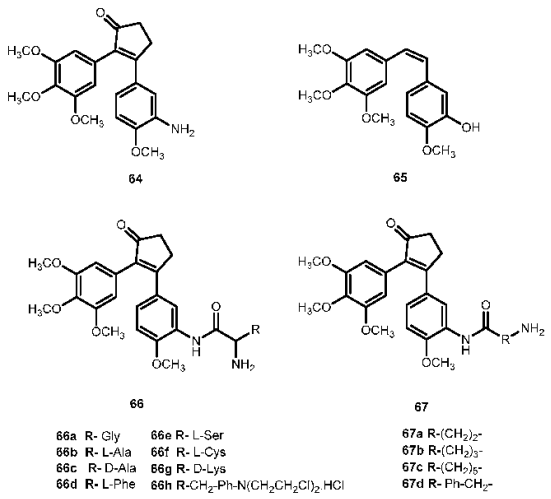

Figure 28. Structures of prodrugs of **64**.

The introduction of different amino acids and phosphate improved water solubility of the prodrug. In addition, their antitumor activity was also improved with several amino acids prodrugs **66a**, **66b**, **66d**–**f**, **66h**, **66a**, and **67c** exhibiting more potent antitumor activity compared to the parent drug. Cytotoxicity of the prodrugs was determined in two tumor cell lines, B16 (murine melanoma) and HCT 116 (human colon tumor). Most of the amino acid prodrugs of **66**–**67** showed potent cytotoxicity in both tumor cell lines. Nonetheless, it is not clear if prodrugs **66a**–**h** and **67a**–**d** would be cytotoxic *per se* or their toxicity is related to their conversion into parent drug. It should be noted it that none of the prodrugs were significantly toxic in mice [116]. Considering the introduction of amino acids and phosphate group lead to an increase of bioactivity and improvement of water solubility this strategy might be applied to other aromatic amines drugs that have poorly soluble in the aqueous system.

3.2.6. Other Compounds

Quercetin (3′-4′-3-5-7-tetrahydroxyflavone, **68**, Figure 29) is emerging as anticancer drug candidate and its prodrug QC-12 (**69**, Figure 27) has entered the phase I clinical trials [117]. The **69** is an amino acid prodrug of **68**, where one of the phenol groups of the parent drug is attached to amino acid glycine via carbamate bond which should be cleavage in the bloodstream by hydrolysis to yield the parent drug [118]. Although **68** has many biological activities, the drug is almost water insoluble which requires the use of dimethyl sulfoxide (DMSO) for its use in clinical trials. The introduction of amino acid moiety leading to the formation of **69**, has increased aqueous solubility when compared to the parent drug. The prodrug is activated by cellular hydrolyzing enzymes, however, it is unknown if this activation occurs before or during absorption [119].

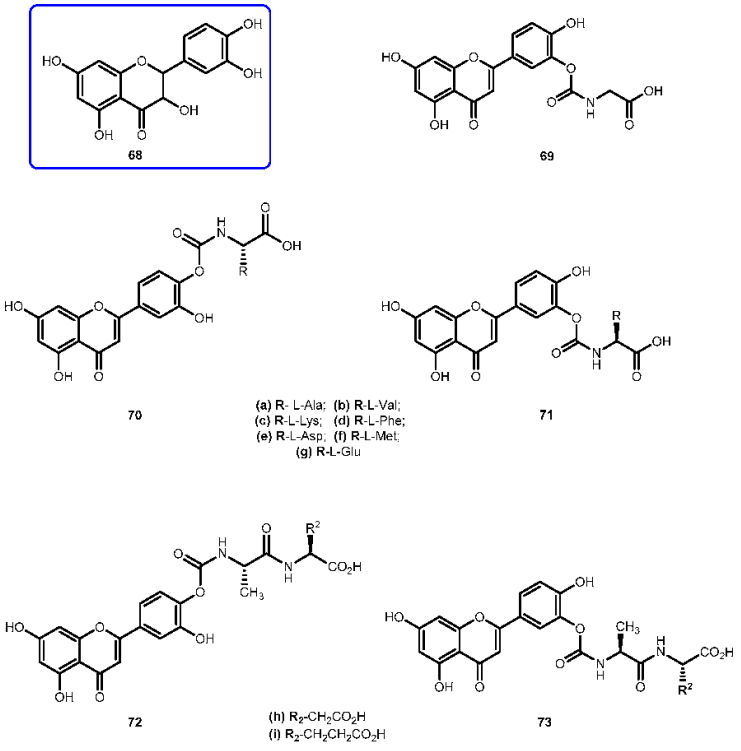

Figure 29. Quercetin (**68**), prodrug QC-12 (**69**) and its amino acids **70**–**71** and dipeptides **72**–**73** conjugates.

The advantage presented by **69** is its high aqueous solubility compared to the parent drug. However, its utility for oral dosage is limited due to the low bioavailability, which presumably results from the fast metabolism and excretion of the prodrug. With intent to improve bioavailability, it was synthesized a novel amino acid/dipeptides conjugates of **69** and assessed their pharmacokinetic properties, including water solubility, stability against chemical or enzymatic hydrolysis and cell permeability across MDCK (Madin-Darby canine kidney) cells. The moieties used to their synthesis were non-polar amino acids (Ala, Val, Phe, Met), positively charged (Lys) and negatively charged (Asp, Glu) (Figure 29) [119].

The prodrugs of **68** showed remarkable increases of 6.8–53.0-fold of water solubilities, increased relative to **68**. In particular, amino acids such as aspartic acid and glutamic acid increased the water solubilities of their corresponding quercetin conjugates **70e/71e** and **70g/71g** by 45.2 and 53.0 folds respectively. The introduction of amino acid chains provided additional solubilities to novel analogs of **69** by blocking hydrolysis on carbamate link. Like **68**, its prodrugs were stable in PBS buffer but susceptible to enzymatic hydrolysis in a cell lysate, which contained various activated hydrolyzing enzymes. Amino acid conjugates of **68** such as **70c/71c** and **70g/71g** showed strong resistance against hydrolysis and consequently has extended half-lives compared with that of **69**. The prodrugs **70e/71e**, **70g/71g** and **72i/73i** also showed significantly increased intestinal permeability at MDCK cells in comparison with parent drug. Due to these results, Kim et al. considered to have identified a novel quercetin-amino acid conjugate **70g/71g**, of which warrant further development as prodrugs of **68** and **69** [119].

More recently, it has been proposed that **64** might act as a prodrug itself since it is rapidly transformed into active metabolites, 3-4-dihydroxyphenylacetic acid (**74**) Figure 30) and *m*-hydrophenylacetic acid (**75**) (Figure 30) by intestinal microflora [120].

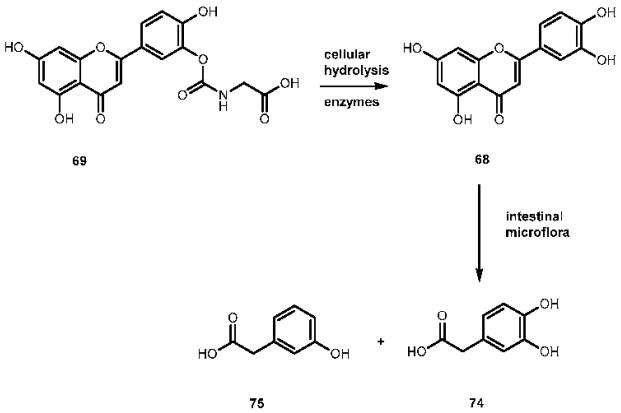

Figure 30. Bioconversion of a carbamate of **69** by cellular hydrolyzing enzymes and the proposed biotransformation to active metabolites, **74** and **75**, by intestinal microflora (Reproduced from [4]).

Docetaxel (**76**, Figure 31), is an important chemotherapeutic drug widely used for the treatment of several types of cancer. Like other drugs, **76** has poor water solubility and consequently has limited clinical application. Moreover, it induces several adverse effects as allergic reactions, neurotoxicity and cardiovascular toxicity [121,122].

In order to improve its antitumor activity and water solubility, Ma et al. developed a novel derivative of **76** by linking an amino acid to the hydroxyl group of C′2 position (Figure 31). Its stability and solubility were assessed on PBS buffer (pH 7.0) and human plasma. Through linkage of amino acid moiety improved its water solubility 200–600 times compared to **76**. Therefore, this new derivative might suitable for injection by preparing a lyophilized powder. In addition, after administration of LK-196 in human plasma, it was demonstrated that the new derivative acts as a prodrug of **76**. This fact might be related to the strong-electron effect caused by fluorine atom in α-position of the

amino acid linker. Regard to its antitumor activity, LK-196 significantly inhibited the growth of human prostate tumor PC-3 in nude mice. In fact, LK-196 shown a stronger activity than **76** [123]. Despite these encouraging results, after administration of LK-196 at higher LD_{50}, several adverse effects were observed. Nonetheless, its toxicity was not increased when compared to **76** [123]. Apparently, the introduction of the amino acid linker with a fluorine moiety improved the water solubility and stability and did not alter its toxicity. Therefore, this strategy should develop novel derivatives with lower toxicity in vivo.

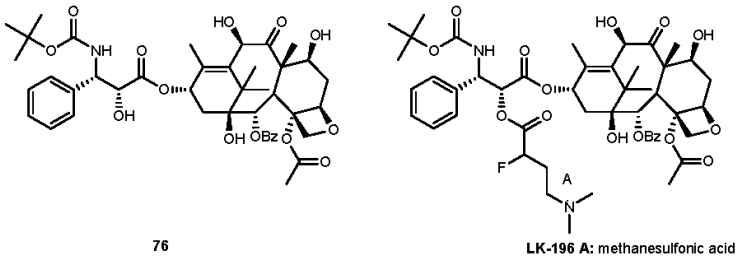

Figure 31. Chemical structure of docetaxel (**76**) and its novel prodrug LK-196.

3.3. Antiparasitic Drugs

Parasitic diseases, caused by a diverse spectrum of eukaryotic organisms, represent a major global health problem. Malaria, leishmaniasis, Chaga's disease and African sleeping sickness (both caused by *Trypanosoma* species) affects hundreds of millions of people worldwide causing millions of deaths annually and present an immense social and economic burden [124]. Most of the current drugs used to treat these diseases, especially the neglected ones, are old and have many limitations, including the emergence of drug resistance [125,126]. Therefore, it is urgent to develop new control tools (vaccines or new molecule-drugs) exhibiting different modes of action by exploring and combining a wide variety of chemical structures or improving pharmacological properties of drugs that are already used.

3.3.1. Trypanosomiasis

American trypanosomiasis (Chaga's disease) represents a serious public health problem in the American continent, where approximately 100 million is at the risk of infection. Current therapy is unsatisfactory and accomplished with the only two available trypanocidal drugs, nifurtimox (**77**) and benzindazole (**78**) (Figure 32) [127] which are only effective in the acute phase of the disease.

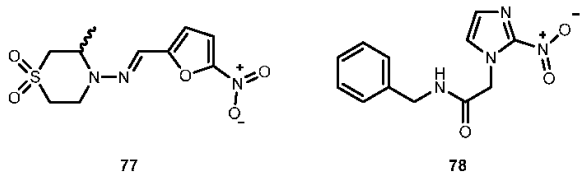

Figure 32. Chemical structures of trypanocidal drugs, nifurtimox (**77**) and benzindazole (**78**).

One of the major challenges in trypanosomiasis chemotherapy is the related efficacy of drugs, they are only effective in the acute phase of the infection. However, early stage of the infection is difficult to diagnose. On the other hand, both drugs have serious adverse side effects. The antimalarial **4**, has also been used in human acute and congenital cases of Chaga's disease [128]. Chung and co-workers synthesized dipeptide prodrugs of **4** (Figure 33) and evaluated in vitro trypanocidal activity.

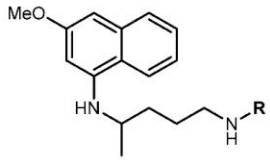

79
79a R-Lys-Arg
79b R-Phe-Ala
79c R-Phe-Arg

Figure 33. Dipeptide prodrugs of **6** tested against trypanosomiasis.

Dipeptide prodrugs of **4** (Figure 33) were active against trypomastigotes forms of *Trypanosoma cruzi* (*T. cruzi*) that were present on Rhesus monkey kidney epithelial cells LLC-MK2. It was demonstrated that **79a** was active on *T. cruzi* development inside host cells, probably by interfering in the initial steps of trypomastigote-amastigote transformation. These prodrugs proved to be more active than **79b** and **c**, suggesting that the specific cleavage has an important role in the release of **6**. In addition, it was a good carrier for **4** and has a potential to be used as a spacer group for the development of other prodrugs of **4** against trypanosomiasis [127]. Therefore, **79a** should be considered for in vivo test provide information regarding to its bioavailability and other pharmacological parameters.

Pentamidine (**80**, Figure 34) is effective in therapy for the hemolymphatic stage of trypanosomiasis and antimony-resistant leishmaniasis [129]. As an aromatic diamine, pentadimine requires an intravenous or inhalation application. Unfortunately, most of the serious parasitic infections occur in tropical or subtropical countries that usually have poor medical care system. Consequently, this way of application limits the medicinal use of **80** in most regions and emerging need for a derivative of **80** that can be administered orally.

Moreover, the intravenous application is associated with toxic side effects [130]. Generally, drugs containing amidines has poor oral bioavailability and are often converted into amidoxime prodrugs to overcome low uptake from GI tract. Esterification of amidoxime with amino acids represent a newly developed double prodrug principle. In order to reduce toxicity, Kotthaus and co-workers designed a model compound *N*-valoxybenzamidine (**81**, Figure 34) and investigated it's biological transformation in vitro and in vivo, with a special interest in oral bioavailability and the tissue distribution after application. Afterwards, the prodrug principle was transferred to *N*,*N*′-bis(valoxy)pentamidine (**82**, Figure 34). Kotthaus and co-workers examined water solubility, stability, in vitro bioactivation, and organ distribution of **81**, including post absorptive conversion to the active metabolite pentamidine in rats [131].

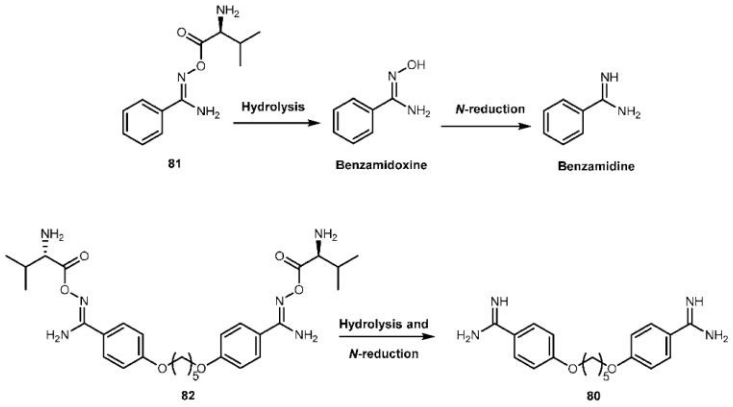

Figure 34. Metabolic activation of *N*-valoxybenzamidine and *N*,*N*′-bis(valoxy)pentamidine (reproduced from [131]).

Both **81** and **82** were activated in vitro by all enzyme preparations investigated (i.e., porcine and human subcellular enzyme fractions, hmARC1, hmARC2, and hepatocytes). The activation relies on esterases and mitochondrial amidoxime reducing components (mARC) and is thus independent of P450 enzymes, minimizing the risk for drug-drug interactions and undesired effects. Kotthaus and co-workers results demonstrated the increase of solubility in comparison to the amidoxime prodrugs leading to an excellent oral bioavailability. In addition to absorption by diffusion, the transport by amino acid and peptide transporters in the GI tract is feasible. After oral administration in rats was observed an oral bioavailability of prodrug about 88% was observed **81**. The high bioavailability also excludes the possibility of an ester hydrolysis prior to absorption. Compound **80** entered into the cells of all tissues investigated. This effect is essential for the antiprotozoal effect of **80** considering that the parasites are spread throughout the body. More important, **81** was transformed completely to the parent drug. Also, its solubility was improved over 100-fold in comparison to **80**, diamoxidine and *N*,*N*′-bis(acetoxy)pentamidine. The authors considered that these observations indicate that the development of this new prodrug principle may also valuable for the treatment of the second stage of African sleeping sickness. Furthermore, Kotthaus and co-workers detected active drug **80** in the brain, although only in small amounts. They considered that the development of prodrugs of **80** based on other amino acids might be an interesting strategy leading to prodrugs able to cross the blood-brain barrier more efficiently [131].

3.3.2. Malaria

Malaria is one of the major public health problems in tropical areas. The rapid emergence and spread of chloroquine-resistant *Plasmodium falciparum* (*P. falciparum*) throughout the African continent is the major obstacle to present efforts to control the disease. *P. falciparum* strains are resistant to newer drugs such as mefloquine which might result from the loss of drug activity on the asexual blood forms of the parasite, called blood schizonts, that are responsible for the clinical symptoms of disease [132].

Current, **4** is the drug of choice against malaria since it is active against both of latent liver forms of relapsing malaria caused by *P. vivax* and *P. ovale* and the gametocytes from all species of the parasite causing human malaria [132]. The short plasma half-life of **4** might be related to its rapid oxidative deamination to carboxyprimaquine [133], which is inactive against malaria. Also, **4** induces oxidation of oxyhemoglobin to methemoglobin leading to a considerable blood toxicity [134]. In order to improve some limitations of **4**, several prodrugs have been developed.

Portela and co-workers developed dipeptide derivatives of **4** to (i) evaluate the gametocytocidal activity of novel dipeptides derivatives **83**–**85** of **4** (Figure 35) and their potential as transmission-block antimalarials; (ii) compare the side effects of chains containing natural and non-natural amino acids on the gametocytocidal activity and (iii) to assess the effect of aliphatic side-chain acylation on the formation of carboxyprimaquine in rat liver homogenates [37].

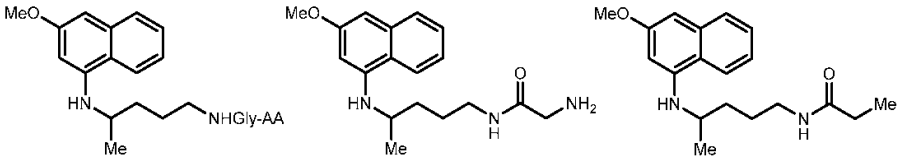

83 **84** **85**

83a AA-Gly;
83b AA-L-Phe;
83c AA-L-Ala;
83d AA-D-Phe;
83e AA-Sar

Figure 35. Dipeptides derivatives of **6** synthesized by Portela et al. [37].

Equal roles of CYP450, monoamine oxidase (MAO) and aldehyde dehydrogenase in the conversion of **4** into carboxyprimaquine, rat liver homogenates were selected to study the metabolism

of derivatives **83**. Simultaneous formation of **4** and **84** was observed with compounds **83a**–**c**. In contrast, derivatives **83d**–**e** were stable in the incubation mixtures and their concentrations remaining constant for at least 3 h. Under the same conditions, **84** failed to regenerate the parent drug [37]. Thus, it was considered that acylation of the aliphatic side-chain protects the terminal amino group against oxidative deamination, thereby preventing the formation of carboxyprimaquine [37].

The mefloquine-resistant *P. berghei* ANKA 25R/10 strain, *Balb c* mice, and *Anopheles stephensi* mosquitoes were used throughout the course of the assay for sporogonic development. The criteria used to assess the antimalarial activity of each compound were: (i) the minimal effective dose that prevents the appearance of oocysts in the midgut of mosquitoes; (ii) the percentage of mosquitoes with oocysts; (iii) the mean number of oocysts per injected mosquito; and (iv) % of mosquitoes with sporozoites in their salivary glands. All the derivatives of **83** were able to prevent the development of the sporogonic cycles of *P. berghei* in *A. stephensi* mosquitoes at dose levels of 15 and 7.5 mg/kg. Most likely, the gametocytocidal activity of derivatives of **83** is not related to their rate of peptidase-catalyzed hydrolysis to **4**. The derivatives **83d**–**e** which are not hydrolyzed by peptidases display an intrinsic activity. In contrast, *N*-acetyl-PQ **84**, which lacks a terminal basic amino group, did not present a gametocytocidal activity. Carboxyprimaquine, which itself lacks a terminal group, is also inactive, implying that the presence of a terminal amino group is a major structural requirement for the gametocytocidal activity. Thus, the acylation of the primary amino group at C'-4 with dipeptides containing natural and non-natural amino acids, is a new approach to preventing the oxidative deamination of **4**. Also, they considered this may be useful to the design of new antimalarials based compounds that are rapidly metabolized [37].

Some peptide and amino acid derivatives of **4** and other 8-aminoquinoline antimalarials have been synthesized in order to reduce the metabolic oxidative deamination pathway, as well as to reduce the toxicity of parent drug. Despite the encouraging results, it has been shown that amino acid and dipeptide derivatives of **4** are rapidly hydrolyzed to parent drug by aminopeptidases and endopeptidases [37] suggesting that they might undergo extensive hydrolysis to the parent drug in GI tract when is orally administered. With intent to enhance the enzymatic stability of amino acid or peptides derivatives of **4** toward proteolytic degradation, Araújo and co-workers introduced an imidazolidin-4-one formation as a useful prodrug approach to protecting the *N*-terminal amino acid residue. They hypothesized that imidazolidin-4-ones derivatives **87a**–**l** (Figure 36) would release the corresponding amino acid derivative via a non-enzymatic reaction, which in turn, could be enzymatically hydrolyzed to **6** [135].

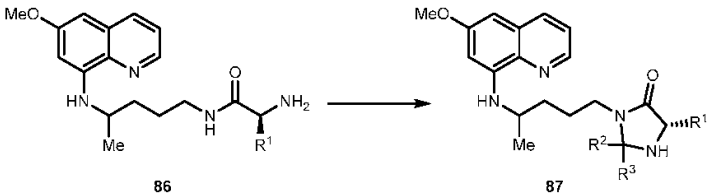

87a	R^1- H	R^2- $(CH_2)_5$	R^3- $(CH_2)_5$
87b	R^1- H	R^2- Me	R^3- Me
87c	R^1- Me	R^2- $(CH_2)_5$	R^3- $(CH_2)_5$
87d	R^1-CHPh	R^2- $(CH_2)_6$	R^3- $(CH_2)_6$
87e	R^1-CHPh	R^2- $(CH_2)_5$	R^3- $(CH_2)_5$
87f	R^1-CHPh	R^2- $(CH_2)_4$	R^3- $(CH_2)_4$
87g	R^1-CHPh	R^2- Me	R^3- Me
87h	R^1-$CHMe_2$	R^2- $(CH_2)_6$	R^3- $(CH_2)_6$
87i	R^1-$CHMe_2$	R^2- $(CH_2)_5$	R^3- $(CH_2)_5$
87j	R^1-$CHMe_2$	R^2- $(CH_2)_4$	R^3- $(CH_2)_4$
87k	R^1-$CHMe_2$	R^2- Me	R^3- Me
87l	R^1-CH_2CHMe_2	R^2- Me	R^3- Me

Figure 36. Formation of imidazolidin-4-ones derivatives of **4** (Adapted from [135]).

The hydrolysis of imidazolidin-4-one **87a**–**l** in 80% of human plasma was monitored by HPLC for the simultaneous disappearance of substrate and formation of the amino acid derivatives and **6**. With exception of compound **87b**, all imidazolidin-4-ones display unusually high stability when incubated in human plasma, with no significant disappearance of the starting material over 3 days of incubation. Results obtained by Araújo and co-workers showed that stability of **87** is not significantly affected by the R^2 and R^3 substituents in the imidazolidin-4-ones moiety. In contrast, the corresponding amino acid derivatives **87**, are hydrolyzed quantitatively to **4** with rates depending on the nature of amino acid chain [135] (Figure 37).

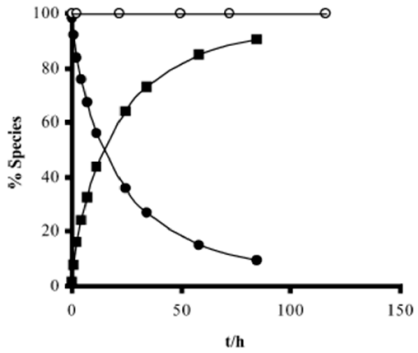

Figure 37. Time courses for components (**87c**) (○), Ala-PQ (●) and PQ (■) when (**87c**) and Ala-PQ were incubated in 80% human plasma at 37 °C (reproduced from [135]).

While simple amino acid derivatives behave as prodrugs of **4**, the corresponding imidazolidin-4-ones **87** are too stable to be considered prodrugs. In contrast to their behavior in plasma, the derivatives **87**, hydrolyze to the corresponding amino acid derivatives in pH 7.4 buffer, with half-lives ranging from 9 to 30 days. Moreover, the compounds **87** are hydrolyzed 50–100 times slower than dipeptides or pentapeptides. Araújo et al. thought that the explanation for this observation could be related to the mechanism of hydrolysis [135].

The potential of compounds **87** to prevent the transmission of malaria was studied using a method described above [37]. The parent drug and the imidazolidin-4-one derivatives **87a**–**g** (i.e., those with Gly-, Ala-, and Phe-) completely inhibited the production of oocyst at a dose of 50 μmol/kg. Although imidazolidin-4-one with Val- and Leu-, **87i**–**l**, significantly affecting the sporogonic development of *P. berghei*, it did not completely inhibit the production of oocyst at 50 μmol/kg. At dose of 10 μmol/kg, derivatives **78a**–**c** and **78j**–**l** significantly affects the number of oocysts. This activity was similar to **4** [135].

However, derivatives **87d**–**g** (derived from Phe-) and **97h**, **i** (derived from Val-) did not significantly reduce the oocyst production when compared to control. Araújo and co-workers concluded that the imidazolidin-4-ones derived from Gly-PQ **87a**–**b**, and Ala-PQ **97c** are the most effective gametocytocidal agents, displaying an antimalarial activity reported from glycine derivative of **4** [37], suggesting that incorporation of the imidazolidin-4-one scaffold does not significantly alter s the antimalarial activity. In contrast, imidazolidin-4-one **87** derived from more lipophilic amino acids Phe, Val and Leu was less active when compared to **4** [135]. Vangapandu and co-workers reported that the attachment of a hydrophobic amino acid to the terminal amino group of an analog of **4** led to decreased blood-schizontocidal antimalarial activity, suggesting that the hydrophobic amino acid side chains have a detrimental effect on the activity of 8-aminoquinoline derivatives both in blood schizonts and gametocytes [136]. Imidazolidin-4-ones synthesized are very stable both in chemical and enzymatic conditions, suggesting that they are active per se [135].

In view of the results described above, Vale and co-workers undertook the *N*1-acylation of imidazolidin-4-ones with amino acid in order to (i) fully suppress the hydrolysis of imidazolidin-4-one

ring through acylation of its *N*1 nitrogen; (ii) increase the aqueous solubility of novel compounds by insertion of basic amino acid promoieties and; (iii) potentially increase antimalarial activity, given the relevant role usually attributed to the basic amino group of **4**. A set of different structures (Figure 38) was prepared using several amino acid chains (R_1 and R_2) in order to check the influence of these substituents on compounds properties.

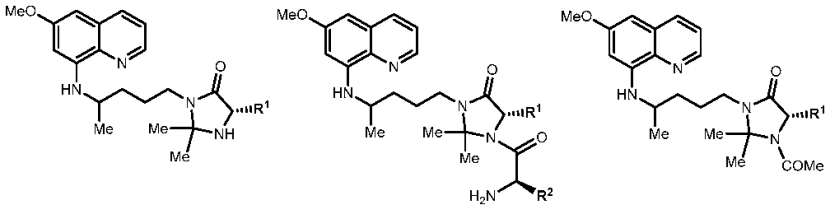

Figure 38. Structures synthesized of imidazolidin-4-one derivative of **4** and tested against *P. berghei*.

All compounds **89** were evaluated for in vitro antiplasmodial activity against the chloroquine-resistant *P. falciparum* strain W2. Results demonstrated that: (i) in vivo antiplasmodial activity of compound **89** is not significantly affected by the nature of the amino acid residue at the imidazolidin-4-one *N*1 atom; (ii) activity of compounds **89** is also not significantly affected by the nature of the R1 substituent at the C-5 position of the imidazolidin-4-one moiety **80a** and **b**, had similar values of IC_{50} contrasting with **88a** and **b** in which the incorporation of a methyl group at C-5 leads to complete loss of activity); (iii) acetylation of the imidazolidin-4-one's N1 atom leads to complete loss of activity (e.g., **90** vs. **89a**), suggesting that the presence of a basic amino group is a major requirement for antiplasmodial activity. In general, compounds **89** displayed greater cytotoxicity than **4** against A549 cells, with exception of **89a** and **89h**, which showed no toxicity. Vale and co-workers believed that the antiplasmodial activity of compounds benefits from the *N*1-acylation of the imidazolidin-4-one ring with an amino acid, which may be partly due to the presence of the primary amino group brought by the inserted amino acid residue. To assess the ability of compounds to inhibit the development of *P. berghei* schizonts in human hepatoma cells (Huh-7 cells), Vale and co-workers used fluorescence activated-cell sorting (FACS)-based method. This method is based on the measurement of the fluorescence of Huh-7 cells, following infection with GFP-expressing *P. berghei* sporozoites. At given time after injection, the percentage of parasitized cells is given by the percentage of GFP-positive events. The extent of intracellular development is proportional to the number of GFP copies in the cell, measured as the intensity of fluorescence. The hepatic anti-plasmodial activity of compounds **89** was monitored by measuring infection of Huh-7 cells incubated with various concentrations of each, 48 h after sporozoite addition. All compounds **89** displayed a marked dose-dependent effect on parasite development. Despite IC_{50} were higher than of 6, several compounds displayed marked antiplasmodial activity. The potential of compounds **89** to inhibit the sporogonic cycle of *Plasmodium* within the mosquito gut was once again studied using a model previously described [37,135]. Compounds were tested at 10 and 50 μmol/kg and although none of them was particularly good at decreasing the percentage of infected mosquitoes, all of them were active at effectively reducing the mean number of oocysts formed per infected mosquito. Moreover, while none of them was superior to **4** at the highest dose, at the lowest dose **89g** and **h** were comparable to the parent drug, and **89a** and **89f** were better than **4**. Compound **89a** significantly reduced the sporogonic development of the parasite at both doses tested, while compound **89b** was inactive at 10 μmol/kg; **89e** was clearly active but did not rank the

best of the set, in contrast to its relative activity against liver-stage *P. berghei*. Even though most of the compounds **89** were generally not as active as **4**. Nonetheless, their remarkable chemical and enzymatic stability, as well as preliminary data on ADME properties, suggest that they are promising leads toward novel hydrolytically and enzymatically stable drugs with therapeutic indices superior to those of **4** [137].

Recently, a novel series of side chains modified 4-amino-quinolines with a reduced amide bond (Figure 39) were developed and its antimalarial activity was assessed on both chloroquine-sensitive (3D7) and chloroquine-resistant (K1) strains of *P. falciparum* [138]. Although chloroquine (**91**, Figure 39) is an important therapeutic agent against malaria, *P. falciparum* strains resistant to **91** has emerged through years in endemic areas [139]. Thus, it is necessary to develop or improve chemotherapeutic agents in order to prevent resistance.

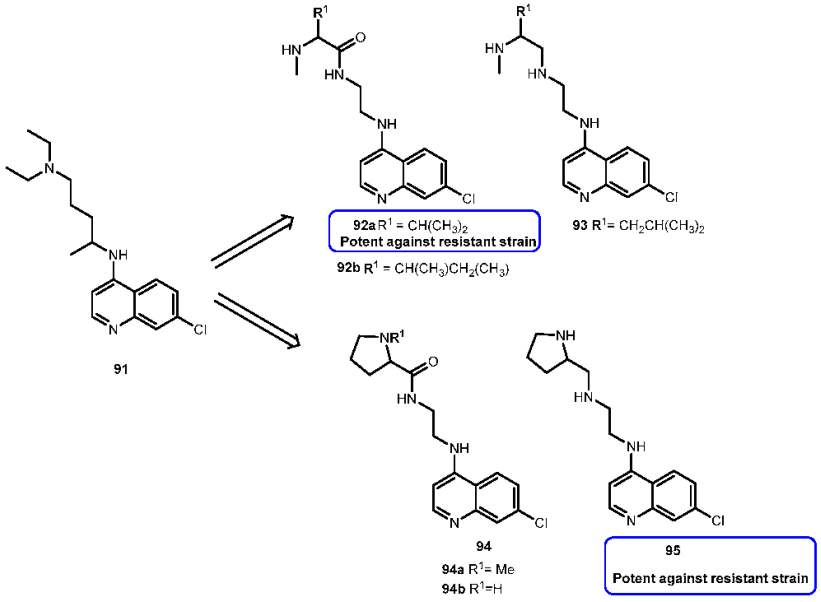

Figure 39. Chloroquine (**91**) and its side-chain modified 4-aminoquinoles (**92**–**95**). Derivative **95** was the most potent against resistant strain wheres **92a** was the most potent against the sensitive strain.

The novel derivatives of **91** designed in order to increase lipophilicity and antimalarial activity. Since amide bond is unstable on biological milieu it was hypothesized that its reduction increased the lipophilicity and therefore might enhance theirs in vivo activity. Yet, so far, the authors did not evaluate the antimalarial activity in vivo. Regarding in vitro activity, the derivatives with a basic nitrogen atom at the side chain showed significant antimalarial activity. The most promising compounds tested, **92a** and **b** showed significant inhibition (IC_{50} 0.28 and 0.31 μM) of parasite growth against K1 of *P. falciparum* whereas compounds **93**, **94b** and **95** (IC_{50} 0.18, 0.22 and 0.17 μM) exhibited a higher activity against this strain as compared to reference drug, **91** (IC_{50} 0.255 μM) [138]. Apparently, the introduction of the methyl group in the side chain (e.g., **94a**) results in increased activity against the 3D7 strain. In fact, this derivative showed better activity than **91** against K1 of *P. falciparum*. The novel derivatives demonstrated less cytotoxicity when incubated in VERO cells and higher selectivity index. It was also demonstrated that all derivatives formed a strong complex with hematin and inhibited the β-hematin formation in vitro, suggesting that they act as heme polymerization target [138]. These results suggest that these derivatives might be promising for further lead optimization in order to obtain novel compounds against resistant strains of *P. falciparum*.

3.3.3. Leishmaniasis

Visceral Leishmaniasis (VL) is the most severe form of the disease, being fatal if untreated [139]. Currently, there are no effective vaccines to prevent *Leishmania* infections and, therefore, management of VL relies on chemotherapy with first-line drugs (e.g., pentavalent antimonials) second-line drugs (e.g., pentamidine) or its lipid formulations and miltefosine [140]. However, these drugs have several problems as specific toxicities, elevated costs, prolonged treatment regimens, low patient compliance, and parasite resistance [141]. The antimalarial **4** is known to exhibit activity against visceral leishmania.

In light of previously relevant findings about peptidomimetic derivatives of **87** [135,137], Vale-Costa and co-workers evaluated the compounds previously synthesized as imidazolidin-4-one derivatives **89a**–**c**,**f**–**g**, PQ-Pro-AA derivative (**96**) and ferrocene derivatives of **4** (**97**–**98**, Figure 40), against both the promastigote and intramacrophage amastigote forms of *Leishmania infantum*, the agent of Mediterranean visceral leishmaniasis.

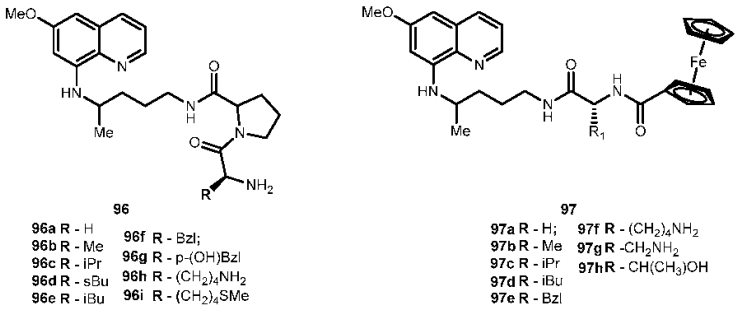

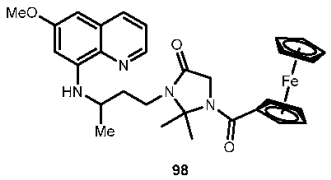

Figure 40. Peptidomimetic derivatives, imidazolidin-4-one derivatives and Ferrocene derivatives of **4** evaluated *for Leishmania infantum*.

Among the compounds tested, compounds **89c** and **96c** were the most active with IC_{50} similar to **6**. Although these compounds are among the derivatives of **6** with the highest lipophilicity values, there was no direct correlation between clogP values and IC_{50}. Compounds **89c** and **96c** are closely related, as compound **96c** is the imidazolidin-4-one peptidomimetic surrogate of dipeptide derivative **84c**, suggesting that valine residue common to the two derivatives is beneficial for in vitro antileishmanial activity against promastigotes [142].

When the compounds were tested for antileishmanial activity inside macrophages using **4**, sitamaquine and miltefosine as reference drugs, compound **96c** was much more active than compound **89c**. This might be related to the fact that compound **89c** is more susceptible than compound **96c** to proteolytic degradation and the fact that protease activity is increased in Leishmania-infected macrophages. Hypothetically, proteolytic degradation would cause the cleavage of the dipeptide moiety in compound **96c**, leading to release of **6**. If this was the case, compound **89c** would be expected to display an activity similar to the parent drug, which did not occur. This fact might be due to macrophage metabolization of compound **89c**, but not **6** or **96c**, to originate a compound which is more toxic to *L. infantum*.

Afterwards, Vale-Costa and co-workers, evaluated the efficacy of compound **87c** in a mouse model of VL which was as effective as **4**, at low doses, at reducing hepatic parasite loads, with no

evidence of negative side effects. It was possible observed that peptidomimetic derivatives of **4** were less prone that **6** to metabolic conversion mediated by rat liver enzymes. The peptidomimetic derived **89c** displays higher in vivo antileishmanial activity, lower toxicity, and higher stability compared to its parent drug [142].

Concerning the ferrocenes (Fc) derivatives of **4** (i.e., **97**, **98**), the results obtained for promastigotes were very variable, reflecting the structural diversity of these organometallic compounds. Compounds **97a**–**h**, where **4** is linked to Fc through a variable amino acid spacer, was generally not very promising. One of the most active compounds against *L. infantum* promastigotes was compound **98**, with an activity comparable to that of miltefosine. This is interesting since this compound includes structural modifications imidazolidin-4-one and Fc moiety, which can be seen as an organometallic surrogate of peptidomimetic compound **89**. Similar to peptidomimetics, the most promising organometallic derivatives of **4** against promastigotes were tested in intramacrophagic amastigote form from *Leishmania*. Compound **98** revealed a significant activity in this setting. Nonetheless, the most striking observation was related to the potent activity of **97a** against amastigotes that was not differen from miltefosine. Thus, the presence of an imidazolidin-4-one ring seems to be not necessary for intramacrophagic activity in the case of organometallic derivatives. Most likely the joining of the constrained cyclic imidazolidin-4-one motif with the bicyclic Fc in compound **98**, represents a structure too large or too stiff to easily enter the macrophage and/or the amastigote. By removing the imidazolidin-4-one ring (as in compound **97a**) such problem might be minimized or eliminated, explaining the higher activity of compound **97a** comparatively to **98**. Since these compounds, have interesting or highly potent activities combined with very low toxicity for host cells, they should be considered as leads for the development of a novel and safer antileshmanial derivatives of **4** [142].

3.4. Bacterial Diseases

The increasing incidence of infections caused by the rapid onset of bacterial resistance to available antibiotics is a serious health problem. As multidrug-resistant bacterial strains proliferate, the need for effective therapy has stimulated research into the design and synthesis of novel antibacterial/antimicrobial agents [143].

3.4.1. Gram(+) and Gram(−) Microorganisms

Cell permeating antimicrobial agents can potentially play an important role in eliminating infections by intracellular pathogens. Unfortunately, many antibiotic classes do not penetrate the plasma membrane effectively [144].

Ibrahimi and co-workers synthesized amino acid conjugates of fluoroquinolone, ciprofloxacin and norfloxacin, metronidazole and sulfadiazine, and screened for their activity against *Staphylococcus aureus*, *Escherichia coli*, *Pseudomonas aeruginosa* and *Bacillus subtilis*. These strains were used due to their pathophysiological relevance and close relation to pathogenic strains related to human diseases. The antibiotics chosen for chemical modification have a wide range of activity [144]. All agents are considered broad-spectrum antibiotics with activity against Gram(+) and Gram(−) bacteria. However, they present some limitations, for example, fluoroquinolones can cause adverse reactions in central nervous system, skin and gastrointestinal tract [145].

Several conjugation drugs showed greater inhibitory activity compared to the parent drug, which may be a result of several independent or combined mechanisms. Probably, the conjugate may increase the concentration of the compound inside the cell and block the compound sites that interact with antibacterial resistance proteins, thus preventing the inactivation of the drug. Lipophilicity is higher for conjugates comparatively to the corresponding parent antibiotic, which is important since it is believed that the strong lipophilic character of a drug plays an essential role in producing an antimicrobial effect, being related to membrane permeation in biological systems [144].

Ciprofloxacin (**99**) and its conjugates (**100a**–**c**) Figure 41) were screened and showed growth inhibition in all strains. At lower concentrations, **99** demonstrated to be highly active and might be

considered a much more potent antibiotic. Despite the good activities, this conjugate family showed a variable result among strains, where **100a** and **100b** inhibited over 90% of growth in *B. subtilis* and **100b** did not show significant inhibition in any strain and **100a** only inhibits 50.26% of growth in *S. aureus* [144].

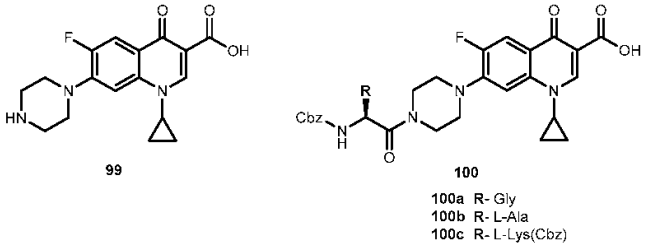

Figure 41. Structures of ciprofloxacin (**99**) and amino acid ciprofloxacin (**100a–c**) conjugates.

Norfloxacin (**101**, Figure 42) inhibited the growth of all screened strains but the strength of its conjugates is variable among bacteria strains. At 60 μg/mL, conjugates **102a–d** inhibited a higher percentage of *S. aureus* growth than the parent antibiotic whereas in *P. aeruginosa*, only **102a** shows activity [144].

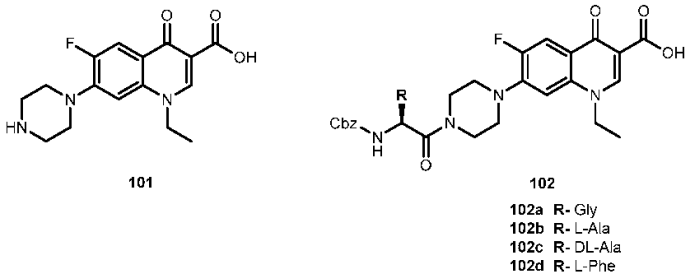

Figure 42. Structures of norfloxacin (**101**) and amino acid norfloxacin conjugates (**102a–c**).

The pipemidic acid derivatives of **102** (Figure 43) were active only against Gram(+) bacteria as *S. aureus* and *B. subtilis*. *B. subtilis* showed high sensitivity to all pipemidic conjugates at a concentration 40 μg/mL. Prodrugs **103a** and **103e** also presented higher growth inhibition than the parent antibiotic. At a fixed dose 200 μg/mL, *S. aureus* showed the greatest sensitivity to conjugates **103c** and **103d** [144].

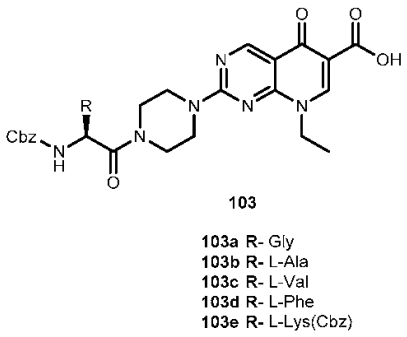

Figure 43. Structures amino acid pipemidic conjugates (**103a–e**).

Finally, metronidazole (**104**), sulfadiazine (**105**) and conjugates (**106–107**, Figure 44) did not inhibit the growth of any strain [144].

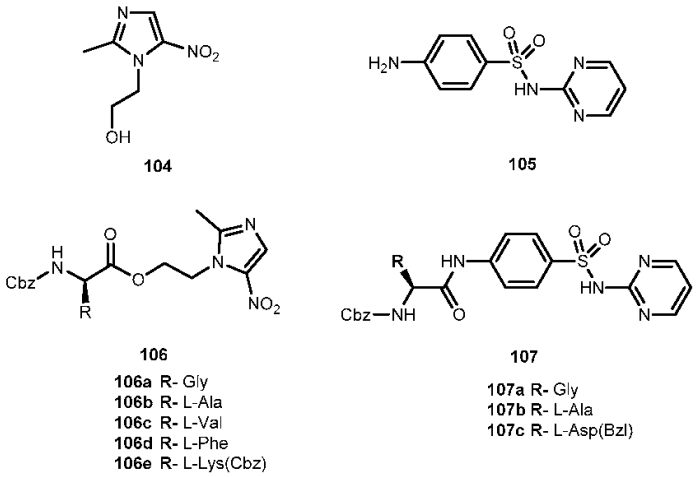

Figure 44. Structures of metronidazole (**104**) and its conjugates (**106a**–**e**) and sulfadiazine (**105**) and its conjugates (**107a**–**c**).

Ibrahimi and co-workers considered that the inclusion of amino acids in antibiotics, may provide alternative options for treatment of bacterial-resistant strains, with the benefit of increasing drug uptake and/or eliminate or alleviate adverse side effects [144].

3.4.2. Tuberculosis (TB)

The emergence of drug-resistant tuberculosis worldwide is alarming [146]. It is estimated that one-third of the world's population is currently infected with *Mycobacterium tuberculosis* (*M. tuberculosis*), and every year 8–9 million new cases arise. In addition, almost 500,000 people per year are infected with multi-resistant TB (MDR-TB) and 40,000 new cases of drug-resistant TB (XDR-TB) are estimated. XDR-TB was defined as a resistance to any fluoroquinolones and to at least one of the three injectable drugs capreomycin, kanamycin or amikacin. Moreover, unlike MDR-TB, XDR-TB is often untreatable. In addition, HIV co-infection with MDR-TB in immunocompromised patients is a serious challenge. Therefore, it is urgent develop novel types of drugs or prodrugs with a new mechanism of action [147].

A novel series of halogenated salicylanilides and *N*-acetyl-*L*-phenylalanine (**108a**–**k**, Figure 45) were synthesized and their antibacterial activity was assessed against *M. tuberculosis* including MDR-TB strains and atypical mycobacteria [148].

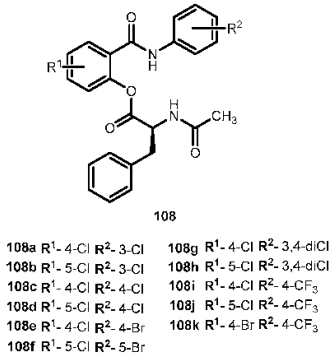

Figure 45. Structures of halogenated salicylanilides and *N*-acetyl-L-phenylalanine tested against *M. tuberculosis* strains [148].

The novel esters showed high antituberculous activity (minimum inhibitory concentration, MIC 0.25 μmol/L). Generally, the compounds synthesized were more active than the starting salicylanilides, with exception for **108j** that was less active. The derivatives **108c** and **108d**, that present similar MIC values, were more active on *M. tuberculosis* than salicylanilides, in some cases MIC decrease 8-fold (e.g., **108e**, **g** and **92i**) [148]. As mentioned, it seems that lipophilicity influences the activity, but the relationship is not direct. In general, the most lipophilic **108g**, **i**, **k** and partly **e** showed the highest anti-mycobacterial activity [148].

The MDR-TB results (MIC 1–2 μM) of **108 g**, **k** and **i** suggesting that they might be promising candidates for MDR-TB treatment. Comparing **108i** and **k**, the late had almost the same antitubercular efficacy as **108i**. Based on these results, Krátý and co-workers considered **108k** an optimal candidate for further investigation as a promising antimycobacterial agent. In general, to increase the activity against bacteria it seems that the most convenient substituents are 4-CF_3 (e.g., **108i** and **k)** and 4-Br (e.g., **108f**). Through comparison of substituents on the salicylic ring, those that present 5-Cl rather 4-Cl are more active against bacteria, with exception of **108i**. Therefore, some of these esters could be potential agents against Gram-positive infections [148]. Considering the results, salicylanilides of *N*-acetylphenylalanine esters could be a new highly active group with promising wide-range antibacterial activity [148].

3.4.3. Leprosy

Dapsone (diamino-diphenyl sulfone) (**109**, Figure 46) is a bacteriostatic and antileprosy agent with a low aqueous solubility. In order to overcome this limitation, Pochopin and co-workers developed novel amino acid amides derivatives of dapsone **110a**–**m** (Figure 46).

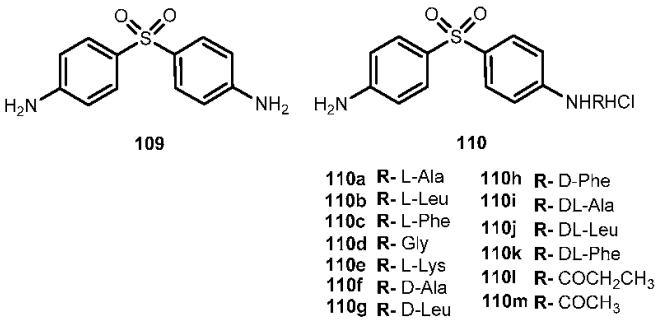

Figure 46. Structures of dapsone (**109**) and its amino acid amines derivatives (**110a**–**m**).

Through chemical stabilities studies of prodrugs, the only degradation product observed at any pH value was the parent drug, suggesting that no other routes of degradation apart from hydrolysis of the amide bond occur [149]. The addition of the amino acid residues to **109** resulted in improvement of 2–3 orders of magnitude in water solubility for the HCl salts, with exception of *L*-Phe-dapsone **110c**. *L*-Lys-dapsone **110e**.The greatest solubility over the widest pH range might be due to the ionizable α-amino which is protonated at physiological pH. The derivatives **110a**–**e** were all substrates for leucine aminopeptidase. The corresponding *D*-amino acid derivatives were completely stable in the presence of leucine aminopeptidases over 8 h, which is consistent with the specificity of leucine aminopeptidases for amino acids in *L*-configuration, excluding glycine, which does not have a chiral center. Hydrolysis of **110a**–**e** to **109** occurred in human plasma and human, rat, and rabbit blood. Of all compounds studied, derivative **110e** presented the best results concerning to half-life (>2 years at pH 4) and is rapidly and quantitatively hydrolyzed in the systemic circulation after intravenous administration. Therefore, **110e** might a good prodrug example for further development of other poorly soluble amides [149].

3.5. Brain and Central Nervous System (CNS) Diseases

Currently, one of the most significant challenges in pharmaceutical research is the development of new drugs targeting the central nervous system (CNS). Despite recent advances in brain research, adequate efficient drug therapies against many CNS disorders have not been discovered. A successful treatment of the CNS diseases requires not only the identification of appropriate targets within the CNS but also strategies to improve the transport of therapeutics across the relatively insurmountable blood brain barrier (BBB) into the CNS at sufficient levels to achieve the desired effect. It has been estimated that more than 2% of the small molecular weight drugs and practically none of the large molecules weight drugs developed for CNS disorders cross the BBB at adequate levels [150]. The carriers for glucose (glucose transporter 1,GLUT1) and large amino acid (LAT1), have been found to have a sufficiently high transport capacity to hold promise for significant drug delivery to the brain [151,152].

3.5.1. Epilepsy and Bipolar Disease (Anticonvulsants)

Epilespsy is not one condition, but a complex set of cerebral disorders that in common the occurrence and recurrence of seizures [153]. Nowadays, about 65 million people worldwide live with epilepsy, and only 70% of them control the seizures with the available medication [154], at expenses of the significant adverse side effects that increase their toxic actions when a lifelong medication is required [155]. The remaining 30% of patients are still resistant to anticonvulsant drugs [156].

Recently, a novel series of β-alanine derived sulfamides (**111**–**116**), and derivatives that had *L*-valine and *L*-phenyl alanine skeleton (**117**,**118**) instead β-alanine moiety of methyl [*N*-(*p*-fluorobenzyl)-sulfamoyl]-β-alaninate were synthesized and assessed for maximal electroshock seizures (MES) (Figure 47).

Despite all the derivatives showed protection against the maximal electroshock seizure test in mice at the lowest dose tested (30 mg/kg). They did not show significant protection against chemical-induced convulsion by pentylenetretrazole (PTZ) [157]. It should be pointed out that most of the structures did not induce toxic effects, which support the use of amino acids for design and development of novel anticonvulsant compounds. Based on biological results, it seems that the substitution of the sulfamide moiety by branched alkyl groups lead to increase of anti-MES activity [157].

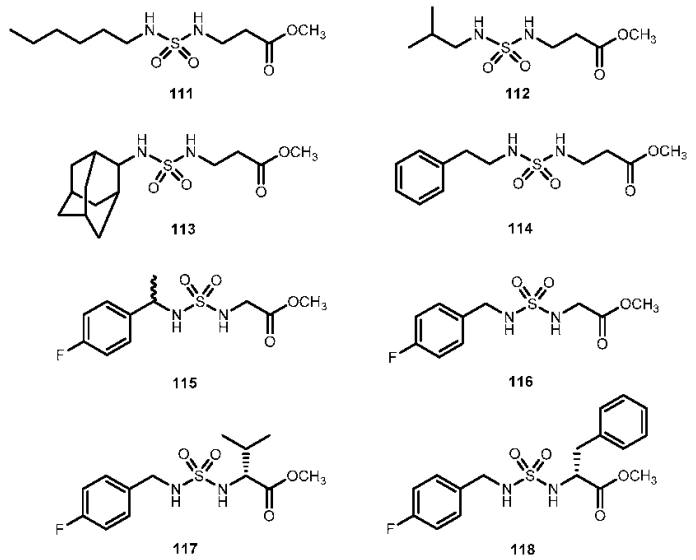

Figure 47. Amino acid derived sulfamides evaluated on maximal electroshock seizure.

Peura and co-workers synthesized and evaluated novel ester *L*-phenylalanine amide and ester prodrugs (**120a**–**b** and **121a**–**b**) of valproic acid (**119**, Figure 48), an anticonvulsant used in the treatment of epilepsy and bipolar mania which is extensively bound to plasma proteins, metabolize to toxic species in the liver and is assymmetrically transported across the BBB [158–160]. The main aim of Peura and co-workers was to demonstrate the potential of the amino acid as carriers for the drug targeting the CNS via LAT1 [161].

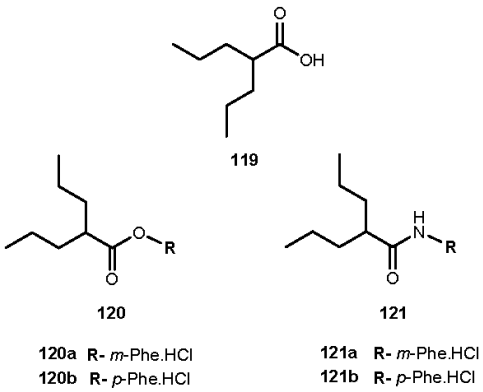

Figure 48. *L*-Phenylalanine amide (**121a**–**b**) and ester prodrugs (**120a**–**b**) of valproic acid (**119**).

The stability of the prodrugs synthesized was evaluated in aqueous buffer (pH 7.4) and their bioconversion to the parent drug was determined in rat brain (20%), rat liver homogenates (50%) and human plasma (75%). All prodrugs demonstrated adequate chemical stability. Ester derivatives **120a**–**b** were rapidly hydrolyzed to parent drug in tissue homogenates and plasma. On the other hand, the enzymatic hydrolysis of amides **121a**–**b** in brain, liver homogenates and plasma resulted only in a slight degradation of the prodrugs in vivo. Although the biodegradation of **121a**–**b** was determined to be quite slow, Peura and co-workers thought that was reasonable to determine their transport-binding mechanism and the brain uptake. In fact, the slow release of an active drug in CNS might provide a sustained therapeutic effect for a prodrug [161].

The transport mechanisms across the BBB and the LAT1 affinity of the prodrugs **120a**–**b** and **121a**–**b** as well the amount of the prodrug uptake into the brain were determined by using the modified in situ rat brain perfusion technique. All prodrugs were able to bind the LAT1 at the BBB. The regioselective positioning of valproate in the *L*-phenylalanine structure significantly affects the binding of the prodrug to LAT1. There were no significant differences between the affinities to LAT1 whether **119** was linked to the promoiety by amide or ester bond. However, a significant difference between affinities of the prodrug to LAT1 was observed when **119** was linked to the para- or meta-position of *L*-phenylalanine promoiety. The affinities of **120a** and **121a** were more than 10-fold compared with those of **120b** and **121b** [161].

Reversibility of the prodrugs by rat LAT1 was also examined to confirm that prodrugs do not inhibit the LAT1 transport irreversibly since this parameter is an essential requirement for the brain uptake of prodrugs via specific transporters. Thus, total amounts of all the prodrugs in the brain after the in situ rat brain perfusion were studied to confirm that all prodrugs do not only bind to LAT1 but are also transported across BBB into the brain. The valproate prodrugs were able to cross the rat BBB and gain entry into the brain [161].

Amide prodrugs **120b** and **121b** were shown to cross the rat BBB more efficiently than the esters **120a** and **121a**. These difference between these two groups of compounds may be due to the exposure of the esters to the degrading enzymes at the BBB during the perfusion. Nonetheless, the difference between the rate of uptake of **120b** and **121b** is not significant and could be explained according to their affinities. One plausible explanation for the limited uptake capacity of prodrug

120a may be related to steric restriction. In addition, this prodrug may strongly bind to LAT1 that it does not leave the transporter relatively as easily as prodrug **121b**. Thus, *L*-phenylalanine derivatives, especially substituted in meta-position of the phenolic group could be highly used as prodrug designed for LAT1-mediated CNS delivery of small molecular weight drugs with poor brain penetration properties [161].

More recently, seven amino acids prodrugs of **119** targeted for LAT1 were evaluated in order to provide insights related to brain uptake and systemic pharmacokinetics of parent drug. In general, all prodrugs presented affinity for LAT1, with prodrugs that were derivatized at the *meta*-position of phenylalanine moiety exerting higher inhibitions than prodrugs that were derivatized at the *para*-position. Their bioconversion in vitro revealed that ester prodrugs (**122**–**125**, Figure 49) were converted to parent drug in rat and human-derived biological media more effectively than their corresponding amide prodrugs **121a**, **121b** and **126** (Figure 49).

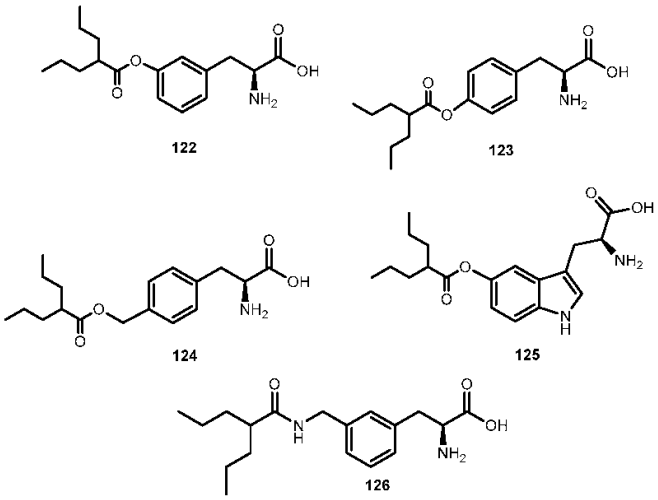

Figure 49. Chemical structures of amino acid esters (**122**–**125**) and amide prodrug (**126**) of **119** studied by Gynther et al. [161].

Since esters prodrugs were too unstable to be studied in a rat model, only the corresponding uptake of amides was assessed in vivo. The amide prodrugs bound to human plasma proteins to a greater than **119** and this linkage is independent of prodrug concentration. It was also demonstrated that amide prodrugs were delivered into the brain after intravenous bolus injection of equivalent doses. One of amide prodrugs, **126**, achieved a great brain uptake and high selectivity for LAT-1 and released parent drug slowly into the brain. Therefore, this prodrug has a great potential to stabilize the parent drug concentration within the brain [162].

Gabapentin (**127**, Figure 50) is a structural analog of GABA (gamma amino butyric acid) used for the treatment of epilepsy [163] and postherpetic neuralgia [164]. The drug has structural features of amino acids and has also shown efficacy in the treatment of anxiety disorders [165] and diabetic neuropathy [166]. The bioavailability of **127** is dose-dependent, decreasing from approximately 60% (at a 300 mg dose) to 35% or less (at doses are used to treat neuropathic pain). The underlying mechanism of this dose dependence is thought to be saturation of absorption of **127** that occurs in the intestine [167]. The absorption of **127** in the upper small intestine is mediated by the low-capacity solute transporter, possibly an L-type amino acid transporter. Following oral absorption, the drug is rapidly excreted in urine and therefore, **127** must be administered three or four times per day to maintain therapeutic levels [168]. Efforts to develop a sustained release formulation for **128** have failed, primarily due to the lack of significant absorption of the drug in the large intestine [169].

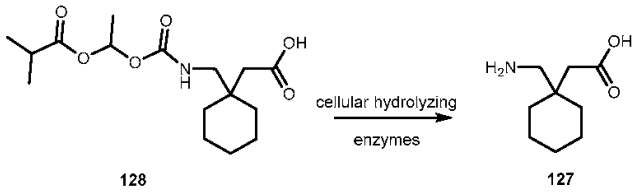

Figure 50. Bioconversion of XP13512 (**128**) to parent drug (**127**) by cellular hydrolyzing enzymes (Adapted from [4]).

The prodrug of **127** was stable at physiological pH but was rapidly converted to the parent drug in intestinal and liver tissues from rats, dogs, monkeys, and humans. In addition, **128** was not a substrate or inhibitor of major cytochrome P450 isoforms. The prodrug had an active apical to basolateral transport across Caco-2 cell monolayers and pH-dependent passive permeability across artificial membranes. In addition, it inhibited the uptake ^{14}C-lactate by human embryonic kidney cells expressing monocarboxylate transporter type 1 (MCT-1) as well as inhibited uptake of ^{3}H-biotin into Chinese Hamster Ovary cells overexpressing human sodium-dependent multivitamin transporter (SMV1), suggesting that transport of prodrug is mediated through these transporters [170].

Baclofen (**129**, Figure 51) is a racemic $GABA_B$ receptor, used for treating spasticity and other neurological diseases. Similar to **127**, **129** has structural features of amino acid. In humans, **129** is rapidly absorbed after oral administration and the drug is rapidly eliminated, largely unchanged, via renal excretion. Moreover, it is only absorbed in the upper small intestinal by the saturable active transport mechanism. Similarly to **128**, **129** needs to be administered frequently to maintain its therapeutic effects [171]. In order to overcome these limitations, Lal et al. developed a new prodrug of **129**, XP19986 (**130**, Figure 51), which is a pharmacologically active *R*-isomer of **129**. Unlike the parent drug, this prodrug was designed to be well absorbed from the colon, allowing the drug to be delivered in a sustained release formulation that may reduce the frequency of administration and reduce fluctuations in plasma exposure. This, in turn, may lead to improved efficacy through a combination of a greater duration of action, greater subject convenience and therefore, adherence, and improved safety profile compared with **129** [172].

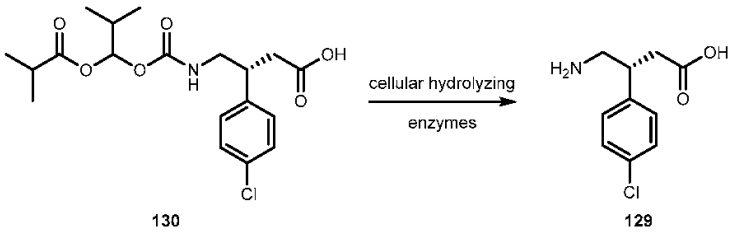

Figure 51. Bioconversion of XP19986 (**130**) to *R*-baclofen (**129**) by cellular hydrolyzing enzymes (adapted from [4]).

The prodrugs **128** and **130** (of **127** and **129**, respectively) further exemplify the utility of amino acid prodrugs targeted to transporters other than oligopeptide transporters expressed in the gastrointestinal tract [4].

The anticonvulsant carbamazepine (**131**, Figure 52) is the most frequently prescribed first-line drug for the treatment of partial and generalized tonic-clonic epileptic seizures [173]. It is effective as a treatment of epilepsy in the majority of cases, but it hampers the parenteral administration of the drug [174]. It has been reported that **131** has slow and somewhat erratic oral absorption and presents incomplete oral bioavailability in some cases. Hemenway and co-workers synthesized a novel water-soluble analog of **131**, *N*-Gly-CBZ (**132**, Figure 52) where the amino acid glycine has been linked to the urea nitrogen of parent drug, leading to a peptide link acyl urea functionality. The stability of

132 was found to range over four orders of magnitude with the greatest stability in the pH range 3–4 where an injectable solution of >50 mg/mL of **131** equivalent (697 mg/mL) appeared to be possible. The introduction of *N*-Gly increased the aqueous solubility of the parent drug. However, due to its chemical instability ($t_{90\%}$ = 5.9 days at pH 4.0, 25 °C), the parenteral formulation of prodrug was limited only to the freeze-dried product for reconstitution prior to use [175]. The enzymatic stability in vivo performance of **132** in rats after oral administration was evaluated by Hemenway and Stella [176].

The stability of the prodrug in rat blood and plasma was adequate to ensure minimal *ex-vivo* conversion during blood sample processing and analysis, allowing pharmacokinetic studies to be conducted in rats. The prodrug was readily converted to the parent drug following IV administration to rats (Figure 51).

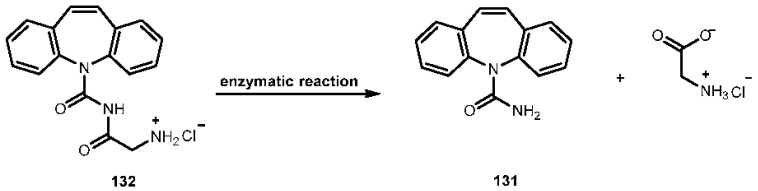

Figure 52. Bioconversion of *N*-Gly-CBZ (**132**) to CBZ (**131**) in vivo (Adapted from [4]).

The rate of appearance of **131** following IV administration of the prodrug was approximated by a $t_{1/2}$ value of about 1 min, which is very similar to the $t_{1/2}$ value for prodrug elimination. The prodrug gives an equivalent dose of the parent drug compared to an equimolar dose of **131** as control following IV dosing. This result is consistent with **132** acting as a viable prodrug candidate with rapid and complete conversion to the parent drug using the rat animal model. The oral administration of **132** resulted in the appearance of plasma levels of **131** but not prodrug in rat blood samples. It appears that most of the conversion occurs prior to **132** reaching systemic circulation. It is likely that a high degree of **132** bioconversion to **131** occurs in GI tract, facilitated by non-specific peptidases present in high levels in the lumen and at the brush border of intestinal mucosa. The prodrug also demonstrated superior oral bioavailability due to its greater aqueous solubility [176].

Another prodrug of **131**, *N*-cysteamine carbamazepine (**133**, Figure 53), has also been developed for IV use. The aqueous solubility of the *N*-cysteamine derivative exceeded 100 mg/mL, at pH 2.6, and its predicted shelf-life ($t_{90\%}$) was 320 days, at pH 4.0 and 25 °C. After an IV dose of **133** in rats, the parent drug was immediately seen in plasma, whereas no intact drug was observed, suggesting that the conversion of prodrug to parent drug occurred rapidly and most probably via reaction with glutathione (Figure 53) [177].

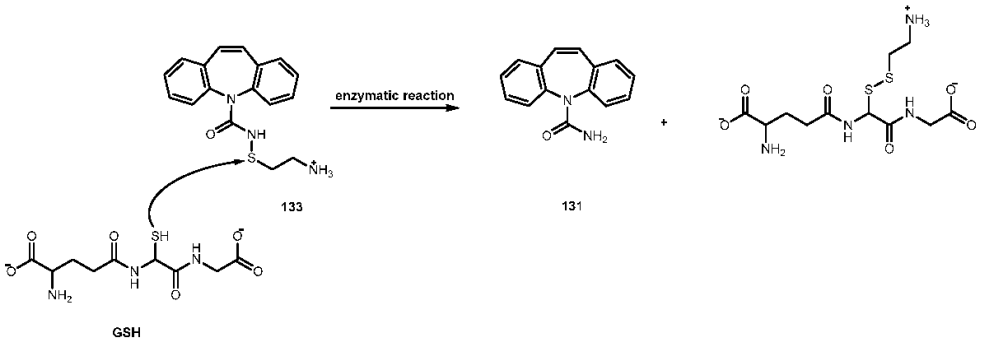

Figure 53. Possible conversion mechanism of *N*-cysteamine carbamazepine **(133)** to the parent drug **131** by the nucleophilic attack by GSH (adapted from [4]).

3.5.2. Anxiety Disorders

LY354740 or eglumetad (**134**, Figure 54) was an investigational drug, which was expected to be useful in the treatment of many psychiatric diseases, including psychosis and anxiety [178]. However, due to its low membrane permeability, **134** presents limited oral bioavailability. In order to overcome this limitation, an amino acid prodrug was developed, LY544344 (**135**, Figure 54), by introducing an alanyl promoiety attached to the amine of the parent drug.

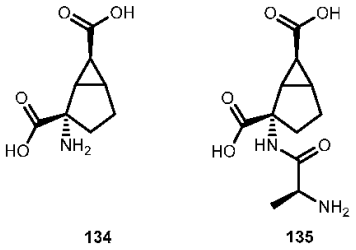

Figure 54. Chemical structures of LY354740 (**134**) and its amino acid prodrug LY544344 (**135**).

After oral administration of **135** there was a 10-fold increase in brain, plasma and cerebrospinal fluid (CBS) concentrations. The rate of increase in **134** concentration was faster in dose group of **135**, consistent with rapid intestinal absorption of the prodrug via active PepT1-mediated transport. Initial uptake of parent drug into the brain was similarly rapid, but there was a large period of at least several hours between the peak concentrations in plasma and brain. Despite the rapid appearance of parent drug in the CNS, the concentrations were relatively low in brain and CSF compared with plasma, indicating limited passive penetration of **134**. Furthermore, Rorick-Kenh and co-workers compared the oral efficacy of the **134** and its prodrug in rodent models of psychosis and anxiety. Orally administered prodrug (30 mg/kg) and subcutaneously administered parent drug (10 mg/kg) were able to attenuate stress-induced hyperthermia in DBA/2 mice, with the prodrug producing anxiolytic effects at lower oral doses than the parent drug. Oral administration of parent drug did not significantly affect fear-induced suppression of operant responding in rats. However, subcutaneously administration of **135** and orally administered prodrug produced significant anxiolytic effects in this model [179].

Varma and co-workers attempted to elucidate the mechanism of intestinal absorption of **134** and its prodrug **135**. Transport of both compounds was affected by P-glycoprotein-mediated efflux, as shown in transport and uptake inhibition studies in MDCK multidrug resistance 1-transfected cell line and inverted membrane vesicles. Their results suggest that prodrug is (i) a substrate for the intestinal apical uptake PepT1 transporter and for enterocytic peptidase(s) that cleave the peptide bond to release parent drug; (ii) has an affinity for specific efflux transporter present on the apical membrane; and (iii) is able to use the paracellular pathway. The **134** has limited entry into enterocytes and its transepithelial transport is via the paracellular pathway [180]. Despite these results, the clinical development of **135** was recently discontinued [4].

3.5.3. Attention Deficit/Hyperactivity Disorder (ADHD)

Lisdexamfetamine dimesylate (LDX, Vyvane®, **136**, Figure 55) is an *L*-lysine amino acid amide prodrug which is used as a psychostimulant for attention-deficit/hyperactivity disorder, a neuropsychiatric condition, in children aged 6–12 years and adults [181]. Unlike other formulations that rely on mechanical release of the active drug that may be affected by GI factors, such as transit time and pH, **136** is a prodrug that has a biological mechanism of drug delivery that uses enzymatic hydrolysis to convert the therapeutically inactive molecule to the active drug, *D*-amphetamine (**137**, Figure 55). The naturally occurring amino acid *L*-lysine is a by-product of the hydrolysis [182].

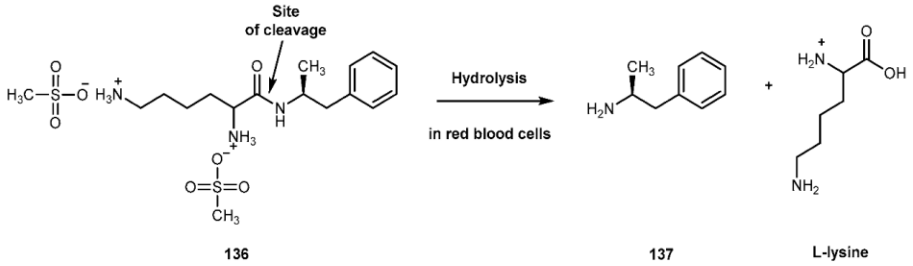

Figure 55. The enzymatic conversation of LDX (**136**) to active *D*-amphetamine (**137**) (adapted from [182]).

The prodrug has been shown to provide a long duration effect allowing a once-daily dosing [183] and is the only prodrug available for treatment of ADHD. Therefore, it is important to understand the absorption and enzymatic conversion of intact **136** to the active moiety, **137**. With this in mind, Pennick conducted studies in order to investigate the absorption and enzymatic conversion of **136** in rat and human tissues and cell culture models [182].

Pharmacokinetic studies in portal and jugular vein-cannulated rats showed that after administration of a single dose of **136**, intact prodrug was rapidly absorbed from GI tract. **137** was measurable in both portal and systemic plasma shortly after dosing, suggesting a rapid conversion of **136** to **137** in both portal and systemic circulations, peaked between one and two hours post dosing. The post blood levels of **136** were approximately 10-fold higher than systemic levels, indicating the occurrence of pre-systemic conversion of **136** to **137** in a rat model. The absorption of **136** likely occurs via high-capacity carrier-mediated transport system involving PepT1 in the small intestine. The subsequent metabolism of the drug to its active metabolite by red blood cells also appears to be via the high-capacity system. Thus, saturation of enzymatic conversion of **136** in the blood is unlikely to occur at therapeutic doses. The findings of high-capacity absorption and enzymatic conversion may contribute to the consistent and reproducible pharmacokinetic profile of **136** in humans. The biotransformation process, and not the dissolution of intact **136**, appears to control the rate of delivery of active **137** [182].

3.5.4. Parkinson's Disease (PD)

Parkinson's Disease is a degenerative disorder of the CNS that presents with resting tremor, bradykinesia, postural instability, and rigidity and is associated with the loss of dopamine (**138**, Figure 56) in the nigro-statal dopamine system [184]. Prodrugs of **138** were developed since several pharmacokinetic problems were found in its use to treat Parkinson's disease. First, both amino-terminal and the catechol hydroxyl groups of **138** are rapidly and extensively metabolized after oral administration. Furthermore, **138** is largely ionized, and thus, it is not able to cross the BBB via passive diffusion [185].

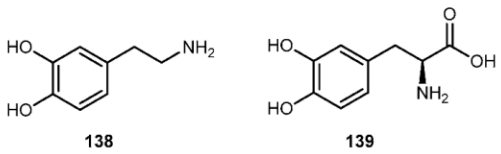

Figure 56. Chemical structure of dopamine (**138**) and its prodrug levodopa (**139**).

Levodopa (**139**, Figure 56) is the only clinically used prodrug of **138** that is transported into the brain via LAT1-transporters as a "pseudonutrient". The "pseudonutrient" structure of **139** is metabolically transformed to the parent drug in the brain, while its metabolic transformation in peripheral tissues is prevented by simultaneous administration of peripheral

inhibitors of **139** metabolizing enzymes, i.e., aromatic *L*-amino acid decarboxylase (AADC) and catechol-*O*-methyltransferase (COMT). The need for these inhibitors complicates treatment with **139**. Furthermore, chronic treatment with **139** has many problematic pharmacokinetic obstacles, e.g., extensive metabolism, plasma fluctuations, erratic oral absorption and variability in the extent of the first-pass effect. In advanced Parkinson's disease, an extensive loss of nigrostriatal dopaminergic neurons leads to a significant decreased of AADC activity that is essential to convert **139** to **138**. However, **139** with AADC- and COMT inhibitor still remains the cornerstone of the drug treatment of Parkinson's disease [185].

Despite the improvement of symptoms during therapy with **139** in Parkinson's disease patients, the drug has several disadvantages, as mentioned above. This has prompted the search for compounds that could replace **139** in the treatment of this neurodegenerative disease. **139** offers several possibilities for derivatives formation containing biodegradable linkages and useful for prodrug approach. Felix et al. proposed and examined antiparkinson activity in mice of a series of di- and tripeptides (**140a**–**x**, Figure 57) containing **139** [186].

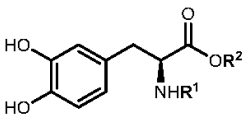

140

140a	R^1- H	R^2- Gly	**140m**	R^1- 3-MeO-Tyr	R^2- H
140b	R^1- H	R^2- Tyr	**140n**	R^1- D-dopa	R^2- H
140c	R^1- H	R^2- 3-MeO-Tyr	**140o**	R^1- Glu	R^2- H
140d	R^1- H	R^2- L-dopa	**140p**	R^1- Ser	R^2- H
140e	R^1- H	R^2- Lys	**140q**	R^1- a-Glu	R^2- H
140f	R^1- H	R^2- Glu	**140r**	R^1- Lys	R^2- H
140g	R^1- Gly	R^2- H	**140s**	R^1- y-Glu	R^2- H
140h	R^1- Ala	R^2- H	**140t**	R^1- Gly-Gly	R^2- H
140i	R^1- Leu	R^2- H	**140u**	R^1- Gly-Gly	R^2- H
140j	R^1- Val	R^2- H	**140v**	$R^1 = R^2$ = Gly	
140k	R^1- Pro	R^2- H	**140w**	$R^1 = R^2$ = L-dopa	
140l	R^1- Tyr	R^2- H	**140x**	R^1- Pro	R^2- L-dopa

Figure 57. Di- and tripeptides prodrugs of **140**.

Some of the peptides were more effective in reversing reserpine-induce catatonia and were relatively non-toxic and resulted in a low degree of stereotypic behavior than **140** [186].

Wang and co-workers developed a tripeptide mimetic prodrug of **138** (**141**, Figure 58) as a delivery system for improving oral absorption, in which D-*p*-hydroxyphenylglycine-L-proline was attached to **140** [187].

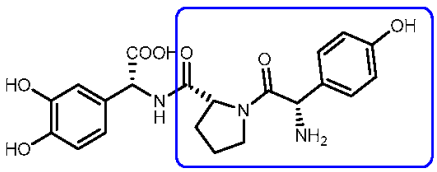

141

Figure 58. Tripeptide mimetic prodrug of **138**. A D-*p*-hydroxyphenylglycine-L-proline group (blue square) was attached to parent drug.

The tripeptide was well absorbed during a perfusion study in rat intestine, devoid of side effect of **138** on isolated muscles and significantly decreased the methamphetamine-induced rotational behavior

in nigrostriatal-lesioned rats, suggesting that it might be an effective agent for Parkinson's disease [187]. In order to enhance the brain uptake of cationic dopamine, Peura et al. synthesized three amino acid prodrugs of **138** (**142a**–**c**, Figure 59) and evaluated their physicochemical properties, as well as (i) their LAT1-binding and BBB permeation; (ii) brain uptake after IV administration and releasing of **138** ability in rat brain after intraperitoneal administration [188].

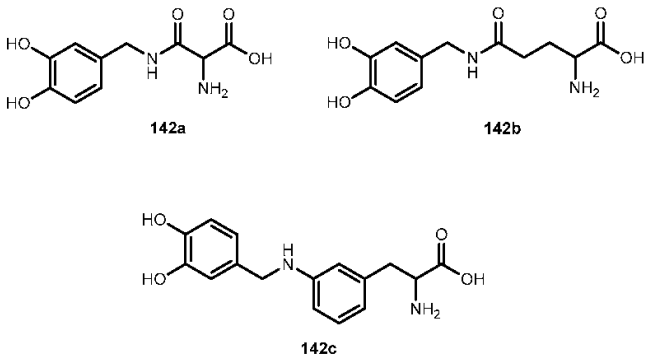

Figure 59. Amino acid prodrugs of **142** synthesized by Peura and co-workers [188].

Synthesized dopamine prodrugs **142a**–**c** possess affinity for LAT1 at rat BBB during the in situ rat brain perfusion and evoked a sustained release of the parent drug as shown by in vitro stability studies fulfilling the specifications required for tissue-targeted prodrugs. The prodrugs appeared to be reasonably stable in the aqueous buffer at pH 7.4 having half-lives of approximately 10 h, in case of prodrug **142b** or longer, **142a** and **142c**. The half-lives of prodrugs in rat plasma and liver homogenates were notably shorter than those determined in the aqueous buffer solution, suggesting that the prodrugs released the parent drug predominantly enzymatically. Peura and co-workers showed that only the meta-substituted phenylalanine promoiety attached to **138** via an amide bond as **142c** exhibited adequate affinity for LAT1 for carrier-mediated brain uptake. The aspartic acid of **142a** and adipic acid of **142b** did not possess favorable properties as LAT1 substrates as **142c**, showing that translocation of the LAT1 prodrugs across the BBB is dependent on their affinity to LAT1. In addition to the in situ studies, **142c** was also taken up into the rat brain after its intravenous administration in vivo in rats. Peura and co-workers could not find enhanced concentrations of **141** in the rat striata after IV administration of **142c** when compared with the corresponding equimolar dose of **138**. Thus, authors hypothesized that **142c** is too quickly eliminated from the brain due to its high polarity [188]. As seen before with **119** [161], the attachment of phenylalanine to parent drug via an amide bond from meta-position of its aromatic ring could be a feasible promoiety for LAT1-targeting of cationic drugs [188].

3.5.5. Neuropathic Pain

Glycine is the most abundant inhibitory neurotransmitter in the spinal cord [189]. Blockage of strychnine-sensitive glycine receptors, with strychnine, in the spinal cord elicits allodynia, a condition in which normally innocuous tactile stimuli provoke intensive aversive responses suggestive of pain [190]. Furthermore, blockage of glycine receptors by strychnine enhances neuropathic pain [191]. Intracerebroventricular intrathecal injection of glycine produces analgesia in thermal and chemical nociception [192] suggesting that glycine modulates pain responses to a variety of nociceptive *stimuli.*

The potential therapeutic use of glycine as an analgesic has been hindered by its limited penetrability into CNS [193], as a large amount of the amino acid is being required to produce significant levels in CNS [194]. Some percursors like melacemide (2-*n*-pentyaminoacetamide) (**143**, Figure 60), readily penetrate into the CNS and elevate glycine concentrations in the brain [195]. This precursor is used as an antiepileptic drug and interferes with the production of allodynia by strychnine, and is

metabolized primarily by monoamine oxidase (MAO-B) to glycinamide (**144**, Figure 60), which is the immediate precursor of glycine. Beyer and co-workers suggested that **144** is more effective than **143** in producing analgesia due to the magnitude duration, and effectiveness of the oral administrations rout, of this anti-nociceptive effect of **144** [196].

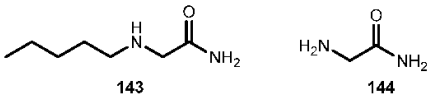

Figure 60. Chemical structures of melacemide (**143**) and glycinamide (**144**).

Gynther and co-workers described a feasible means to achieve carrier-mediated drug transport into rat brain via LAT1, by conjugating a model compound to *L*-tyrosine and *L*-lysine (Figure 61). A hydrophilic drug, ketoprofen (**145**, Figure 61), that is not a substrate for LAT1, was chosen as a model compound [197]. This drug is used for the treatment of some nerve pain such as sciatica and postherpetic neuralgia.

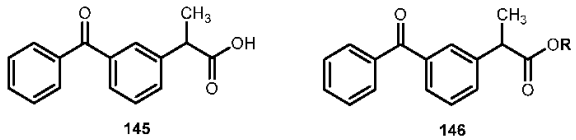

Figure 61. Chemical structures of ketoprofen (**145**) and its amino acid prodrugs.

The **146a** and **146b** prodrugs of **145** showed a concentration-dependent, yet saturable, brain uptake during in situ rat perfusion experiments. The uptake was inhibited by 2-aminobicyclo (2,2,1)heptan-2-carboxylic acid (BCH), a well-known LAT1 inhibitor, suggesting that the brain uptake of prodrugs was mediated by LAT1, even though **145** is not a LAT1 substrate. Probably the conjugation of amino acid and **145** turns prodrugs more suitable to link to LAT1. Furthermore, after bolus injection of **146b** in rats, both prodrugs and parent drug were detected in the whole rat brain tissue. The in vivo microdialysis in rat stratia studies showed that **146b** was able to deliver parent drug to its site of action, i.e., into intracellular compartments of brain cells [151,197].

3.5.6. Depression

CAM-4451 (**147**, Figure 62) is a selective high-affinity NK_1, neurokinin receptor, antagonist that is used as an antidepressant agent [97]. The **147** has a very low aqueous solubility (<2 μg/mL) and consequently poor oral bioavailability [97]. Chan and co-workers used a targeted prodrug strategy to increase the absorption of the poorly water-soluble parent drug, synthesizing amino acid ester prodrugs of **147** (**148a** and **b**, Figure 62). Bioconversion of prodrugs CAM-4562 (**148a**) and CAM-4580 (**148b**) by aminopeptidases to parent drug is depicted in Figure 62.

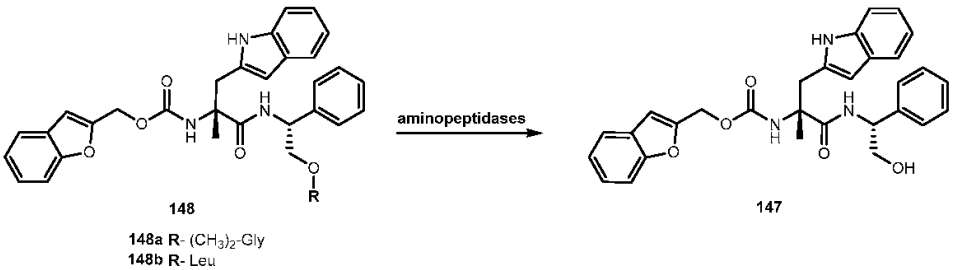

Figure 62. Bioconversion of amino acid ester prodrugs (**148a**) and CAM-4580 (**148b**) to its parent drug.

Amino acid leucine, **148b**, has a modest increase in solubility of **147**, while the dimethylglycine prodrug, **148a** has a 1500-fold greater solubility and nearly 3-times better oral bioavailability than of its parent drug [97]. Moreover, **148a** showed more selective hydrolysis compared to the parent drug by aminopeptidases at the brusher border membrane of the GI tract, whereas **148b** was more susceptible to hydrolysis before reaching the brush border membrane, which may cause potential precipitation problems after absorptions [97].

3.5.7. Anaesthetic

Propofol (2,6-disopropylphenol) (**149**, Figure 63) is an intravenous agent used for anesthesia. Due to its very low solubility, **149** is formulated as an oil-water emulsion (1% *w*/*v*) of soya bean oil, glycerol and purified egg phosphatide (Diprivan®). As a lipid-based emulsion, it suffers from a number of limitations, such as poor physical stability, a potential for embolism, and need for strictly aseptic handling [198]. These drawbacks have stimulated an active research for safe alternative dosage forms, and, in particular, aqueous formulations.

Several α-amino acid ester derivatives (**150a**–**c**, Figure 63) were investigated by Trapani and co-workers. Generally, the derivatives showed low-to-moderate solubility and high stability in water solution [199].

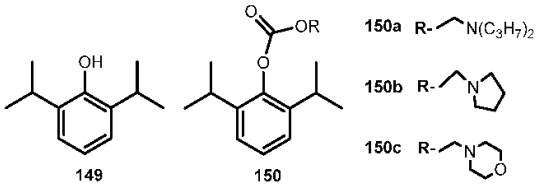

Figure 63. Chemical structure of amino acid derivatives of **149** [199].

The amino acid derivatives exhibited resistance in plasma and brain homogenates that were too high for them to consider them as true prodrugs. Interestingly, some of them have been found to interact with subtype A of $GABA_A$ receptor, a major target mediating pharmacological actions of **149** and other general anesthetics [200].

Different derivatives of **149** (**150d**–**g**, Figure 64) were prepared by coupling, via an ester bond, the drug with cyclic amino acids, namely *L*-proline (106 band positional isomers of piperidine carboxylic acid). Their solubility and stability in aqueous system solution, lipophilicity, susceptibility to enzymatic hydrolysis in animal plasma and liver, as well as their ability to modulate $GABA_A$ receptors were evaluated [201].

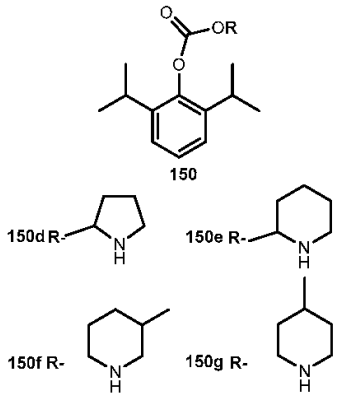

Figure 64. Cyclic amino acid derivates of propofol synthesized by Altomare et al. [201].

The *L*-proline (**150d**) and racemic nipecotic acid (**150f**) esters were found to be highly soluble in water and sufficiently stable at physiological pH (half-lives > 6 h) whereas the α-amino acid esters (**150d** and **150e**) were found to be quantitatively hydrolyzed in plasma and liver esterase solutions, within a few minutes, showing prodrug behavior. The in vitro activity of esters demonstrated a mechanism involving allosteric modulation of $GABA_A$ receptors. The in vivo anticonvulsant and anesthetic activities of prolinate **150d**, administered intraperitoneally in aqueous solution, made Altomare and co-workers consider this prodrug as a candidate for developing formulations useful for parenteral administration [201].

Phosphate ester prodrugs of **149**, fosfopropofol (**151**) and HX0969w (**152**) (Figure 65) were designed to avoid the unsatisfactory water solubility of the parent drug. However, in previous clinical trials, there were reported prodrug side effects such as paresthesia and pruturius which might be related to the accumulation of phosphate ester [202]. To exclude this potential risk, Lang and co-workers designed two amino acid prodrugs, HX0969-Gly-F_3 (**153a**) and HX0969-Ala-HCl (**153b**) (Figure 65), based on the lead compound **152**, by introducing the amino acid group into the structures of the prodrugs of **149** [203].

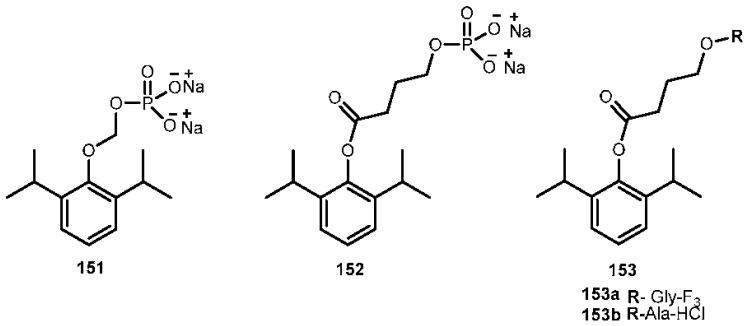

Figure 65. Chemical structures of phosphate and amino acids prodrugs of **149**.

The hydrolysis assays in both rat and rhesus monkey plasma revealed that two amino acid prodrugs release parent drug to a greater extent at a more rapid rate than the phosphate prodrug during a period of five hours. All prodrugs released **149** rapidly in the presence of rat hepatic enzymes. The in vivo studies showed that amino acid prodrugs, administered intravenously could have a more rapid onset of action in a smaller dose than **151** and **152** [203]. Therefore, the application of the amino acid group to the prodrug of **149** could be a good strategy to improve water solubility and the onset of action.

4. Conclusions

In conclusion, amino acid prodrugs have a proven track of improving several pharmacological parameters, such as oral bioavailability of drugs that have poor solubility and permeability. More recently, amino acid prodrugs have successfully been used to achieve sustained release, intravenous delivery, and improved metabolic stability. Moreover, amino acid promoieties have been described as an important tool to enhance the transposition of the blood-barrier brain, which is important for several central nervous diseases that have few drugs available to combat them. In addition, these promoieties are safe pharmacological agents and do not increase the toxicity of compounds but might alleviate side effects of most drugs, especially those used as anticancer agents. We hope that this review stimulates the research on use of amino acid prodrug to overcome delivery changes and to discover effective new or improve older drugs.

Author Contributions: All authors contributed equally.

Funding: This research received no external funding.

Acknowledgments: NV acknowledges support from Fundação para a Ciência e Tecnologia (FCT, Lisbon, Portugal) and FEDER (European Union), award number IF/00092/2014/CP1255/CT0004. NV also thanks FCT for the IF position and Fundação Manuel António da Mota (FMAM, Porto, Portugal) and Pfizer (Portugal) for support for the Nuno Vale Research Group. The contents of this report are solely the responsibility of the authors and do not necessarily represent the official views of the FCT, FMAM and Pfizer.

Conflicts of Interest: The authors declare no conflict of interest.

References

1. Han, H.-K.; Amidon, G.L. Targeted prodrug design to optimize drug delivery. *AAPS Pharm. Sci.* **2000**, *2*, 48–58. [CrossRef]
2. Longqin, H. The prodrug approach to better targeting. *Curr. Drug Dis.* **2004**, *4*, 28–32.
3. Rautio, J.; Kumpulainen, H.; Heimbach, T.; Oliyai, R.; Oh, D.; Järvinen, T.; Savolainen, J. Prodrugs: Design and clinical applications. *Nat. Rev. Drug Discov.* **2008**, *7*, 255–270. [CrossRef] [PubMed]
4. Vig, B.S.; Huttunen, K.M.; Laine, K.; Rautio, J. Amino acids as promoities in prodrug design and development. *Adv. Drug Deliv. Rev.* **2013**, *65*, 1370–1385. [CrossRef] [PubMed]
5. Huttunen, K.M.; Raunio, H.; Rautio, J. Prodrugs—From serendipity to rational design. *Pharmacol. Rev.* **2011**, *63*, 750–771. [CrossRef] [PubMed]
6. Mazák, K.; Noszál, B. Drug delivery: A process governed by species-specific lipophilicities. *Eur. J. Pharm. Sci.* **2014**, *62*, 96–104. [CrossRef] [PubMed]
7. Buckley, S.T.; Fischer, S.M.; Fricker, G.; Brandl, M. In vitro models to evaluate the permeability of poorly soluble drug entities: Challenges and perspectives. *Eur. J. Pharm. Sci.* **2012**, *45*, 235–250. [CrossRef] [PubMed]
8. Lipinski, C.A.; Lombardo, F.; Dominy, B.W.; Feeney, P.J. Experimental and computational approaches to estimate solubility and permeability in drug discovery and development settings. *Adv. Drug Deliv. Rev.* **2001**, *46*, 3–26. [CrossRef]
9. Nielsen, P.B.; Müllertz, A.; Norling, T.; Kristensen, H.G. The effect of alpha-tocopherol on the in vitro solubilisation of lipophilic drugs. *Int. J. Pharm.* **2001**, *222*, 217–224. [CrossRef]
10. Saetern, A.M.; Flaten, G.E.; Brandl, M. A method to determine the incorporation capacity of camptothecin in liposomes. *AAPS PharmSciTech* **2004**, *5*, 30–37. [CrossRef] [PubMed]
11. Rathore, M.S.; Gupta, V.B. Functional characterization of amino acid transport system for transport of phenylalanine on mammalian cornea for better ocular drug delivery. *J. Pharm. Sci. Res.* **2010**, *2*, 329–337.
12. Gupta, G.; Gupta, S.V.; Lee, K.D.; Amidon, G.L. Chemical and enzymatic stability of amino acid prodrugs containing methoxy, ethoxy and propylene glycol linkers. *Mol. Pharm.* **2009**, *6*, 1604–1611. [CrossRef] [PubMed]
13. Del Amo, E.M.; Urtti, A.; Yliperttula, M. Pharmacokinetic role of L-type amino acid transporters LAT1 and LAT2. *Eur. J. Pharm. Sci.* **2008**, *35*, 161–174. [CrossRef] [PubMed]
14. Ylikangas, H.; Malmioja, K.; Peura, L.; Gynther, M.; Nwachukwu, E.O.; Leppänen, J.; Laine, K.; Rautio, J.; Lathela-Kakkonen, M.; Huttunen, K.M.; et al. Quantitative insight into design of compounds recognized by L-Type Amino Acids Transporter 1 (LAT1). *ChemMedChem* **2014**, *9*, 2699–2707. [CrossRef] [PubMed]
15. Amidon, G.L.; Lennernäs, H.; Shah, V.P.; Crison, J.R. A theoretical basis for a biopharmaceutic drug classification: The correlation of in vitro drug product dissolution and in vivo bioavailability. *Pharm. Res.* **1995**, *12*, 413–420. [CrossRef] [PubMed]
16. Mitra, A.K. Role of transporters in ocular drug delivery system. *Pharm. Res.* **2009**, *26*, 1192–1196. [CrossRef] [PubMed]
17. Katragadda, S.; Gunda, S.; Hariharau, S.; Mitra, A.K. Ocular pharmacokinetics of acyclovir amino acid ester prodrugs in the anterior chamber. Evaluation of their utility in treating ocular HSV infections. *Int. J. Pharm.* **2008**, *359*, 15–24. [CrossRef] [PubMed]
18. Katragadda, S.; Xiadong, Z.; Ravi, T.S.; Mitra, A.K. Small neutral amino acid ester prodrugs of acyclovir targeting amino acid transporters on the cornea: Possible antiviral agents against ocular HSV-1 infections. *Ophthal. Eye Dis.* **2010**, *2*, 43–56.

19. Bier, D.M.; Young, V.R. A kinetic approach to assessment of amino acid and protein replacement needs of individual sick patient. *J. Parenter. Enteral. Nutr.* **1987**, *11*, 95S–97S. [CrossRef] [PubMed]
20. Hatanaka, T.; Haramura, M.; Fei, Y.J.; Miyauchi, S.; Bridges, C.C.; Ganapathy, P.S.; Smith, S.B.; Ganapathy, V.; Ganapathy, M.E. Transport of amino acid-based prodrugs by the Na^+ and Cl^- coupled amino acid transporter $ATB^{0,+}$ and expression of the transporter in tissues amenable for drug delivery. *J. Pharmacol. Exp. Ther.* **2004**, *308*, 1138–1147. [CrossRef] [PubMed]
21. Nashed, Y.E.; Mitra, A.K. Synthesis and characterization of novel dipeptide ester prodrugs of acyclovir. *Spectrochim. Acta Part A* **2003**, *59*, 2033–2039. [CrossRef]
22. Colla, L.; De Clercq, E.; Busson, R.; Vanderhaeghe, H. Synthesis and antiviral activity of water-soluble esters of acyclovir [9-[(2-hydroxyethoxy)methyl]guanine]. *J. Med. Chem.* **1983**, *26*, 602–604. [CrossRef] [PubMed]
23. Maudgal, P.C.; De Clerqc, E.; Descamps, J.; Missotten, L. Topical treatment of experimental herpes simplex keratouveities with 2′-*O*-glycylacyclovir. A water-soluble ester of acyclovir. *Arch. Ophtalmol.* **1984**, *102*, 140–142. [CrossRef]
24. Shao, Z.; Park, G.-B.; Krishnamoorthy, R.; Mitra, A.K. The physicochemical properties, plasma enzymatic hydrolysis, and nasal absorption of acyclovir and its 2-ester prodrugs. *Pharm. Res.* **1994**, *11*, 237–242. [CrossRef] [PubMed]
25. Gao, H.; Mitra, A.K. Regioselective synthesis of acyclovir and its prodrugs. *Synth. Commun.* **2001**, *31*, 1399–1419. [CrossRef]
26. Beutner, K.R.; Friedman, D.J.; Forszpaniak, C.; Andersen, P.L.; Wood, M.J. Valaciclovir compared with acyclovir for improved therapy for herpes zoster in immunocompetent adults. *Antimicrob. Agents Chemother.* **1995**, *39*, 1546–1553. [CrossRef] [PubMed]
27. Soul-Lawton, J.; Seaber, E.; On, N.; Wootton, R.; Rolan, P.; Posner, J. Absolute bioavailability and metabolic disposition of valaciclovir, the *L*-valyl ester of acyclovir, following oral administration to humans. *Antimicrob. Agents Chemother.* **1995**, *39*, 2759–2764. [CrossRef] [PubMed]
28. Wang, L.H.; Schultz, M.; Weller, S.; Smiley, M.L.; Blum, M.R. Pharmacokinetics and safety of multiple dose valaciclovir in geriatric volunteers with and without concomitant diuretic therapy. *Antimicrob. Agents Chemother.* **1996**, *40*, 80–85. [PubMed]
29. Anand, B.; Nashed, Y.; Mitra, A. Novel dipeptide prodrugs of acyclovir for ocular herpes infections: Bioreversion, antiviral activity and transport across rabbit cornea. *Curr. Eye Res.* **2003**, *26*, 151–163. [CrossRef] [PubMed]
30. Ganapathy, M.E.; Huang, W.; Wang, H.; Ganapathy, V.; Leibach, F.H. Valacyclovir: A substrate for the intestinal and renal peptide transporters PEPT1 and PEPT2. *Biochem. Biophys. Res. Commun.* **1998**, *246*, 470–475. [CrossRef] [PubMed]
31. Han, H.K.; Oh, D.M.; Amidon, G.L. Cellular uptake mechanism of amino acid ester prodrugs in Caco-2/hPEPT1 cells overexpressing a human peptide transporter. *Pharm. Res.* **1998**, *15*, 1382–1386. [CrossRef] [PubMed]
32. Vrueh, R.L.; Smith, P.L.; Lee, C.P. Transport of *L*-valine-acyclovir via the oligopeptide transporter in the human intestinal cell line Caco-2. *J. Pharmacol. Exp. Ther.* **1998**, *286*, 1166–1170. [PubMed]
33. Han, H.; Oh, D.M.; Amidon, G.L. 5′-amino acid esters of antiviral nucleosides, acyclovir, and AZT are absorbed by the intestinal PEPT1 peptide transporter. *Pharm. Res.* **1998**, *15*, 1154–1159. [CrossRef] [PubMed]
34. Patel, K.; Trivedi, S.; Luo, S.; Zhu, X.; Pal, D.; Kern, E.R.; Mitra, A.K. Synthesis, physicochemical properties and antiviral activities of ester prodrugs of ganciclovir. *Int. J. Pharm.* **2005**, *305*, 75–89. [CrossRef] [PubMed]
35. Santos, C.R.; Capela, R.; Pereira, C.S.; Valente, E.; Gouveia, L.; Pannecouque, C.; De Clercq, E.; Moreira, R.; Gomes, P. Structure-activity relationships for dipeptide prodrugs of acyclovir: Implications for prodrug design. *Eur. J. Med. Chem.* **2009**, *44*, 2339–2346. [CrossRef] [PubMed]
36. Larsen, S.W.; Ankersen, M.; Larsen, C. Kinetics of degradation and oil solubility of ester prodrugs of a model dipeptide (Gly-Phe). *Eur. J. Pharm. Sci.* **2004**, *22*, 399–408. [CrossRef] [PubMed]
37. Portela, M.J.; Moreira, R.; Valente, E.; Constantino, L.; Iley, J.; Pinto, J.; Rosa, R.; Cravo, P.; Rosário, V.E. Dipeptide derivatives of primaquine as transmission-blocking antimalarials: Effect of aliphatic side-chain acylation on the gametocytocidal activity and on the formation of carboxyprimaquine in rat liver homogenates. *Pharm. Res.* **1999**, *16*, 942–954. [CrossRef]

38. Thomsen, A.E.; Christensen, M.S.; Bagger, M.A.; Steffansen, B. Acyclovir prodrug for the intestinal di/tri-peptide transporter PEPT1: Comparison of the in vivo bioavailability in rats and transport in Caco-2 cells. *Eur. J. Pharm. Sci.* **2004**, *23*, 319–325. [CrossRef] [PubMed]
39. Steingrimsdottir, H.; Gruber, A.; Palm, C.; Grimfors, G.; Kalin, M.; Eksborg, S. Bioavailability of aciclovir after oral administration of aciclovir and its prodrugs valaciclovir to patients with leucopenia after chemotherapy. *Antimicrob. Agents Chemother.* **2000**, *44*, 207–209. [CrossRef] [PubMed]
40. Höglund, M.; Ljungman, P.; Weller, S. Comparable aciclovir exposures by oral valaciclovir and intravenous acyclovir in immunocompromised cancer patients. *J. Antimicrob. Chemother.* **2001**, *47*, 855–861. [CrossRef] [PubMed]
41. Shen, W.; Kim, J.-S.; Kish, P.E.; Zhang, J.; Mitchell, S.; Gentry, B.G.; Breitenbach, J.M.; Drach, J.C.; Hilfinger, J. Design and synthesis of vidarabine prodrugs as antiviral agents. *Bioorg. Med. Chem. Lett.* **2009**, *19*, 792–796. [CrossRef] [PubMed]
42. Boyd, M.R.; Bacon, T.H.; Sutton, D.; Cole, M. Antiherpesvirus activity of 9-(4-hydroxy-3-hydroxy-methylbut-1-yl)guanine (BRL39123) in cell culture. *Antimicrob. Agents Chemother.* **1987**, *31*, 1238–1242. [CrossRef] [PubMed]
43. Harnden, M.R.; Jarvest, R.L.; Boyd, M.R.; Sutton, D.; Hodge, R.A.V. Prodrugs of selective antiherpesvirus agent 9-[4-hydroxy-3-(hydroxymethoxyl)but-1-yl]guanidine (BRL-39123) with improved gastroinstestinal absorption properties. *J. Med. Chem.* **1989**, *30*, 1738–1743. [CrossRef]
44. Beauchamp, L.M.; Orr, G.F.; de Miranda, P.; Burnette, T.; Krenitsky, T.A. Amino acid ester prodrugs of acyclovir. *Antiviral Chem. Chemother.* **1992**, *3*, 157–169. [CrossRef]
45. Kim, D.-K.; Lee, N.; Im, G.J.; Kim, Y.-G.; Chang, K.; Kim, H.-T.; Cho, Y.-G.; Choi, W.-S.; Jung, I.; Kim, K.H. Synthesis and evaluation of amino acid ester prodrugs of penciclovir. *Bioorg. Med. Chem. Lett.* **1996**, *6*, 1849–1854. [CrossRef]
46. Zou, R.; Drach, J.C.; Townsend, L.B. Design, synthesis and viral evaluation of 2-chloro-5,6-dihalo-1-(β-D-ribofuranosyl)-benzimidazoles as potential agents for human cytomegalovirus infection. *J. Med. Chem.* **1997**, *40*, 811–818. [CrossRef] [PubMed]
47. Underwood, M.R.; Harvey, R.J.; Stanat, S.C.; Hemphil, M.L.; Miller, T.; Drach, J.C.; Townsend, L.B.; Biron, K.K. Inhibition of human cytomegalovirus DNA maturation by a benzimidazole ribonucleoside is mediated through the UL89 gene product. *J. Virol.* **1998**, *72*, 717–725. [PubMed]
48. Song, X.; Vig, B.S.; Lorenzi, P.L.; Drach, J.C.; Townsend, L.B.; Amidon, G.L. Amino acid ester prodrugs of the antiviral agent 2-bromo-5,6-dichloro-1-(β-D-ribofuranosyl)benzimidazole as potential substrates of hPEPT1 transporter. *J. Med. Chem.* **2005**, *48*, 1274–1277. [CrossRef] [PubMed]
49. Lorenzi, P.L.; Landowski, C.P.; Song, X.; Borysko, K.Z.; Breitenbach, J.M.; Kim, J.S.; Hilfinger, J.M.; Townsend, L.B.; Drach, J.C.; Amidon, G.L. Amido acid ester prodrugs of 2-bromo-5,6-dichloro-1-(β-D-ribofuranosyl)benzimidazole enhance metabolic stability in vitro and in vivo. *J. Pharm. Exp. Ther.* **2005**, *314*, 883–890. [CrossRef] [PubMed]
50. McKenna, C.E.; Kashemirov, B.A.; Eriksson, U.; Amidon, G.L.; Kish, P.E.; Mitchell, S.; Kim, J.-S.; Hilfinger, J.M. Cidofovir peptide conjugates as prodrugs. *J. Organomet. Chem.* **2005**, *690*, 2673–2678. [CrossRef]
51. De Clerqc, E. Antiviral drugs: Current state of the art. *J. Clin. Virol.* **2001**, *22*, 73–89. [CrossRef]
52. Hasegawa, T.; Kawaguchi, T. Future of prodrugs in antiviral therapy. *Clin. Pharmacokinet.* **1994**, *27*, 331–336. [CrossRef] [PubMed]
53. World Health Organization (WHO). *Malaria and HIV Interactions and Their Implications for Public Health Policy*; Report of a Technical Consultation; WHO: Geneva, Switzerland, 2005.
54. Fischl, M.A.; Richman, D.D.; Grieco, M.H.; Gottlieb, M.S.; Volberding, P.A.; Laskin, O.L.; Leedom, J.M.; Groopman, J.E.; Mildvan, D.; Schooley, R.T.; et al. The efficacy of azidothymidine (AZT) in treatment of patients with AIDS and AIDS-related complex. A double-blind, placebo-controlled trial. *N. Engl. J. Med.* **1987**, *317*, 185–191. [CrossRef] [PubMed]
55. Mohan, P. Problems and perspectives in the design of anti-HIV-1 agents. *Drug Dev. Rev.* **1993**, *29*, 1–17. [CrossRef]
56. Klecker, R.W., Jr.; Collins, J.M.; Yarchoan, R.; Thomas, R.; Jenkins, J.F.; Broder, S.; Meyers, C.E. Plasma and cerebrospinal fluid pharmacokinetics of 3′-azido-3′-deoxythymidine: A novel pyrimidine analog with potential application for the treatment of patients with AIDS and related diseases. *Clin. Pharmacol. Ther.* **1987**, *41*, 407–412. [CrossRef] [PubMed]

57. Styrt, B.A.; Piazza-Hepp, T.D.; Chikami, G.K. Clinical toxicity of antiretroviral nucleoside analogs. *Antivir. Res.* **1996**, *31*, 121–135. [CrossRef]
58. Turk, G.; Moroni, G.; Pampuro, S.; Briñon, M.C.; Salomón, H. Antiretroviral activity and cytotoxicity of novel zidovudine (AZT) derivatives and their relation to their chemical structure. *Int. J. Antimicrob. Agents* **2002**, *20*, 282–288. [CrossRef]
59. Santos, C.; Capela, R.; Pereira, C.S.; Valente, E.; Gouveia, L.; Pannecouque, C.; De Clercq, E.; Moreira, R.; Gomes, P. Dipeptide derivatives of AZT: Synthesis, chemical stability, activation in human plasma, hPEPT1 affinity, and antiviral activity. *ChemMedChem* **2008**, *3*, 970–978. [CrossRef] [PubMed]
60. Zhang, L.; Zhang, L.; Luo, T.; Zhou, J.; Sun, L.; Xu, Y. Synthesis and evaluation of a dipeptide-drug conjugate library as substrates for PEPT1. *ACS Comb. Sci.* **2012**, *14*, 108–114. [CrossRef] [PubMed]
61. Lai, L.; Xu, Z.; Zhou, J.; Lee, K.D.; Amidon, G.L. Molecular basis of prodrug activation by human valacyclovirase, an alpha-amino acid ester hydrolase. *J. Biol. Chem.* **2008**, *283*, 9318–9327. [CrossRef] [PubMed]
62. Liang, Y.; Sharon, A.; Grier, J.P.; Rapp, K.L.; Schinazi, R.F.; Chu, C.K. 5′-*O*-aliphatic and amino acid ester prodrugs of (−)-β-D-(*2R,4R*)-dioxolane-thymide (DOT): Synthesis, anti-HIV activity, cytotoxicity and stability studies. *Bioorg. Med. Chem.* **2009**, *17*, 1404–1409. [CrossRef] [PubMed]
63. Kumar, G.N.; Jayanti, V.K.; Johnson, M.K.; Uchic, J.; Thomas, S.; Lee, R.D.; Grabowski, B.A.; Sham, H.L.; Kempf, D.-J.; Denissen, J.F.; et al. Metabolism and disposition of the HIV-1 protease inhibitor lopinavir (ABT-378) given in combination with ritonavir in rats, dogs, and humans. *Pharm. Res.* **2004**, *21*, 1622–1630. [CrossRef] [PubMed]
64. Argawal, S.; Boddu, S.H.; Jain, R.; Samanta, S.; Pal, D.; Mitra, A.K. Peptide prodrugs: Improved oral absorption of lopinavir, a HIV protease inhibitor. *Int. J. Pharm.* **2008**, *359*, 7–14.
65. Lavanchy, D. Hepatitis B virus epidemiology, disease burden, treatment, and current and emerging prevention and control measures. *J. Virol. Hep.* **2004**, *11*, 97–107. [CrossRef]
66. Chen, Z.; Zheng, M. Patents and development of HBV and HCV clinical treatment: From 2001 to April 2005. *Exp. Opin. Ther. Patents* **2005**, *15*, 1027–1039. [CrossRef]
67. Hwang, J.-T.; Choi, J.-R. Novel phosphate nucleoside as antiviral agents. *Drugs Fut.* **2004**, *29*, 163–177. [CrossRef]
68. Fu, X.; Jiang, S.; Li, C.; Xin, J.; Yang, Y.; Ji, R. Design and synthesis of novel bis(*L*-amino acid) ester prodrug of 9-[2-phosphonomethoxy)ethyl)adenine (PMEA) with improved anti HBV-activity. *Bioorg. Med. Chem. Lett.* **2007**, *17*, 465–470. [CrossRef] [PubMed]
69. Hodge, R.A. Telbivudine/torcitabine idenix/Novartis. *Curr. Opin. Investig. Drug* **2004**, *5*, 232–241.
70. Pierra, C.; Amador, A.; Benzaria, S.; Cretton-Scott, E.; D'Amours, M.; Mao, J.; Mathieu, S.; Moussa, A.; Bridges, E.G.; Standring, D.N.; et al. Synthesis and pharmacokinetics of valopicitabine (NM 283), an efficient prodrug of the potent anti-HCV agent 2′-C-methylcytidine. *J. Med. Chem.* **2006**, *49*, 6614–6620. [CrossRef] [PubMed]
71. Li, F.; Maag, H.; Alfredson, T. Prodrugs of nucleoside analogues for improved oral absorption and tissue targeting. *J. Pharm. Sci.* **2008**, *97*, 1109–1134. [CrossRef] [PubMed]
72. Zhou, X.J.; Knox, S.; Fielman, B.; Chao, G.; Brown, N. Safety and pharmacokinetics of NM107 following intravenous infusion of escalating doses in healthy volunteers: Determination of absolute oral bioavailability of valopicitabine (NM283). *J. Hepatol.* **2006**, *44*, S231–S232. [CrossRef]
73. Sorbera, L.A.; Castaner, J.; Leeson, P.A. Valopicitabine: Anti-hepatitis C virus drug, RNA-directed RBA polymerase (NS5B) inhibitor. *Drugs Fut.* **2006**, *3*, 320–324. [CrossRef]
74. Sinhababu, A.K.; Thakker, D.R. Prodrugs of anticancer agents. *Adv. Drug Deliv. Res.* **1996**, *19*, 241–273. [CrossRef]
75. Landowski, C.P.; Lorenzi, P.L.; Song, X.; Amidon, G.L. Nucleoside ester prodrugs substrate specificity of liver carboxylesterase. *J. Pharmacol. Exp. Ther.* **2006**, *316*, 241–273. [CrossRef] [PubMed]
76. Gonzalez, D.E.; Covitz, K.-M.; Sadée, W.; Mrsny, R.J. An oligopeptide transporter is expressed at high levels in the pancreatic carcinoma cell lines AsPc-1 and Capan-2. *Cancer Res.* **1998**, *58*, 519–525. [PubMed]
77. Nakanishi, T.; Tamai, I.; Takaki, A.; Tsuji, A. Cancer cell-targeted drug delivery utilizing oligopeptide transport activity. *Int. J. Cancer* **2000**, *88*, 274–280. [CrossRef]

78. Vig, B.S.; Lorenzi, P.L.; Mittal, S.; Landowski, C.P.; Shin, H.-C.; Mosberg, H.I.; Hilfinger, J.M.; Amidon, G.L. Amino acid ester prodrugs of floxuridine: Synthesis and effects of structure, stereochemistry and site of esterification on the rate of hydrolysis. *Pharm. Res.* **2003**, *20*, 1381–1388. [CrossRef] [PubMed]
79. Song, X.; Lorenzi, P.L.; Landowski, C.P.; Vig, B.S.; Hilfinger, J.M.; Amidon, G.L. Amino acid ester prodrug of the anticancer agent gemcitabine: Synthesis, bioconversion, metabolic bioevasion and hPEPT1-mediated transport. *Mol. Pharm.* **2005**, *2*, 157–167. [CrossRef] [PubMed]
80. Landowski, C.P.; Vig, B.S.; Song, X.; Amidon, G.L. Targeted delivery to PEPT1-overexpresssing cells: Acidic, basic, and secondary floxuridine amino acid ester prodrugs. *Mol. Cancer Ther.* **2005**, *4*, 659–667. [CrossRef] [PubMed]
81. Landowski, C.P.; Song, X.; Lorenzi, P.L.; Hilfinger, J.M.; Amidon, G.L. Floxuridine amino acid ester prodrugs: Enhancing Caco-2 permeability and resistance to glycosidic bond metabolism. *Pharm. Res.* **2005**, *22*, 1510–1518. [CrossRef] [PubMed]
82. Tsume, Y.; Hilfinger, J.M.; Amidon, G.L. Enhanced cancer cell growth inhibition by dipeptide prodrugs of Floxuridine: Increased transporter affinity and metabolic stability. *Mol. Pharm.* **2008**, *5*, 717–727. [CrossRef] [PubMed]
83. Tsume, Y.; Hilfinger, J.M.; Amidon, G.L. Potential of amino acid/dipeptide monoester prodrug of floxuridine in facilitating enhanced delivery of active drug to interior sites of tumors: A two-tier monololayer in vitro stability. *Pharm. Res.* **2011**, *28*, 2575–2588. [CrossRef] [PubMed]
84. Tsume, Y.; Amidon, G.L. The feasibility of enzyme targeted activation for amino acid/dipeptide monoester prodrugs of floxuridine; cathepsin D as potential targeted enzyme. *Molecules* **2012**, *17*, 3672–3689. [CrossRef] [PubMed]
85. Huang, P.; Chubb, S.; Hertel, L.W.; Grindey, G.B.; Plunkett, W. Action of 2′,2′-difluorodeoxycytidine on DNA synthesis. *Cancer Res.* **1991**, *51*, 6110–6117. [PubMed]
86. Tsume, Y.; Incecayir, T.; Song, X.; Hilfinger, S.M.; Amidon, G.L. The development of orally administrable gemcitabine prodrugs with *D*-enantiomer amino acid: Enhanced membrane permeability and enzymatic stability. *Eur. J. Pharm. Sci.* **2014**, *86*, 514–523. [CrossRef] [PubMed]
87. Vale, N.; Ferreira, A.; Fernandes, I.; Alves, C.; Araújo, M.J.; Mateus, N.; Gomes, P. Gemcitabine anti-proliferative activity significantly enhanced upon conjugation with cell-penetrating peptides. *Bioorg. Med. Chem. Lett.* **2017**, *27*, 2898–2901. [CrossRef] [PubMed]
88. Diaz-Padilla, I.; Siu, L.L. Brivanib alaninate for cancer. *Exp. Opin. Investig. Drugs* **2011**, *20*, 577–586. [CrossRef] [PubMed]
89. Huynth, H.; Fargnoli, J. Brivanib alaninate: VEGFR/FGFR inhibitor oncolytic. *Drug Fut.* **2009**, *34*, 881–895. [CrossRef]
90. Marathe, P.H.; Kamath, A.V.; Zhang, Y.; D'Arienzo, C.; Bhide, R.; Fargnoli, J. Preclinical pharmacokinetics and in vitro metabolism of brivanib (BMS-540215) a potent VEGFR2 inhibitor and its alanine ester prodrug brivanib alaninate. *Cancer Chemother. Pharmacol.* **2009**, *65*, 55–66. [CrossRef] [PubMed]
91. Gong, J.; Gan, J.; Caceres-Cortes, J.; Christopher, L.J.; Arora, V.; Masson, E.; Williams, D.; Pursley, J.; Allentoff, A.; Lago, M.; et al. Metabolism and disposition of [^{14}C] brivanib alaninate after oral administration to rats, monkeys, and humans. *Drug Metab. Dispos.* **2011**, *39*, 891–903. [CrossRef] [PubMed]
92. Vale, N.; Correia-Branco, A.; Patrício, B.; Duarte, D.; Martel, F. In vitro studies on the inhibition of colon cancer by amino acid derivatives of bromothiazole. *Bioorg. Med. Chem. Lett.* **2017**, *27*, 3507–3510. [CrossRef] [PubMed]
93. Senkowski, W.; Zhang, X.; Olofsson, M.H.; Isacson, R.; Höglund, U.; Gustafsson, M.; Nygren, P.; Linder, S.; Larsson, R.; Frynknäs, M. Three-dimensional cell culture-based screening identifies the anthelminthic drug nitazoxanide as a candidate for treatment of colorectal cancer. *Mol. Cancer Ther.* **2015**, *14*, 1504–1516. [CrossRef] [PubMed]
94. Stockis, A.; Deroubaix, X.; Lins, R.; Jeanbaptiste, B.; Calderon, P.; Rossignol, J. Pharmacokinetics of nitazoxanide after single oral dose administration in 6 healthy volunteers. *Int. J. Clin. Pharmacol. Ther.* **1996**, *34*, 349–351. [PubMed]
95. Borrego, S.L.; Fahrmann, J.; Datta, R.; Stringari, C.; Grapov, D.; Zeller, M.; Chen, Y.; Wang, P.; Baldi, P.; Gratton, E.; et al. Metabolic changes associated with methionine stress sensitivity in MDA-MB-468 breast cancer cells. *Cancer Metabol.* **2016**, *4*, 9. [CrossRef] [PubMed]

96. Jones-Bolin, S.; Zhao, H.; Hunter, K.; Klein-Szanto, A.; Ruggeri, B. The effect of the oral, pan-VEGFR kinase inhibitor CEP-7055 and chemotherapy in orthopedic models of glioblastoma and colon carcinoma in mice. *Mol. Cancer Ther.* **2006**, *5*, 1744–1753. [CrossRef] [PubMed]
97. Chan, O.H.; Schmid, H.L.; Stilgenbauer, L.A.; Howson, W.; Horwell, D.C.; Stewart, S.B.H. Evaluation of a targeted prodrug strategy of enhanced oral absorption of poorly-water-soluble compounds. *Pharm. Res.* **1998**, *15*, 1012–1018. [CrossRef] [PubMed]
98. Ruggeri, B.; Singh, J.; Gingrich, D.; Angeles, T.; Albom, M.; Yang, S.; Chang, H.; Robinson, C.; Hunter, K.; Dobrzanski, P.; et al. CEP-7055, a novel orally active pan inhibitor of vascular endothelial growth factor receptor tyrosine kinase with potent antiangiogenic activity and antitumor efficacy in preclinical models. *Cancer Res.* **2003**, *63*, 5978–5991. [PubMed]
99. Barth, R.F.; Yang, W.; Al-Madhoun, A.S.; Johnsamuel, J.; Byun, Y.; Chandra, S.; Smith, D.R.; Tjarks, W.; Eriksson, S. Boron-containing nucleosides as potential delivery agents for neutron capture therapy of brain tumors. *Cancer Res.* **2004**, *64*, 6287–6295. [CrossRef] [PubMed]
100. Barth, R.F.; Coderre, J.A.; Vicente, M.; Blue, T.E. Boron neutron capture therapy of cancer: Current status and future prospects. *Clin. Cancer Res.* **2005**, *11*, 3987–4002. [CrossRef] [PubMed]
101. Hasabelnaby, S.; Goudah, A.; Agarwal, H.K.; abd Alla, M.S.M.; Tjarks, W. Synthesis, chemical and enzymatic hydrolysis, and aqueous solubility of amino acid ester prodrugs of 3-carboranyl thymidine analogs for boron neutron capture therapy of brain tumors. *Eur. J. Med. Chem.* **2012**, *55*, 325–334. [CrossRef] [PubMed]
102. Houchens, D.P.; Ovejera, A.A.; Riblet, S.M.; Slagel, D.E. Human brain tumor xenografts in nude mice as a chemotherapy model. *Eur. J. Cancer Clin. Oncol.* **1983**, *19*, 799–805. [CrossRef]
103. Supko, J.G.; Malspeis, L. Dose-dependent pharmacokinetics of rapamycin-28-*N*,*N*-dimethylglycinate in the mouse. *Cancer Chemother. Pharmacol.* **1994**, *33*, 325–330. [CrossRef] [PubMed]
104. Spataro, A.; Kessel, D. Studies on camptothecin-induced degradation and apparent reaggregation of DNA from L1210 cells. *Biochem. Biophys. Res. Commun.* **1972**, *48*, 643–648. [CrossRef]
105. Yurkovetskiy, A.V.; Fram, R.J. XMT-1001, a novel polymeric camptothecin pro-drug in clinical development for patients with advanced cancer. *Adv. Drug Deliv. Rev.* **2009**, *61*, 1193–1202. [CrossRef] [PubMed]
106. Pantazis, P.; Hinz, H.R.; Mendoza, J.T.; Kozielski, A.J.; Williams, L.J., Jr.; Stehlin, J.S., Jr.; Giovanella, B.C. Complete inhibition of growth followed by death of human malignant melanoma cells in vitro and regression of human melanoma xenografts in immunodeficient mice induced by camptothecins. *Cancer Res.* **1992**, *52*, 3980–3987. [PubMed]
107. Deshmukh, M.; Chao, P.; Kutscher, H.L.; Gao, D.; Sinko, P.J. A series of α-amino acid ester prodrugs of camptothecin: In vitro hydrolysis and A549 human lung carcinoma cell cytotoxicity. *J. Med. Chem.* **2010**, *53*, 1038–1047. [CrossRef] [PubMed]
108. Chua, M.-S.; Kashiyama, E.; Bradshaw, T.D.; Stinson, S.F.; Brantley, E.; Sausville, E.A.; Stevens, M.F.G. Role of CYP1A1 in modulation of antitumor properties of the novel agent 2-(4-amino-3-methylphenyl)-benzothiazole (DF 203, NSC 674495) in human breast cancer cells. *Cancer Res.* **2000**, *60*, 5196–5203. [PubMed]
109. Hose, C.; Riviera, M.; Sausville, E.; Monks, A. Induction of cytochrome P450 CYP1A1 and cytochrome P450 CYP1B1 by 2-(4-amino-3-methylphenyl)benzothiazole (BZ) in 60 human tumor cell lines: Correlation with BZ toxicity. *Proc. Am. Assoc. Cancer Res.* **2001**, *42*, 511.
110. Bradshaw, T.D.; Bibby, M.C.; Double, J.A.; Fichtner, I.; Cooper, P.A.; Alley, M.C.; Donohue, S.; Stinson, S.F.; Tomaszewjsti, J.E.; Sausville, E.A.; et al. Preclinical evaluation of amino acid prodrugs of a novel antitumor 2-(4-amino-3-methylphenyl)benzothiazoles. *Mol. Cancer Ther.* **2002**, *1*, 239–246. [PubMed]
111. Farmer, P.B. Metabolism and reactions of alkylating agents. *Pharmacol. Ther.* **1987**, *35*, 301–358. [CrossRef]
112. Chrzanowski, K.; Bielawska, A.; Palka, J. Proline analogue of melphalan as a prodrug susceptible to the action of prolidase in breast cancer MDA-MB 231. *Il Farmaco* **2003**, *58*, 1113–1119. [CrossRef]
113. Wu, Z.; Shah, A.; Patel, N.; Yuan, X. Development of methotrexate proline prodrug to overcome resistance by MDA-MB-231 cells. *Bioorg. Med. Chem. Lett.* **2010**, *20*, 5108–5112. [CrossRef] [PubMed]
114. Mittal, S.; Song, X.; Vig, B.S.; Landowski, C.P.; Kim, I.; Hilfinger, J.M.; Amidon, G. Prolidase, a potential enzyme targeted for melanoma: Design of proline-containing dipeptide-linker prodrugs. *Mol. Pharm.* **2005**, *2*, 37–46. [CrossRef] [PubMed]
115. Nam, N.H.; Kim, Y.; You, Y.J.; Hong, D.H.; Kim, H.M.; Ahn, B.Z. Synthesis and anti-tumor activity of a novel combretastatins: Combretocyclopentenones and related analogues. *Bioorg. Med. Chem. Lett.* **2002**, *12*, 1955–1958. [CrossRef]

116. Nam, N.H.; Kim, Y.; You, Y.J.; Hong, D.H.; Kim, H.M.; Ahn, B.Z. Water soluble prodrugs of the antitumor agent 3-[(3-amino-4-methoxy)phenyl]-2-(3,4,5-trimethoxyphenyl)cyclopent-2-ene-1-one. *Bioorg. Med. Chem.* **2003**, *11*, 1021–1029. [CrossRef]
117. Hirpara, K.; Aggarwal, P.; Mukherjee, A.K.; Joshi, N.; Burman, A.C. Quercetin and its derivatives: Synthesis, pharmacological uses with special emphasis on anti-tumor properties and prodrug with enhanced bio-availability. *Anti-Cancer Agent Med. Chem.* **2009**, *9*, 138–161. [CrossRef]
118. Mulholand, P.J.; Ferry, D.R.; Anderson, D.; Hussain, S.A.; Young, A.M.; Cook, J.E.; Hodgkin, E.; Seymour, L.W.; Kerr, D.J. Pre-clinical and clinical study of QC-12, a water-soluble prodrug of quercetin. *Ann. Oncol.* **2001**, *12*, 245–248. [CrossRef]
119. Kyoung, M.K.; Oh, Y.M.; Park, K.-S.; Chong, Y. A novel prodrug of quercetin, 3-*N*,*N*-dimethyl carbamoyl quercetin (DCQ), with improved stability against hydrolysis in cell culture medium. *Bull. Korean Chem. Soc.* **2009**, *30*, 2114–2116.
120. Vissiennon, C.; Nieber, H.; Kelber, O.; Butterweck, V. Route of administration determines the anxiolytic activity of the flavonols kampferol, quercetin and myricetin-are they prodrugs? *J. Nutr. Biochem.* **2012**, *23*, 733–740. [CrossRef] [PubMed]
121. Mu, L.; Feng, S.S. A novel controlled release formulation for the anticancer drug paclitaxel (Taxol®): PLGA nanoparticles containing vitamin E TPGS. *J. Control. Release* **2003**, *86*, 33–48. [CrossRef]
122. Lundberg, B.B.; Risovic, V.; Ramaswamy, M.; Wasan, K.M. A lipophilic paclitaxel derivative incorporated in a lipid emulsion for parenteral administration. *J. Control. Release* **2003**, *86*, 93–100. [CrossRef]
123. Ma, H.; Chen, G.; Wang, T.; Li, Q.; Liu, Y. Design, synthesis, and biological evaluation of a novel water-soluble prodrug of docetaxel with amino acid as a linker. *Chem. Biol. Drug Des.* **2016**, *88*, 363–369. [CrossRef] [PubMed]
124. McKerrow, M.H.; Caffrey, C.; Kelly, B.; Loke, P.; Sajid, M. Proteases in parasitic diseases. *Annu. Rev. Pathol. Mech. Dis.* **2006**, *1*, 497–536. [CrossRef] [PubMed]
125. Molyneux, D.H. Control of human parasitic diseases: Context and overview. *Adv. Parasitol.* **2006**, *61*, 1–45. [PubMed]
126. Renslo, A.R.; McKerrow, J.H. Drug discovery and development for neglected parasitic diseases. *Nat. Chem. Biol.* **2006**, *2*, 701–710. [CrossRef] [PubMed]
127. Chung, M.C.; Gonçalves, M.F.; Colli, N.; Ferreira, E.I.; Miranda, M.T.M. Synthesis and in vitro evaluation of potential antichagasic dipeptide prodrugs of primaquine. *J. Pharm. Sci.* **1997**, *86*, 1127–1131. [CrossRef] [PubMed]
128. Howard, J.E.; Rios, C.; Ebensperger, I.; Olivos, P. Congenital Chagas disease. *Bol. Chil. Parasitol.* **1957**, *12*, 42–45. [PubMed]
129. Denise, H.; Barrett, M.P. Uptake and mode of action of drugs used against sleeping sickness. *Biochem. Pharmacol.* **2001**, *61*, 1–5. [CrossRef]
130. Sands, M.; Kron, M.A.; Brown, R.B. Pentamidine, a review. *Rev. Infect. Dis.* **1985**, *7*, 625–634. [CrossRef] [PubMed]
131. Kotthaus, J.; Hungeling, H.; Reeh, C.; Kotthaus, J.; Schade, D.; Wein, S.; Wolffram, S.; Clement, B. Synthesis and biological evaluation of *L*-valine-amidoxiesters as double prodrugs of amidines. *Bioorg. Med. Chem.* **2011**, *19*, 1907–1914. [CrossRef] [PubMed]
132. Hanboonkunupakarn, B.; White, N.J. The threat of antimalarial resistance. *Trop. Dis. Travel Med. Vaccines* **2016**, *2*, 10. [CrossRef] [PubMed]
133. Baker, J.K.; Yarber, R.H.; Nanayakkara, N.P.D.; McChesney, J.D.; Homo, F.; Landau, I. Effect of aliphatic side-chain substituents on the antimalarial activity and on the metabolism of primaquine studied using mitochondria and microsome preparations. *Pharm. Res.* **1990**, *7*, 91–95. [CrossRef] [PubMed]
134. Umbreit, J. Methemoglobin-It's not just blue: A concise review. *Am. J. Hematol.* **2007**, *82*, 134–144. [CrossRef] [PubMed]
135. Araújo, M.J.; Bom, J.; Capela, R.; Casimiro, C.; Chambel, P.; Gomes, P.; Iley, J.; Lopes, F.; Morais, J.; Moreira, R.; et al. Imidizolidin-4-one derivatives of primaquine as novel transmission-blocking antimalarials. *J. Med. Chem.* **2005**, *48*, 888–892. [CrossRef] [PubMed]
136. Vagapandu, S.; Sachdeva, S.; Jain, M.; Singh, S.; Singh, P.P.; Kaul, C.L.; Jain, R. 8-aminoquinoamides conjugates with amino acids are exhibiting potent blood-schizontocidal antimalarial activities. *Bioorg. Med. Chem.* **2004**, *12*, 239–247. [CrossRef]

137. Vale, N.; Matos, J.; Gut, J.; Nogueira, F.; do Rosário, V.; Rosenthal, P.J.; Moreira, R.; Gomes, P. Imidazolidin-4-one peptidomimetic derivatives of primaquine: Synthesis and antimalarial activity. *Bioorg. Med. Chem. Lett.* **2009**, *18*, 4150–4153. [CrossRef] [PubMed]
138. Srinivasarao, K.; Argawal, P.; Srivastava, K.; Haq, W.; Puri, S.K.; Katti, S.B. Design, synthesis and in vitro antiplasmodial activity of 4-aminoquinolines containing modified amino acid conjugates. *Med. Chem. Res.* **2016**, *25*, 1148–1162. [CrossRef]
139. World Health Organization (WHO). *Control of the Leishmaniasis*; Technical Report Series; WHO: Geneva, Switzerland, 2010; pp. 1–186.
140. Chappuis, F.; Sundar, S.; Hailu, A.; Ghalib, H.; Rijal, S.; Peeling, R.W.; Alvar, J.; Boelaert, M. Visceral leishmaniasis: What are the needs for diagnosis, treatment, and control? *Nat. Rev. Microbiol.* **2007**, *5*, 873–882. [CrossRef] [PubMed]
141. Maltezou, H.C. Drug resistance in visceral leishmaniasis. *J. Biomed. Biotechnol.* **2010**, *2010*, 617521. [CrossRef] [PubMed]
142. Vale-Costa, S.; Vale, N.; Matos, J.; Tomás, A.; Moreira, R.; Gomes, P.; Gomes, M.S. Peptidomimetic and organometallic derivatives of primaquine active against *Leishmania infantum*. *Antimicrob. Agent Chemother.* **2012**, *56*, 5774–5781. [CrossRef] [PubMed]
143. Goodman, D.A.; Huskins, W.C. Control of nosocomial antimicrobial-resistant bacteria: A strategic priority for hospitals worldwide. *Clin. Infect. Dis.* **1997**, *24*, S139–S145. [CrossRef]
144. Ibrahim, M.A.; Panda, S.S.; Birds, A.S.; Serrano, J.C.; Gonzalez, C.F.; Alamry, K.A.; Katrizky, A.R. Synthesis and antibacterial evaluation of amino-acid antibiotic conjugates. *Bioorg. Med. Chem.* **2014**, *24*, 1856–1861. [CrossRef] [PubMed]
145. De Sarro, A.; De Sarro, G. Adverse reactions to fluoroquinolones. An overview on mechanistic aspects. *Curr. Med. Chem.* **2001**, *8*, 371–384. [CrossRef] [PubMed]
146. Jain, A.; Dixit, P. Multidrug-resistant to extensively drug resistant tuberculosis: What is next? *J. Biosci.* **2008**, *33*, 605–616. [CrossRef] [PubMed]
147. World Health Organization (WHO). *Anti-Tuberculosis Drug Resistance in the World: 4th Global Report*; WHO: Geneva, Switzerland, 2008.
148. Krátký, M.; Vinšová, J.; Butcha, V.; Horvati, K.; Bösze, S.; Stolaříková, J. New amino acid esters of salicylanilides active against MDR-TB and other microbes. *Eur. J. Med. Chem.* **2008**, *45*, 6106–6113. [CrossRef] [PubMed]
149. Pochopin, N.L.; Charman, W.N.; Stella, V.J. Aminoacid derivatives of dapsone as water-soluble prodrugs. *Int. J. Pharm.* **1995**, *121*, 157–167. [CrossRef]
150. Pardridge, W.M. *Brain Drug Targeting: The Future of Brain Development*; Cambridge University Press: Cambridge, UK, 2001; Volume 1, pp. 1–12.
151. Gynther, M.; Laine, K.; Ropponen, J.; Leppänen, J.; Mannila, A.; Nevalainen, T.; Savolainen, J.; Järvinen, T.; Rautio, J. Large neutral amino acid transporter enables brain drug delivery via prodrugs. *J. Med. Chem.* **2008**, *51*, 932–936. [CrossRef] [PubMed]
152. Gynther, M.; Ropponen, J.; Laine, K.; Leppänen, J.; Haapakoski, P.; Peura, L.; Järvinen, T.; Rautio, J. Glucose promoiety enables glucose transporter mediated brain uptake of ketoprofen and imdomethacin prodrugs in rats. *J. Med. Chem.* **2009**, *52*, 3348–3353. [CrossRef] [PubMed]
153. Fisher, R.S.; Acevedo, C.; Arzimanoglou, A.; Bogacz, A.; Cross, J.H.; Elger, C.E.; Engel, J., Jr.; Forsgren, L.; French, J.A.; Glynn, M.; et al. A practical clinical definition of epilepsy. *Epilepsia* **2014**, *55*, 475–482. [CrossRef] [PubMed]
154. Moshé, S.L.; Perucca, E.; Ryvlin, P.; Tomson, T. Epilepsy: New advances. *Lancet* **2015**, *385*, 884–898. [CrossRef]
155. Bialer, M.; Johannessen, S.I.; Levy, R.H.; Perucca, E.; Tomson, T.; White, S.H. Progress report on new antiepileptic drugs: A summary of the Eight Eilat Conference (EILT XI). *Epilepsy Res.* **2013**, *103*, 2–30. [CrossRef] [PubMed]
156. French, J.A. Refractory epilepsy: Clinical overview. *Epilepsia* **2007**, *48* (Suppl. 1), 3–7. [CrossRef] [PubMed]
157. Villalba, M.L.; Enrique, A.V.; Higgs, J.; Castaño, R.A.; Goicoechea, S.; Taborda, F.D.; Gavernet, L.; Lick, I.D.; Marder, M.; Blanch, L.E.B. Novel sulfamides and sulfamates derived from amino esters: Synthetic studies and anticonvulsant activity. *Eur. J. Pharmacol.* **2016**, *774*, 55–63. [CrossRef] [PubMed]

158. Barré, J.; Chamouard, J.M.; Houin, G.; Tillement, J.P. Equilibrium dialysis, ultrafiltration, and ultracentrifugation compared for determining the plasma-protein-binding characteristics of valproic acid. *Clin. Chem.* **1985**, *31*, 60–64.
159. Svennebring, A.M. Investigation of the prerequisites for the optimization of specific plasma protein binding as a strategy for the reduction of first-pass hepatic metabolism. *Xenobiotica* **2015**, *45*, 286–301. [CrossRef] [PubMed]
160. Cornford, E.M.; Diep, C.P.; Pardridge, W.M. Blood-brain barrier transport of valproic acid. *J. Neurochem.* **1985**, *44*, 1541–1550. [CrossRef] [PubMed]
161. Peura, L.; Malmioja, K.; Laine, K.; Leppänen, J.; Gynther, M.; Isotalo, A.; Rautio, J. Large amino acid transporter 1 (LAT1) prodrugs of valproic acid: New prodrug design ideas for central nervous system delivery. *Mol. Pharm.* **2011**, *8*, 1857–1866. [CrossRef] [PubMed]
162. Gynther, M.; Peura, L.; Vernerová, M.; Leppänen, J.; Kärkkäinen, J.; Lehtonen, M.; Rautio, J.; Huttunen, K.M. Amino acid promoieties alter valproic acid pharmacokinetics and enable extended brain exposure. *Neurochem. Res.* **2016**, *41*, 2797–2809. [CrossRef] [PubMed]
163. McLean, M.J. Gabapentin in the management of convulsive disorders. *Epilepsia* **1999**, *40*, S39–S50. [CrossRef] [PubMed]
164. Rice, A.S.; Maton, S.; Postherpetic Neuralgia Study Group. Gabapentin in postherpetic neuralgia: A randomized double-blind placebo controlled study. *Pain* **2001**, *94*, 215–224. [CrossRef]
165. Pollack, M.H.; Matthews, J.; Scott, E.L. Gabapentin as a potential treatment for anxiety disorders. *Am. J. Phsychiatry* **1998**, *155*, 992–993. [CrossRef] [PubMed]
166. Backonja, M.; Beydoun, A.; Edwards, K.R.; Schwartz, S.L.; Fonseca, V.; Hes, M.; LaMoreaux, L.; Garofalo, E. Gabapentin for the symptomatic treatment of painful neuropathy in patients with diabetes mellitus: A randomized controlled trial. *JAMA* **1998**, *280*, 1831–1836. [CrossRef] [PubMed]
167. Uchino, H.; Kanai, Y.; Kim, K.; Wempe, M.F.; Chairoungdua, A.; Morimoto, E.; Anders, M.W.; Endou, E. Transport of amino acid-related compound mediate to L-type amino acid transporter 1 (LAT-1): Insights into mechanisms of substrate recognition. *Mol. Pharm.* **2002**, *61*, 729–737. [CrossRef]
168. Richter, A.; Anton, S.E.; Koch, P.; Dennett, S.L. The impact of reducing dose frequency on health outcomes. *Clin. Ther.* **2003**, *25*, 2307–2335. [CrossRef]
169. Kriel, R.L.; Birnbaum, A.K.; Cloyd, J.C.; Ricker, B.J.; Jones Saete, C.; Caruso, K.J. Failure of absorption of gabapentin after rectal administration. *Epilepsia* **1997**, *38*, 1242–1244. [CrossRef] [PubMed]
170. Cundy, C.K.; Branch, R.; Chernov-Rogan, T.; Dias, T.; Estrada, T.; Hold, K.; Koller, K.; Liu, X.; Mann, A.; Panuwat, M.; et al. XP13515 [(±)-1([α-isobutanoyloxyethoxylcarbonyl]aminomethyl)-1-cyclohexane acetic acid], a novel gabapentin prodrug: I. Design, synthesis, enzymatic conversion to gabapentin, an a intestinal transport by intestinal solute transporters. *J. Pharm. Ther.* **2004**, *311*, 315–323. [CrossRef] [PubMed]
171. Wuis, E.W.; Dirkis, M.J.; Termond, E.F.; Vree, T.B.; Van der Kleijn, E. Plasma and urinary excretion kinetics of oral baclofen in healthy subjects. *Eur. J. Clin. Pharmacol.* **1989**, *37*, 181–184. [CrossRef] [PubMed]
172. Lal, R.; Sukbuntherng, J.; Tai, E.H.L.; Upadhay, S.; Yao, F.; Warren, M.S.; Luo, W.; Bu, L.; Nguyen, S.; Zamora, J.; et al. Arbaclofen placarbil, a novel R-baclofen prodrug: Improved absorption, distribution, metabolism, and elimination properties compared with R-baclofen. *J. Pharm. Exp. Ther.* **2009**, *330*, 911–921. [CrossRef] [PubMed]
173. Loiseau, P.; Duche, B.; Pedespan, J.M. Absence epilepsies. *Epilepsia* **1985**, *36*, 1182–1186. [CrossRef]
174. Chen, X.-Q.; Venkatesh, S. Miniature device for aqueous and non-aqueous solubility measurements during drug discovery. *Pharm. Res.* **2004**, *21*, 1758–1761. [CrossRef] [PubMed]
175. Hemenway, J.N.; Jarho, P.; Henri, J.T.; Nair, S.K.; VanderVelde, D.; Georg, G.I.; Stella, V.J. Preparation and physicochemical characterization of a novel water-soluble prodrug of carbamazepine. *J. Pharm. Sci.* **2010**, *99*, 1810–1825. [CrossRef] [PubMed]
176. Hemenway, J.N.; Stella, V.J. In vitro and in vivo evaluation of a novel water-soluble *N*-glycyl prodrug (*N*-Gly-CBZ) of carbamazepine. *J. Pharm. Sci.* **2010**, *99*, 4565–4575. [CrossRef] [PubMed]
177. Hemenway, J.N.; Nti-Addae, K.; Guarino, V.R.; Stella, V.J. Preparation, characterization and in vivo conversion of new water-soluble sulfenamide prodrugs of carbamazepine. *Bioorg. Med. Chem. Lett.* **2007**, *17*, 6629–6632. [CrossRef] [PubMed]

178. Dunayevich, E.; Erickson, J.; Levine, L.; Landbloom, R.; Schoepp, D.D.; Tollefson, G.D. Efficacy and tolerability of an mGlu2/3 agonist in the treatment of generalized anxiety disorder. *Neuropsychopharmacology* **2008**, *33*, 1603–1610. [CrossRef] [PubMed]
179. Rorick-Kehn, L.M.; Perkins, E.J.; Knitowski, K.M.; Hart, J.C.; Johnson, B.G.; Schoepp, D.D.; McKinzie, D. Improved bioavailability of the mGlu213 receptor agonist LY354740 using a prodrug strategy: In vivo pharmacology of LY544344. *J. Pharm. Exp. Ther.* **2005**, *316*, 905–913. [CrossRef] [PubMed]
180. Varma, M.V.; Eriksson, A.H.; Sawada, G.; Pak, Y.A.; Perkins, E.J.; Zimmerman, C.L. Transepithelial transport of the group II metabotropic glutamate 2/3 receptor agonist (1*S*,2*S*,5*R*,6*S*)-2-aminobicyclo[3.1.0]hexane-2,6-dicarboxylate (LY354740) and its prodrug (1*S*,2*S*,5*R*,6*S*)-2-[(2′*S*)-(2′-amino)propionyl]aminobicyclo[3.1.0]hexane-2,6-dicarboxylate (LY544344). *Drug Metabol. Dis.* **2009**, *37*, 211–220.
181. Goodman, D.W. Lisdexamfetamine dimesylate (Vyvanase), a prodrug stimulant or attention deficit/hyperactivity disorder. *Pharm. Ther.* **2010**, *35*, 273–387.
182. Pennick, M. Absorption of lisdexamphetamine dismesylate and its enzymatic conversion to d-amphetamine. *Neuropsychiatr. Dis. Treat.* **2010**, *6*, 317–327. [CrossRef] [PubMed]
183. Cowles, B.J. Lisdexamfetamine for treatment of attention-deficit/hyperactivity disorder. *Ann. Pharmacother.* **2009**, *43*, 669–676. [CrossRef] [PubMed]
184. Fearnley, J.M.; Lees, A.J. Ageing and Parkinson's disease: Substantia nigra regional selectivity. *Brain* **1991**, *114*, 2283–2301. [CrossRef] [PubMed]
185. Di Stefano, A.; Sazio, P.; Cuasa, L.S. Antiparkison prodrug. *Molecules* **2008**, *13*, 46–58. [CrossRef] [PubMed]
186. Felix, A.M.; Winter, D.P.; Wang, S.S.; Kulesha, I.D.; Pool, W.R.; Hane, D.L.; Sheppard, H. Synthesis and antineserpine activity of peptides of *L*-dopa. *J. Med. Chem.* **1974**, *17*, 422–426. [CrossRef] [PubMed]
187. Wang, H.; Lee, J.; Tsai, M.; Lu, H.; Hsu, W. Synthesis and pharmacological activities of a novel tripeptide mimetic dopamine prodrug. *Bioorg. Med. Chem. Lett.* **1995**, *5*, 2195–2198. [CrossRef]
188. Peura, L.; Malmioja, K.; Huttunen, K.; Leppänen, J.; Hämäläinen, M.; Forsberg, M.M.; Gynther, M.; Rautio, J.; Laine, K. Design, synthesis and brain uptake of LAT1-targeted aminoacid prodrugs of dopamine. *Pharm. Res.* **2013**, *30*, 2523–2537. [CrossRef] [PubMed]
189. Zeilhofer, H.U.; Wildner, H.; Yévenws, G.E. Fast synaptic inhibition in spinal sensory processing and pain control. *Physiol. Rev.* **2012**, *92*, 193–235. [CrossRef] [PubMed]
190. Sherman, S.E.; Loomis, C.W. Morphine insensitive allodynia is produced by intrathecal strychnine in the lightly anesthetized rat. *Pain* **1994**, *56*, 17–26. [CrossRef]
191. Yamamoto, T.; Yaksh, T.L. Effects of intrathecal strychnine and bicuculine on nerve compression-induced thermal hyperalgesia and selective antagonism by MK-801. *Pain* **1993**, *54*, 79–84. [CrossRef]
192. Haranishi, Y.; Hara, K.; Terada, T.; Nakamura, S.; Sata, T. The antinociceptive effect of intrathecal administration of glycine transporter-2 inhibition ALX 1393 in rat acute pain model. *Anesth. Anal.* **2010**, *110*, 615–621. [CrossRef] [PubMed]
193. Seta, K.; Sershen, H.; Lajtha, A. Cerebral amino acid uptake in vivo in newborn mice. *Brain Res.* **1972**, *47*, 415–425. [CrossRef]
194. Toth, E.; Lajtha, A. Elevation of cerebral levels of non-essential amino acids in vivo by administration of large doses. *Neurochem. Res.* **1981**, *6*, 1309–1317. [CrossRef] [PubMed]
195. Doheny, M.; Nagaki, S.; Patsalos, P.N. A microdialysis study of glycinamide, glycine and other amino acid neurotransmitters in rat frontal cortex and hippocampus after the administration of milacemide, a glycine prodrug. *Naunyn Schmiedebergs Arch. Pharmacol.* **1996**, *354*, 157–163. [CrossRef] [PubMed]
196. Beyer, C.; Komisaruk, B.K.; González-Flores, O.; Gómora-Arrati, P. Glycinamide a glycine prodrug, induces antinociception by intraperitoneal or oral ingestion in ovariectomized rats. *Life Sci.* **2013**, *92*, 576–581. [CrossRef] [PubMed]
197. Gynther, M.; Jalkanen, A.; Lethonen, M.; Forsberg, M.; Laine, K.; Ropponen, J.; Leppänen, J.; Knuuti, J.; Rautio, J. Brain uptake of ketoprofen-lysine prodrug in rats. *Int. J. Pharm.* **2010**, *399*, 121–128. [CrossRef] [PubMed]
198. Bennet, S.N.; McNeil, M.M.; Bland, L.A.; Arduino, M.J.; Villarino, M.E.; Perrotta, D.M.; Burwen, D.R.; Welbel, S.F.; Pegues, D.A.; Stroud, L.; et al. Post-operative infections traced to contamination of an intravenous anesthetic, Propofol. *N. Engl. J. Med.* **1995**, *33*, 147–154. [CrossRef] [PubMed]

199. Trapani, G.; Latrofa, A.; Franco, M.; Lopedota, A.; Maciocco, E.; Liso, G. Water-soluble salts of amino acid esters of the anesthetic agent Propofol. *Int. J. Pharm.* **1998**, *175*, 195–204. [CrossRef]
200. Trapani, G.; Altomare, C.; Sanna, E.; Biggio, G.; Liso, G. Propofol in anaesthesic. Mechanism of action, structure-activity relationships and drug delivery. *Curr. Med. Chem.* **2000**, *7*, 249–271. [CrossRef] [PubMed]
201. Altomare, C.; Trapani, G.; Latrofa, A.; Serra, M.; Sanna, E.; Biggio, G.; Liso, G. Highly water-soluble derivatives of the anesthetic agent propofol: In vitro and in vivo evaluation of cyclic amino acid esters. *Eur. J. Pharm. Sci.* **2003**, *20*, 17–26. [CrossRef]
202. Zhou, Y.; Yang, J.; Liu, J.; Wang, Y.; Zhang, W.S. Efficacy comparison of the novel water-soluble propofol prodrug HX0969w and fosfopropofol in mice and rats. *Br. J. Anaesth.* **2013**, *111*, 825–832. [CrossRef] [PubMed]
203. Lang, B.C.; Yang, J.; Wang, Y.; Luo, Y.; Kang, Y.; Liu, J.; Zhang, W.S. An improved design of water-soluble propofol prodrugs characterized by rapid onset of action. *Anesth. Anal.* **2014**, *118*, 745–754. [CrossRef] [PubMed]

Sample Availability: Samples of the compounds are not available from the authors.

➢ Development of potent CPP6–gemcitabine conjugates against human prostate cancer cell line (PC-3)

RSC Medicinal Chemistry

ROYAL SOCIETY OF CHEMISTRY

RESEARCH ARTICLE

View Article Online
View Journal

Cite this: DOI: 10.1039/c9md00489k

Development of potent CPP6–gemcitabine conjugates against human prostate cancer cell line (PC-3)†

Cristiana Correia,[abc] Cristina P. R. Xavier,[bc] Diana Duarte,[abc] Abigail Ferreira,[ad] Sara Moreira,[abc] M. Helena Vasconcelos[bce] and Nuno Vale[*abcf]

Received 18th October 2019,
Accepted 31st December 2019

DOI: 10.1039/c9md00489k

rsc.li/medchem

Gemcitabine (dFdC) is a nucleoside analogue used in the treatment of various cancers, being a standard treatment for advanced pancreatic cancer. The effect of gemcitabine is severely compromised due to its rapid plasma degradation, systemic toxicity and drug resistance, which restricts its therapeutic efficacy. Our main goal was to develop new active conjugates of dFdC with novel cell-penetrating hexapeptides (CPP6) to facilitate intracellular delivery of this drug. All new peptides were prepared by solid phase peptide synthesis (SPPS), purified and characterized by HPLC and LC-MS. Cell-penetrating peptides (CPP) contain a considerably high ratio of positively charged amino acids, imparting them with cationic character. Tumor cells are characterized by an increased anionic nature of their membrane surface, a property that could be used by CPP to target these cells. The BxPC-3, MCF-7 and PC-3 cancer cell lines were used to evaluate the *in vitro* cytotoxicity of conjugates and the results showed that conjugating dFdC with CPP6 significantly enhanced cell growth inhibitory activity on PC-3 cells, with IC_{50} between 14 and 15 nM. These new conjugates have potential to become new therapeutic tools for cancer therapy.

Gemcitabine (2′,2′-difluoro-2′-deoxycytidine, dFdC, **1**, Scheme 1), a nucleoside analogue, is a chemotherapeutic drug that acts against an extensive range of solid tumors, such as pancreatic, non-small cell lung, breast and ovarian cancers.[1] This anticancer drug has different mechanisms of action, including the inhibition of thymidylate synthetase,[2] the inhibition of DNA synthesis, and the activation of two major stress-activated signalling pathways, c-Jun N-terminal kinase (JNK) and p38 mitogen activated protein kinase (p38 MAPK), leading to increased apoptosis.[3] Gemcitabine is a prodrug whose activity occurs as a result of intracellular conversion into two active metabolites, gemcitabine diphosphate (dFdCDP) and gemcitabine triphosphate (dFdCTP), by the enzyme deoxycytidine kinase.[4] dFdCDP also inhibits ribonucleotide reductase, the enzyme responsible for catalyzing the synthesis of deoxynucleoside triphosphates required for DNA synthesis.[5] dFdCTP competes with endogenous deoxynucleoside triphosphates for incorporation into DNA.[1] Nevertheless, treatment with gemcitabine has limited efficacy due to its high toxicity and inactivation in the serum, through deamination of its 4-*N* amine by cytidine deaminase (CDA).[6] Due to the high levels of this enzyme in both human plasma and liver,[7] gemcitabine metabolic inactivation represents one of the major obstacles to its efficacy.[8] Another important drawback associated with gemcitabine therapy is the drug resistance related to nucleoside transporter deficiency, which is developed by some tumor cells after initial tumor regression. Gemcitabine is transported into cells by concentrative and equilibrative nucleoside transporters,[9–14] such as human equilibrative nucleoside transporter-1 (hENT-1). Therefore, the expression of this transporter plays a key role in gemcitabine intracellular uptake.[15]

The plasma level of gemcitabine can quickly drop below the effective threshold level due to its short half-life (8–17 min), thus limiting its clinical benefit. Therefore, much higher doses are required to reach an effective plasma concentration, increasing the risk of adverse side effects.[1] In

[a] *Laboratory of Pharmacology, Department of Drug Sciences, Faculty of Pharmacy, University of Porto, Rua de Jorge Viterbo Ferreira 228, 4050-313 Porto, Portugal. E-mail: nuno.vale@ff.up.pt*
[b] *Institute of Molecular Pathology and Immunology of the University of Porto (IPATIMUP), Rua Júlio Amaral de Carvalho, 45, 4200-135 Porto, Portugal*
[c] *Instituto de Investigação e Inovação em Saúde (i3S), University of Porto, Rua Alfredo Allen, 208, 4200-135 Porto, Portugal*
[d] *LAQV/REQUIMTE, Department of Chemical Sciences, Faculty of Pharmacy, University of Porto, Rua de Jorge Viterbo Ferreira 228, 4050-313 Porto, Portugal*
[e] *Laboratory of Microbiology, Department of Biological Sciences, Faculty of Pharmacy, University of Porto, Rua de Jorge Viterbo Ferreira, 228, 4050-313 Porto, Portugal*
[f] *Department of Molecular Pathology and Immunology, Abel Salazar Biomedical Sciences Institute (ICBAS), University of Porto, Rua de Jorge Viterbo Ferreira 228, 4050-313 Porto, Portugal*

† Electronic supplementary information (ESI) available. See DOI: 10.1039/c9md00489k

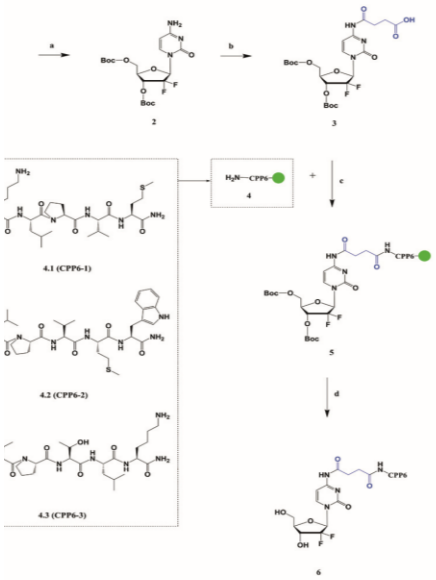

thetic pathway to CPP6-C2-dFdC conjugates (**6**) and sentations of new CPP6 (**4**). a) $(Boc)_2O$, KOH 1 M, b) succinic anhydride, *N*,*N*-dimethylformamide (DMF), sopropylamine (DIEA), rt, magnetic agitation, 24 h to F, *O*-(benzotriazol-1-yl)-*N*,*N*,*N*′,*N*′-tetramethyluronium phate (HBTU), DIEA, rt, manual agitation, 2 h; d) cid (TFA) : H_2O : triisopropylsilane (TIS) 95 : 2.5 : 2.5, 4 h,

ove its metabolic stability and cytotoxic activity, rug resistance, many alternatives have emerged, ne synthesis of prodrugs.[16–18] Chemical could potentially lead to new therapeutic Numerous modifications have already been 4-(*N*)- and 5′-positions of gemcitabine, such as tion of poly(ethylene glycol) (PEG), valproic acid, squalenoic acid (squalene) or valeroyl, uroyl and stearoyl linear acyl derivatives in the the addition of fatty acid chains or phosphate tecting groups to the 5′-position.[1,16–19] The enzymatic profiles of 5′-D-valyl-gemcitabine and nyl-gemcitabine have shown potential to oral uptake and delay the enzymatic , as well as to enhance the uptake and cytotoxic ncitabine in cancer cells.[20] More recently, the f cell-penetrating peptides (CPP) to the aniline dCDP, through suitable bio-/chemo-reversible eported.[19] The use of a CPP represents a good he formulation of new prodrugs due to their y as vectors for the achievement of cellular ug delivery in a non-cytotoxic way.[21–23]
he above-mentioned problems, we hypothesized ion of dFdC with CPP6 could enhance the owth. We were supported by our experience in the conjugation of dFdC with classical CPP,[19] and also encouraged by the recent prodrug conjugates of dFdC using amino acids as linker, that showed enhanced anti-proliferative activity of parental drug on A549 cells,[24] and by the combination of this drug with polysaccharides, with reported enhanced antitumor activity and reversed apoptosis caused by dFdC in both spleen and bone marrow.[25] Our new family of CPP6 was inspired by two peptides (KLPVM and VPMLK) that were reported to have high percentage of cell penetration, from a family of CPP5.[26]

The amino acid tryptophan (Trp) was added in order to further improve their capacity of cell penetration, since tryptophan (Trp) has high propensity to be inserted into membranes.[27,28] Specifically, the Trp residues appear to prefer to be positioned near the lipid carbonyl region.[29,30] Using standard Fmoc chemistry and solid phase peptide synthesis (SPPS) method,[31] one Trp residue was coupled to the N-terminal and to the C-terminal position of the first CPP5 and to the N-terminal of the second CPP5, yielding three novel hexapeptides: CPP6-1 (**4.1**), CPP6-2 (**4.2**), and CPP6-3 (**4.3**) (Table 1). The use of the succinic anhydride linker aimed to enhance the rate of drug delivery, due to the presence of amide bonds, which have resonance stabilization, being relatively unreactive under physiological conditions, and thus protecting the drug from cytidine deaminase (CDA, Fig. 1).

In parallel, two –OH groups of dFdC (**1**) were selectively protected with Boc groups,[32] resulting in compound **2**. The success of the protection was verified by NMR and LC-MS.[33] Then, compound **2** was conjugated with succinic anhydride[34] and the reaction progress was followed by TLC. This reaction nearly completed, yielding one major product (**3**), which was then conjugated with CPP6 by SPPS. Conjugates were then cleaved[35] from the solid support, purified by reverse phase medium-pressure liquid chromatography (RP-MPLC) to >95% purity[36] and tested in cells from the human pancreatic adenocarcinoma BxPC-3,[37] human breast adenocarcinoma MCF-7,[38] and human prostate adenocarcinoma PC-3[38] cell lines.

The cell growth inhibitory activity of native dFdC (**1**), novel CPP6 (**4**) and conjugates (**6**) was evaluated following 72 h treatment of BxPC-3 cells, with the sulforhodamine (SRB) assay, and of MCF-7 and PC-3 cells, with the MTT assay. The SRB colorimetric assay is used to determine cell density, based on the measurement of cellular protein content, which infers the cellular growth.[39] In the MTT assay, the yellow tetrazolium MTT (3-(4,5-dimethylthiazol-2-yl)-2,5-diphenyltetrazolium bromide) is reduced by metabolically active cells, in part by the action of dehydrogenase enzymes, to generate reducing equivalents such as NADH and NADPH.[38] These assays have been used to evaluate the cytotoxicity of drugs and conjugates in the indicated cancer cell lines.

Since the efficacy of dFdC is dependent on the hENT-1 transporter,[40] we further investigated if the activity of conjugates **6** also relies on the presence of this transporter.

View Article Online
RSC Medicinal Chemistry Research Article

Table 1 Sequence of peptides and conjugates evaluated on the human adenocarcinoma cell lines (BxPC-3, MCF-7 and PC-3). "I" is the human equilibrative nucleoside transporter-1 (hENT-1) inhibitor (nitrobenzylthioinosine, NBMPR)

#	Compound	Sequence	MW (g mol^{-1})	BxPC-3[a] IC_{50} 72 h (nM) (−I)	BxPC-3[a] IC_{50} 72 h (nM) (+I)	MCF-7[b] IC_{50} 72 h (nM)	PC-3[b] IC_{50} 72 h (nM)
1	dFdC (gemcitabine)	—	263.20	130 ± 20	190 ± 40	1.4 ± 0.1	74 ± 6.1
4.1	CPP6-1	WKLPVM	772.02	>1000	>1000	223 ± 46	>1000
4.2	CPP6-2	KLPVMW	772.02	>1000	>1000	>1000	>1000
4.3	CPP6-3	WVPTLK	741.94	>1000	>1000	>1000	>1000
6.1	dFdC-C2-CPP6-1	dFdC-$(CH_2)_2$-WKLPVM	1117.28	180 ± 10	380 ± 10	5.1 ± 0.7	15 ± 0.6
6.2	dFdC-C2-CPP6-2	dFdC-$(CH_2)_2$-KLPVMW	1117.28	170 ± 20	384 ± 70	6.9 ± 1.0	>1000
6.3	dFdC-C2-CPP6-3	dFdC-$(CH_2)_2$-WVPTLK	1087.19	200 ± 10	381 ± 20	4.0 ± 0.8	14 ± 0.4
7	Tamoxifen	—	371.52	N.D.	N.D.	20 ± 1.5	>1000
8	Metformin	—	129.16	N.D.	N.D.	9.9 ± 0.9	189 ± 25

[a] SRB assay was performed in the BxPC-3 cells following 72 h treatment. [b] Cytotoxicity of drugs and peptides using the MTT assay.

Thus, BxPC3 cells were incubated with conjugates **6** in the presence or in the absence of a known inhibitor of this transporter. Nitrobenzylthioinosine (NBMPR), a small molecule inhibitor of equilibrative nucleoside transporter (ENT) proteins,[41] was selected. The effect on cell growth was assessed with the SRB assay[42] and the IC_{50} of the conjugates *versus* controls was calculated (Table 1).

Results showed that the IC_{50} of the conjugates was always higher in the presence of the inhibitor, suggesting that, in BxPC3 cells, conjugates **6** are preferentially transported by hENT-1. We suggest (Fig. 1) that conjugates **6** are preferentially transported by this hENT-1, and that once in the cytoplasm, dFdC-CPP6 conjugates may undergo sequential phosphorylations, disrupting DNA synthesis and causing apoptosis.

All peptides developed in this project have proline (Pro) in the sequence of amino acids, which allows the peptide to cyclize.[43,44] However, the position of the Trp residues greatly influences the cell growth results (Table 1). It has been reported that a minimum of two Trp residues with amidated C-terminal end is essential for the antimicrobial activity of short synthetic peptides.[45–49] Trp is an aromatic, neutral amino acid, and is the largest amino acid containing its characteristic indole functional group. Trp can be considered hydrophobic due to its uncharged side chain. However, Trp side chain is not embedded in the hydrocarbon region of lipid bilayers and positions itself towards the hydrophilic side.[50] So, Trp prefers to be located specifically near the lipid-carbonyl region and partitions near the membrane-water interface, showing a strong tendency to insert itself into membranes.[28,29] Due to its aromatic side chain, Trp is able to rapidly form hydrogen bonds with the bilayer components, having a dipole moment of ~2.1 debyes.[51] These hydrophilic and hydrophobic attributes of Trp make it ideal for insertion into membranes.[52] So, it can be understood that the Trp that is closest to a region with more carbonyl groups is more likely to make bonds and thus present a greater conformational stability. These two evidences attributed to Trp can be established in the context showed in Fig. 2.

The results observed for compounds **6.1** and **6.3** prove that activity in MCF-7 and PC-3 cells is much better when Trp is in the middle of the conjugate (N-terminal position of the peptide). For PC-3 cells, dFdC IC_{50} decreased from 74 nM to 15 nM and 14 nM, after conjugation with CPP6-1 and CPP6-3, respectively, demonstrating an increase in the cell growth inhibitory activity in the presence of the conjugates. Also, the three new conjugates of dFdC with CPP6 presented more potent cell growth inhibitory activity in MCF-7 and PC-3 cells than the reference drugs tamoxifen or metformin,[53] except conjugate **6.2** in the PC-3 cell line.

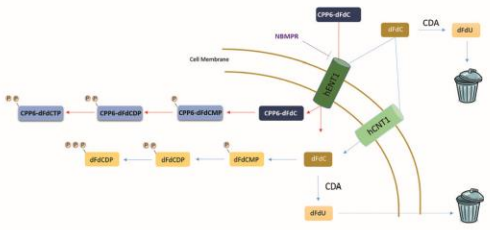

Fig. 1 Schematic representation of our proposed hypothetic mechanism for the transport of CPP6–dFdC conjugates and gemcitabine (dFdC) across cell membrane. hENT-1: human equilibrative nucleoside transporter; hCNT-1: human concentrative nucleoside transporter; dFdCMP: gemcitabine monophosphate; dFdCDP: gemcitabine diphosphate; dFdCTP: gemcitabine triphosphate; dFdU: 2′,2′-difluoro-2′-deoxyuridine; CDA: cytidine deaminase; CPP6–dFdC: conjugates of dFdC with CPP6 developed in this project.

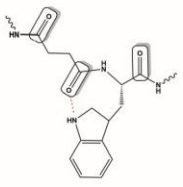

Fig. 2 Representation for conjugates **6.1** and **6.3** of Trp near the carbonyl region and hydrogen bond with succinic anhydride. The Trp that is closest to a region with higher carbonyl groups is more likely to make bonds and thus present a greater conformational stability.

Conclusions

In summary, dFdC inhibits the growth of prostate cancer cell line but only at high concentrations,[54,55] which is in accordance with clinical data suggesting only modest activity when this drug is used as a single agent for metastatic androgen-independent prostate cancer.[56] Additionally, it has been reported that PC-3 cells acquire dFdC resistance by gradual loss of HMGN5 expression.[57] In the present study, three novel dFdC prodrug conjugates with CPP6 were synthesized and tested in BxPC-3, MCF-7 and PC-3 cell lines. Conjugates **6.1** and **6.3** have significantly enhanced cell growth inhibitory activity against human prostate adenocarcinoma cells, as demonstrated by the lower IC_{50} in the PC-3 cell line, when compared with dFdc alone. These results suggest that dFdC conjugation with CPP, in particular hexapeptides, can be an interesting approach to develop therapeutic tools for prostate cancer treatment.

Conflicts of interest

There are no conflicts to declare.

Acknowledgements

D. D. and A. F. thank the Fundação para a Ciência e Tecnologia (FCT, Portugal) for the Ph.D. grants SFRH/BD/140734/2018 and PD/BD/135120/2017, respectively. C. P. R. X. acknowledges support from FCT through the post-doc grant SFRH/BPD/122871/2016. N. V. acknowledges support from FCT and FEDER (European Union) for financial support through IF/00092/2014/CP1255/CT0004 project. N. V. also thanks FCT for IF position and Fundação Manuel António da Mota (FMAM, Portugal) for the support to Nuno Vale's Research Group. The contents of this report are solely the responsibility of the authors and do not necessarily represent the official views of the FCT or FMAM. All cell lines used in our Labs were obtained from European Collection of Authenticated Cell Cultures (ECACC).

Notes and references

1 E. Moysan, G. Bastiat and J. P. Benoit, *Mol. Pharmaceutics*, 2013, **10**, 430–444.
2 R. J. Honeywell, V. W. R. van Haperen, G. Veerman, K. Smid and G. J. Peters, *Int. J. Biochem. Cell Biol.*, 2015, **60**, 73–81.
3 F. Liu, A. J. Gore, J. L. Wilson and M. Korc, *PLoS One*, 2014, **9**, e84982.
4 E. Mini, S. Nobili, B. Caciagli, I. Landini and T. Mazzei, *Ann. Oncol.*, 2006, **17**(Suppl 5), v7.
5 V. Heinemann, Y. Z. Xu, S. Chubb, A. Sen, L. W. Hertel, G. Grindey and W. Plunkett, *Mol. Pharmaceutics*, 1990, **38**, 567–572.
6 A. M. Storniolo, S. R. Allerheiligen and H. L. Pearce, *Semin. Oncol.*, 1997, **24**(Suppl 7), 72–77.
7 J. R. Kroep, C. J. A. van Moorsel, G. Veerman, V. A. Voorn, R. M. Schultz, J. F. Worzalla and G. J. Peters, *Purine and Pyrimidine Metabolism in Man Ix*, Springer US, 1998.
8 H. Ueno, K. Kiyosawa and N. Kaniwa, *Br. J. Cancer*, 2007, **97**, 145–151.
9 J. Baselga, L. Norton, J. Albanell, Y. M. Kim and J. Mendelsohn, *Cancer Res.*, 1998, **58**, 2825–2831.
10 C. Chang, P. W. Swaan, L. Y. Ngo, P. Y. Lum, S. D. Patil and J. D. Unadkat, *Mol. Pharmacol.*, 2004, **65**, 558–570.
11 M. Podgorska, K. Kocbuch and T. Pawelczyk, *Acta Biochim. Pol.*, 2005, **52**, 749–758.
12 X. Fang, F. E. Parkinson, D. A. Mowles, J. D. Young and C. E. Cass, *Biochem. J.*, 1996, **317**, 457–465.
13 J. R. Hammond, S. Lee and P. J. Ferguson, *J. Pharmacol. Exp. Ther.*, 1999, **288**, 1185–1191.
14 M. W. Ritzel, A. M. Ng, S. Y. Yao, K. Graham, S. K. Loewen, K. M. Smith, R. J. Hyde, E. Karpinski, C. E. Cass, S. A. Baldwin and J. D. Young, *Mol. Membr. Biol.*, 2001, **18**, 65–72.
15 G. Hu, F. Li, K. Ouyang, F. Xie, X. Tang, K. Wang and X. Qin, *Int. J. Oncol.*, 2012, **40**, 798–806.
16 T. Karampelas, O. Argyros, N. Sayyad, K. Spyridaki, C. Pappas, K. Morgan and D. Fokas, *Bioconjugate Chem.*, 2014, **25**, 813–823.
17 M. Dasari, A. P. Acharya, D. Kim, S. Lee, S. Lee, J. Rhea and N. Murthy, *Bioconjugate Chem.*, 2013, **24**, 4–8.
18 J. S. Ryu and D. Raucher, *Cancer Lett.*, 2014, **348**, 177–184.
19 N. Vale, A. Ferreira, I. Fernandes, C. Alves, M. J. Araújo, N. Mateus and P. Gomes, *Bioorg. Med. Chem. Lett.*, 2017, **27**, 2898–2901.
20 Y. Tsume, T. Incecayir, X. Song, J. M. Hilfinger and G. L. Amidon, *Eur. J. Pharm. Biopharm.*, 2014, **86**, 514–523.
21 D. M. Copolovici, K. Langel, E. Eriste and Ü. Langel, *ACS Nano*, 2014, **8**, 1972–1994.
22 F. Wang, Y. Wang, X. Zhang, W. Zhang, S. Guo and F. Jin, *J. Controlled Release*, 2014, **174**, 126–136.
23 J. Regberg, A. Srimanee and Ü. Langel, *Pharmaceuticals*, 2012, **5**, 991–1007.
24 L. Ma, Y. Chen, X. Wang, M. Xiong, Y. Sun, X. Zhang and Y. Zhao, *Bioorg. Med. Chem. Lett.*, 2018, **28**, 2920–2924.
25 X. Xie, Y. Zhou, X. Wang, J. Guo, J. Li, H. Fan, J. Dou, B. Shen and C. Zhou, *Carbohydr. Polym.*, 2017, **173**, 360–371.
26 J. A. Gomez, J. Chen, J. Ngo, D. Hajkova, I. J. Yeh, V. Gama and S. Matsuyama, *Pharmaceuticals*, 2010, **3**, 3594–3613.
27 K. Kachel, E. Asuncion-Punzalan and E. London, *Biochemistry*, 1995, **34**, 15475–15479.
28 D. J. Schibli, R. F. Epand, H. J. Vogel and R. M. Epand, *Biochem. Cell Biol.*, 2002, **80**, 667–677.
29 W. M. Yau, W. Wimley, K. Gawrisch and S. H. White, *Biochemistry*, 1998, **37**, 14713–14718.
30 M. R. de Planque, J. A. Kruijtzer, R. M. Liskamp, D. Marsh, D. V. Greathouse, R. E. Koeppe and J. A. Killian, *J. Biol. Chem.*, 1999, **274**, 20839–20846.
31 Solid-phase peptide synthesis (SPPS): all peptides were synthesised using solid phase Fmoc chemistry by manual synthesis, in a polypropylene syringe with a polyethylene porous filter. A Teflon™ rod was used to manually stir the

resin throughout the synthesis. Couplings were performed using *O*-(benzotriazol-1-yl)-*N*,*N*,*N*′,*N*′-tetramethyluronium hexafluorophosphate (HBTU) and *N*-ethyl-*N*,*N*-diisopropylamine (DIEA) in *N*,*N*-dimethylformamide (DMF). Removal of Fmoc protecting groups was achieved using piperidine for 20 minutes (20% in DMF). The peptides were synthesized on Fmoc-Rink Amide MBHA resin (Novabiochem, loading: 0.78 mmol g^{-1}). Coupling of the first amino acid was carried out manually on the syringe. The resin was first swollen in DMF and then in dichloromethane (DCM), followed by addition of the first amino acid (5 equivalents dissolved in DMF), HBTU (5 equivalents) and DIEA (10 equivalents). The reaction proceeded for 1 hour after which the solution was rejected and the resin was washed 3 times with DMF and another 3 times with DCM. The success of the coupling was verified by the Kaiser test. To grow the chain, each amino acid was added according to the desired sequence and this procedure was repeated for every single amino acid.

32 Gemcitabine (500 mg, 1.90 mmol) was dissolved in 50 mL of KOH 1M aqueous solution and stirred for 1 h. A solution of Boc_2O (6.22 g, 28.5 mmol) in 40 mL of dioxane was added dropwise over 40 min. The mixture was stirred at room temperature for 5 h and then extracted by ethyl acetate. The organic layer was washed 3 times with brine, dried over anhydrous Na_2SO_4, and concentrated by rotary evaporation under vacuum. The residue was further purified by column chromatography with hexane–acetone (8 : 1) to give 3′,5′-*O*-bis(*tert*-butoxycarbonyl)-gemcitabine (2) as a white solid (90% yield).

33 The ^{1}H-NMR spectrum (600 MHz, $CDCl_3$) showed the following resonances: d = 7.45 (s, 1H), 6.40 (s, 1H), 5.92 (s, 1H), 5.22 (m, 1H), 4.42–4.18 (m, 3H), 1.50 (m, 9H), 1.35 (m, 9H). ESI-MS, m/z 464.18 [positive, (M + H)], 927.36 [positive, (2M + H)].

34 Conjugation of dFdC with succinic anhydride: a suspension of dFdC-Boc_2 and succinic anhydride (1.2 eq.) was prepared in 2 to 3 mL of DMF, at room temperature, under magnetic agitation. Then, DIEA was added (2 eq.) and the reaction elapses from 24 h to 48 h.

35 Cleavage of conjugates: a cleavage cocktail consisting of TFA/H_2O/TIS (95 : 2.5 : 2.5 v/v, 5 mL) was added to the dry peptidyl resin. The reaction mixture was gently agitated at room temperature for 4 h. The resulting content was filtered on a D4 funnel, and the resin was washed with TFA followed by removal of solvent under reduced pressure. Conjugates were precipitated using cold *tert*-butyl methyl ether (14 mL of ether per 1 mL of peptide solution), cooled to −22 °C for about 30 minutes and then centrifuged at 3500 rpm for 5 minutes at −5 °C. The ether was carefully rejected and "fresh" ether was added again. The addition of ether and centrifugation was repeated 2 more times and finally the tubes were left in a vacuum desiccator until the crude conjugates were dry.

36 Purification of conjugates: dry conjugate pellets were solubilized in 10% aqueous acetic acid and analysed by high-performance liquid chromatography with diode-array detection (HPLC-DAD) and liquid chromatography-mass spectrometry (LC-MS).

37 Cell viability assay on BxPC-3 cells: cell growth was assessed by the SRB assay. Cells were seeded into a 96-well plate at a concentration of 7.5×10^4 cells per mL with RPMI medium supplemented with 5% FBS for 24 h. The following day (24 h after), 100 μL per well of different concentrations of the synthesized conjugates or appropriate controls (dFdC or CPP6) were added to the cells and these were further incubated for 72 h. After the incubation, cells were fixed by trichloroacetic acid (TCA) (0 °C, 1 h, 10% per well), washed 3 times using deionized water and left to dry. Dry cells were stained for 30 min with sulforhodamine (SRB) solution (sulforhodamine B 0.4% + acetic acid 1%), washed with 1% acetic acid and left to dry. Finally, the protein-bound dye was solubilized with 100 μL of 10 mM Tris base per well and the absorbance was read in an automated microplate reader (Sinergy HT, Biotek Instruments Inc, Vermont, USA) at 510 nm.

38 Cell viability assays on PC-3 and MCF-7 cells: human PC-3 metastatic prostate cells and MCF-7 breast cancer cell lines were seeded in 96-well plates with 200 μL per well, with an initial cell density of 5000 cells per well. Cells were allowed to attach for 24 h and were next either left untreated or treated with 4.1, 4.2, 4.3, 6.1, 6.2, 6.3 or gemcitabine (0.001, 0.01, 0.1, 1 and 3 μM) for 72 h. During all the experimental period, cells were maintained at 37 °C with 5% CO_2. Vehicle control experiments (cells exposed to DMSO at maximum final concentration of 0.1% v/v) were also performed in parallel. After cell treatment, viability was evaluated using the MTT protocol. At the end of incubations, cell medium was removed and 100 μL per well of MTT solution (0.5 mg mL^{-1} in PBS) were added. Then, plates were incubated for 3 h protected from light. After this period, MTT solution was removed and DMSO (100 μL per well) was added to solubilize the formazan crystals. Absorbance was measured at 570 nm in an automated microplate reader (Sinergy HT, Biotek Instruments Inc, Vermont, USA). Results were compared with the respective control whose average of values was set to 100%. All conditions were performed in triplicate.

39 V. Vichai and K. Kirtikara, *Nat. Protoc.*, 2006, **1**, 1112–1116.
40 S. Nordh, D. Ansari and R. Andersson, *World J. Gastroenterol.*, 2014, **20**, 8482–8490.
41 M. Tsujie, S. Nakamori, S. Nakahira, Y. Takahashi, N. Hayashi, J. Okami, H. Nagano, K. Dono, K. Umeshita, M. Sakon and M. Monden, *Anticancer Res.*, 2007, **27**, 2241–2249.
42 Study with NBMPR (nitrobenzylthioinosine): assay performed in exact equal conditions as the assay described[37] but, before the addition of compounds, cells were incubated with NBMPR for 5 min (1 μM per well).
43 M. Maleševi, M. Schumann, G. Jahreis, G. Fischer and C. Lücke, *ChemBioChem*, 2012, **13**, 2122–2127.
44 M. Hollosi, L. Radics and T. Wieland, *Int. J. Pept. Protein Res.*, 1977, **10**, 286–290.

45 J. Choi and E. Moon, *J. Microbiol. Biotechnol.*, 2009, **19**, 792–802.
46 M. B. Strøm, O. Rekdal and J. S. Svendsen, *J. Pept. Sci.*, 2002, **8**, 431–437.
47 M. Strom, T. Hansen, M. Havelkova and V. Torfoss, *Therapeutic Peptides*, US8809280 B2, 2014.
48 X. Bi, C. Wang, L. Ma, Y. Sun and D. J. Shang, *Appl. Microbiol.*, 2013, **115**, 663–672.
49 M. Arias, L. T. Nguyen, A. M. Kuczynski, T. Lejon and H. J. Vogel, *Antibiotics*, 2014, **3**, 595–616.
50 G. Trinquier and Y. H. Sanejouand, *Protein Eng., Des. Sel.*, 1998, **11**, 153–169.
51 H. Khandelia and Y. N. Kaznessis, *J. Phys. Chem. B*, 2007, **111**, 242–250.
52 M. B. Strøm, O. Rekdal and J. S. Svendsen, *J. Pept. Res.*, 2000, **56**, 265–274.
53 Chemical structures of tamoxifen and metformin are represented in Fig. S20 in the ESI.†
54 H. Khandelia and Y. N. J. Kaznessis, *J. Phys. Chem. B*, 2007, **111**, 242–250.
55 M. V. Cronauer, H. Klocker, H. Talasz, F. H. Geisen, A. Hobisch, C. Radmayr, G. Böck, Z. Culig, M. Schirmer, A. Reissigl, G. Bartsch and G. Konwalinka, *Prostate*, 1996, **28**, 172–181.
56 H. J. Muenchen, M. M. Quigley, M. J. Pilat, J. E. Lehr, S. K. Brumfield, M. Mahoney and K. J. Pienta, *Anticancer Res.*, 2000, **20**, 735–740.
57 R. Morant, J. Bernhard, R. Maibach, M. Borner, M. F. Fey, B. Thürlimann, E. Jacky, F. Trinkler, J. Bauer, G. Zulian, S. Hanselmann, C. Hürny and F. Hering, *Ann. Oncol.*, 2000, **11**, 183–188.

REFERENCES

REFERENCES

REFERENCES

1. Tozer, T.N.; Rowland, M. Essentials of Pharmacokinetics and Pharmacodynamics; *Wolters Kluwer*, **2015**.
2. Fan, J.; de Lannoy, I.A. Pharmacokinetics. *Biochemical Pharmacology*, **2014**, 87, 93-120, DOI: 10.1016/j.bcp.2013.09.007.
3. Nordberg, M.; Duffus, J.; Templeton, D.M. Glossary of terms used in toxicokinetics (IUPAC Recommendations 2003). *Pure and Applied Chemistry*, **2004**, 76, 1033-1082, DOI: 10.1351/pac200476051033.
4. Lynch, T.; Price, A. The effect of cytochrome P450 metabolism on drug response, interactions, and adverse effects. *American Family Physician*, **2007**, 76, 391-396.
5. McDonnell, A.M.; Dang, C.H. Basic review of the cytochrome p450 system. *Journal of the Advanced Practitioner in Oncology*, **2013**, 4, 263-268, DOI: 10.6004/jadpro.2013.4.4.7.
6. Research and Development in the Pharmaceutical Industry. Availabe online: *https://www.cbo.gov/publication/57126* (accessed in July 2021).
7. Sertkaya, A.; Wong, H.-H.; Jessup, A.; Beleche, T. Key cost drivers of pharmaceutical clinical trials in the United States. *Clinical Trials*, **2016**, 13, 117-126, DOI: 10.1177/1740774515625964.
8. Mullard, A. New drugs cost US$2.6 billion to develop. *Nature Reviews Drug Discovery*, **2014**, 13, 877-877, DOI: 10.1038/nrd4507.
9. Food and Drug Admistration, U. The Drug Development Process. Availabe online: *https://www.fda.gov/patients/learn-about-drug-and-device-approvals/drug-development-process* (accessed in July 2021).
10. Drug Discovery and Development Process. Availabe online: *https://www.nebiolab.com/drug-discovery-and-development-process/* (accessed in July 2021).
11. Di, L.; Feng, B.; Goosen, T.C.; Lai, Y.; Steyn, S.J.; Varma, M.V.; Obach, R.S. A Perspective on the Prediction of Drug Pharmacokinetics and Disposition in Drug Research and Development. *Drug Metabolism and Disposition*, **2013**, 41, 1975-1993, DOI: 10.1124/dmd.113.054031.

12. Schultz, A.; Saville, B.R.; Marsh, J.A.; Snelling, T.L. An introduction to clinical trial design. *Paediatric Respiratory Reviews*, **2019**, 32, 30-35, DOI: 10.1016/j.prrv.2019.06.002.

13. FDA Approval Process. Availabe online: *https://www.drugwatch.com/fda/approval-process/* (accessed in July 2021).

14. Questions and Answers on FDA's Adverse Event Reporting System (FAERS). Availabe online: *https://www.fda.gov/drugs/surveillance/questions-and-answers-fdas-adverse-event-reporting-system-faers* (accessed in July 2021).

15. Alavijeh, M.; Palmer, A. The pivotal role of drug metabolism and pharmacokinetics in the discovery and development of new medicines. *IDrugs : the investigational drugs journal*, **2004**, 7, 755-763.

16. Pappalardo, F.; Russo, G.; Tshinanu, F.M.; Viceconti, M. In silico clinical trials: concepts and early adoptions. *Briefings in Bioinformatics*, **2019**, 20, 1699-1708, DOI: 10.1093/bib/bby043.

17. Marsousi, N.; Desmeules, J.A.; Rudaz, S.; Daali, Y. Usefulness of PBPK Modeling in Incorporation of Clinical Conditions in Personalized Medicine. *Journal of pharmaceutical sciences*, **2017**, 106, 2380-2391, DOI: 10.1016/j.xphs.2017.04.035.

18. Michelson, S.; Sehgal, A.; Friedrich, C. In silico prediction of clinical efficacy. *Current Opinion in Biotechnology*, **2006**, 17, 666-670, DOI: 10.1016/j.copbio.2006.09.004.

19. Kimko, H.; Pinheiro, J. Model-based clinical drug development in the past, present and future: a commentary. *British Journal of Clinical Pharmacology*, **2015**, 79, 108-116, DOI: 10.1111/bcp.12341.

20. Bolger, M.B.; Fraczkiewicz, R.; Lukacova, V. Simulations of Absorption, Metabolism, and Bioavailability. In *Drug Bioavailability*, 2008; 10.1002/9783527623860.ch17pp. 453-495.

21. Huang, Q.; Riviere, J.E. The application of allometric scaling principles to predict pharmacokinetic parameters across species. *Expert Opinion on Drug Metabolism & Toxicology*, **2014**, 10, 1241-1253, DOI: 10.1517/17425255.2014.934671.

22. Cho, H.J.; Kim, J.E.; Kim, D.D.; Yoon, I.S. In vitro-in vivo extrapolation (IVIVE) for predicting human intestinal absorption and first-pass elimination of drugs: principles and applications. *Drug Development and Industrial Pharmacy*, **2014**, 40, 989-998, DOI: 10.3109/03639045.2013.831439.

23. Khan, M.T. Predictions of the ADMET properties of candidate drug molecules utilizing different QSAR/QSPR modelling approaches. *Current Drug Metabolism*, **2010**, 11, 285-295, DOI: 10.2174/138920010791514306.

24. Norinder, U.; Bergström, C.A. Prediction of ADMET properties. *ChemMedChem: Chemistry Enabling Drug Discovery*, **2006**, 1, 920-937.

25. Van der Graaf, P.H.; Nilsson, J.; Van Schaick, E.A.; Danhof, M. Multivariate quantitative structure-pharmacokinetic relationships (QSPKR) analysis of adenosine A1 receptor agonists in rat. *Journal of Pharmaceutical Sciences*, **1999**, 88, 306-312, DOI: 10.1021/js980294a.

26. van de Waterbeemd, H.; Gifford, E. ADMET in silico modelling: towards prediction paradise? *Nature Reviews Drug Discovery*, **2003**, 2, 192-204, DOI: 10.1038/nrd1032.

27. Gabrielsson, J.; Weiner, D. Pharmacokinetic and Pharmacodynamic Data Analysis: Concepts and Applications, Third Edition; *Taylor & Francis*, **2001**.

28. Marchenko, O.V.; Katenka, N.V. Quantitative Methods in Pharmaceutical Research and Development: Concepts and Applications; *Springer International Publishing*, **2020**.

29. Gabrielsson, J.; Weiner, D. Non-compartmental analysis. *Methods in Molecular Biology*, **2012**, 929, 377-389, DOI: 10.1007/978-1-62703-050-2_16.

30. Chen, B.; Abuassba, A.O.M. Compartmental Models with Application to Pharmacokinetics. *Procedia Computer Science*, **2021**, 187, 60-70, DOI: 10.1016/j.procs.2021.04.033.

31. Parrott, N.; Lave, T. Applications of physiologically based absorption models in drug discovery and development. *Molecular Pharmaceutics*, **2008**, 5, 760-775, DOI: 10.1021/mp8000155.

32. Jones, H.; Rowland-Yeo, K. Basic concepts in physiologically based pharmacokinetic modeling in drug discovery and development. *CPT: Pharmacometrics & Systems Pharmacology*, **2013**, 2, e63, DOI: 10.1038/psp.2013.41.

33. Sager, J.E.; Yu, J.; Ragueneau-Majlessi, I.; Isoherranen, N. Physiologically Based Pharmacokinetic (PBPK) Modeling and Simulation Approaches: A Systematic Review of Published Models, Applications, and Model Verification. *Drug Metabolism and Disposition: The Biological Fate of Chemicals*, **2015**, 43, 1823-1837, DOI: 10.1124/dmd.115.065920.

34. Upton, R.N.; Foster, D.J.R.; Abuhelwa, A.Y. An introduction to physiologically-based pharmacokinetic models. *Pediatric Anesthesia*, **2016**, 26, 1036-1046, DOI: 10.1111/pan.12995.

35. Nestorov, I. Whole Body Pharmacokinetic Models. *Clinical Pharmacokinetics*, **2003**, 42, 883-908, DOI: 10.2165/00003088-200342100-00002.

36. Charles, B. Population pharmacokinetics: An overview. *Australian Prescriber*, **2014**, 37, 210-213, DOI: 10.18773/austprescr.2014.078.

37. Ette, E.I.; Williams, P.J. Population Pharmacokinetics I: Background, Concepts, and Models. *Annals of Pharmacotherapy*, **2004**, 38, 1702-1706, DOI: 10.1345/aph.1D374.

38. About Simulations Plus, Inc. Availabe online: *https://www.simulations-plus.com/about/* (accessed in July 2021).

39. Simulations Plus, Inc: Global Regulatory Strategies. Availabe online: *https://www.simulations-plus.com/services/regulatory-strategies/* (accessed in July 2021).

40. GastroPlus™. Availabe online: *https://www.simulations-plus.com/software/gastroplus/* (accessed in July 2021).

41. Daga, P.R.; Bolger, M.B.; Haworth, I.S.; Clark, R.D.; Martin, E.J. Physiologically Based Pharmacokinetic Modeling in Lead Optimization. 1. Evaluation and Adaptation of GastroPlus To Predict Bioavailability of Medchem Series. *Molecular Pharmaceutics*, **2018**, 15, 821-830, DOI: 10.1021/acs.molpharmaceut.7b00972.

42. Xia, B.; Yang, Z.; Zhou, H.; Lukacova, V.; Zhu, W.; Milewski, M.; Kesisoglou, F. Development of a Novel Oral Cavity Compartmental Absorption and Transit Model for Sublingual Administration: Illustration with Zolpidem. *The American Association of Pharmaceutical Scientists Journal*, **2015**, 17, 631-642, DOI: 10.1208/s12248-015-9727-7.

43. Santos, J.; Lobato, L.; Vale, N. Clinical pharmacokinetic study of latrepirdine via in silico sublingual administration. *In Silico Pharmacology*, **2021**, 9, 29, DOI: 10.1007/s40203-021-00083-0.

44. Kostewicz, E.S.; Aarons, L.; Bergstrand, M.; Bolger, M.B.; Galetin, A.; Hatley, O.; Jamei, M.; Lloyd, R.; Pepin, X.; Rostami-Hodjegan, A., et al. PBPK models for the prediction of in vivo performance of oral dosage forms. *European Journal of Pharmaceutical Sciences*, **2014**, 57, 300-321, DOI: 10.1016/j.ejps.2013.09.008.

45. Weinberg, B.A.; Marshall, J.L.; Hartley, M.; Salem, M.E. A paradigm shift from one-size-fits-all to tailor-made therapy for metastatic colorectal cancer. *Clinical Advances in Hematology & Oncology: H&O*, **2016**, 14, 116-128.

46. Gastmeier, P. From 'one size fits all' to personalized infection prevention. *The Journal of Hospital Infection*, **2020**, 104, 256-260, DOI: 10.1016/j.jhin.2019.12.010.

47. Clarke, W.; Dasgupta, A. Clinical Challenges in Therapeutic Drug Monitoring: Special Populations, Physiological Conditions and Pharmacogenomics; *Elsevier Science*, **2016**.

48. Kang, J.S.; Lee, M.H. Overview of therapeutic drug monitoring. *The Korean Journal of Internal Medicine*, **2009**, 24, 1-10, DOI: 10.3904/kjim.2009.24.1.1.

49. Buclin, T.; Thoma, Y.; Widmer, N.; André, P.; Guidi, M.; Csajka, C.; Decosterd, L.A. The Steps to Therapeutic Drug Monitoring: A Structured Approach Illustrated With Imatinib. *Frontiers in Pharmacology*, **2020**, 11, 177, DOI: 10.3389/fphar.2020.00177.

50. Holford, N.H.G.; Buclin, T. Safe and Effective Variability—A Criterion for Dose Individualization. *Therapeutic Drug Monitoring*, **2012**, 34, 565-568, DOI: 10.1097/FTD.0b013e31826aabc3.

51. Abrantes, J.A.; Jönsson, S.; Karlsson, M.O.; Nielsen, E.I. Handling interoccasion variability in model-based dose individualization using therapeutic drug monitoring data. *British Journal of Clinical Pharmacology*, **2019**, 85, 1326-1336, DOI: 10.1111/bcp.13901.

52. Widmer, N.; Bardin, C.; Chatelut, E.; Paci, A.; Beijnen, J.; Levêque, D.; Veal, G.; Astier, A. Review of therapeutic drug monitoring of anticancer drugs part two-Targeted therapies. *European Journal of Cancer*, **2014**, 50, 2020-2036, DOI: 10.1016/j.ejca.2014.04.015.

53. Muller, A.E.; Huttner, B.; Huttner, A. Therapeutic Drug Monitoring of Beta-Lactams and Other Antibiotics in the Intensive Care Unit: Which Agents, Which Patients and Which Infections? *Drugs*, **2018**, 78, 439-451, DOI: 10.1007/s40265-018-0880-z.

54. Maitre, T.; Muret, P.; Blot, M.; Waldner, A.; Duong, M.; Si-Mohammed, A.; Chavanet, P.; Aho, S.; Piroth, L. Benefits and Limits of Antiretroviral Drug Monitoring in Routine Practice. *Current HIV Research*, **2019**, 17, 190-197, DOI: 10.2174/1570162x17666190903232053.

55. Papamichael, K.; Cheifetz, A.S. Therapeutic drug monitoring in patients on biologics: lessons from gastroenterology. *Current Opinion in Rheumatology*, **2020**, 32, 371-379, DOI: 10.1097/bor.0000000000000713.

56. Schoretsanitis, G.; Paulzen, M.; Unterecker, S.; Schwarz, M.; Conca, A.; Zernig, G.; Gründer, G.; Haen, E.; Baumann, P.; Bergemann, N., et al. TDM in psychiatry and neurology: A comprehensive summary of the consensus guidelines for therapeutic drug monitoring in neuropsychopharmacology, update 2017; a tool for clinicians. *The World Journal of Biological Psychiatry*, **2018**, 19, 162-174, DOI: 10.1080/15622975.2018.1439595.

57. Keller, F.; Schröppel, B.; Ludwig, U. Pharmacokinetic and pharmacodynamic considerations of antimicrobial drug therapy in cancer patients with kidney dysfunction. *World Journal of Nephrology*, **2015**, 4, 330-344, DOI: 10.5527/wjn.v4.i3.330.

58. Holford, N.; Ma, G.; Metz, D. TDM is dead. Long live TCI! *British Journal of Clinical Pharmacology*, n/a, DOI: 10.1111/bcp.14434.

59. Keizer, R.J.; ter Heine, R.; Frymoyer, A.; Lesko, L.J.; Mangat, R.; Goswami, S. Model-Informed Precision Dosing at the Bedside: Scientific Challenges and Opportunities. *CPT: Pharmacometrics & Systems Pharmacology*, **2018**, 7, 785-787, DOI: 10.1002/psp4.12353.

60. Guidi, M.; Csajka, C.; Buclin, T. Parametric Approaches in Population Pharmacokinetics. *The Journal of Clinical Pharmacology*, n/a, DOI: 10.1002/jcph.1633.

61. Goutelle, S.; Woillard, J.-B.; Neely, M.; Yamada, W.; Bourguignon, L. Nonparametric Methods in Population Pharmacokinetics. *The Journal of Clinical Pharmacology*, n/a, DOI: 10.1002/jcph.1650.

62. Xu, X.S.; Yuan, M.; Zhu, H.; Yang, Y.; Wang, H.; Zhou, H.; Xu, J.; Zhang, L.; Pinheiro, J. Full covariate modelling approach in population pharmacokinetics: understanding the underlying hypothesis tests and implications of multiplicity. *Br J Clinical Pharmacology*, **2018**, 84, 1525-1534, DOI: 10.1111/bcp.13577.

63. Gupta, S.K. Use of Bayesian statistics in drug development: Advantages and challenges. *International Journal of Applied & Basic Medical Research*, **2012**, 2, 3-6, DOI: 10.4103/2229-516x.96789.

64. Donagher, J.; Barras, M.A. Therapeutic drug monitoring: using Bayesian methods to evaluate hospital practice. *Journal of Pharmacy Practice and Research*, **2018**, 48, 522-529, DOI: 10.1002/jppr.1432.

65. Drennan, P.; Doogue, M.; Hal, S.J.v.; Chin, P. Bayesian therapeutic drug monitoring software: past, present and future. *International Journal of Pharmacokinetics*, **2018**, 3, 109-114, DOI: 10.4155/ipk-2018-0005.

66. Bray, F.; Ferlay, J.; Soerjomataram, I.; Siegel, R.L.; Torre, L.A.; Jemal, A. Global cancer statistics 2018: GLOBOCAN estimates of incidence and mortality worldwide for 36 cancers in 185 countries. *CA: A Cancer Journal for Clinicians*, **2018**, 68, 394-424, DOI: 10.3322/caac.21492.

67. National Cancer Institute: Cancer Statistics. Availabe online: *https://www.cancer.gov/about-cancer/understanding/statistics* (accessed in July 2021).

68. National Cancer Institute: Types of Cancer Treatment. Availabe online: *https://www.cancer.gov/about-cancer/treatment/types* (accessed in July 2021).

69. Gegechkori, N.; Haines, L.; Lin, J.J. Long-Term and Latent Side Effects of Specific Cancer Types. *The Medical Clinics of North America*, **2017**, 101, 1053-1073, DOI: 10.1016/j.mcna.2017.06.003.

70. National Cancer Institute - Side Effects of Cancer Treatment. Availabe online: *https://www.cancer.gov/about-cancer/treatment/side-effects* (accessed in

71. Pucci, C.; Martinelli, C.; Ciofani, G. Innovative approaches for cancer treatment: current perspectives and new challenges. *Ecancer medical science*, **2019**, 13, 961, DOI: 10.3332/ecancer.2019.961.

72. Pushpakom, S.; Iorio, F.; Eyers, P.A.; Escott, K.J.; Hopper, S.; Wells, A.; Doig, A.; Guilliams, T.; Latimer, J.; McNamee, C., et al. Drug repurposing: progress, challenges and recommendations. *Nature Reviews Drug Discovery*, **2019**, 18, 41-58, DOI: 10.1038/nrd.2018.168.

73. Bayat Mokhtari, R.; Homayouni, T.S.; Baluch, N.; Morgatskaya, E.; Kumar, S.; Das, B.; Yeger, H. Combination therapy in combating cancer. *Oncotarget*, **2017**, 8, 38022-38043, DOI: 10.18632/oncotarget.16723.

74. Fisusi, F.A.; Akala, E.O. Drug Combinations in Breast Cancer Therapy. *Pharmaceutical Nanotechnology*, **2019**, 7, 3-23, DOI: 10.2174/2211738507666190122111224.

75. van Meerbeeck, J.P.; Fennell, D.A.; De Ruysscher, D.K. Small-cell lung cancer. *Lancet*, **2011**, 378, 1741-1755, DOI: 10.1016/s0140-6736(11)60165-7.

76. Sleire, L.; Førde, H.E.; Netland, I.A.; Leiss, L.; Skeie, B.S.; Enger, P.Ø. Drug repurposing in cancer. *Pharmacological Research*, **2017**, 124, 74-91, DOI: 10.1016/j.phrs.2017.07.013.

77. Fong, W.; To, K.K.W. Drug repurposing to overcome resistance to various therapies for colorectal cancer. *Cellular and Molecular Life Sciences*, **2019**, 76, 3383-3406, DOI: 10.1007/s00018-019-03134-0.

78. Bertolini, F.; Sukhatme, V.P.; Bouche, G. Drug repurposing in oncology—patient and health systems opportunities. *Nature Reviews. Clinical Oncology*, **2015**, 12, 732-742, DOI: 10.1038/nrclinonc.2015.169.

79. Souza, C.; Pellosi, D.S.; Tedesco, A.C. Prodrugs for targeted cancer therapy. *Expert Review of Anticancer Therapy*, **2019**, 19, 483-502, DOI: 10.1080/14737140.2019.1615890.

80. Giang, I.; Boland, E.L.; Poon, G.M.K. Prodrug applications for targeted cancer therapy. *The American Association of Pharmaceutical Scientists Journal*, **2014**, 16, 899-913, DOI: 10.1208/s12248-014-9638-z.

81. Singh, Y.; Palombo, M.; Sinko, P.J. Recent trends in targeted anticancer prodrug and conjugate design. *Current Medicinal Chemistry*, **2008**, 15, 1802-1826, DOI: 10.2174/092986708785132997.

82. Ettmayer, P.; Amidon, G.L.; Clement, B.; Testa, B. Lessons Learned from Marketed and Investigational Prodrugs. *Journal of Medicinal Chemistry*, **2004**, 47, 2393-2404, DOI: 10.1021/jm0303812.

83. Hashida, M. Role of pharmacokinetic consideration for the development of drug delivery systems: A historical overview. *Advanced Drug Delivery Reviews*, **2020**, 157, 71-82, DOI: 10.1016/j.addr.2020.06.015.

84. Connors, T.A.; Knox, R.J. Prodrugs in cancer chemotherapy. *Stem Cells*, **1995**, 13, 501-511, DOI: 10.1002/stem.5530130507.

85. Vale, N.; Ferreira, A.; Matos, J.; Fresco, P.; Gouveia, M.J. Amino Acids in the Development of Prodrugs. *Molecules*, **2018**, 23, DOI: 10.3390/molecules23092318.

86. Vig, B.S.; Huttunen, K.M.; Laine, K.; Rautio, J. Amino acids as promoieties in prodrug design and development. *Advanced Drug Delivery Reviews*, **2013**, 65, 1370-1385, DOI: 10.1016/j.addr.2012.10.001.

87. Katragadda, S.; Gunda, S.; Hariharan, S.; Mitra, A.K. Ocular pharmacokinetics of acyclovir amino acid ester prodrugs in the anterior chamber: evaluation of their utility in treating ocular HSV infections. *International Journal of Pharmaceutics*, **2008**, 359, 15-24, DOI: 10.1016/j.ijpharm.2008.03.015.

88. Rathore, M.; Gupta, V. Functional characterization of amino acid transport system for transport of phenylalanine on mammalian cornea for better ocular drug delivery. *Journal of Pharmaceutical Sciences,* **2010**, 2, 329-337.

89. del Amo, E.M.; Urtti, A.; Yliperttula, M. Pharmacokinetic role of L-type amino acid transporters LAT1 and LAT2. *European Journal of Pharmaceutical Sciences*, **2008**, 35, 161-174, DOI: 10.1016/j.ejps.2008.06.015.

90. Ylikangas, H.; Malmioja, K.; Peura, L.; Gynther, M.; Nwachukwu, E.O.; Leppänen, J.; Laine, K.; Rautio, J.; Lahtela-Kakkonen, M.; Huttunen, K.M., et al. Quantitative insight into the design of compounds recognized by the L-type amino acid transporter 1 (LAT1). *ChemMedChem*, **2014**, 9, 2699-2707, DOI: 10.1002/cmdc.201402281.

91. Song, X.; Lorenzi, P.L.; Landowski, C.P.; Vig, B.S.; Hilfinger, J.M.; Amidon, G.L. Amino acid ester prodrugs of the anticancer agent gemcitabine: synthesis, bioconversion, metabolic bioevasion, and hPEPT1-mediated transport. *Molecular Pharmaceutics*, **2005**, 2, 157-167, DOI: 10.1021/mp049888e.

92. Diaz-Padilla, I.; Siu, L.L. Brivanib alaninate for cancer. *Expert Opinion on Investigational Drugs*, **2011**, 20, 577-586, DOI: 10.1517/13543784.2011.565329.

93. Agarwal, S.; Boddu, S.H.S.; Jain, R.; Samanta, S.; Pal, D.; Mitra, A.K. Peptide prodrugs: Improved oral absorption of lopinavir, a HIV protease inhibitor. *International Journal of Pharmaceutics*, **2008**, 359, 7-14, DOI: 10.1016/j.ijpharm.2008.03.031.

94. Chin, C.M.; Chiba, D.E.; Machado, M.G.; Vizioli Ede, O.; Santos, J.L. Peptide prodrugs for the treatment of CNS disorders: a perspective for new drugs. *Current medicinal chemistry*, **2014**, 21, 2599-2609, DOI: 10.2174/09298673216661402171255 26.

95. Wang, Y.; Cheetham, A.G.; Angacian, G.; Su, H.; Xie, L.; Cui, H. Peptide-drug conjugates as effective prodrug strategies for targeted delivery. *Advanced Drug Delivery Reviews*, **2017**, 110-111, 112-126, DOI: 10.1016/j.addr.2016.06.015.

96. Lee, J.; Huang, W.; Broering, J.M.; Barron, A.E.; Seo, J. Prostate tumor specific peptide-peptoid hybrid prodrugs. *Bioorganic & Medicinal Chemistry Letters*, **2015**, 25, 2849-2852, DOI: 10.1016/j.bmcl.2015.04.092.

97. Ma, Y.; He, P.; Tian, X.; Liu, G.; Zeng, X.; Pan, G. Mussel-Derived, Cancer-Targeting Peptide as pH-Sensitive Prodrug Nanocarrier. *ACS Applied Materials & Interfaces*, **2019**, 11, 23948-23956, DOI: 10.1021/acsami.9b09031.

98. Copolovici, D.M.; Langel, K.; Eriste, E.; Langel, U. Cell-penetrating peptides: design, synthesis, and applications. *ACS Nano*, **2014**, 8, 1972-1994, DOI: 10.1021/nn4057269.

99. Shin, M.C.; Zhang, J.; Min, K.A.; Lee, K.; Byun, Y.; David, A.E.; He, H.; Yang, V.C. Cell-penetrating peptides: Achievements and challenges in application for cancer treatment. *Journal of Biomedical Materials Research Part A*, **2014**, 102, 575-587, DOI: 10.1002/jbm.a.34859.

100. He, H.; Sun, L.; Ye, J.; Liu, E.; Chen, S.; Liang, Q.; Shin, M.C.; Yang, V.C. Enzyme-triggered, cell penetrating peptide-mediated delivery of anti-tumor agents. *Journal of Controlled Release*, **2016**, 240, 67-76, DOI: 10.1016/j.jconrel.2015.10.040.

101. Nasrolahi Shirazi, A.; Tiwari, R.; Chhikara, B.S.; Mandal, D.; Parang, K. Design and Biological Evaluation of Cell-Penetrating Peptide–Doxorubicin Conjugates as Prodrugs. *Molecular Pharmaceutics*, **2013**, 10, 488-499, DOI: 10.1021/mp3004034.

102. Cheng, H.; Zhu, J.-Y.; Xu, X.-D.; Qiu, W.-X.; Lei, Q.; Han, K.; Cheng, Y.-J.; Zhang, X.-Z. Activable Cell-Penetrating Peptide Conjugated Prodrug for Tumor Targeted Drug Delivery. *ACS Applied Materials & Interfaces*, **2015**, 7, 16061-16069, DOI: 10.1021/acsami.5b04517.

103. Szabó, I.; Orbán, E.; Schlosser, G.; Hudecz, F.; Bánóczi, Z. Cell-penetrating conjugates of pentaglutamylated methotrexate as potential anticancer drugs against resistant tumor cells. *European Journal of Medicinal Chemistry*, **2016**, 115, 361-368, DOI: 10.1016/j.ejmech.2016.03.034.

104. Duan, Z.; Chen, C.; Qin, J.; Liu, Q.; Wang, Q.; Xu, X.; Wang, J. Cell-penetrating peptide conjugates to enhance the antitumor effect of paclitaxel on drug-resistant

lung cancer. *Drug Delivery*, **2017**, 24, 752-764, DOI: 10.1080/10717544.2017.1321060.

105. Zakeri-Milani, P.; Mussa Farkhani, S.; Shirani, A.; Mohammadi, S.; Shahbazi Mojarrad, J.; Akbari, J.; Valizadeh, H. Cellular uptake and anti-tumor activity of gemcitabine conjugated with new amphiphilic cell penetrating peptides. *Experimental and Clinical Sciences Journal*, **2017**, 16, 650-662, DOI: 10.17179/excli2017-249.

106. Vale, N.; Duarte, D.; Silva, S.; Correia, A.S.; Costa, B.; Gouveia, M.J.; Ferreira, A. Cell-penetrating peptides in oncologic pharmacotherapy: A review. *Pharmacological Research*, **2020**, 162, 105231, DOI: 10.1016/j.phrs.2020.105231.

107. Mini, E.; Nobili, S.; Caciagli, B.; Landini, I.; Mazzei, T. Cellular pharmacology of gemcitabine. *Annals of Oncology*, **2006**, 17 Suppl 5, v7-12, DOI: 10.1093/annonc/mdj941.

108. FDA Approval for Gemcitabine Hydrochloride. Availabe online: *http://www.cancer.gov/about-cancer/treatment/drugs/fda-gemcitabine-hydrochloride#Anchor-PanCan* (accessed in November 11th, 2015).

109. FDA, U.I. GEMZAR® (Gemcitabine HCl) for injection; FDA label. Availabe online: *https://www.accessdata.fda.gov/drugsatfda_docs/label/2011/020509s069lbl.pdf* (accessed in November 2020).

110. Abdel-Rahman, O.; Elsayed, Z.; Elhalawani, H. Gemcitabine-based chemotherapy for advanced biliary tract carcinomas. The *Cochrane Database of Systematic Reviews*, **2018**, 4, Cd011746, DOI: 10.1002/14651858.CD011746.pub2.

111. Shelley, M.D.; Jones, G.; Cleves, A.; Wilt, T.J.; Mason, M.D.; Kynaston, H.G. Intravesical gemcitabine therapy for non-muscle invasive bladder cancer (NMIBC): a systematic review. *BJU Int*, **2012**, 109, 496-505, DOI: 10.1111/j.1464-410X.2011.10880.x.

112. Ducoulombier, A.; Cousin, S.; Kotecki, N.; Penel, N. Gemcitabine-based chemotherapy in sarcomas: A systematic review of published trials. *Critical Reviews in Oncology/Hematology*, **2016**, 98, 73-80, DOI: 10.1016/j.critrevonc.2015.10.020.

113. Hioki, M.; Shimada, T.; Yuan, T.; Nakanishi, T.; Tajima, H.; Yamazaki, M.; Yokono, R.; Takabayashi, M.; Sawamoto, K.; Akashita, G., et al. Contribution of equilibrative nucleoside transporters 1 and 2 to gemcitabine uptake in pancreatic cancer cells. *Biopharmaceutics & Drug Disposition*, **2018**, 39, 256-264, DOI: 10.1002/bdd.2131.

114. Moysan, E.; Bastiat, G.; Benoit, J.-P. Gemcitabine versus modified gemcitabine: a review of several promising chemical modifications. *Molecular pharmaceutics*, **2013**, 10, 430-444.

115. World Health, O. Antimicrobial resistance: global report on surveillance; *World Health Organization*, Geneva, **2014**.

116. WHO's first global report on antibiotic resistance reveals serious, worldwide threat to public health. Availabe online: *https://www.who.int/southeastasia/news/detail/30-04-2014-who-s-first-global-report-on-antibiotic-resistance-reveals-serious-worldwide-threat-to-public-health* (accessed in July 2021).

117. Pollack, L.A.; Srinivasan, A. Core elements of hospital antibiotic stewardship programs from the Centers for Disease Control and Prevention. *Clinical Infectious Diseases*, **2014**, 59 Suppl 3, S97-S100, DOI: 10.1093/cid/ciu542.

118. Roberts, J.A.; Abdul-Aziz, M.H.; Lipman, J.; Mouton, J.W.; Vinks, A.A.; Felton, T.W.; Hope, W.W.; Farkas, A.; Neely, M.N.; Schentag, J.J., et al. Individualised antibiotic dosing for patients who are critically ill: challenges and potential solutions. *The Lancet. Infectious Diseases*, **2014**, 14, 498-509, DOI: 10.1016/s1473-3099(14)70036-2.

119. Cunha, C.B.; Opal, S.M. Antibiotic Stewardship: Strategies to Minimize Antibiotic Resistance While Maximizing Antibiotic Effectiveness. *The Medical Clinics of North America*, **2018**, 102, 831-843, DOI: 10.1016/j.mcna.2018.04.006.

120. Antibiotic Stewardship. Availabe online: *https://penallergytest.com/antibiotic-stewardship/* (accessed in July 2021).

121. Leekha, S.; Terrell, C.L.; Edson, R.S. General Principles of Antimicrobial Therapy. *Mayo Clinic Proceedings*, **2011**, 86, 156-167, DOI: 10.4065/mcp.2010.0639.

122. Abdul-Aziz, M.H.; Alffenaar, J.C.; Bassetti, M.; Bracht, H.; Dimopoulos, G.; Marriott, D.; Neely, M.N.; Paiva, J.A.; Pea, F.; Sjovall, F., et al. Antimicrobial therapeutic drug monitoring in critically ill adult patients: a Position Paper. *Intensive Care Medicine*, **2020**, 46, 1127-1153, DOI: 10.1007/s00134-020-06050-1.

123. Mabilat, C.; Gros, M.F.; Nicolau, D.; Mouton, J.W.; Textoris, J.; Roberts, J.A.; Cotta, M.O.; van Belkum, A.; Caniaux, I. Diagnostic and medical needs for therapeutic drug monitoring of antibiotics. *European Journal of Clinical Microbiology & Infectious Diseases*, **2020**, 39, 791-797, DOI: 10.1007/s10096-019-03769-8.

124. Wicha, S.G.; Märtson, A.G.; Nielsen, E.I.; Koch, B.C.P.; Friberg, L.E.; Alffenaar, J.W.; Minichmayr, I.K. From Therapeutic Drug Monitoring to Model-Informed Precision Dosing for Antibiotics. *Clinical Pharmacology and Therapeutics*, **2021**, 109, 928-941, DOI: 10.1002/cpt.2202.

125. Choi, R.; Woo, H.I.; Park, H.D.; Lee, S.Y. A nationwide utilization survey of therapeutic drug monitoring for five antibiotics in South Korea. *Infection and Drug Resistance*, **2019**, 12, 2163-2173, DOI: 10.2147/idr.S208783.

126. Begg, E.J.; Barclay, M.L.; Kirkpatrick, C.M. The therapeutic monitoring of antimicrobial agents. *British Journal of Clinical Pharmacology*, **2001**, 52 Suppl 1, 35s-43s, DOI: 10.1046/j.1365-2125.2001.0520s1035.x.

127. Reeves, D.; Lovering, A.; Thomson, A. Therapeutic drug monitoring in the past 40 years of the Journal of Antimicrobial Chemotherapy. *Journal of Antimicrobial Chemotherapy*, **2016**, 71, 3330-3332, DOI: 10.1093/jac/dkw408.

128. Cunha, B.A. Antibiotic side effects. *The Medical Clinics of North America*, **2001**, 85, 149-185, DOI: 10.1016/s0025-7125(05)70309-6.

129. Yılmaz, Ç.; Özcengiz, G. Antibiotics: Pharmacokinetics, toxicity, resistance and multidrug efflux pumps. *Biochemical Pharmacology*, **2017**, 133, 43-62, DOI: 10.1016/j.bcp.2016.10.005.

130. Ye, Z.K.; Tang, H.L.; Zhai, S.D. Benefits of therapeutic drug monitoring of vancomycin: a systematic review and meta-analysis. *PloS One*, **2013**, 8, e77169, DOI: 10.1371/journal.pone.0077169.

131. Rybak, M.; Lomaestro, B.; Rotschafer, J.C.; Moellering, R., Jr.; Craig, W.; Billeter, M.; Dalovisio, J.R.; Levine, D.P. Therapeutic monitoring of vancomycin in adult patients: a consensus review of the American Society of Health-System Pharmacists, the Infectious Diseases Society of America, and the Society of Infectious Diseases Pharmacists. *American Journal of Health-System Pharmacy*, **2009**, 66, 82-98, DOI: 10.2146/ajhp080434.

132. Jenkins, A.; Thomson, A.H.; Brown, N.M.; Semple, Y.; Sluman, C.; MacGowan, A.; Lovering, A.M.; Wiffen, P.J. Amikacin use and therapeutic drug monitoring in adults: do dose regimens and drug exposures affect either outcome or adverse events? A systematic review. The *Journal of Antimicrobial Chemotherapy*, **2016**, 71, 2754-2759, DOI: 10.1093/jac/dkw250.

133. Kovačević, T.; Avram, S.; Milaković, D.; Špirić, N.; Kovačević, P. Therapeutic monitoring of amikacin and gentamicin in critically and noncritically ill patients.

Journal of Basic and Clinical Pharmacy, **2016**, 7, 65-69, DOI: 10.4103/0976-0105.183260.

134. de Velde, F.; Mouton, J.W.; de Winter, B.C.M.; van Gelder, T.; Koch, B.C.P. Clinical applications of population pharmacokinetic models of antibiotics: Challenges and perspectives. *Pharmacological Research*, **2018**, 134, 280-288, DOI: 10.1016/j.phrs.2018.07.005.

135. Hodiamont, C.J.; Janssen, J.M.; de Jong, M.D.; Mathôt, R.A.; Juffermans, N.P.; van Hest, R.M. Therapeutic Drug Monitoring of Gentamicin Peak Concentrations in Critically Ill Patients. *Therapeutic Drug Monitoring*, **2017**, 39, 522-530, DOI: 10.1097/ftd.0000000000000432.

136. Drennan, P.G.; Thoma, Y.; Barry, L.; Matthey, J.; Sivam, S.; van Hal, S.J. Bayesian Forecasting for Intravenous Tobramycin Dosing in Adults With Cystic Fibrosis Using One Versus Two Serum Concentrations in a Dosing Interval. *Therapeutic Drug Monitoring*, **2021**, 43, 505-511, DOI: 10.1097/ftd.0000000000000900.

137. Möhlmann, J.E.; van Luin, M.; Mascini, E.M.; van Leeuwen, H.J.; de Maat, M.R. Monitoring of tobramycin serum concentrations in selected critically ill patients receiving selective decontamination of the digestive tract: a retrospective evaluation. *European Journal of Clinical Pharmacology*, **2019**, 75, 831-836, DOI: 10.1007/s00228-019-02644-x.

138. Coulthard, K.P.; Peckham, D.G.; Conway, S.P.; Smith, C.A.; Bell, J.; Turnidge, J. Therapeutic drug monitoring of once daily tobramycin in cystic fibrosis--caution with trough concentrations. *Journal of Cystic Fibrosis*, **2007**, 6, 125-130, DOI: 10.1016/j.jcf.2006.05.015.

139. Roberts, J.A.; Lipman, J. Pharmacokinetic issues for antibiotics in the critically ill patient. *Critical Care Medicine*, **2009**, 37, 840-851; quiz 859, DOI: 10.1097/CCM.0b013e3181961bff.

140. Model-Based Bayesian Precision Dosing. Availabe online: *https://precisepk.com/* (accessed in July 2021).